U. S. Department of Energy
1000 Independence Avenue, S.W.
Washington, D.C. 20585

Fiscal Year 2020: Fourth Quarter

Progress Reports:
Advanced Battery Materials Research (BMR) Program
&
Battery500 Consortium

Released December 2020
for the period of July – September 2020

Approved by

Tien Q. Duong, Program Manager
Advanced Battery Materials Research Program & Battery500 Consortium
Vehicle Technologies and Electrification Program
Energy Efficiency and Renewable Energy

TABLE OF CONTENTS

Advanced Battery Materials Research Program

Battery500 Consortium Program

TABLE OF FIGURES

TABLE OF TABLES

A MESSAGE FROM THE MANAGER: ADVANCED BATTERY MATERIALS RESEARCH PROGRAM AND BATTERY500 CONSORTIUM

The Office of Energy Efficiency and Renewable Energy (EERE) has two programs that perform cutting edge research to advance battery technology for electric vehicles. The Advanced Battery Materials Research (BMR) Program focuses on discovering high-performance materials, comprehensive modeling, and diagnostics analyses of materials and electrochemical cell behavior to address chemical, physical, and mechanical instabilities. It is composed of seven research task areas including: Liquid/Polymer Solid-State Electrolytes; Diagnostic Analysis; Modeling; Metallic Lithium; Sulfur Electrodes; Air-Electrodes/Electrolytes; and Sodium-Ion Batteries. The Battery500 Consortium focuses on designing a cell that can achieve 500 Wh/Kg and 1000 cycles through novel cell architectures utilizing a lithium anode, a compatible electrolyte, and high-capacity cathodes. To accomplish this aggressive goal, the program is divided into 3 key areas: Materials and Interfaces; Electrode Architecture; and Cell Fabrication, Testing, and Diagnosis.

In this document, we report on the progress made on these efforts from July 1, 2020, through September 30, 2020. A few notable achievements from the BMR investigators this quarter are summarized below:

- B. McCloskey's group at the University of California at Berkeley used coarse-grained molecular dynamics simulations to characterize the Onsager transport coefficients of polyelectrolyte solutions as a function of chain length and concentration. They found that the rigorously computed transference number is substantially lower than that approximated by the Nernst–Einstein equations typically used to characterize these systems due to the presence of strong anion–anion and cation–anion correlations. The Team demonstrated that the Nernst–Einstein assumption does not provide a physically meaningful estimate of the transference number in these solutions and calls into question the expectation of polyelectrolytes to exhibit a high cation transference number.
- The Stanford University group (Z. Bao and Y. Cui) investigated novel electrolytes based on a design strategy of incorporating an ionic polymer coating at the electrode-electrolyte interface. The cycling stability of the ionic polymer coatings in a Li||Cu configuration was analyzed using the conventional electrolyte of 1 M $LiPF_6$ in EC/EMC with 10% FEC. They found that the ionic polymer coating shows improved performance for at least 150 cycles in comparison to the bare electrode that fails at about 50 cycles. They also observed that the polymer coating significantly enhances the lifetime of the full cell.
- S. Martin's group at Iowa State University demonstrated that the mixed oxy-sulfide nitride (MOSN) mixed-glass-former (MGF) glassy solid electrolyte (GSE) compositions have ionic conductivity > 1 mS/cm at 25^{o}C; have electronic area specific resistance > 0.1 M Ohm-cm^2; are stable in the potential window of 0 to 5 V versus Li/Li^+; and are chemically stable.
- The Pacific Northwest National Laboratory group (C. Wang) demonstrated the correlations among lithium deposition conditions, dendrite growth kinetics, and SEI formation mechanisms, offering insights on how to regulate the microstructure and chemical features of electrochemically deposited lithium metal and SEI.
- The Argonne National Laboratory (ANL) group (Z. Chen) revealed that the reactions between Li-metal anode and LLZO electrolyte accelerate with increasing current density. Their study showed micron-sized clustered cracks on flat LLZO pellet surface after repeated lithium stripping/plating, revealing that damages to the electrolyte originate from within instead of from outside.

- K. Amine's group at ANL implemented scanning electron microscopy (SEM) combined with time-of-flight secondary ion mass spectrometry to visualize the impact of the shuttling effect of polysulfides on the morphology and composition of a Se-S cathode and Li-metal anode during cycling. Cells utilizing DME-based electrolytes showed the presence of irregular deposition products of sulfur and selenium on the surface of the lithium, while a fluorinated ether-based electrolyte exhibited a uniform and homogeneous morphology with no detectable selenium and only a weak signal for sulfur. The results demonstrate the benefit of using fluorinated ether solvents in Li-S systems.

Highlights from the Battery500 Consortium team include the following:

Keystone Project 1: Materials and Interfaces

- A novel electrolyte, 1 M LiFSI/FDMB, was shown to improve lithium metal deposition morphology and SEI nanostructure. Cryo-TEM results revealed a very thin SEI with extraordinary uniformity. When 1 M LiFSI/DME or 1 M LiFSI/DMB was applied in Cu|NMC-532 anode-free cells after 10 cycles, the lithium structure on copper was dendritic and porous. By contrast, with the 1 M LiFSI/FDMB electrolyte, the 2.7 mAh cm^{-2} lithium deposited on copper (~ 14-µm thick theoretically, while ~ 20-µm observed) showed densely packed flat and large grains, even after 70 cycles.
- Studies revealed that cathode capacity retention does not directly correlate to nickel content. By adjusting calcination parameters, such as temperature and oxygen pressure, pure-nickel $LiNO_2$ can give superior capacity retention compared to $LiNi_{0.94}Co_{0.06}O_2$. This, however, is at the cost of reduced capacity.

Keystone Project 2: Electrode Architecture

- Scanning transmission electron microscopy – electron energy loss spectroscopy (STEM-EELS) and synchrotron studies revealed the chemistries both within the sulfurized polyacrylonitrile (SPAN) bulk electrode and at the electrode-electrolyte interphase. These studies provide insight for designing electrolytes that enable high areal loading (> 6.5 mAh cm^{-2}) SPAN with promising electrochemical performance.
- SEM images revealed the effect of 3D current collector tortuosity on lithium deposition behavior: high tortuosity can hinder the diffusion of lithium ions and lead to inhomogeneous lithium deposition, while small tortuosity can reduce the specific surface area and cause whisker-like lithium prone to deactivation.

Keystone Project 3: Cell Fabrication, Testing, and Diagnosis

- Electrochemical characterization methods were enhanced to understand utilization of electrode materials. These methods will allow the Battery500 team to directly compare different cycling experiments and advance new cell and electrode design concepts.

We encourage you to follow our progress as we proceed. Our first quarter FY 2021 report is expected to be available in March 2021.

Sincerely,

Tien Q. Duong

Tien Q. Duong
Manager, Advanced Battery Materials Research Program & Battery500 Consortium
Batteries & Electrification R&D
Energy Efficiency and Renewable Energy
U.S. Department of Energy

TASK 1 – Liquid/Polymer Solid-State Electrolytes

Summary and Highlights

The BMR Program goal is to develop long-life batteries superior to commercial Li-ion systems in terms of cost, vehicle range, and safety. The BMR Program addresses the fundamental problems of electrode chemical and mechanical instabilities that have slowed development of affordable, high-performance, automotive batteries. The aim is to identify electrode/electrolyte materials that yield enhanced battery performance and lead to greater acceptance of electric vehicles (EVs). Currently, the U. S. Department of Energy (DOE) Vehicle Technologies Office (VTO) supports 16 projects in the BMR Program under this Electrolytes Task. These projects can be categorized into four general topics:

- **Liquid.** The projects for liquid electrolyte (LE) aim to develop electrolyte formulations, based on fluoro-chemistries, to achieve significantly improved operating voltage, increased durability, and increased energy density of Li-ion batteries at a reasonable cost. Nonaqueous polyelectrolyte solutions with high Li^+ transference numbers will be developed to achieve high rate capabilities at room temperature. In addition, electrolytes with new polymer binders bearing a pentafluorophenyl group on the backbone will be designed, synthesized, and tested.
- **Polymer.** The targets of polymer electrolyte (PE) projects include inorganic/polymer and polymer/gel hybrid electrolytes that have flexibility, mechanical strength, thermal stability, high ionic conductivity, stable interfaces against lithium metal, and polysulfide-trapping capability enabling energy density Li-S batteries, with comparable cycle life.
- **Self-Forming & Self-Healing.** The self-forming, self-healing electrolyte projects are focused on developing and implementing Li-metal-based metal fluorite and metal iodide batteries, capable of energy densities > 400-500 Wh/kg and 1000 Wh/L.
- **Solid-State.** The solid-state projects are to develop high conductivities solid electrolytes (SEs) / composite SEs that are scalable, are chemically and electrochemically stable, and will enable low-cost, high-energy-density solid-state lithium batteries (SSLBs).

Highlights

At the Daikin group (J. Sunstrom, R. Hendershot, and A. Falzone), the team studied crystalline structural changes following cycling at high voltage (≥ 4.5V), using 200 mAh NMC-532/Graphite cells with different electrolytes, undergoing 600 continuous CC-CC cycles at 0.7C (3.0-4.5 V or 3.0-4.6 V). Rapid degradation in cells was observed in the hydrocarbon cells at 4.6 V after the 100th cycle, whereas the fluorinated met the project performance target of ≥ 80% capacity retention at 4.6 V after at least 300 cycles. This further supports that electrolyte degradation is the dominating degradation mechanism in NMC-532/Graphite cells, with a small (if any) contribution from bulk crystallinity changes in the cathode. Additional pouch cells were tested this quarter to determine both the reversible and irreversible thickness changes as a function of time/voltage/electrolyte. The team finds no overall irreversible thickness change in the pouch cell.

At Stony Brook University (SBU, E. Takeuchi), extended cycle life testings were performed. Comparisons of cycling efficiency over 60 cycles demonstrated the ability of the Li-SE-C (IV) configuration to maintain a higher Coulombic efficiency (CE) compared to the other cell types.

The University of California (UC) at Berkeley group (B. McCloskey) completed Milestone 4 and its related progress measure, writing an article (in press at *Macromolecules*) on coarse-grained molecular dynamics (MD) simulations of polyelectrolyte solutions, demonstrating that trends in cation-anion correlations cannot be predicted from static analysis of the fraction of ion pairs, as is conventional in the MD literature, but rather must be understood through a dynamic analysis of ion pair residence times. They also investigated polymerized ionic liquids, that is, polyelectrolyte solutions with no added solvent, and observed anti-correlated cation-anion motion, as has been previously observed in non-polymeric ionic liquids.

The Stanford University group (Z. Bao and Y. Cui), based on a design strategy of incorporating an ionic polymer coating at the electrode-electrolyte interface, used perfluoropolyether-dimethacrylate (PFPE-DMA) as polymer network backbone, pentaerythritol-tetrakis(3-mercaptopropionate) (PETMP) as the crosslinker, and lithium-styrene-trifluoromethanesulfonyl-imide (Li-STFSI) as salt linker in different ratios. The cycling stability of the ionic polymer coatings in Li||Cu configuration was analyzed using conventional electrolyte of 1 M $LiPF_6$ in ethylene carbonate (EC) / ethyl methyl carbonate (EMC) with 10% fluoroethylene carbonate (FEC). They found that the ionic polymer coating shows improved performance for at least 150 cycles in comparison to the bare electrode that fails at about 50 cycles. They also observed that the polymer coating significantly enhances the lifetime of the full cell. In addition, they found that the polymer design reported in this work can stabilize metal-electrolyte interfaces independent of the electrolyte and cathode chemistries.

The Lawrence Berkeley National Laboratory (LBNL) group (N. Balsara) found that the POSS-PEO-POSS [polyhedral oligomeric silsesquioxane, (POSS); poly(ethylene oxide), (PEO)] hybrid triblock electrolyte shows an exceptionally high limiting current between 1.8 and 6 mA cm^{-2} for a membrane of 25-30 µm thicknesses. Additionally, the polymers exhibit stability against lithium metal after cycling experiments. The operating current density is an important factor in the lifetime of lithium symmetric cells with solid PEs.

The Iowa State University (ISU) group (S. Martin) has demonstrated that the mixed-oxy-sulfide-nitride (MOSN) mixed-glass-former (MGF) glassy solid electrolyte (GSE) compositions have ionic conductivity >1 mS/cm at 25°C; electronic area specific resistance (ASR) > 0.1 M Ohm-cm^2; are stable in the potential window of 0 to 5 V versus Li/Li^+; and are chemically stable. This quarter, the use of the vertical furnace for large-scale melting of MOSN MGF GSEs was further optimized.

The Wildcat group (K. Carroll / C. Peebles) has shown significant effort on designing high ceramic loading composite films. They found that lower the boiling point of the co-solvent improves the overall ionic conductivity of the composite film; and that by adjusting the calendering parameters, they can further improve the ionic conductivity of the film. The team also began testing interfacial resistance (using electrochemical impedance spectroscopy, or EIS) in Li/Li symmetric cells using the solid-state electrolyte (SSE) films they made, to screen Li-metal protection materials.

The University of Michigan (UM) group (J. Sakamoto) successfully fabricated thin film constructs (TFCs), optimized, and delivered to Tasks 2 and 3. The TFCs met the quality assurance criteria for conductivity, surface chemistry, phase purity, and thickness. For Task 2, the TFCs were delivered for *in situ* cycling tests. For Task 3, the TFCs were delivered to study the critical current density (CCD) stripping and CCD plating. Based on the successful delivery of these TFCs, a the result of the *Go/No-Go Decision* is *Go*.

The University of Maryland (UMD) group (C. Wang) has synthesized, characterized Li_5NI_2-LiOH SSEs, and identifies ways of improving the ionic conductivity and interfacial resistance in these materials.

The UMD group (E. Wachsman and Y. Mo) used demonstrated thermodynamic analyses for interface stability based on first-principles computation to perform high-throughput (HT) screening in an effort to identify oxide materials that stabilize with $Li_7La_3Zr_2O_{12}$ (LLZO) – NMC interfaces. The compositions with small chemical and electrochemical reactions with LLZO and NMC are identified as stable coating layers. Therefore, they have successfully achieved the milestone and *Go/No-Go Decision* of computationally determining the mechanism of interfacial stabilization and the appropriate compositions to stabilize the LLZO-NMC interface.

At University of Wisconsin Milwaukee (UWM, D. Qu), the principal investigator's (PI's) research labs and the auxiliary services (for example, machine shop in the university) are only partially opened in order to maintain social distancing during the pandemic. However, they managed to complete all FY 2020 milestones. This quarter, G2 solid-state cells were designed and made for both performance tests and *in situ* observation of dendrite growth. G2 *in situ* gassing analysis cells were also designed, and the analysis will be fully automated.

The team at Virginia Polytechnic Institute and State University (Virginia Tech, L. Madsen) further studied Li-ion transport properties in Molecular Ionic Composite (MIC) electrolytes and their compatibility with lithium metal over a wide temperature range through lithium symmetric cell cycling. The symmetric cell can be cycled at 150°C for 150 hours, demonstrating thermal and electrochemical stability of the MIC electrolyte at an extreme temperature. They also studied the long-term cycling stability of the MIC electrolyte membrane in a Li/MIC/$LiFePO_4$ cell at 23°C using a C/10 charge/discharge rate. The specific discharge capacity reaches a maximum of 150 mAh g^{-1}, with a high retention of 94% after 400 cycles, again signifying the strong stability of MIC membrane.

The team at Solid Power (P. Zhang) with UC at San Diego (S. Meng, UCSD) has developed the multifunctional electrolyte materials meeting Year 1 performance targets on both the Li-ion conductivity and the CCD against lithium metal. In addition, a post-treatment method has been developed to improve the purity of the material, which improves the electrolyte CCD (that is, lithium stability) significantly. Furthermore, the SSE separator coating process has been developed at pilot scale. Their full cell demonstrates 250 cycles with 80% capacity retention and 350 cycles with 75% capacity retention, exceeding the first year goal of 200 cycles.

The team at Pennsylvania State university (PSU, D. Wang) continued their previous work on developing new solid electrolyte introducing nitrogen and aluminum in the basic Li_2S-P_2S_5 solid electrolyte system. They have developed a new glass-ceramic solid electrolyte $65Li_2S$-$65Li_2S$-$26P_2S_5$-$10Li_3N$-$12Al_2S_3$ (LPSNAl-12) with high ionic conductivity of 5.19 mS cm^{-1} at 25°C and low activation energy of 0.159 eV. Such high ionic conductivity meets their proposed milestone for synthesizing new solid electrolyte in budget period 1. In addition, sulfur cathode with sulfur content of ~ 50 wt% and areal loading of ~ 1.5 mg cm^{-2} demonstrated high initial discharge capacity of over 1400 mAh g^{-1}, and even after 50 cycles, the specific capacity could still retain above 1200 mAh g^{-1} at 0.3 charge/discharge rate at 60°C. Li-In alloy was employed as anode and 75 $Li_2S \cdot 25\ P_2S_5$ glass type SSE was employed as solid electrolyte membrane and electrolyte used in the cathode. Such superior performance fulfilled the electrochemically active molecules (EAMs) additives demonstration milestone as well as the project progress cell demonstration target of *Go/No Go Decision* for budget period 1.

Task 1.1 – Advanced Lithium-Ion Battery Technology: High-Voltage Electrolyte (Joe Sunstrom, Ron Hendershot, and Alec Falzone, Daikin)

Project Objective. The project objective is to identify electrolyte formulations, based on fluoro-chemistries, that will allow significantly improved operating voltage, increased durability, and increased energy density of Li-ion batteries at a reasonable cost. The project seeks to understand the conditions under which the electrolyte degrades, the effect on battery performance, and solutions that can overcome current limitations of the electrolyte. Gassing in Li-ion batteries is one of the most common failure mechanisms and poses the greatest safety risk in consumer devices. This project aims to investigate gas composition pas a function of cathode material, electrolyte formulation, and operating voltage, and proposes optimal cell compositions at decomposition voltages.

Project Impact. Developing an understanding of the operating conditions in which gases form in Li-ion batteries enables the project to propose optimized cell compositions that operate at higher voltages for a longer period. Different fluorinated electrolyte components and additives may suppress and/or eliminate gas generation at or above hypothesized decomposition voltages. To investigate these topics, it is imperative that the project utilize multiple approaches, including, but not limited to, cathode material, electrolyte composition, operating voltage, and cycle number.

Approach. The evolving composition of the electrolyte in the battery will be examined by various analytical instruments to study volatiles [gas chromatography – mass spectrometry / thermal conductivity detection (GC-MS/TCD)], liquid [liquid chromatography MS (LC-MS)], and solid [time-of-flight secondary ion mass spectrometry (TOF-SIMS), thermogravimetric analysis MS (TGA-MS), X-ray photoelectron spectroscopy (XPS), and auger electron spectroscopy (AES)] electrolyte decomposition products during battery operation. In the first year, the team addressed gas composition and kinetics for both hydrocarbon and fluorocarbon as a function of several charge/discharge conditions. In the second year, the project will transition into analysis of the SSE decomposition components of its tested batteries to obtain valuable information about solid electrolyte interphase (SEI) layer formation and how it manifests change in both the anode (graphite) and cathode (LCO and NMC). The third year is focused on measuring changes in the solid-state structure of the cathode following high-voltage operation. The project aims to quantify any dissolved metal ions originating from the cathode and deposited on the anode using inductively coupled plasma – mass spectrometry (ICP-MS). It will also study changes in the cathode structure using powder XRD.

Out-Year Goals. Work will progress toward understanding how electrolyte formulation and cell operation affect stability of transition metals (TMs) in the cathode structure. The project aims to quantify metal ions, if any, dissolved into solution as a function of operating parameters (that is, voltage, time, etc.) and electrolyte formulation. In addition, measurements will be made using powder XRD to detect changes in the crystal structure of the cathode (LCO and NMC). Understanding effects on the solid-state structure in Li-ion batteries will provide valuable information on the required cathode chemistry for increased performance at high voltage.

Collaborations. The project has initiated a collaboration with J. Chan (University of Texas, or UT, at Dallas) for powder XRD measurements to investigate changes in cathode structure as a function of operating conditions. Results from this collaboration were reported in the second quarter of FY 2020.

Milestones

1. Cathode structure versus time/voltage. (Q3, FY 2020; Complete)
2. Data compilation and selection of new electrolyte composition. (Q4, FY 2020; Complete)

Progress Report

Comparisons of crystalline structural changes following cycling at high-voltage (≥ 4.5 V) is extremely valuable to elucidate any degradation observed either during cycling or post-mortem. 200 mAh NMC-532/graphite cells underwent 600 continuous CC cycles at 0.7C (3.0-4.5 V or 3.0-4.6 V). This was performed as a function of electrolyte by comparing the baseline hydrocarbon formulation to the optimized fluorinated analog. Rapid degradation in cells was observed in the hydrocarbon cells at 4.6 V after the 100th cycle; whereas, the fluorinated met the project performance target of ≥ 80% capacity retention at 4.6 V after at least 300 cycles. This further supports that electrolyte degradation is the dominating degradation mechanism in NMC-532/graphite cells, with a small (if any) contribution from bulk crystallinity changes in the cathode. Figures 1 and 2 depict the diffraction pattern from cells post-mortem at various states of charge (SOC) as a function of electrolyte. No defect crystalline phases were detected outside the layered $Li(Ni_xMn_yCo_z)O_2$ structure post-mortem.

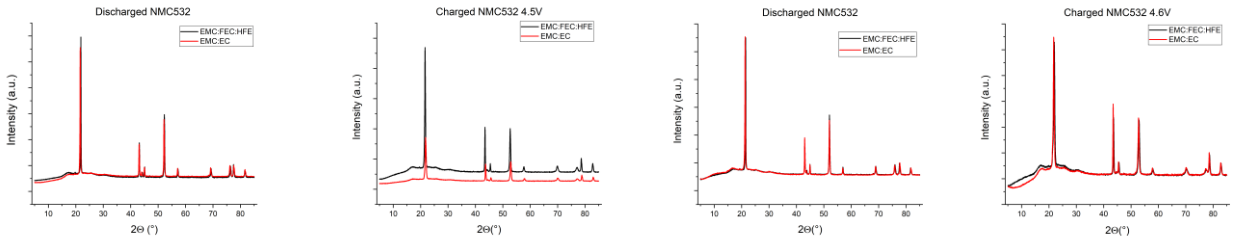

Figure 1. Diffraction patterns as a function of state of charge and electrolyte. Charged cells were measured *ex situ* nominally at their upper cutoff voltage (4.5 or 4.6 V), whereas discharged cells were at 3.4 V.

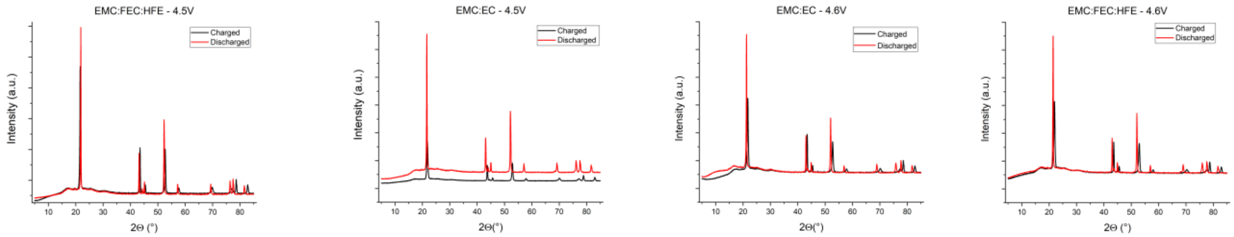

Figure 2. Diffraction patterns as a function of electrolyte at 4.5 and 4.6 V. Electrolyte formulation does not appear to have an effect on bulk changes in the crystalline structure, at the detection limits of *ex situ* powder X-ray diffraction.

Additional pouch cells were tested this quarter to determine both the reversible and irreversible thickness changes as a function of time/voltage/electrolyte. Figure 3 depicts the project's optimized cell chemistry, NMC-532, as a function of SOC with the baseline hydrocarbon electrolyte formulation [1.2M $LiPF_6$ 80:20 (EMC:EC, v/v) + 1% PS (w/w)].

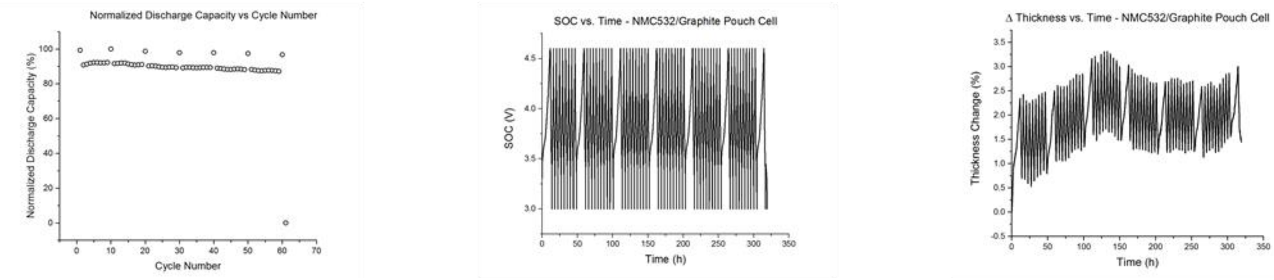

Figure 3. Normalized discharged capacity (left), state of charge versus time (middle), and Δ thickness versus time (right). Cell was cycled at C/2, with a CC-CV every 10 cycles to benchmark capacity degradation (C/20). Thickness changes were obtained using the contactless laser method outlined in previous reports.

On a cycle-by-cycle basis, the pouch cell gains approximately 1.5% in thickness (~ 56 μm) when a 100% SOC is reached at 4.6 V. Over the course of the 60 charge/discharge cycle life test, this change appears to be both reproducible and reversible within experimental error. There does appear to be an overall irreversible thickness change seen in the pouch cell. The start and end of the experiment both represent identical SOC at 3.0 V. This SOC indicates an overall irreversible thickness increase of approximately 1.5% over the 60 cycles, with a visible upward trend following the 50th cycle.

Patents/Publications/Presentations

The project has no patents, publications, or presentations to report this quarter.

Task 1.2 – Dual Function Solid-State Battery with Self-Forming, Self-Healing Electrolyte and Separator
(Esther Takeuchi, Stony Brook University)

Project Objective. The project objective is to demonstrate a solid-state rechargeable battery based on a Li-metal anode and iodine cathode with a self-forming, self-healing electrolyte and separator with high gravimetric and volumetric energy density.

Project Impact. This program will enable demonstration of the proposed rechargeable battery with improved power capability, high energy density, and a self-forming, self-healing SSE/separator. Technical insight will be gained regarding improved conductivity of the solid LiI based electrolyte, power capability of the proposed system, the self-healing nature of the LiI layer, the nature of the electrode-electrolyte interfaces, and feasibility of the system to reach the DOE targets.

Approach. The proposed concept is a dual function rechargeable SSB utilizing LiI combined with silver iodide (AgI) as the electrolyte, with lithium metal (and small quantities of silver metal) as the anode and iodine as the cathode, and with a self-forming, self-healing separator/electrolyte. The battery will be assembled in the discharged state, where the anode and cathode will be created during the first formation (charge) step. Initially, silver ion (Ag^+) will diffuse toward the negative electrode and be reduced to silver metal (Ag^0), and iodine ion (I^-) will be oxidized to elemental iodine (I_2) at the cathode side. As the formation of the battery continues, lithium ion (Li^+) will form a Li-metal layer at the anode, with generation of iodine at the cathode. LiI will remain and serve as both the separator and electrolyte.

Out-Year Goals. This is a multi-year program where the effort is divided into three major tasks.

- Year 1 involves electrolyte preparation and characterization including preparation of SSEs and conductivity measurements.
- Year 2 will focus on cell construction and testing including both *in situ* and *ex situ* analysis.
- Year 3 will focus on cell characterization. Under the program, cycle life, efficiency, energy density, and the functional capacity of cells will be determined.

Collaborations. This project collaborates with A. Marschilok and K. Takeuchi of SBU.

Milestones

1. Determine cycling performance at elevated temperature. (Q1, FY 2020; Completed)
2. Determine behavior of conductivity as a function of temperature to determine resistance as well as fundamental thermodynamic parameters of the SSEs. (Q2, FY 2020; Completed)
3. Conduct destructive analysis of tested cells. (Q3, FY 2020; Completed)
4. Perform extended cycle life testing. (Q4, FY 2020; Completed)

Progress Report

The milestone for this quarter was extended cycle life testing. For this series of extended cycling, four types of interfaces were tested, where the solid electrolyte (SE) interface was either modified on the negative-SE interface, positive-SE interface, or both negative-SE and positive-SE interfaces. Interfaces tested included the following four configurations: (I) SE only (no modification), (II) Li-metal SE, (III) SE – carbon nanotube (CNT), and (IV) Li-metal-SE-CNT, as shown in Figure 4. A composite electrolyte of LiI and lithium iodide(3-hydroxypropionitrile) ($LiI(HPN)_2$) was incorporated for all interface testing.

Figure 4. Cell designs of (I) solid electrolyte (SE) only, (II) Li-metal SE, (III) SE – carbon nanotube, and (IV) Li-metal-SE-CNT.

Each cell design was tested in a coin-cell configuration by galvanostatic charge-discharge cycling under a current density of 10 µA/cm^2 and a lower voltage limit of 0.005 V. Extended cycling was conducted at 30°C, for 60 cycles, and CE was compared among interfaces (Figure 5).

Figure 5a shows the voltage profiles of the varied interface cells, over the initial charge-discharge cycles. In comparing the voltage profiles, the CNT-containing cell configurations (III and IV) had notable shorting events during cycling. Despite instances of shorting, particularly in configuration IV, CE was not notably reduced, and cycling was able to continue post-shorting, noting the ability of the cells to recover fully and continue cycling after a shorting event. The ability of cell recovery was potentially attributed to the self-healing capability of the Li/I_2 based chemistry, where the formation of excess LiI on discharge from a lithium dendrite in contact with iodine would reduce the impact of the dendrite on the shorting event and allow for continued cell cycling. Notable differences were observed in the 1st cycle discharge profiles, as shown in Figure 5b, where the Li-SE-CNT configuration (IV) demonstrated the highest loaded voltage, as well as a distinct voltage plateau compared to the sloping voltage profiles of the other configurations (I-III).

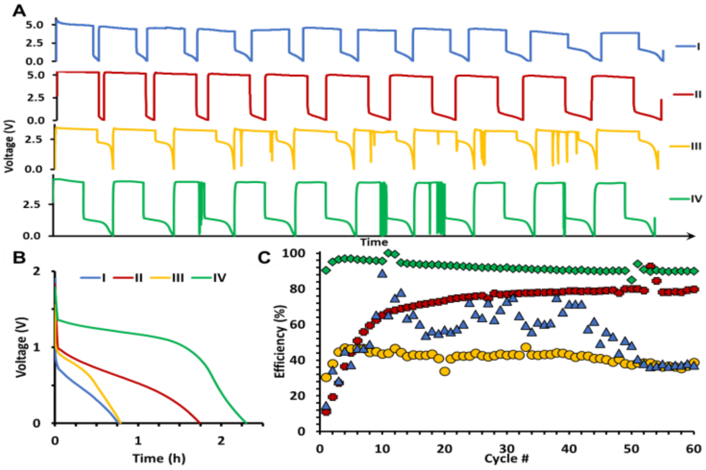

Figure 5. Voltage profiles of cell configurations I (blue), II (red), III (yellow), and IV (green) for (a) the first 11 cycles, and (b) 1st cycle discharge profiles. (c) Coulombic efficiencies over 60 cycles comparing each cell configuration.

Comparisons of cycling efficiency over 60 cycles demonstrated the ability of the Li-SE-CNT (IV) configuration to maintain a higher CE compared to the other cell types. Interestingly, cell configuration II consisting only of SE and lithium metal showed notable improvements in CE with continued cycling, increasing from ~ 10% to ~ 80% efficiency. These results highlight both the impact of having an excess lithium metal source present in the cell, as well as considering the impact of the solid electrolyte-positive interface modification and its role in efficiency over extended cycling.

Patents/Publications/Presentations

Publication

- Submitted manuscript is under revision.

Task 1.3 – Characterization and Modeling of Li-Metal Batteries: Characterization of Li$^+$ Transport in Polyelectrolytes
(Bryan D. McCloskey, University of California at Berkeley)

Project Objective. This task aims to understand lithium plating and stripping in non-traditional electrolyte systems (specifically, polyelectrolyte solutions and concentrated binary salt electrolytes) that have been proposed to reduce dendrite formation during lithium stripping and plating due to their high Li$^+$ transference numbers (t_+). The team will develop capabilities that allow them to understand how ion dynamics in these electrolytes impact macroscale transport properties and Li-metal plating and stripping.

Impact. Ultimately, this task will develop an understanding of how electrolyte composition and molecular interactions can be manipulated to positively impact ion transport of potential electrolytes for Li-metal batteries. This will provide a set of general design rules for novel electrolytes enabling stable, efficient high capacity Li-metal stripping and plating.

Approach. To understand various aspects of lithium plating and ion transport in these systems, the team will develop novel diagnostic and computational modeling techniques. Model polyelectrolytes, with pendant triflimide anions, will be used as polyanions, as their properties can be easily tuned via changes in the polymerization chemistry. Solution parameters that can be varied for both polyelectrolyte solutions and concentrated electrolytes include solvent and salt composition, additive inclusion, and the aforementioned polymer properties, all of which can have a profound impact on electrostatic interactions between charged species in solution, as well as interfacial stability and reaction kinetics of the lithium electrode. The team will develop capabilities that allow them to understand how molecular-level ion dynamics in these electrolytes impact macroscale transport properties and Li-metal plating and stripping. These computational simulations will be validated and refined by comparing results to experimentally measured transport properties of these electrolytes. They will optimize electrochemical methods for these electrolytes to evaluate relevant transport properties under the Newman Concentrated Solution Theory framework, which has never been performed on these non-traditional electrolytes. ^{1}H and ^{19}F nuclear magnetic resonance (NMR) diffusometry will also be used to measure single-ion self diffusion coefficients without an applied electric field; solution viscosity measurements using a state-of-the-art rotating sphere viscometer can be performed under entirely air/water-free conditions. The team will develop capabilities to quantitatively understand degradation mechanisms of various electrolytes during Li-metal stripping and plating. Specifically, differential electrochemical MS (DEMS) will be used to study outgassing that occurs from electrolyte degradation processes.

Out-Year Goals. The ultimate goal of this project is to understand the influence of electrolytes with novel transport characteristics on the performance of Li-metal electrodes. Work will continue to build toward a complete understanding of Li-ion and counterion transport in polyelectrolyte solutions and concentrated electrolytes, as well as the impact of electrolyte transport properties on Li-metal uniformity during electrochemical stripping and plating. Outgassing measurements using differential electrochemical MS will be developed to further probe the interfacial reactivity of lithium metal with electrolytes created in this project.

Collaborations. Collaborators on this project include K. Persson (atomistic and coarse-grained modeling) and N. Balsara (electrochemical characterization of PEs), both at LBNL.

Milestones

1. Complete study of solvent influence of transport in polysulfone-based polyelectrolyte solutions. (Q1, FY 2020; Completed)
2. Complete development and validation (using known LEs) of electrochemical transport methods. (Q2, FY 2020; Completed)

3. Complete synthesis and transport characterization of model triflimide-based polyion (pTFSI) solutions in symmetric cells with Li-metal electrodes. (Q3, FY 2020; Delayed due to COVID, with expected completion in early Q1, FY 2021)
4. Complete development of coarse-grained polyelectrolyte model to study effect of polyelectrolyte composition on transport of model polyelectrolyte systems. Progress measure: publish article on scaling of transport properties of polyelectrolyte solutions as a function of polymer and solvent properties. (Q4, FY 2020; Completed)

Progress Report

Note: Portions of the following text are adapted from Fong et al. (Fong, K. D., J. Self, B. D. McCloskey, and K. A. Persson. "Onsager Transport Coefficients and Transference Numbers in Polyelectrolyte Solutions and Polymerized Ionic Liquids." *Macromolecules*).

This quarter, the team completed Milestone 4 and its related progress measure, writing an article (in press at *Macromolecules*) on coarse-grained MD simulations of polyelectrolyte solutions. The simulations were performed using the classical Kremer-Grest bead-spring model and evaluated transport as a function of chain length and concentration. The focus of the work is analysis of the Onsager transport coefficients of these polyelectrolytes, which provide insight into the ion correlations dictating ion motion and allow the team to rigorously compute the cation transference number (t_+) of the solutions. Despite the intuitive expectation that these systems should yield high t_+ and the high t_+ predicted by the Nernst-Einstein equation (t_+^{NE}), none of the polyelectrolyte solutions studied exhibit t_+ greater than that of the conventional monomeric (binary salt) electrolytes (Figure 6). The trends in t_+ are cleanly rationalized via the systems' strong anion-anion and cation-anion correlations, which the Nernst-Einstein assumption neglects. For long chain lengths and low concentrations, the team observes negative cation transference number ($t_+ < 0$), making this work one of the first instances in which negative transference numbers—a contentious topic in the field of polymer-based battery electrolytes—have been rigorously computed using MD. They attribute this phenomena of negative t_+ to the presence of long-lived negatively charged aggregates in solution, for example, a single cation bound to a long polyanion. Importantly, they demonstrate that trends in cation-anion correlations cannot be predicted from static analysis of the fraction of ion pairs, as is conventional in the MD literature, but rather must be understood through a dynamic analysis of ion pair residence times. The team's work thus repudiates some of the intuitive assumptions typically made for understanding transport phenomena in polyelectrolytes.

They have also used the coarse-grained MD model to investigate polymerized ionic liquids, that is, polyelectrolyte solutions with no added solvent. The team has derived the special theoretical considerations necessary for two-component systems, which dictate that the transference number is only a function of the ions' charge and molar masses. For the current model, this corresponds to a transference number of exactly 0.5 for all chain lengths. In these systems, they also observe anti-correlated cation-anion motion, as has been previously observed in non-polymeric ionic liquids.

Although this work suggests that unentangled, short-chain polyelectrolyte solutions may not be useful as high t_+ alternatives to conventional Li-ion battery electrolytes, the insights gained here suggest several avenues for more promising systems. It is possible that polyelectrolyte solutions or gel-like single-ion conductors may be able to attain high cation transference number if the chains are entangled or cross-linked such that the polymer is effectively immobile. The slow dynamics and complex structure of these systems precludes the team from studying them with MD, so they will focus on experimental characterization of these polymers next quarter. The team anticipates that while these systems may have a higher transference number, they will also have lower conductivity. This trade-off will need to be considered when developing optimal electrolyte formulations.

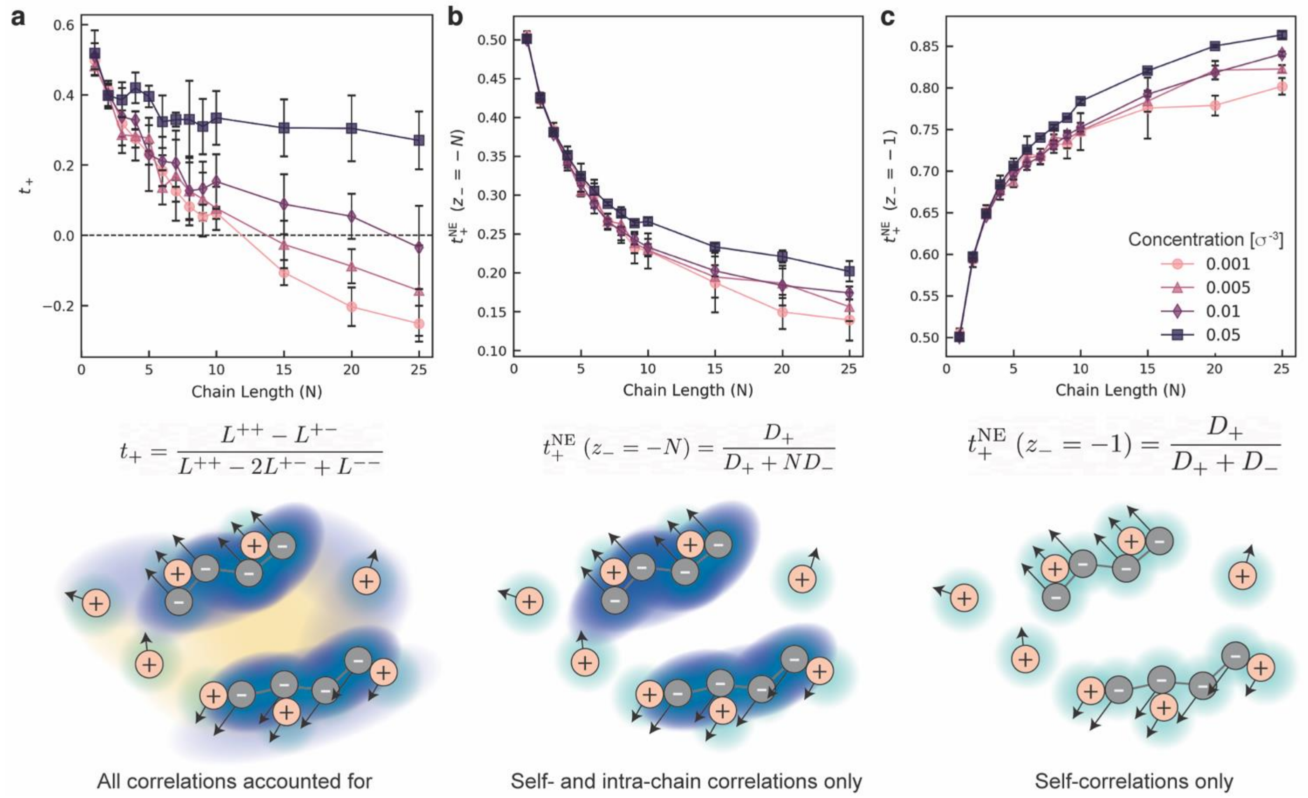

Figure 6. Cation transference number as a function of chain length computed from coarse-grained molecular dynamics simulations. (a) Rigorously computed t_+ obtained from the Onsager transport coefficients and accounting for all ion correlations present in solution. (b-c) t_+^{NE}, the ideal solution transference number ignoring correlations between ions. (b) Treating entire polymer chains as the anionic species ($z_- = -N$) accounts for intra-chain correlations, but ignores correlations between chains and between cations and anions. (c) Treating individual monomers as the anionic species ($z_- = -1$) ignores all ionic correlations.

Patents/Publications/Presentations

Publications

- Fong, K. D., J. Self, B. D. McCloskey, and K. A. Persson. "Onsager Transport Coefficients and Transference Numbers in Polyelectrolyte Solutions and Polymerized Ionic Liquids." *Macromolecules*. In press.
- Fong, K. D., H. K. Bergstrom, B. D. McCloskey, and K. K. Mandadapu. "Transport Phenomena in Electrolyte Solutions: Non-Equilibrium Thermodynamics and Statistical Mechanics." *American Institute of Chemical Engineers (AIChE) Journal* (2020): e17091.

Presentations

- The Electrochemical Society (ECS) PRiME 2020 (Joint Meeting of the ECS, ECS of Japan, and Korean ECS) 2020, Virtual (October 4–9, 2020): "Characterizing Ion Transport in Non-Aqueous Electrolyte Solutions for Li-Ion and Li- Metal Batteries"; H. Bergstrom.
- Battery Modeling Webinar Series, Virtual (October 6, 2020): "Transport Phenomena in Electrolyte Solutions: Non-Equilibrium Thermodynamics and Statistical Mechanics"; K. Fong.

Task 1.4 – Advanced Polymer Materials for Batteries
(Zhenan Bao and Yi Cui, Stanford University)

Project Objective. This project will develop new polymer materials for batteries. The team will develop polymer coatings with specific mechanical properties that can accommodate the volume expansion and contraction of the Li-metal anode associated with deposition and stripping (charging and discharging).

Project Impact. The cycling stability and CE of Li-metal electrodes will be increased by implementation of a polymer-based protective layer that functions as an artificial SEI with desired properties. The improved performance will enable further development toward practical utilization of Li-metal anodes with higher cycling efficiency and less susceptibility to dendrite-based failure.

Approach. The project uses soft polymer coatings with dynamic crosslinking to give the resulting polymers liquid-like rheological properties and stretchable and self-healing properties. In previous work, the project has shown that such coatings resulted in uniform deposition/stripping of lithium metal and improved cycling stability of Li-metal electrodes. To understand the design rules for effective polymer coatings, the team chose a few representative polymers to systematically understand structure property relationships. Here, the team investigates the correlation between surface energy of the polymer and exchange current for lithium deposition.

Out-Year Goals. Work will progress toward the correlation between dielectric constant and exchange current. These findings will enable further understanding and development of various polymer coatings for protecting Li-metal anodes.

Collaborations. This quarter, the team is collaborating with J. Qin at Stanford University.

Milestones

1. Analyze the solvation structure and lithium diffusivity of polymer/electrolyte using NMR, Fourier transform infrared (FTIR) spectroscopy, electrochemical tests, and molecular simulations. (Q1, FY 2020; Completed)
2. Evaluate the polymer basic cycling performance: 0.5 and 1 mA/cm² conditions in Li|Li and Li|Cu cells using carbonate electrolyte. (Q2, FY 2020; Completed)
3. Self–healing polymer coated Li||NMC battery: Stable cycling at C/3 rate for 150 cycles using 15 µl/mAh electrolyte. (Q3, FY 2020; Completed)
4. Self–healing polymer coated Li||NMC battery: Stable cycling at C/3 rate for at least 50 cycles using 50-µm lithium. (Q4, FY 2020; Completed)

Progress Report

Introduction

Li-metal anode suffers from several instabilities during electrodeposition process in battery charging. Specifically, lithium deposition leads to inhomogeneous coverage on the electrode substrate, resulting in concentration of electric field at the tip of these deposits, ultimately resulting in dendritic growth that shorts the battery. The high surface area metal deposition also causes faster parasitic reactions between the lithium metal and organic electrolyte that is responsible for the rapid fade of battery capacity. According to conventional understanding, the primary sources of instabilities in electrodeposition are diffusion limitations in ion transport processes, both in the bulk electrolyte and at electrode-electrolyte interfaces. Consequently, many theoretical efforts have been focused on modeling dendritic growth in a purely diffusion limited condition by varying transport properties like ion conductivity, and relative mobility of anions and cations (transference number), and studying their effect on electrolyte modulus or electrode geometry. Likewise, several experimental efforts have reported improved electrodeposition stability with electrolytes with high transference number, conductivity, or modulus. While ion transport and mechanics are important determinants of morphological evolution of the metal electrode, other coupled parameters like electrochemical kinetics and electrostatic potential landscape can play a critical role. For example, several experimental findings have reported observation of fractal structures during electrodeposition of metallic lithium, even at rates much below the diffusion limited current density. This further indicates that transport parameters in the electrolyte may not be the sole determinant of morphological stability. The relative effect of electrochemical kinetics and ion transport is particularly important considering the metal electrode does not have a smooth surface, which is aggravated even at earlier stages of deposition. The physical perturbations on the metal surface result in abrupt enhancement of local electric field causing the ions to be preferentially directed toward the dendritic tips, ultimately leading to unstable growth. In addition, a major challenge in understanding this phenomenon is that the transport and kinetics essentially rely on the same physical factors as ion concentration, viscosity, and temperature, among others. Here, the team leverages ultrafast scanning voltammetry and pulse-field gradient NMR to decouple the effects of kinetics and transport, respectively. Based on these analyses, they design a polymer interface that stabilizes electrodeposition by maintaining a uniform ion flux to the electrode. Subsequently, they intend to utilize the polymer interface for improving Li-metal battery cycling, both in Li||Cu and Li||NMC configurations.

Polymer Coating Design

Based on the aforementioned theoretical understanding, the team proposes a design strategy of incorporating an ionic polymer coating at the electrode-electrolyte interface that can enable interfacial ion transport, while reducing the charge transfer kinetics. The chemical design of the polymer network is shown in Figure 7a. Specifically, PFPE-DMA is used as polymer network backbone, PETMP as the crosslinker, and Li-STFSI as the salt linker in different ratios. The PFPE polymer is known to be resistive to chemical corrosions, while the salt molecules are incorporated to facilitate ion transport. The variation in the salt content in the polymer is characterized using NMR and infrared spectroscopy (FTIR). Figure 7b shows the varying ^{1}H NMR peak intensities of the polymers for the specific methyl groups labeled in Figure 7a, where it is seen that as linkable Li-STFSI is increased in the feed, the immobilized salt content in the polymer network is progressively higher. The team further analyzed the IR-spectra of the ionic polymer networks, where they observe that on crosslinking, the representing vibrational mode of the thiol group (-SH) at 2550 cm^{-1} disappears for all the polymers synthesized here; thus, they can conclude that all the PETMP linkers are reacted. Also, the vibration modes of the double bonds (1650 cm^{-1}) in the styrene molecule present in the Li-STFSI monomers were compared for different cases, and it is confirmed that increasing the Li-STFSI in the feed indeed leads to stronger intensity of this peak. Thus, the team confirms to be able to systematically vary immobilized salt content in the polymer network to ultimately lead to fundamental understanding of the effect of ionic polymers in stabilizing electrodeposition.

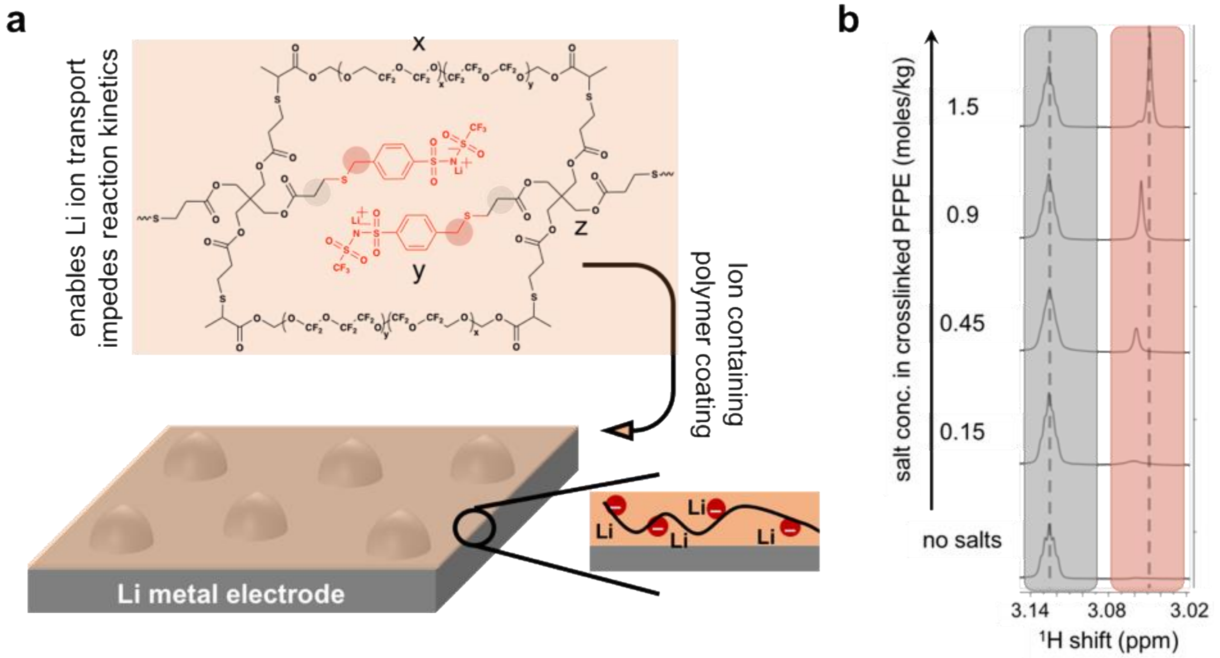

Figure 7. Polymer coating on Li-metal electrode. (a) Schematic showing the structure of ionic polymer coated on the Li-metal electrode. The ionic polymer comprises of x: perfluoropolyether-dimethacrylate (PFPE-DMA) backbone, y: pentaerythritol tetrakis(3-mercaptopropionate) or PETMP crosslinker, and z: (4 styrenesulfonyl) (trifluoromethanesulfonyl) imide (STFSI-Li) monomeric salts. The PFPE polymer acts as blocking agents for the liquid electrolyte, while the SFTFSI anions provide Li-ion transport pathways. (b) Comparison of peak heights obtained from ^{1}H NMR measurements showing the relative content of the methyl groups in the polymer backbone and the tethered anions (spectra referenced to residual protons in CD_3OD). The NMR trend follows the trend of varying salt moieties in the polymer backbone.

Battery Performance

The cycling stability of the ionic polymer coatings in Li||Cu configuration was analyzed using conventional electrolyte of 1 M $LiPF_6$ in EC/EMC with 10% FEC. The CE comparison of the control (bare electrode) and polymer coating is presented in Figure 8a. It is seen that the ionic polymer coating shows improved performance for at least 150 cycles in comparison to the control that fails at about 50 cycles. Finally, the polymer-coated thin 25-μm Li-metal electrode (N = 5mAh/cm^2) was paired against $LiNiMnCoO^2$ cathode having capacity (P) 1.7 mAh/cm^2; the batteries (N/P = 3) were cycled using the electrolyte 1 M $LiPF_6$ in EC/EMC with 10% FEC. The corresponding capacity and CE for the two cases (with and without polymer coating) are plotted in Figure 8b, while the overall efficiency, measured by the formula C.E. = 100(1-N⁄(n×P)), where n is the cycle number until 80% fade, is plotted as a bar chart in the inset. The team observes that the polymer coating significantly enhances the lifetime of the full-cell, in agreement with findings from the described electrochemical and electrodeposition results.

Additionally, the team believes that the ionic polymer coating utilized in this work is independent of the chemistry of electrolyte. Thus, they pair the polymer-coated lithium with a high-voltage cathode utilizing an electrochemically stable electrolyte that can enhance the high-voltage performance as well as form a stable SEI on the lithium metal synergistically with the effect of the polymer interface. Specifically, efficacy of the coating in Li||NMC full cells is examined using specific conditions to meet practically relevant parameters: ionic polymer coating was applied to a 50-μm (10 mAh/cm^2) thin lithium anode and paired against NMC-622 with 2.0 mAh/cm^2 capacity. The team maintains the electrolyte amount to be ~ 15 μl/mAh. The electrolyte utilized was high performing as reported by the group: 1 M LiTFSI in FDMB. They find that this battery is able to cycle stably for at least 150 cycles (Figure 8a-b). Here, they use a rigorous cycling rate of C/3 charge and C/3 discharge. Clearly, they find that the fluorinated electrolyte based on FDMB and the ionic polymer coating on lithium anode show a synergistic effect, enabling stability. In comparison to previous results involving

Li||NMC full configurations, the cycling results show one of the highest reported improvements in the full-cell configuration. The team believes the polymer design reported in this work can stabilize metal-electrolyte interfaces independent of the electrolyte and cathode chemistries, or even battery geometry. Thus, they provide a facile pathway toward energy-dense, yet stable, Li-metal battery operation.

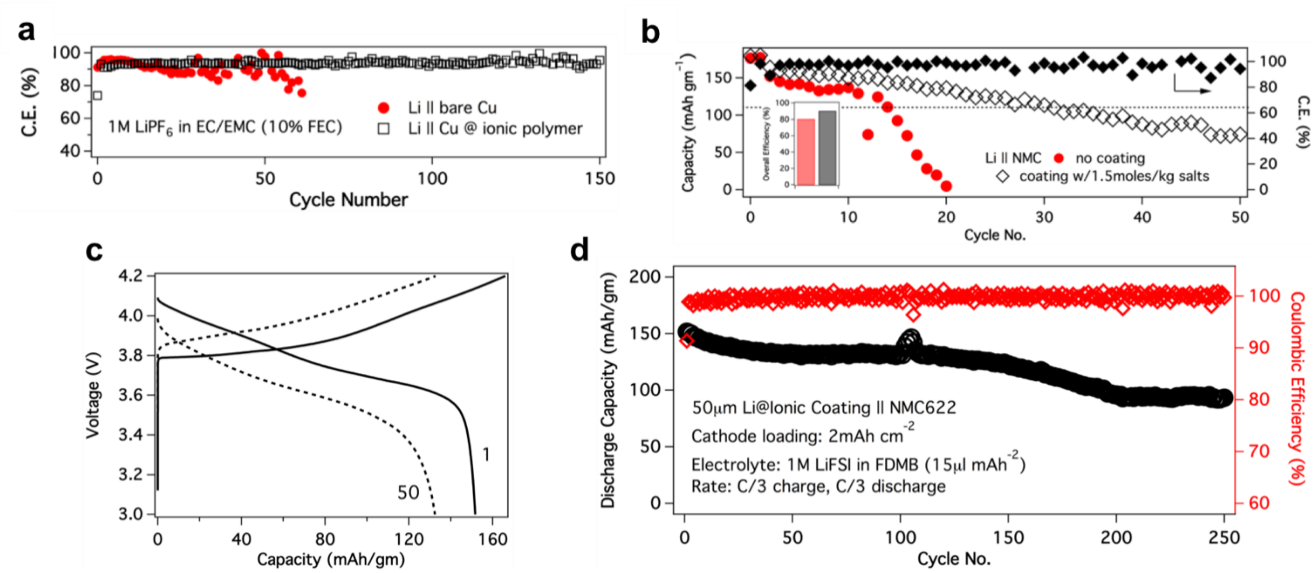

Figure 8. Battery performance. (a) Cycling stability of lithium versus copper cells, where the copper electrodes were either bare or coated with ionic polymers containing 1.5 moles/kg of grafted salts. The bare electrode fails in 50 cycles, while that with coating shows enhanced stability. (b) Li||NMC full cell cycling using 25-µm lithium and 1.7 mAh/cm^2 NMC-532, such that the anode (N) to cathode capacity (P) ratio is 3:1. The lithium metal utilized either bare or coated with the ionic polymer (1.5 moles/kg of salts). The inset shows the comparison of the overall efficiency obtained using the formula: (1–N/ (n × P))100%. The electrolyte in all the subparts was 1 M $LiPF_6$ in EC/EMC with 10% FEC. (c) Voltage profile in a lithium versus NMC-622 cathode for the 1st and 50th cycle. (d) Cycle life of the full cell up to 250 cycles. (c-d) The electrolyte utilized was 1 M LiFSI in FDMB, and the volume was limited to 15 µl/mAh. The lithium utilized was 50-µm thick coated with ~ 1-µm thick layer ionic polymer (1.5 moles/kg of grafted salts). The cathode loading here is 2 mAh/cm^2. The electrolyte utilized was 1 M LiFSI in FDMB, and the volume was limited to 15 µl/mAh.

Patents/Publications/Presentations

Publication

- Yu, Z., Y. Cui, and Z. Bao. "Design Principles of Artificial Solid Electrolyte Interphases for Lithium-Metal Anodes." *Cell Reports Physical Science* 1 (2020): 100119.

Task 1.5 – Improving the Stability of Lithium-Metal Anodes and Inorganic-Organic Solid Electrolytes (Nitash Balsara, Lawrence Berkeley National Laboratory)

Project Objective. The project objective is to establish a new hybrid electrolyte that will be stable against cells with a Li-metal anode.

Project Impact. PEs offer increased stability in lithium batteries in comparison to more widely used LEs. Nanostructured electrolytes containing both soft, ion-conducting domains and rigid, nonconducting domains offer the opportunity to tune both mechanical and electrical properties separately. Such electrolytes are conveniently made by block copolymer self-assembly. Most of the block copolymer electrolytes studied thus far comprise organic polymer chains for both the conducting and rigid domains. The team hopes to synthesize new electrolytes that simulataneously have high transport properties and have greater stability against lithium in comparison to organic diblock copolymers.

Approach. First, the team synthesizes hybrid diblock copolymers by incorporating monomers that contain an inorganic component. Then, electrolytes are prepared by mixing these diblock copolymers with salt. Electrochemical and mechanical characterization of these materials is performed before carrying out cycling X-ray tomography (XRT) experiments. The combination of these approaches enables rational design of materials that exhibit improved stability against lithium metal.

Out-Year Goals. The project will synthesize a new hybrid electrolyte that is designed to be stable against lithium metal. The material is a block copolymer wherein acryloisobutyl POSS is covalently bonded to the chain. The second block is a conventional PE (PEO). Electrochemical characterization of this polymer will include measurement of all transport properties including conductivity, diffusion coefficient, and the transference number. The stability against lithium metal will be evaluated by cyclic voltammetry (CV), while its applications as an electrolyte will be evaluated and visualized using cycling XRT experiments on symmetric Li-hybrid-Li cells.

Collaborations. There are no active collaborations this quarter.

Milestones

1. Synthesize a series of POSS-containing block copolymer electrolytes for electrochemical studies. (Q1, FY 2020; Completed)
2. Create impurity-free lithium layers. (Q2, FY 2020; Completed)
3. Complete electrochemical characterization of POSS-containing block copolymer electrolytes. (Q3, FY 2020; Completed)
4. Provide cycling data for at least two POSS-containing block copolymer electrolytes. (Q4, FY 2020; Completed)

Progress Report

Organic and inorganic-organic block copolymer electrolytes must account for current density effects on lithium dendrite growth when optimizing cell lifetime. One important measurement, thus, is the limiting current of the electrolyte. This measurement can be performed by electrodepositing lithium at different current densities and monitoring the current density at which the measured potential diverges. This quarter, the team conducted cycling and electrochemical characterization using the hybrid organic-inorganic hybrid copolymer POSS-PEO-POSS (chemical structure shown in Figure 9) where the molecular weight of PEO is 35 kg mol^{-1} and POSS is 10 kg mol^{-1}. Three 25-30 µm-thick membranes were fabricated with the salt concentration of [Li]/[EO] = 0.02, 0.04, and 0.06.

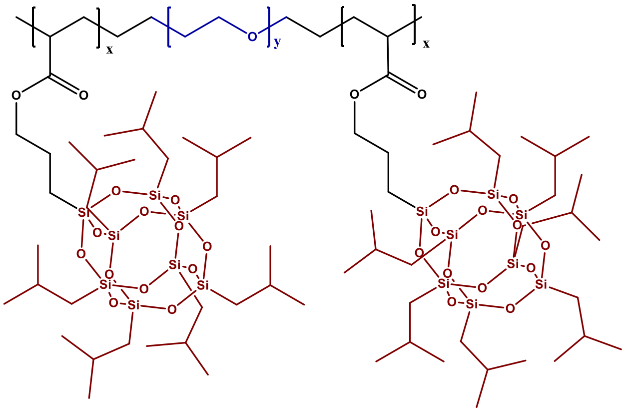

Figure 9. Chemical structure of triblock POSS-PEO-POSS copolymer.

Ionic conductivity using nonblocking electrodes, κ_{nb}, was measured in the three membranes by sandwiching the membrane between lithium electrodes and performing impedance spectroscopy. Temperature was varied from 70-110°C. Figure 10 demonstrates that the ionic conductivity increases with increasing temperature in all electrolytes with a Vogel-Tamman-Fulcher type relationship, as typical with PEs. Additionally, ionic conductivity increases with salt concentration in this salt concentration regime.

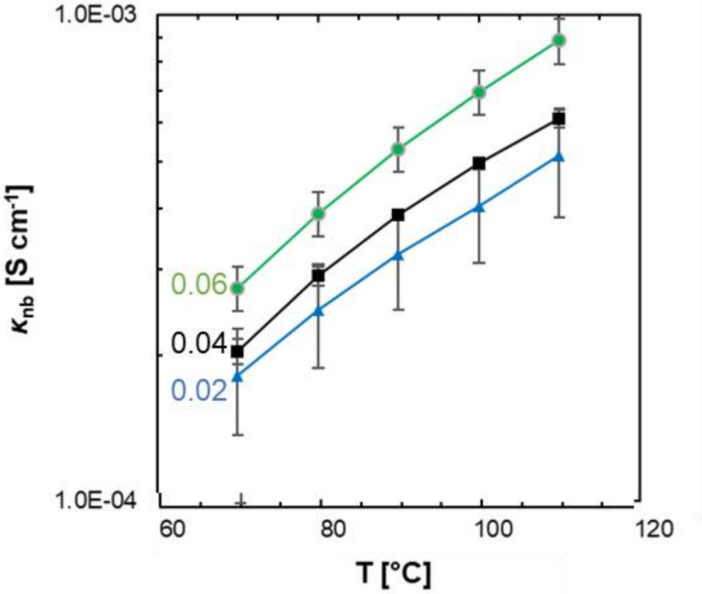

Figure 10. Ionic conductivity, κ_{nb}, as a function of temperature, T, in 3 POSS-PEO-POSS electrolytes at temperatures ranging from 70°C to 110°C.

Limiting current was then measured in POSS-PEO-POSS Li-polymer-Li cells by sandwiching POSS-PEO-POSS membrane between two lithium electrodes and cycling at different current densities. In Figure 11, a routine used to test limiting current measurements is shown. The POSS-PEO-POSS hybrid triblock electrolyte showed an exceptionally high limiting current between 1.8 and 5.7 mA cm^{-2} for a membrane of 25-30 µm thickness, demonstrated in Figure 12.

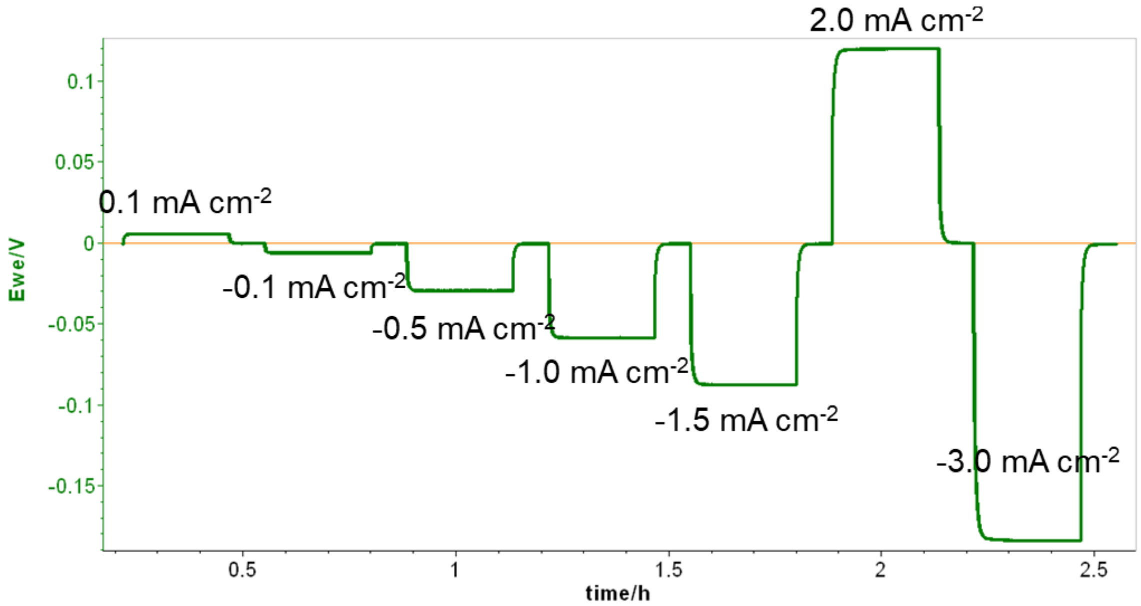

Figure 11. Example of a routine used to test the limiting current of POSS-PEO-POSS (5-35-5) at salt concentration [Li]/[EO] = 0.04. This 30-micron-thick solid hybrid organic-inorganic polymer electrolyte was sandwiched between two lithium electrodes and polarized to electrodeposit lithium from one electrode to the other. The current density was increased systematically until the potential diverged or the cell short-circuited.

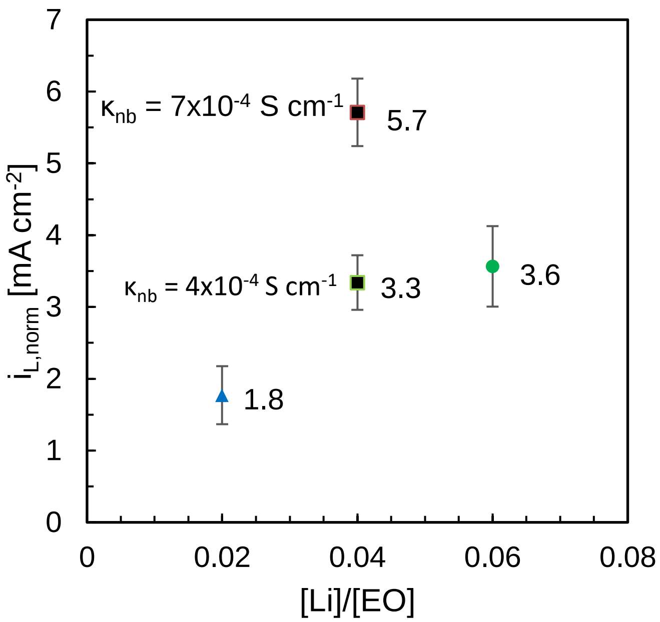

Figure 12. Limiting current ($i_{L,norm}$) measurements in 3 POSS-PEO-POSS electrolytes. Error bars indicate standard deviation from three experiments. All measurements were performed at 90°C. Ionic conductivity measured using non-blocking electrodes (κ_{nb}) is indicated on the left of data points of multiple batches at [Li]/[EO] = 0.04.

To ensure that the lithium interface is stable during limiting current measurements, the interfacial resistance was measured. The interfacial impedance does not change before and after limiting current measurements, as indicated by Figure 13.

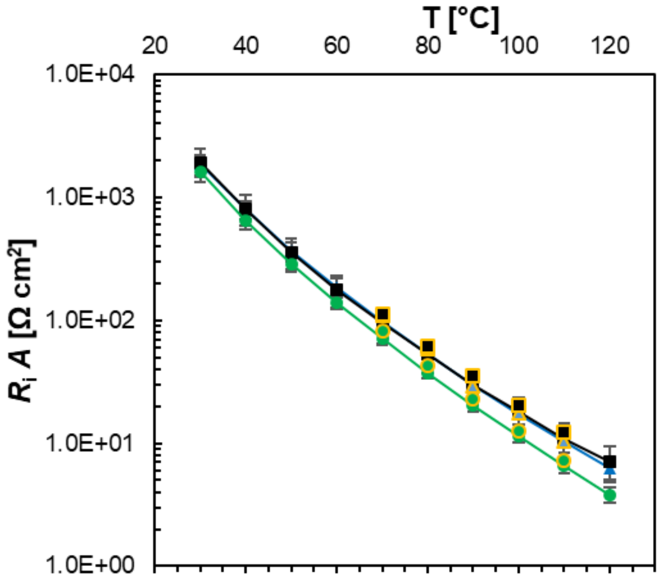

Figure 13. Interfacial resistance multiplied by area (R*iA) measurements in 3 POSS-PEO-POSS electrolytes before and after limiting current measurements, indicating a stable interface during measurements. Error bars indicate standard deviation from three experiments.**

The POSS-PEO-POSS hybrid triblock electrolyte showed an exceptionally high limiting current between 1.8 and 6 mA cm-2 for a membrane of 25-30 µm thicknesses. Additionally, the polymers exhibit stability against lithium metal after cycling experiments. The operating current density is an important factor in the lifetime of lithium symmetric cells with solid PEs.

Patents/Publications/Presentations

Presentation

- ECS, PRiME 2020, Virtual (October 2020): "Predicting Electrolyte Performance in Lithium Metal Batteries at Low and High Current Densities"; M. D. Galluzzo and N. P. Balsara.

Task 1.6 – Development of Thin, Robust, Lithium-Impenetrable, High-Conductivity, Electrochemically Stable, Scalable, and Low-Cost Glassy Solid Electrolytes for Solid-State Lithium Batteries (Steve Martin, Iowa State University of Science and Technology)

Project Objective. The objective of this project is to develop new Li^+-conducting MOSN GSEs that are impermeable to lithium dendrites, have high conductivities, are scalable through low-cost glass manufacturing, are chemically and electrochemically stable, and will enable low-cost, high-energy-density SSLBs. The SSLBs constructed from these new GSEs will meet and exceed all program objectives: usable specific energy @ C/3 ≥ 350 Wh/kg, calendar life 15 years, cycle life (C/3 deep discharge with < 20% energy fade) 1,000, and cost ≤ $100/kWh.

Project Impact. This project will enable the team to demonstrate that (1) thin MOSN GSE films yield superior performance in a much safer, lower-cost, and Li-dendrite impenetrable form and (2) high rate and long cycle life can be achieved in SSLBs using thin-film MOSN GSEs. The new GSEs in SSLBs are anticipated to increase the energy density (anode basis) from ~ 300 mAhr/g to ~ 4,000 mAhr/g, enabling replacement of internal combustion engines in both light and heavy duty vehicles. Each 20% reduction in the ~ 1.6 billion liters of gasoline used per day in the United States would reduce CO_2 emissions by ~ 4 billion kg or 2×10^{12} l of CO_2 per day. The team will also increase scientific and engineering knowledge of thin-film GSEs in SSLBs.

Approach. The MOSN MGF glasses used for the GSEs in this project have been developed in previous work to have the necessary thermal stability and high ionic conductivity for successful use as a drawn-film electrolyte. In this project, the glass chemistry will be tuned for even more desirable properties, by investigating structure-property relationships and testing variations in glass chemistry.

Out-Year Goals. Work will progress toward developing a glass capable of being drawn to 100-micron thickness, while having high conductivity and electrochemical stability and good cycling ability.

Collaborations. There are no active collaborations this quarter.

Milestones

1. Preform redraw capability to form 5-m ribbons verified. (Q1, FY 2020; Completed)
2. Accomplish: MOSN MGF GSEs are thermally stable between -20°C and 100°C, have a Li^+ ion conductivity > 1 mS/cm at 25°C, have a Li^+ ion ASR of ≤ 100 Ohm-cm^2, have an electronic ASR of > 0.1 M Ohm-cm^2, are electrochemically stable between 0 and 4.5 V versus Li/Li^+, and have no more than 1 wt% weight change in 45% relative humidity (RH) air. (Q2, FY 2020; Completed)
3. Accomplish: MOSN MGF GSE are stable against lithium through 100 cycles. (Q3, FY 2020; Completed)
4. *Go/No Go Decision*: MOSN MGF GSE is chemically stable and resistant to crystallization. Analysis indicates technical approach capable of achieving performance targets. (Q4, FY 2020; Completed)

Progress Report

Development of Optimized High Li^+ Ion Conductivity MOSN MGF GSEs

New GSE compositions continue to be developed as the glass properties are optimized for use in a Li-metal battery. Here, the team reports on a new glass composition, ISU-6, Table 1, which exhibits improved glass forming character, an ionic conductivity of 7×10^{-4} S/cm at room temperature, and was found to form a stable interface layer in contact with lithium metal. These improved properties make ISU-6 a viable GSE for scale-up and preform synthesis, which will be reported in future quarters.

Table 1. Tabulated glass chemistry for glassy solid electrolytes testing.

Sample ID	Compositional Formula
ISU 4	$0.55\ Li_2S + 0.35\ SiS_2 + 0.07\ LiPO_3 + 0.03\ LiPO_{2.5}N_{0.33}$
ISU 5	$0.6Li_2S + 0.3\ SiS_2 + 0.1\ LiPO_3$
ISU 6 (new this quarter)	$0.58Li_2S + 0.32\ SiS_2 + 0.1\ LiPO_3$

Thermal Properties. All of the GSEs listed above in Table 1 have achieved Milestone 1.1a and are thermally stable within the described region of -20 to 100°C. As demonstrated in Figure 14, no thermal events occur from -20°C to 100°C. The thermal events above 100°C correspond to the glass transition temperature (T_g) and crystallization temperature (T_C) and are identified with values tabulated in Table 2 below. The team's recent efforts have found that GSEs that possess a working range ($\Delta T = T_C - T_g$) > 100°C are much easier to cast into preforms and draw into films, and for this reason, this criterion is being used to down select to the final composition.

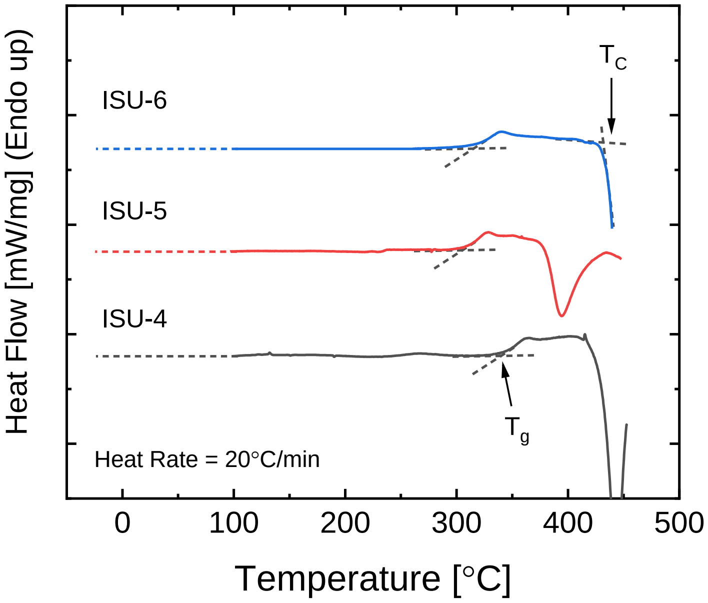

Figure 14. Thermal stability of ISU glasses as shown via differential scanning calorimetry thermograms for selected ISU glassy solid electrolytes (GSEs). All of these GSEs are thermally stable from -20° to 100°C. The newest composition, ISU-6, with the largest working range (see Table 2) was found to form a glass on cooling in bulk pieces.

Table 2. Thermal properties of glassy solid electrolytes.

Sample ID	Thermally Stable (-20°C and 100°C)	Upper Useful Temperature Limit of the Glass (°C)	Working Range $(T_C\text{-}T_g)$ (°C)
ISU 4	Yes	350	70
ISU 5	Yes	305	70
ISU 6	Yes	320	110

Ionic Conductivity > 1 mS/cm at 25°C. The temperature-dependent ionic conductivity of the different ISU GSEs has been measured using impedance spectroscopy (IS). As shown in Figure 15, GSE ISU-6 has a 25°C Li^+ ion conductivity of 0.7 mS/cm ± 0.4 mS/cm. This value is slightly lower than the 1.06 mS/cm reported for the ISU-5 composition last quarter. This slight reduction in the 25°C Li^+ ion conductivity appears to be at the cost of improving the glass forming character and electrochemical stability. The team will continue to optimize this GSE composition to improve all of its thermal, chemical, and electrochemical properties.

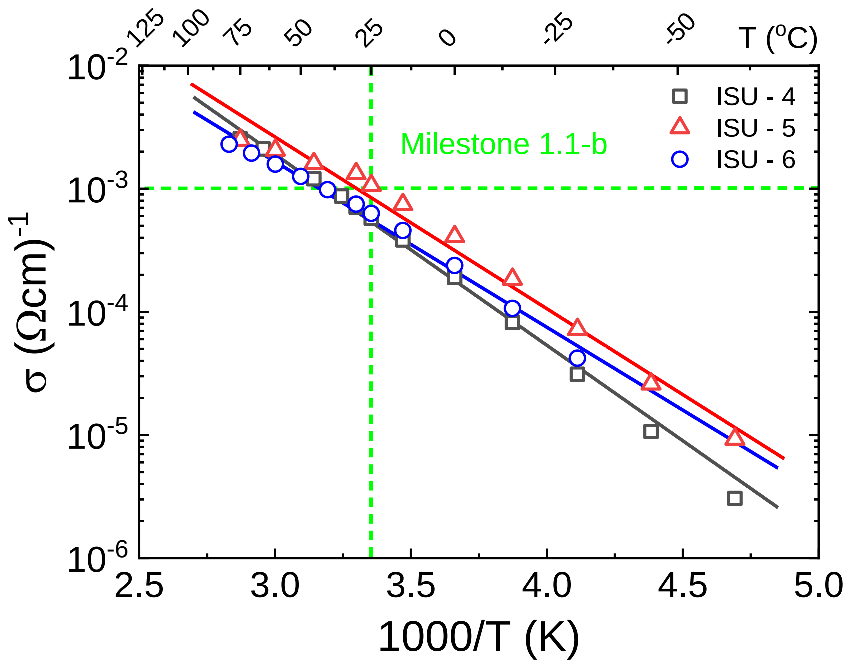

Figure 15. Arrhenius plot comparing the temperature dependence of the ionic conductivity for the three ISU glassy solid electrolytes: ISU-4, ISU-5, and ISU-6. These data show that ISU-5 meets the Milestone 1.1b value of 1 mS/cm at 25°C.

GSE Demonstrates Electronic ASR of > 0.1 M Ohm-cm². The DC polarization technique was used to measure the electronic ASR of the different ISU GSEs. In these experiments, a static, 1V potential was applied across the cell with blocking gold sputtered electrodes, while the responding current was measured as a function of time. The evolution of the electronic ASR as the Li^+ continue to pile up at the interface as a function of time is shown in Figure 16. It was determined that the newest chemistry, ISU-6, demonstrates an electronic ASR of ~ 10 M Ω-cm² after ~ 3 hours of polarization, exceeding the milestone value (0.1 M Ω-cm²**)** by two orders of magnitude.

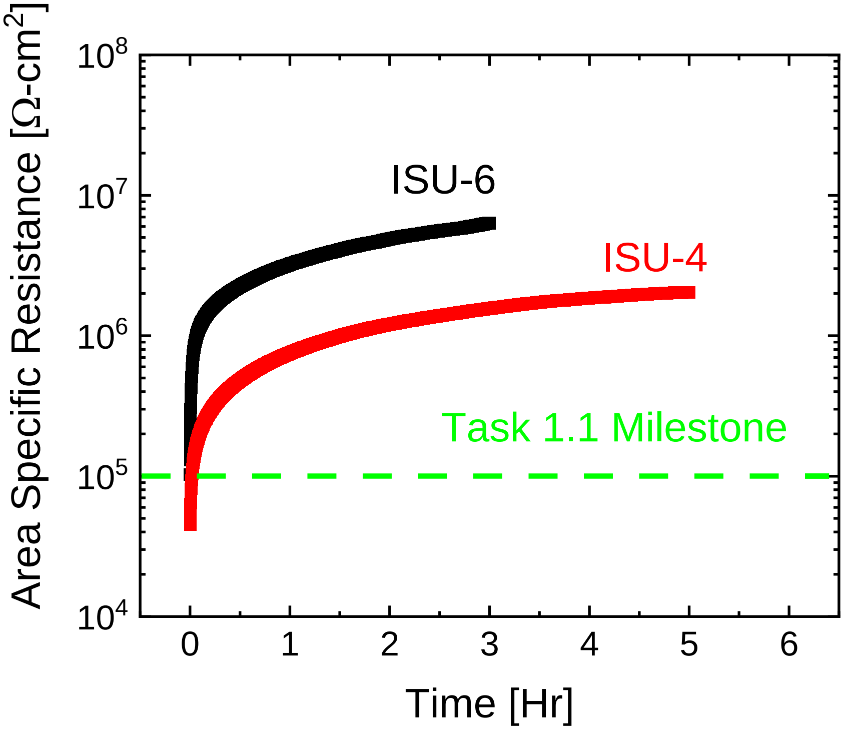

Figure 16. Area specific resistance of ISU-4 and ISU-6 glassy solid electrolytes (GSEs) measured with blocking electrodes using the Static Potential DC polarization technique. Both samples were tested with applied potential of 1 V and measured for 3-5 hours. These data show that ISU-4 and ISU-6 GSEs exceed Milestone 1.1c value of > 0.1 M Ohm-cm^2.

Material Stability

Electrochemically Stable between 0 and 4.5 V versus Li/Li$^+$

The team used CV to test oxidative stability of the ISU-4, ISU-5, and ISU-6 GSE compositions, as shown in Figure 17. The CV experiments were conducted using asymmetric cells, assembled as Li-metal (non-blocking electrode) | GSE | stainless steel (blocking electrode). No major oxidative peaks are present in all three ISU GSE materials. ISU-5 and ISU-6 are found to be more stable than the previous ISU-4 composition due to the consistently lower oxidative currents in the range of 1.5 to 3 V, which the team ascribes to polysulfide -S-S- reduction and oxidation. The lack of major oxidative peaks indicates that these glasses are largely stable in the potential window of 0 to 5 V versus Li/Li$^+$.

The team used IS to determine stability of the GSE in contact with lithium metal, with the ISU-5 composition shown in Figure 18. This composition appears to develop an SEI layer that initially becomes more resistive, but which also quickly stabilizes, as shown in the bulk and interfacial impedances in Figure 18b. This same cell was cycled for 100 cycles at a current density of 0.05 mA/cm^2 and demonstrated good stability, as shown in Figure 18c. When cycled at increasing current densities of 0.1 and 0.2 mA/cm^2, however, cycling behavior was rather poor. It is believed that this may be due to low stack pressure.

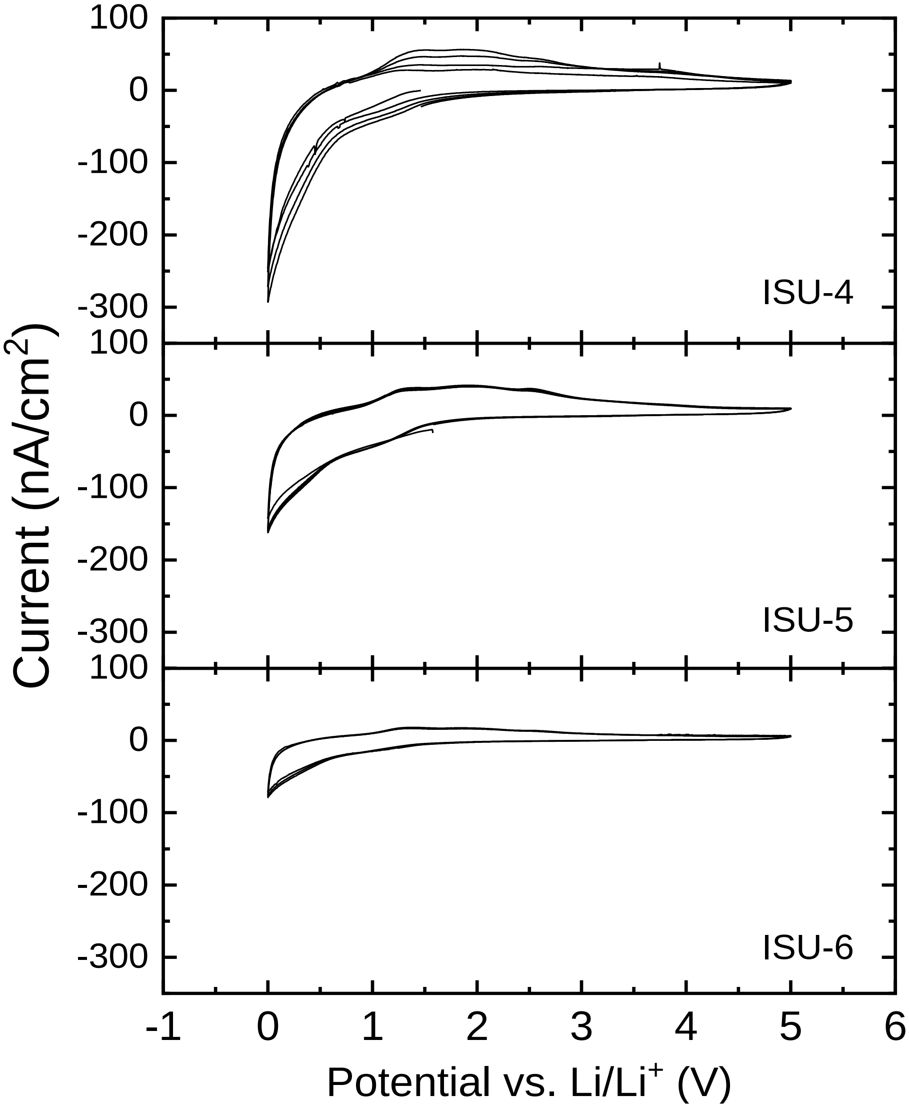

Figure 17. Cyclic voltammograms for the ISU-4, ISU-5, and ISU-6 glassy solid electrolytes (GSEs) over the range from 0 to 5 V. GSE ISU-6 shows little to no reduction/oxidation currents in the range of -S-S- at 1.5 to 2.5 V.

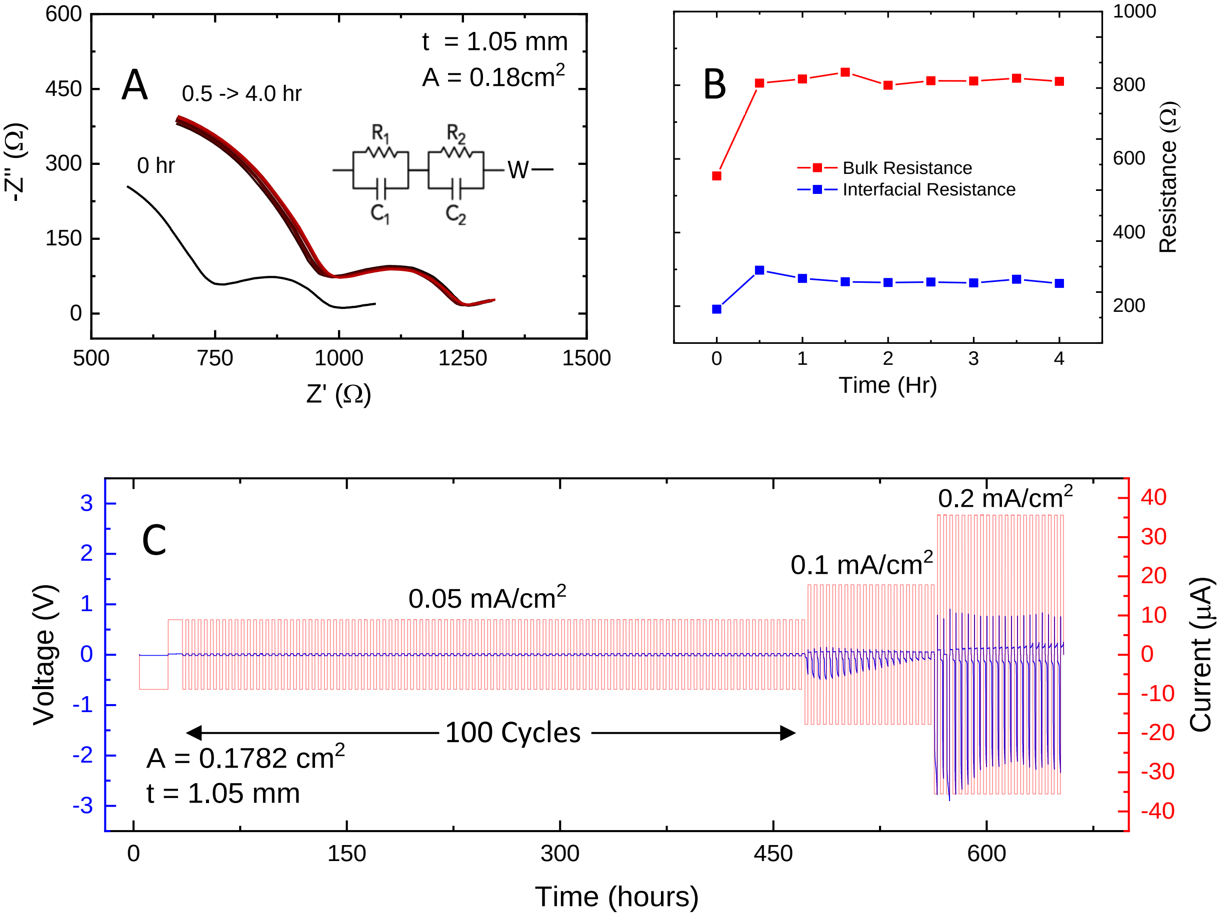

Figure 18. (a) Interfacial and bulk impedances of ISU-5 glassy solid electrolyte in contact with lithium metal tested with electrochemical impedance spectroscopy as a function of time. (b) Time dependent bulk (blue) and interfacial (red) resistances, extracted with a 3-element equivalent circuit model. (c) Low current density symmetric cell cycling data for ISU-5 achieving stable cycling for over 100 cycles.

A new pressure cell was fabricated this quarter and is being used to investigate the effects of stack pressure on symmetric cell performance. Using this new cell, the interfacial resistance of the ISU-5 composition was seen to decrease with time following a nearly logarithmic trend, as seen in Figure 19a-b. These results are in good agreement with recent work published by Wang et al. and indicate that applying pressure along the vertical axis of the cell can decrease the interfacial resistance.[1]

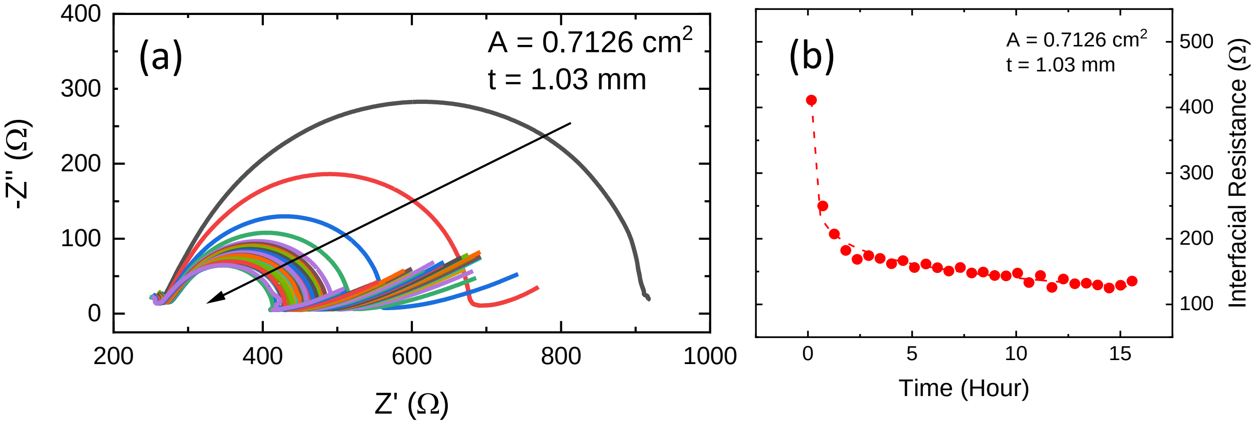

Figure 19. (a) Time-dependent Nyquist plot of ISU-5 composition in contact with lithium metal for 16 hours at ~ 5 Mpa stack pressure at open circuit voltage. Arrow indicates the decrease in the interfacial resistance as a function of time. (b) Interfacial resistance of the symmetric cell extracted using an RC-circuit model, with measurements collected every 30 minutes.

Chemically Stable (No More than 1 wt% Weight Change in 45% RH Air)

Figure 20 shows a TGA thermogram of a typical pure sulfide glass that reacts immediately with humid air, whereas the MOSN GSE ISU-4 and ISU-5 GSEs remain stable for periods of multiple hours in contact with the same humid air. In addition to this, the new MOS GSE (without nitrogen) also shows very promising results, remaining stable for multiple hours in atmospheric conditions. These results indicate that many of the ISU GSEs exhibit the chemical stability required to be handled in a dry room environment for short periods of time with little to no noticeable degradation of the material. This is important for the fabrication of preforms, and even more so for handling GSE thin films.

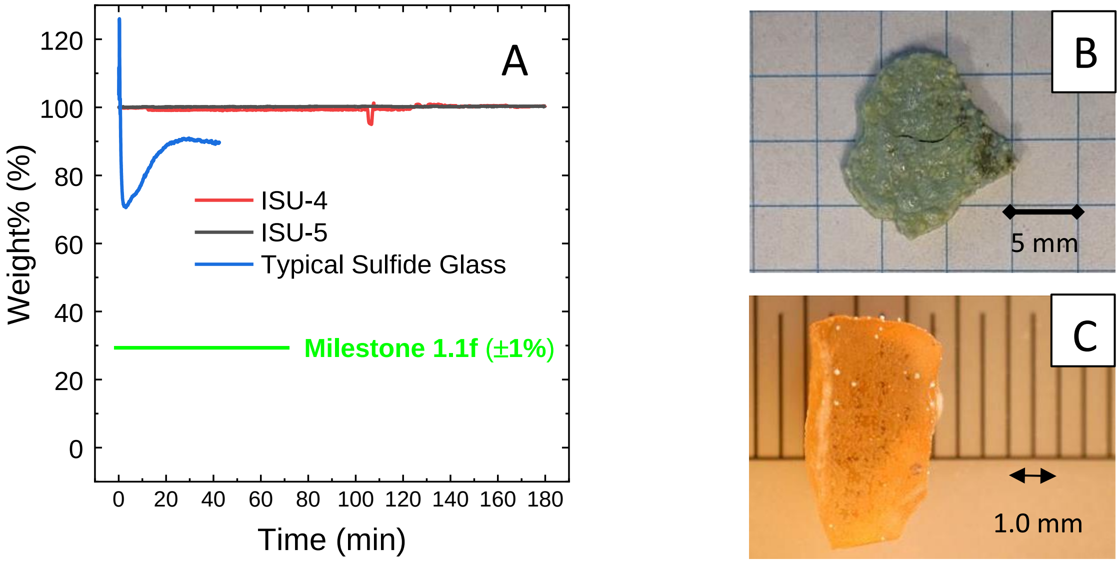

Figure 20. (a) Thermogravimetric analysis results for a typical sulfide glass, which reacts violently with air, compared to the ISU-4 and ISU-5 compositions that do not react at, or react very little with, air. Both the mixed oxy-sulfide (MOS) and mixed oxy-sulfide nitride (MOSN) were found to be stable under standard atmospheric conditions. (b) Photograph of a typical sulfide glass after exposure to atmosphere for an hour. (c) Optical micrograph of a MOS glass exposed to atmosphere for 3 hours. The MOS glass (c) only formed a minimal oxide scale in specific points, whereas the typical pure sulfide GSE fully reacts with air (b) .

Development of Micro-Sheet Glass Ribbon Processing Facility

This quarter, use of the vertical furnace for large-scale melting of MOSN MGF GSEs was optimized, allowing for melts up to 1 kg in mass to be processed. Once melted, the glass must be annealed following a prescribed thermal cycle. Two heated and temperature-controlled 6" x 12" brass plates were used when annealing MOSN MGF GSE preforms for ribbon drawing. The top and bottom plates were independently controlled, with four cartridge heaters allowing for uniform heat distribution. The annealing plates were capable of meeting all parameters of the prescribed thermal cycle with a preform up to ~ 300 g in mass. Developing and testing these capabilities will allow for scale-up in processing of MOSN MGF GSE preforms for drawing of thin film.

Develop Processing Conditions Micro-Sheet Ribbons of MOSN MGF GSEs

This quarter, lithium metaphosphate ($LiPO_3$) was used instead of a borosilicate glass, as the phosphate glass more closely reflects the thermal properties of MOSN glasses. Preforms of $LiPO_3$ were used to continue optimization of thin film fabrication with a specific focus on the initial draw-down conditions prior to the continuous drawing stage. It has been determined that the success of the entire film drawing process is highly dependent on the first steps of the process, and without a proper setup the film drawing will not achieve the appropriate aspect ratio needed for this application. Some of the important aspects include, but are not limited to, the bulk temperature of the glass preform, the viscoelastic liquid dynamics of the glass above the T_g, and the preform feed rate. Through careful optimization of these parameters, many meters of $LiPO_3$ films of were drawn with widths greater than 4 cm and thicknesses reaching between 100-400 µm. These values have met or exceeded all milestones prescribed in Task 3. Future work will report on new work fabricating thin-film, fast-ion conducting, Li^+ MOS GSEs.

Reference

[1] Wang, M. J., R. Choudhury, and J. Sakamoto. "Characterizing the Li-Solid-Electrolyte Interface Dynamics as a Function of Stack Pressure and Current Density." *Joule* 3 (2019): 2165–2178.

Patents/Publications/Presentations

Publications

- Kmiec, S., J Lovi, A. Joyce, D. Bayko, and S. W. Martin. "Anomalously Strong Viscosity Behavior in Mixed Oxy-Sulfide $Na_4P_2S_7O_x$ Invert Glasses." *Journal of Non-Crystalline Solids*. Manuscript number NOC-D-20-00706; Submitted May 18, 2020.
- Joyce, A., S. Kmiec, and S. W. Martin. "Glass Transition Temperature Studies of Planetary Ball Milled $Na_4P_2S_{7-x}O_x$, $0 \leq x \leq 7$, Oxy-Thio Phosphate Glasses." *Journal of Non-Crystalline Solids*. Manuscript number NOC-D-20-00826; Submitted June 11, 2020.
- Zhao, R., G. Hu, S. Kmiec, R. Gebhardt, A. Whale, and S. W. Martin. "A New Amorphous Oxy-Sulfide Solid Electrolyte Material: Anion Exchange, Electrochemical Properties, and Lithium Dendrite Suppression via *In Situ* Interfacial Modification." *American Chemical Society (ACS) Applied Materials and Interfaces*. Accepted; Manuscript number am-2020-09420a.
- Kim, K-H., and S. W. Martin. "A Study on the Improved Structure and Properties of Cation and Anion Double Doped $Li_{10}[Sn_ySi_{1-y}]P_2S_{12-x}O_x$ Solid Electrolytes." *Chemistry of Materials*. Submitted June 15, 2020. Under revision.
- Lazar, M., S. Kmiec, A. Joyce, and S. W. Martin. "Investigations into Reaction between Sodium and Solid-State Sodium Electrolytes." *ACS Applied Energy Materials*. Submitted April 21, 2020. Under revision.

Task 1.7 – Composite Solid Ion Conductor with Engineered Lithium Interface
(Kyler Carroll and Cam Peebles, Wildcat Discovery Technologies)

Project Objective. In this project, Wildcat seeks to perform focused, fundamental research and development on composite polymer/ceramic electrolytes and for the protection of Li-metal anodes to develop an all-solid-state Li-metal battery that achieves DOE requirements for performance that enables potential commercialization of this technology. Wildcat will leverage its HT battery platform to explore a broad composite electrolyte compositional space. Additionally, the HT platform will allow the team to screen hundreds of inorganic and organic coatings for Li-metal protection and translate the best results to all solid cells.

Project Impact. Successful widespread commercialization of EVs is contingent on developing safe high-energy-density batteries capable of long cycle life. Lithium metal affords the highest theoretical capacity (3,860 mAh/g) and lowest electrochemical potential (-3.04 V versus SHE), which offers the highest specific energy density of anode materials today. However, significant progress toward the passivation of lithium metal must occur before the energy density benefit can be realized. The intrinsic high reactivity between lithium metal with conventional Li-ion electrolytes (organic carbonate-based solvents) makes it extremely difficult to overcome these problems. The proposed composite polymer/ceramic electrolyte and a protected Li-metal anode will enable an all-solid-state Li-metal battery. It is expected that the outcomes from this effort will deliver a safe all-solid-state Li-metal pouch cell with over 350 Wh/kg and over 1,000 cycles (C/3) with the cost estimate below $100/kWh.

Approach. The project approach involves (1) identifying a suitable combination of solid ion conductor, polymer, and additive that minimizes overall interfacial impedance between the PE and solid ion conductor, and (2) identifying stable Li-metal protection agent or combination of agents that shows enhanced cycling performance (relative to a non-protected system) using the down-selected cell architectures.

Out-Year Goals. The out-year goals involve screening hundreds of additive, polymer, and solid ion conductor combinations using a HT trilayer cell architecture developed during method development phase. Based on the best combinations, Wildcat will develop a composite polymer/ceramic electrolyte where the Li-ion conductivity is occurring at the ceramic phases of the composite. Additionally, the team will screen hundreds of Li-metal protection agents using the designed HT cell architecture with the goal of identifying those that offer highest stability.

Collaborations. All project tasks will be performed at Wildcat Discovery Technologies.

Milestones

1. Establish baseline performance. (Q1, FY 2020; Completed)
2. Complete synthesis of ceramic ion conductors. (Q2, FY 2020; Completed)
3. Perform down-selection of best ceramic ion conductors for further optimization. (Q3, FY 2020; Completed)
4. Perform down-selection of best composite SE additives for further optimization. (Q4, FY 2020; Completed)
5. Perform down-selection of best high-voltage polymer formulations for further optimization. (Q4, FY 2020; Completed)
6. Lithium-ion conductivity is occurring at the ceramic phase of the composite. Technical progress is acceptable by measurements of ionic conductivity, shear modulus, and film thickness measurements. Analysis of technical results indicates that performance targets are achievable. (Q4, FY 2020; Completed)

Progress Report

This quarter, Wildcat utilized its HT platform to develop a composite polymer ceramic film utilizing the coupling agent that lowers the interfacial impedance developed last quarter. Several parameters were optimized to improve film quality including densifying the films by calendering, the addition processes for making the films, drying temperatures and times, as well as the total amount of ceramic in the composite films. Additionally, Wildcat made progress on the Li-metal portion of the project by beginning to investigate the Li-metal-SSE interface. Using Li/Li symmetric cells, the interface between lithium metal and polymer composite or protected lithium metal and polymer composite was explored. These tests are in progress.

Preparation of Composite Electrolyte

Significant effort was made to design a high ceramic loading composite film. To focus on improving film quality, a non-functionalized LATP ceramic was used with a PEO polymer and lithium salt. Initial tests were aimed to understand the role the solvent had on the film quality as well as the ionic conductivity of the composite films. Figure 21 shows the quality of four films with different co-solvents and the corresponding ionic conductivity. The % ceramic in these composites was set to 60 wt%. It can be seen from the ionic conductivity that the co-solvents directly affect the resulting performance of the films. The trend shows that lowering the boiling point of the co-solvent improves the overall ionic conductivity of the composite film.

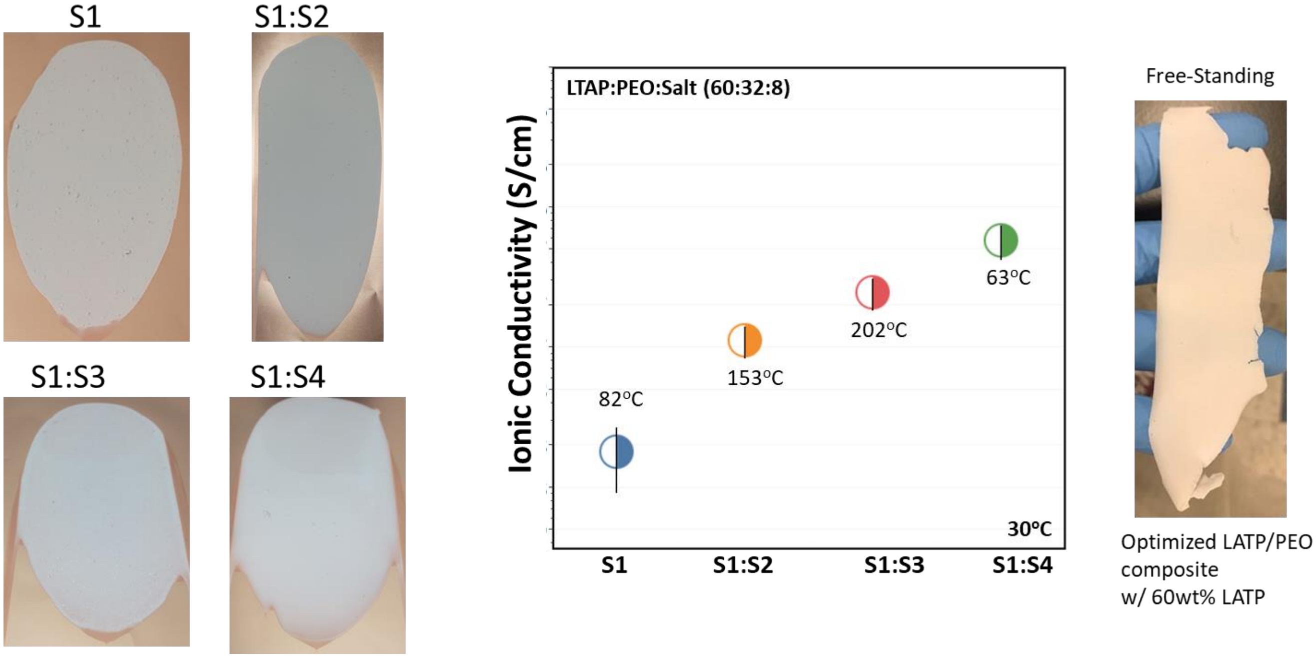

Figure 21. Film quality images of various co-solvents for the composite film and the resulting Ionic conductivity.

To further improve film quality as well as improve ionic conductivity of the composite films, the team investigated the effects of calendering on performance. Figure 22 shows the ionic conductivity of three separate films and shows that by adjusting calendering parameters, the team can improve ionic conductivity of the film.

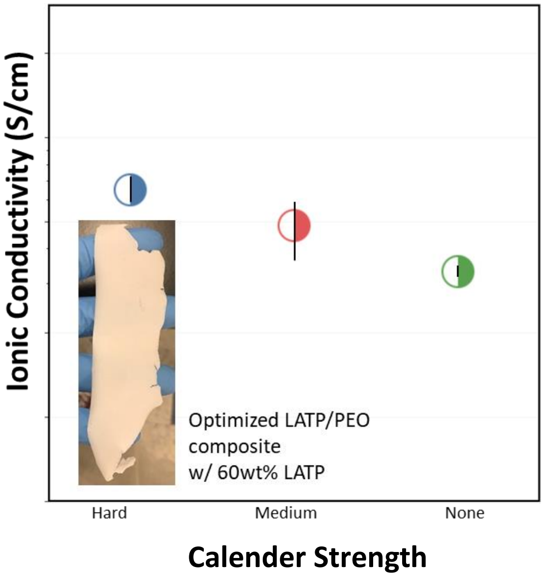

Figure 22. Ionic conductivity values for calendered versus non-calendered PEO composite films with 60 wt% LATP ceramic. The results show the effect of calendering on the ionic conductivity of the films.

Protected Li-Metal Additive Testing

Previous work in the Li-metal additive portion of the project looked at screening Li-metal protection materials in Li/Li symmetric cells using LE. The aim this quarter was to transition to using SSE to begin screening Li-metal protection agents that showed good promise in LE. To this end, Wildcat began testing interfacial resistance (using EIS) in Li/Li symmetric cells using the above-mentioned SSE films. As shown in Figure 23, these interfaces are complex and require careful consideration.

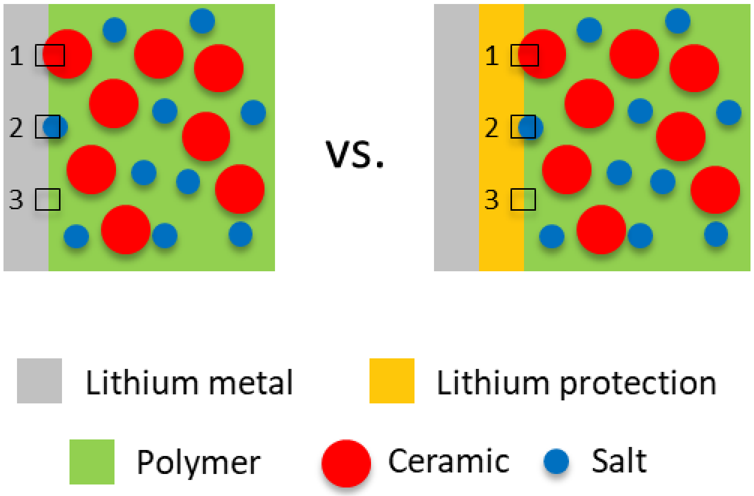

Figure 23. Schematic showing the possible material interactions at the lithium-solid-state electrolyte electrode interface for a non-treated system (left) and a protected Li-metal system (right). The boxed areas show different types of material interfaces.

One of the primary goals was to see how polymer films and ceramics age when in contact with lithium metal. Figure 24 shows the resistance growth between various Li-metal surfaces with a polymer SSE. In Figure 24a, resistance growth between non-protected lithium metal and the SSE is evident, and the overall resistance grows by ~ 250% over 20 days. A poor Li-metal treatment (Figure 24b) leads to high initial (Day 0) resistance as well as dramatic resistance growth over time. Changing the Li-metal protection material (Figure 24c) can lead to low initial resistances (lower than even the bare lithium/SSE system); however, resistance growth is still observed. The team is discovering more Li-metal protection materials similar to that shown in Figure 24d (suppressed resistance growth); they are also working toward lowering initial resistance values.

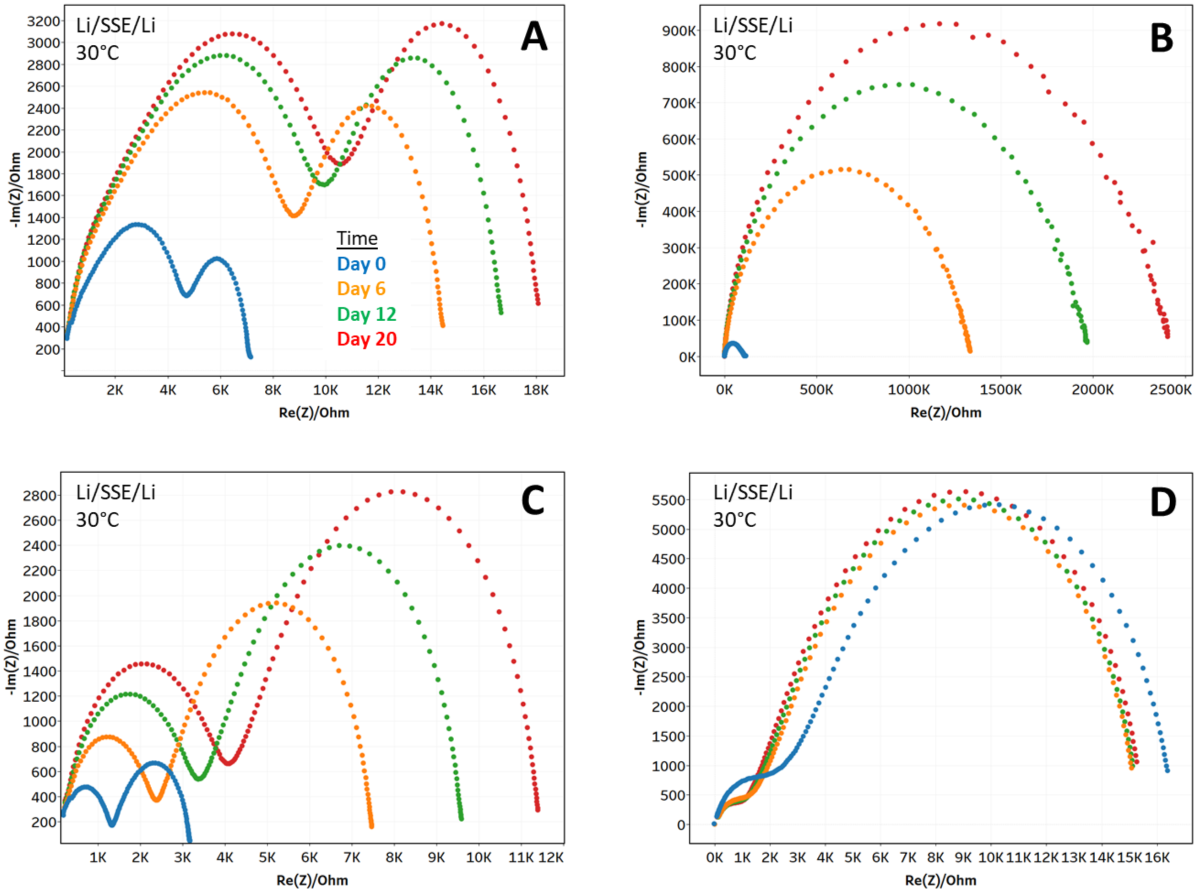

Figure 24. Nyquist plots showing changes to Li/SSE/Li cell resistance after various aging times with and without Li-metal protection. (a) Baseline system (bare lithium, no protection); (b) ASEI_186; (c) ASEI_348; and (d) ASEI_350.

Patents/Publications/Presentations

The project has no patents, publications, or presentations to report this quarter.

Task 1.8 – Physical and Mechano-Electrochemical Phenomena of Thin-Film Lithium-Ceramic Electrolyte Constructs
(Jeff Sakamoto, University of Michigan)

Project Objective. While a small number of SEs exhibit high ionic conductivity (~ 1 mS cm at 298 K), few are stable against lithium metal. The garnet-type SE, based on the nominal formula LLZO, is unique in that it is a fast ion conductor and—as demonstrated in the team's recent project (DE-EE-00006821)—is stable against lithium. Moreover, the team's former project successfully demonstrated a decrease in Li-LLZO interface resistance from 12,000 to 2 Ohms cm^2 and stable cycling at 1 mA cm^2 for 100 cycles (± 15 µm of lithium per cycle). Although the past project demonstrated that LLZO is a viable SE for enabling batteries using metallic lithium, the studies used thick pellets (1 mm) and thick anodes (~ 500 µm). The goal of this project is to acquire a deep fundamental understanding of the physical and mechano-electrochemical phenomena that control the performance of cells consisting of thin LLZO (~ 10 µm), thin lithium anodes (~ 20 µm), and thin solid-state composite cathodes.

Project Impact. If successful, the project will gain knowledge to guide closely related commercialization efforts to scale the production of LLZO-based SSBs.

Approach. The team believes that to achieve a step increase in technology readiness level (TRL), the same performance characteristics previously shown should be demonstrated in technologically relevant cells, for example, thin LLZO and thin lithium.

Out-Year Goals. The out-year goals involve the following: custom TFC development, preliminary cycling studies, Vis cell development, lithium cycling, and polymer gel electrolyte screening.

Collaborations. This project collaborates with Professors N. Dasgupta and D. Siegel of UM, Mechanical Engineering.

Milestones

1. Thin film LLZO integration. (Q1-Q2, FY 2020; Completed / Q4, FY 2020; In progress)
2. Long-term cycling stability. (Q2, FY 2020; Completed / Q4, FY 2020; In progress)
3. Mechanics of the Li-LLZO interface. (Q3, FY 2020; In progress)
4. Stability and kinetics of the LLZO-electrolyte interface. (Q4, FY 2020; In progress)

Progress Report

Thin Film LLZO Integration

Go/No-Go Decision: If Milestone 1.2 is met, continue to deliver TFCs to Tasks 2 to 4. If not demonstrated, consider alternative cell designs: Result: *Go*.

TFCs were successfully fabricated, optimized, and delivered. The TFCs met the quality assurance criteria for conductivity, surface chemistry, phase purity, and thickness. The TFCs were delivered for *in situ* cycling tests and to study the CCD stripping and CCD plating. Based on successful delivery, the result of the *Go/No-Go Decision* is *Go*.

Stability and Kinetics of the LLZO-Electrolyte Interface

To study the behavior of TFC during cycling, cathode technology was developed. Previously, it was determined that state-of-the-art electrolytes react with the TFC to form SEI, which increases the cell resistance with time. To eliminate the SEI reaction, a new cathode technology was developed and implemented to enable preliminary cycling studies of TFC.

Patents/Publications/Presentations

The project has no patents, publications, or presentations to report this quarter.

Task 1.9 – Lithium Dendrite-Free Li_7N_2I-LiOH Solid Electrolytes for High-Energy Lithium Batteries (Chunsheng Wang, University of Maryland)

Project Objective. The objective of this project is to research, develop, and test Li-metal-based batteries that implement solid Li-ion conductors (LICs) equipped with Li_7N_2I-LiOH SE capable of achieving cell performance of 350 Wh/Kg energy density for 1000 cycle life with a cost of ≤ $100/kWh.

Project Impact. Lithium dendrite growth during charge/discharge cycles limits the use of all-solid-state batteries (ASSBs). A criterion for lithium dendrite suppression that is developed through systematical investigation on thermodynamics and kinetics of lithium dendrite growth will guide the electrolyte design. Li_7N_2I-LiOH and Li_3YCl_6 SE with high ionic conductivity and low electronic conductivity will be used to validate the criterion for lithium dendrite suppression, to achieve the project objective.

Approach. The team will establish the relationship among interface energy, lithium plating/stripping overpotential, interface resistance, SE stability with lithium, and CCD. The dendrite suppression criterion will be developed based on the relationship. The dendrite suppression capability for the Li_7N_2I-LiOH pellet will be evaluated by testing the CCD.

Out-Year Goals. In year one, the project will synthesize, modify, and optimize the Li_7N_2I-LiOH and Li_3YCl_6 electrolytes, and Li_7N_2I-LiOH/Li_3YCl_6 bi-layered electrolytes to achieve a high ionic conductivity to $> 5 \times 10^{-4}$ S/cm CCD of > 3.0 mA/cm^2 at a capacity of > 3.0 mAh/cm^2. The team will focus on enhancing the CE for lithium anode to > 99%. The CE of the SE is a powerful indicator of electrolyte stability and lithium dendrite growth.

Collaborations. There are no reported collaborations this quarter.

Milestones

1. Synthesis of Li_7N_2I-LiOH and Li_3YCl_6 electrolytes with high ionic conductivity. (Q1, FY 2020; Completed, December 31, 2019)
2. Electrochemical property of Li_7N_2I-LiOH and Li_7N_2I-LiOH/Li_3YCl_6 bi-layer film. (Q2, FY 2020; Completed)
3. Lithium dendrite suppression capability. (Q3, FY 2020; In progress)
4. High CE for lithium plating/stripping. (Q4, FY 2020)

Progress Report

Synthesis, Characterization, and Optimization of Li_5NI_2-LiOH SSEa

Li_5NI_2-LiOH was prepared using a solid-state reaction. Commercial Li_3N (99.9%, Sigma Aldrich), LiI (99.9%, Sigma Aldrich) and dehydrated LiOH (99.9%, Sigma Aldrich) were mixed according to the molar ratio. The mixture was ball-milled under an argon atmosphere with zirconia balls in a zirconia vial. The collected powder samples were pressed into pellets under isostatic pressure, and then sealed and reacted in a silica tube under the argon atmosphere. The resulting pellet shows a light-yellow color (Figure 25a). As shown in Figure 25c, the XRD pattern of the Li_5NI_2-LiOH powder shows the cubic Li_5NI_2 crystal. A small amount of $H_4Li_2O_4I_{12}$ phase is also detected, which is probably due to contamination of water from the air during the XRD test.

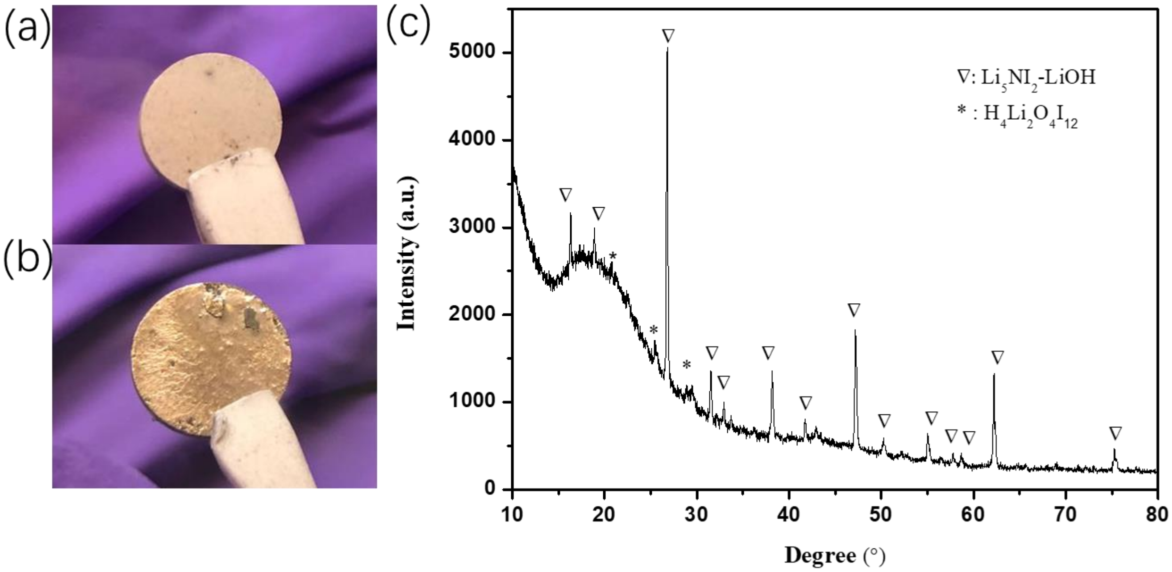

Figure 25. Digital picture of (a) Li_5NI_2-LiOH pellet and (b) Li|Li_5NI_2-LiOH|Li cell. (c) X-ray diffraction pattern of Li_5NI_2-LiOH solid-state electrolyte.

To enhance the ionic conductivity of Li_5NI_2-LiOH SSE, Li_5NI_2-xLiOH electrolytes with different amounts of LiOH were prepared and evaluated. The ionic conductivity of Li_5NI_2-xLiOH electrolytes was measured using Li|Li_5NI_2-xLiOH|Li cells that were prepared by careful painting of molten lithium for 30 minutes in the glovebox (Figure 25b). Figure 26a shows the IS of Li|Li_5NI_2-xLiOH|Li cells. As shown, the semi-circle at high frequency region in IS shrank dramatically with the increase of LiOH addition amount. Therefore, the bulk ionic conductivities (including grain boundary, or GB) of Li_5NI_2 SSEs are increased by LiOH doping. The ionic conductivity of Li_5NI_2-LiOH electrolyte at room temperature is 8×10^{-4} S cm^{-1}. The minor impurities, observed from the XRD pattern, may have an adverse effect on the ionic conductivity. Therefore, higher ionic conductivity is probably reachable with further optimization of preparation conditions.

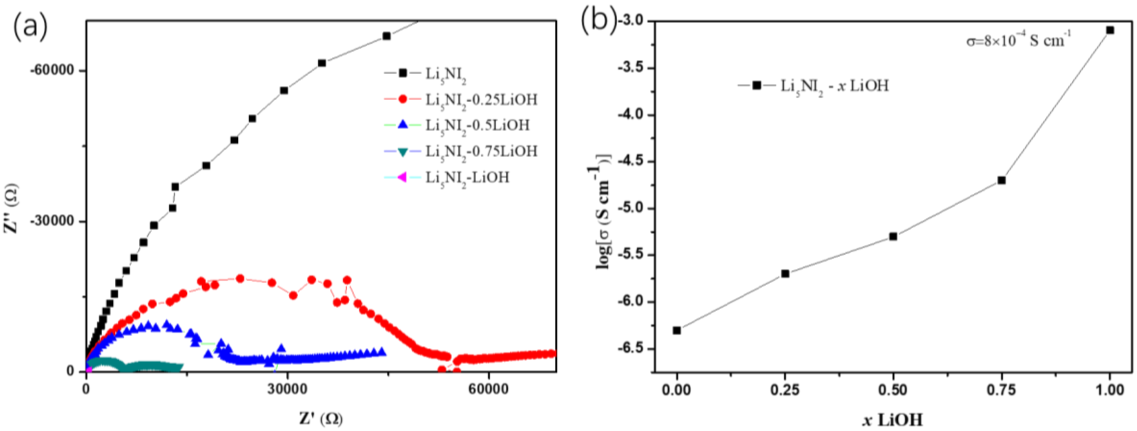

Figure 26. (a) Electrochemical impedance spectroscopies and (b) bulk ionic conductivity of Li|Li$_5$NI$_2$-*x* LiOH|Li cells.

Electrochemical Properties of Li|Li$_5$NI$_2$-LiOH|Li Symmetry Cell

The team planned to investigate the Li$_7$N$_2$I-LiOH electrolyte when they submitted the proposal. However, it was reported that Li$_5$NI$_2$-LiOH electrolytes have a higher ionic conductivity than that of Li$_7$N$_2$I-LiOH electrolytes. This quarter, the electrochemical performance of Li$_5$NI$_2$-LiOH electrolytes was compared with that of Li$_7$N$_2$I-LiOH electrolytes. Li|Li$_7$N$_2$I-LiOH|Li cell was assembled by attaching molten lithium on both sides of the SE pellet. The EIS of both Li$_5$NI$_2$-LiOH and Li$_7$N$_2$I-LiOH at room temperature in the frequency range of 0.01-1×10^6 Hz is shown in Figure 27.

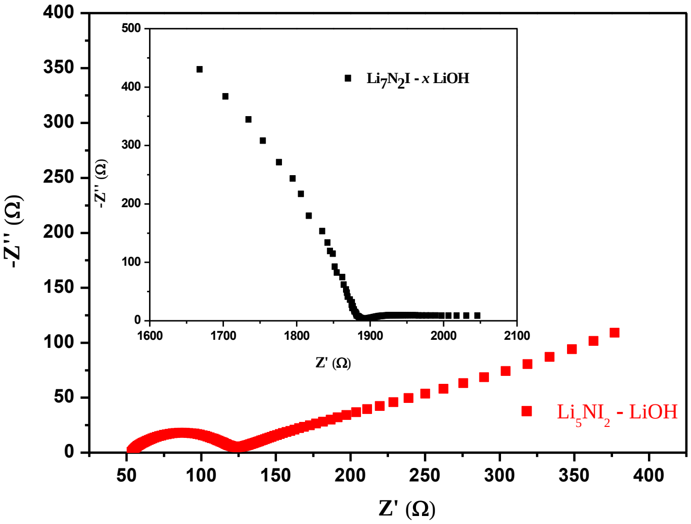

Figure 27. Electrochemical impedance spectroscopy of Li|Li$_5$NI$_2$-LiOH|Li cells and Li|Li$_7$N$_2$I-LiOH|Li cell (inserted).

The EIS plot consists of a small semicircle in the high frequency region, followed by a long slope line in the low frequency region. The large semicircle at high frequency could be assigned to the bulk and GB resistance in the electrolyte, which is estimated to be ~ 125 Ω cm^2. The ionic conductivity of Li$_5$NI$_2$-LiOH is 10 times higher than that of Li$_7$N$_2$I-LiOH. The semicircle in the low frequency region was contributed to ion diffusion. The high interfacial resistance due to ion diffusion dominates the overall resistance, which can be further reduced by optimization of surface modification.

To determine the CCD of Li$_5$NI$_2$-LiOH, a Li|Li$_5$NI$_2$-LiOH|Li symmetric cell was fabricated with a pressure of 5 MPa. A carbon-based intermediate layer was used to assist smooth lithium plating. As shown in Figure 28a, the Li|Li$_5$NI$_2$-LiOH|Li symmetric cell was cycled under step-increasing current densities. Since the Li$_5$NI$_2$-LiOH is thermodynamically stable with lithium metal and has high interface energy against lithium, a common activation process of a physical increase of contact area was observed with lithium plating/stripping cycles. For the first 10 cycles, the overpotential gradually decreases from ~ 0.2 V to 0.1 V, although the currents of lithium plating/stripping increased because the soft lithium metal gradually crawls into the voids of the Li_5NI_2-LiOH SSE without the formation of lithium dendrite due to the high interface energy at the electrolyte/Li interface. This is the merit of thermodynamic stable SE with a high interface energy against lithium that can withstand a high capacity by penetration into the void without forming dendrite. After the “lithium-crawling” gets to its stable state, a stable cycling performance with a high current density of 2.0 mA cm^{-2} and a high capacity of 2.0 mAh cm^{-2} is achieved, which is the milestone for this quarter. Figure 28b shows the EIS of $Li|Li_5NI_2$-$LiOH|Li$ symmetric cell before cycling. At a high-frequency region, two semicircles overlap and can be assigned to electrolyte resistance, and surface resistance, respectively. The total resistance is ~ 205 Ω. After 46 hours of cycling where the current and capacity reached to 2.0 mA cm^{-2} and 2.0 mAh cm^{-2}, respectively, the team measured the EIS of the $Li|Li_5NI_2$-$LiOH|Li$ cell again. As shown in Figure 28b, resistance reduced to 23.4 Ω due to lithium penetration into the pores of Li_5NI_2-LiOH electrolytes. However, the impedance of cycled $Li|Li_5NI_2$-$LiOH|Li$ cell in Figure 28c clearly demonstrates no short circuit, as evidenced by the high-frequency semicircle. After EIS measurement, the $Li|Li_5NI_2$-$LiOH|Li$ symmetric cell is still stably cycling at 2 mA cm^{-2} / 2 mAh cm^{-2}. The team can anticipate longer cycling with this cell.

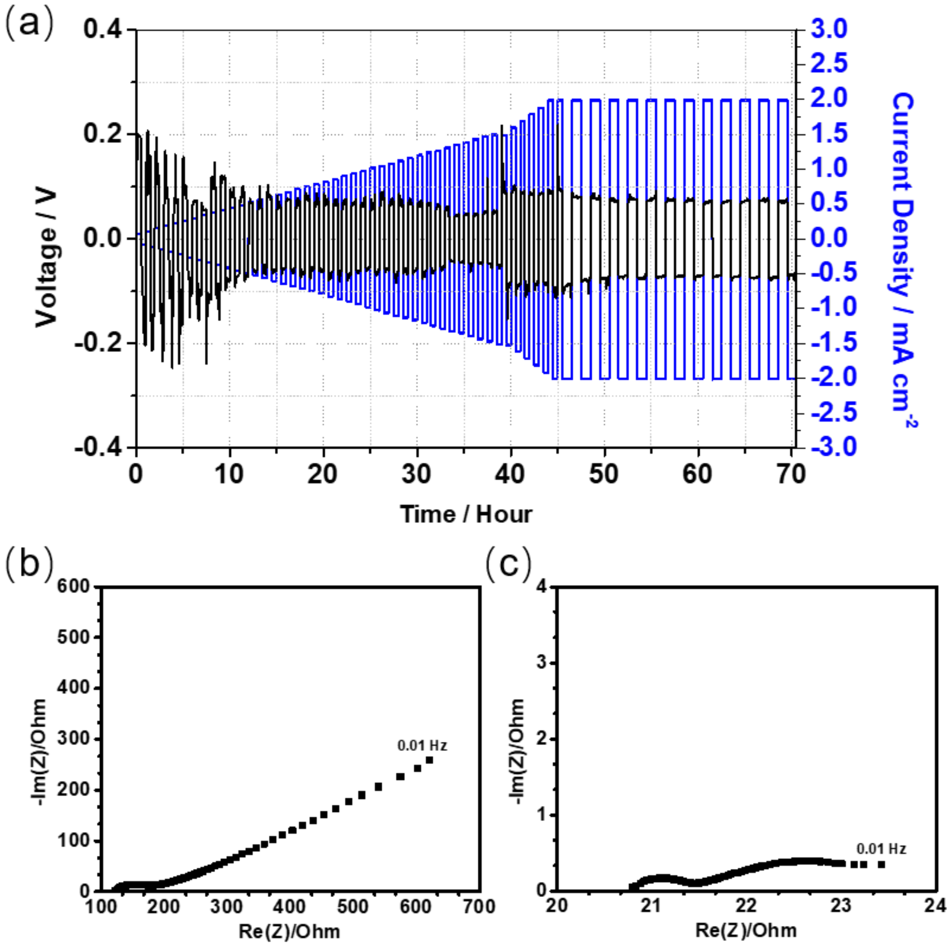

Figure 28. Electrochemical performance of $Li|Li_5NI_2$-$LiOH|Li$ symmetric cell using a carbon-based intermediate layer. (a) Cycle performance of the cell tested at room temperature with 1 hour per cycle for 45 cycles at increasing current densities and 2 hours per cycle afterward at 2 mA cm^{-2}. (b) Impedance spectroscopy (from 106 Hz to 0.01 Hz) of the cell tested at room temperature before cycling. (c) Impedance spectroscopy (from 106 Hz to 0.01 Hz) of the cell tested at room temperature before changing to 2 hours per cycle.

Electrochemical Properties of Li| $Li_{10}N_3I$-LiOH-PTFE |Li Symmetry Thin Film Cell

$Li_{10}N_3I$-LiOH with more lithium content was also prepared using a solid-state reaction similar to that of Li_7N_2I-LiOH by increasing the molar ratio of n(Li_3N)/n(LiI) = 3:1. The obtained materials were ball-milled (PM 100, Retsch) in a zirconia ceramic vial at 400 rpm for 6 hours in argon-filled atmosphere to reduce particle size. By adding PTFE into obtained $Li_{10}N_3I$-LiOH powder, $Li_{10}N_3I$-LiOH-PTFE film with good cold-deformability was fabricated. The total resistance of $Li_{10}N_3I$-LiOH-PTFE film is ~ 530 Ω cm^2, as shown in Figure 29b. The small total resistance can be attributed to the reduced thickness of the film in comparison with the pellet. Figure 29a shows the lithium plating/stripping cycle of Li|$Li_{10}N_3I$-LiOH-PTFE |Li cell at room temperature. No short circuit was observed when the current density increased from 0.01 to 2 mA/cm^2, representing an outstanding lithium dendrite inhibition ability. When the current density was held at 2 mA/cm^2 for 2 hours for each cycle, continuous overpotential decrease was observed. These phenomena can be explained by lithium penetrating into electrolyte as a result of increased plating capacity. After 10 cycles at 2 mA/cm^2, the overpotential stabilized at ~ 0.5 V, corresponding to a small overall resistance in EIS data of cycled sample (Figure 29c). The lithium stabilization can be attributed to the nature of lithiophobic and thermodynamically stable Li-N-I materials against lithium. The role of PTFE in increasing the CCD of $Li_{10}N_3I$-LiOH electrolyte is still being investigated. The team speculates that abundant fluorine group in PTFE enhanced lithiophobicity of the film electrolyte, which makes the electrolyte very resistant to dendrite growth even at a high current density and a large plating capacity.

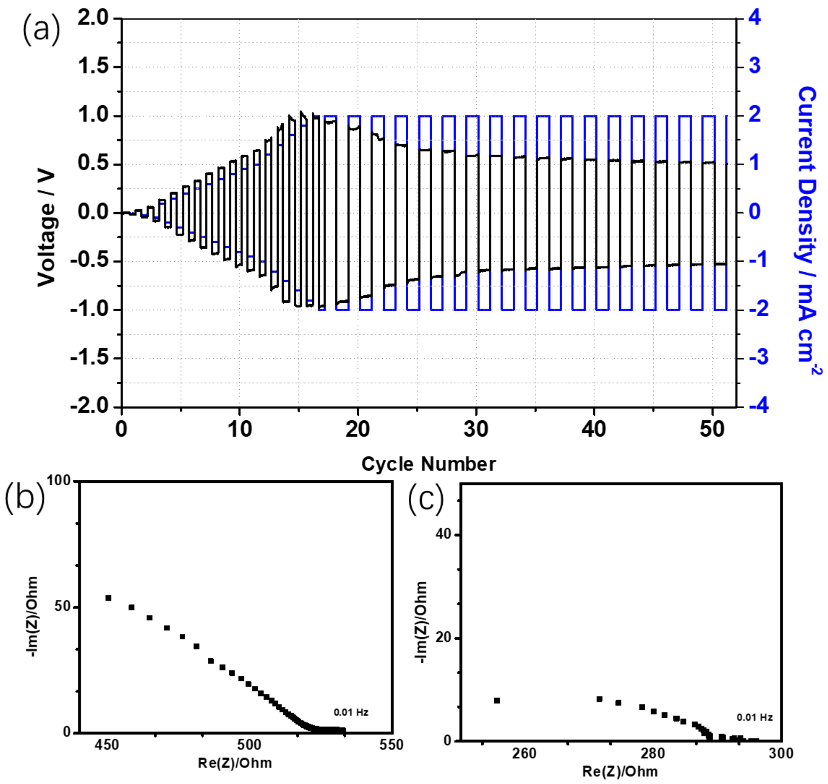

Figure 29. (a) Lithium plating/stripping of Li|$Li_{10}N_3I$-LiOH-PTFE|Li cell at room temperature. The current density first increases with step from 0.01 to 2 mA/cm^2 then holds at 2 mA/cm^2 with 2 hours for each dis/charge cycle; electrochemical impedance spectroscopy data of Li|$Li_{10}N_3I$-LiOH-PTFE|Li (b) before and (c) after cycle at room temperature.

Patents/Publications/Presentations

Publication

- Ji, X., S. Hou, P-F. Wang, X. He, N. Piao, X. Fan, and C. Wang. "Solid-State Electrolyte Design for Lithium Dendrite Suppression." *Advanced Materials* (2020): 2002741.

Task 1.10 – Hot Pressing of Reinforced Lithium-NMC All-Solid-State Batteries with Sulfide Glass Electrolyte

(Thomas Yersak, General Motors)

Project Objective. The objective of this project is to research, develop, and test Li-NMC ASSBs capable of achieving program performance metrics by implementing sulfide glass SSEs and hot press processing in a dry room environment. The performance of ASSBs with sulfide SSEs is limited because they are essentially green tapes with up to 20% porosity. In composite cathodes, the porosity limits energy density and power, while porosity in the separator acts as a conduit for Li-metal deposits if cycling conditions (that is, C-rate, operating temperature, and pressure) are not strictly controlled. The project goal is to demonstrate that the hot pressing method and appropriately formulated sulfide glass SSEs can eliminate porosity to enable Li-NMC ASSBs with energy density of $\geq$ 350 Wh/kg.

Project Impact. The hot press processing method and appropriately formulated sulfide glass SSEs may enable Li-NMC ASSBs with improved energy density > 350 Wh/kg. The GM processing technology depends on heating a sulfide glass SSE above its glass transition temperature, T_g, at which point it can consolidate via viscoplastic flow. In the composite cathode, hot pressing provides liquid-like contact between the NMC cathode and SSE to increase energy density and power by enabling thick composite cathodes with high active material loading. Furthermore, cathode-supported sulfide glass separators can be made dense and thin by hot pressing. A dense separator enables the robust use of a Li-metal anode because lithium deposits may be more effectively blocked, preventing cell shorting.

Approach. The sulfide SSE used in the composite cathode, otherwise known as the catholyte, will dictate the processing specifications for ASSB hot pressing. Thermal stability can be achieved by NMC passivation and proper catholyte formulation. This project will systematically evaluate different NMC coatings, catholyte formulations, and hot-press processing specifications (that is, temperature, time, and pressure). The performance of hot-pressed ASSBs will be compared to green baseline ASSBs and hot-pressed control ASSBs consisting of the β-Li_3PS_4 and Li_6PS_5Cl model SSEs. Electron microscopy will be employed to understand interfacial phenomena and track composite cathode microstructure before and after hot pressing.

Out-Year Goals. In the second year of this project, a sulfide glass SSE will be formulated specifically for use as the separator. The separator glass SSE formulation will be designed to achieve full densification under the hot-press processing specifications determined for the catholyte. Separator glass formulation design will also consider cathodic stability, moisture stability, and ionic conductivity. Once a system of separator glass SSE and catholyte has been determined, the third year of the project will demonstrate hot-pressed full cells at the coin-cell and single-layer pouch cell levels, which meet program target performance metrics.

Collaborations. GM will lead this project with no subrecipients.

Milestones

1. Establish protective coating on cathode: select best coating method and coating chemistry. Confirm conformality of coating using microscopy. (Q2, FY 2020; Completed)
2. Develop suitable baseline system with reversible capacity of ~ 120 mAh/g. (Q3, FY 2020; Completed)
3. Determine parameters required to prepare cathode samples via focused ion beam (FIB) / scanning electron microscopy (SEM) lift-out and to analyze samples via high-resolution transmission electron microscopy (HRTEM). (Q4, FY 2020; In progress)
4. Demonstrate hot-pressed cathode with reversible capacity of 120 mAh/g. Analysis indicates technical approach capable of achieving performance targets. (Q1 FY 2021; In progress)

Progress Report

Due to COVID-related delays, this project has requested a no-cost extension. Reporting will resume next quarter under the extension.

Patents/Publications/Presentations

The project has no patents, publications, or presentations to report this quarter.

Task 1.11 – Low Impedance Cathode/Electrolyte Interfaces for High-Energy-Density Solid-State Batteries
(Eric Wachsman and Yifei Mo, University of Maryland)

Project Objective. The project objective is to research, develop, and test Li-metal-based batteries that implement solid LICs equipped with NMC cathodes integrated into the Li-metal/LLZ tri-layer architecture. Specifically, the team will achieve the following: (1) identify and demonstrate interfacial layers to achieve low-impedance and stable NMC/LLZ interfaces; (2) develop novel processing techniques to fabricate NMC/LLZ composite cathodes with low interfacial resistance; and (3) enable high-performance ASSBs with an energy density of 450 Wh/kg and 1400 Wh/L and negligible degradation for 500 cycles.

Project Impact. Instability or high resistance at the interface of high-energy cathode materials with Li-garnet SEs limits the high-energy-density all-solid-state lithium battery. This project will lead to a fundamental understanding of solid-electrolyte/solid-cathode interfaces and a unique and transformative LLZ framework to enable high-energy-density, safe Li-metal batteries approaching ~ 400 Wh/kg.

Approach. In this new project, the team will build on their demonstrated expertise with garnet electrolytes and ASSB cells to accomplish the following: (1) engineer interfaces to overcome high NMC/LLZ interfacial impedance and interfacial degradation; (2) develop processing and fabrication techniques to achieve high-loading NMC/LLZ composite cathodes with low resistance and high cyclability; and (3) integrate the NMC/LLZ cathodes into all-solid-state Li-metal/LLZ cells to achieve high-energy-density batteries.

Out-Year Goals. The project will solve the current challenges of integrating garnet SE with a cathode to achieve a high-performance ASSB using a high-energy-density Li-metal anode. The resultant high energy density and stability using both high-energy-density Li-metal anodes and NMC cathodes will open new applications in portable electronics, EVs, and beyond.

Collaborations. This project funds work at UMD. The PI, E. Wachsman, will have management responsibility and will lead experimental efforts including garnet synthesis, interface processing, cell fabrication, and testing. The Co-PI, Y. Mo, will lead computational efforts on understanding stability between garnet and cathode and on identifying promising coating materials. No collaborations are reported this quarter.

Milestones

1. Computationally determine interfacial stability between LLZ SEs and NMC cathode. (Q2, FY 2020; Completed)
2. Determine thermochemical stability between LLZ and infiltrated NMC. (Q3, FY 2020; In progress)
3. Computationally determine the mechanism of interfacial stabilization between LLZ and NMC through coating layers. (Q3, FY 2020; Completed)
4. *Go/No-Go Decision*: Computationally determine appropriate compositions to stabilize the LLZ-NMC interface. Achieve design capable of meeting performance requirements. (Q4, FY 2020; Completed)

NOTE: The campus was closed for three months and has only partially reopened, and thus experimental results were limited.

Progress Report

Using demonstrated thermodynamic analyses for interface stability based on first-principles computation, the team performed HT screening to identify oxide materials that stabilize with LLZO-NMC interfaces. They performed HT systematic analysis of these coating materials by investigating the chemical stability of the cathode-LLZO interface, chemical stability of oxide coatings with NMC and LLZO, and electrochemical stability of the coated interfaces. The results of chemical and electrochemical stability of ternary oxides with lithiated and delithiated NMC and LLZO are shown in Figure 30. The results demonstrate the stable oxide coating for LLZO-NMC interfaces and also stabilization mechanisms. In general, LLZO is stable with coating layers with high lithium content, likely because of the high lithium content of LLZO. By contrast, NMC is stable with low lithium content coatings. Due to these differing requirements for lithium content, many materials are not stable with both LLZO and NMC. In summary, the compositions with small chemical and electrochemical reactions with LLZO and NMC are identified as stable coating layers (Figure 30). Notably, the team's analysis identifies several compositions that have been used experimentally to stabilize the LLZO-NMC or LLZO-LCO interface. For example, the Li-Si-O and Li-Nb-O systems have several compositions with low decomposition energies with LLZO and NMC, and these systems have also been widely used experimentally as coating layers. The analysis also identifies the Li- Al, titanium, tin, and tantalum oxides as promising systems for coating layers with LLZO and NMC interfaces. This good agreement with experiments confirms the validity of the project's computation approach, and many promising coatings for the LLZO-NMC interfaces are predicted and will be further tested. In summary, the team has successfully achieved the milestone and *Go/No-Go Decision* of computationally determining the mechanism of interfacial stabilization and the appropriate compositions to stabilize the LLZ-NMC interface.

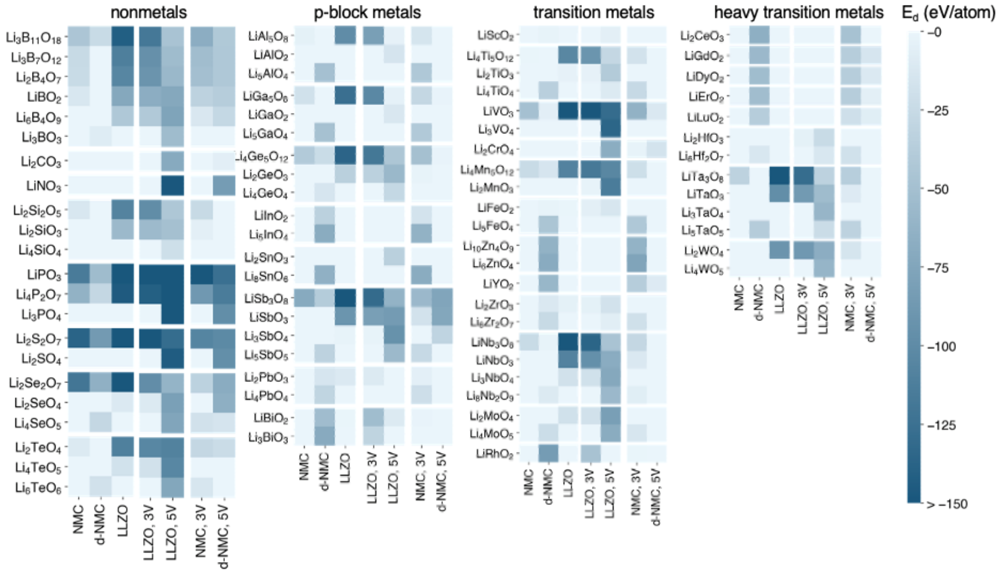

Figure 30. Heatmap showing the chemical decomposition energy of NMC, delithiated NMC, and LLZO with lithium ternary oxide compounds, and the electrochemical decomposition energy of the coating-LLZO and coating-NMC interfaces at 3 V and 5 V.

The team performed XRD experiments on composite pellets of Ta-doped LLZO (LLZTO) and cathode materials (1:1 in weight ratio) prepared by physical mixing, mold pressing, and co-sintering at 500-1000°C for 3 hours. Cathode materials tested include NMC-811, NMC-622, and $LiMnO_4$(LMO). XRD results suggest that LMO can strongly react with LLZTO, even at 500°C (Figure 31a). All NMCs are chemically compatible with LLZTO up to 600°C, after which minimal decomposition phases could be detected (Figure 31b-c). NMC-811 shows greater loss in peak intensity at 1000°C than NMC-622, indicating instability of high nickel content NMC with garnet.

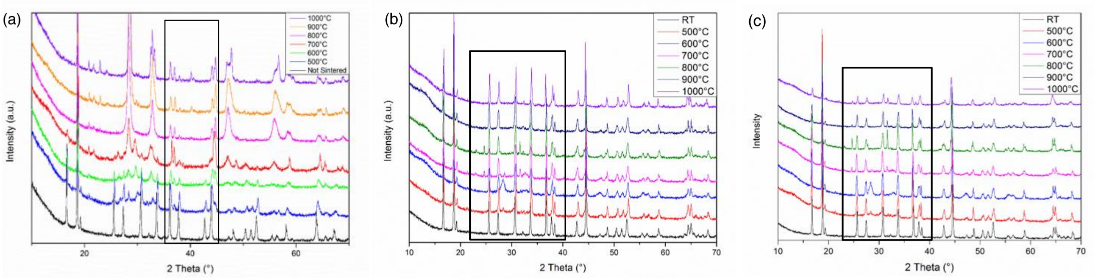

Figure 31. X-ray diffraction patterns of 50/50 w/w mixtures of LLZTO with various cathode materials before and after co-sintering at 500-1000°C. Cathode material for each figure is (a) LMO, (b) NMC-622, and (c) NMC-811. The boxed regions are where the new peaks are appearing.

Patents/Publications/Presentations

Presentations

- ECS PRiME 2020, Virtual (October 4–9, 2020): "Solid-State Chemistries Stable with High-Energy Cathodes for Lithium-Ion Batteries"; A. Nolan, Y. Liu, and Y. Mo. Invited
- ECS PRiME 2020, Virtual (October 4–9, 2020): "Data-Driven Discovery of New Materials for Solid-State Batteries"; Y. Mo.

Task 1.12 – Developing an *In Situ* Formed Dynamic Protection Layer to Mitigate Lithium Interface Shifting: Preventing Dendrite Formation on Metallic Lithium Surface to Facilitate Long Cycle Life of Lithium Solid-State Batteries

(Deyang Qu, University of Wisconsin Milwaukee)

Project Objective. The objective of this project is to research, develop, and test Li-metal-based batteries that implement solid LICs equipped with a formed dynamic protection layer. The proposed project aims to enable safe, long-cycle lithium anodes to achieve cell performance targets of 400 Wh/Kg, over 100 cycles, with 15-year shelf life and < $100/KWh cost.

Project Impact. Project efforts are to contribute an in-depth understanding of the lithium interface and dendrite growth prevention to the field of Li-metal batteries, which will pave the way for eventual development of high-energy-density, low-cost, and long-lasting lithium batteries. This advancement could be a crucial selling point for the greater adoption of EVs. This project will make possible the translation of fundamental research into practical implementation of high-energy lithium anodes, enabling eventual achievement of cell performance targets.

Approach. The novelty of this approach is that the team intends to mitigate the dendrite problem by creating a dynamic protection layer during the interface shift to prevent dendrite formation throughout battery operation.

Out-Year Goals. The project has three out-year goals: (1) *in situ* diagnostic tools are fully functional; (2) potential candidates for Li-anode modifications are identified; and (3) synthesis routes are designed.

Collaborations. The PI is the Johnson Control Endowed Chair Professor, who has close and frequent collaboration with Johnson Controls' scientists and engineers. The collaboration enables the team to validate the outcomes of fundamental research in pilot-scale cells. The PI also has been working closely with top scientists at Argonne National Laboratory (ANL), Brookhaven National Laboratory (BNL), LBNL, and Pacific Northwest National Laboratory (PNNL) and with U. S. industrial collaborators, for example, GM, Millipore Sigma, and Clarios. In addition, the team works with international collaborators in China, Japan, and South Korea. These collaborations will be strengthened and expanded to give this project a vision with both today's state-of-the-art technology and tomorrow's technology in development, while incorporating feed-back from the material designers and synthesizers upstream, as well as from the industrial end users downstream.

Milestones

1. *Baseline*. Conduct literature review and establish baseline for proposed technologies. (Q1, FY 2020; Completed)
2. *Fully functional fixtures and setups*. *In situ* electrochemical-optical and *in situ* electrochemical-MS cells capable of observing dendrite growth and detecting gas generation in real time. (Q1, FY 2020; Completed)
3. *Coating methods*. Physical requirements of each coating technique and adaption of different coating methods for various coating materials based on their properties are identified. (Q2, FY 2020; Completed)
4. *N-type polymer compounds*. N-doped polymer compounds are synthesized. (Q3, FY 2020; Completed)
5. *In situ* diagnostic tools capable of investigating a coated lithium electrode / projected cell performance. Various selected materials can be coated on a lithium surface forming an artificial layer before cell assembly. The dendrite growth and gassing of the coated electrode can be investigated in real-time during cell operation with *in situ* diagnostic tools. Analysis indicates technical approach capable of achieving performance targets. (Q4, FY 2020; Completed)

Progress Report

Due to the pandemic, the PI's research labs and the auxiliary services, for example, the machine shop in the university, are only partially opened to maintain social distancing. However, the team managed to complete all FY 2020 milestones. This quarter, G2 solid-state cells were designed and made for both performance tests and *in situ* observation of the dendrite growth. G2 *in situ* gassing analysis cells were also designed, and the analysis will be fully automated.

G2 Solid-State Cell Design. Figure 32 shows the G2 design of the cell used for performance testing. SSE is pressed and formed in the cell using a pair of rods made by hardened steel. The cathode and the lithium anode are then put on both sides of the SSE; a set of titanium rods with O-ring seals are used as current collectors. A calibrated spring is used to ensure that constant pressure can be maintained during testing. Cells are tested at 60°C. Impedance of a typical LPSCI electrolyte is also shown in Figure 32.

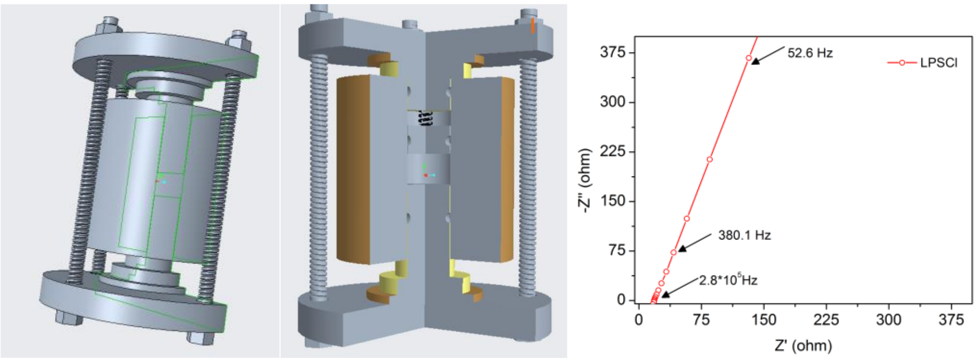

Figure 32. G2 solid-state cell and impedance of the formed solid electrode (LPSCI home synthesized).

Figure 33 shows the G2 design of the cell used for the *in situ* electrochemical optical experiments. The basic design is the same as the G2 cells for the performance tests, but with a window for an optical observation. The window is located right at the electrode/SSE interface. The cell is assembled in a glovebox dedicated to SSE research, and then sealed in an airtight container with a transparent window. The temperature in the box is kept at 60°C with an inside heating element.

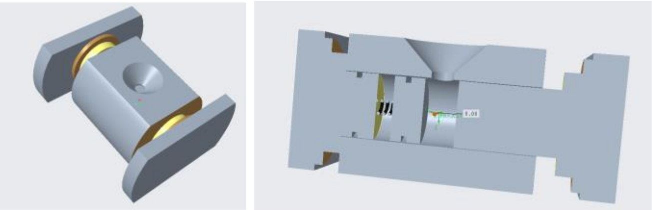

Figure 33. G2 *in situ* electrochemical optical cell for the real-time observation of dendrite growth.

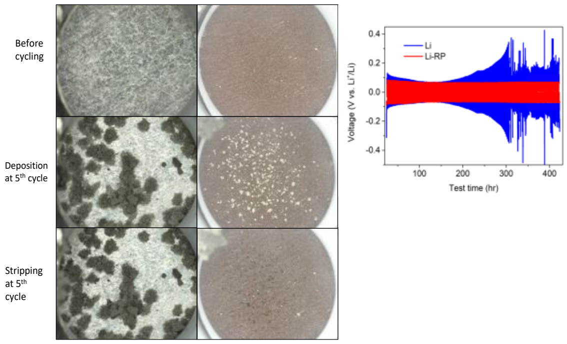

Figure 34. (left) *In situ* observation of a pristine lithium anode and surface treated lithium anode after 5 cycles. (right) The cycling of symmetric Li/Li cells; comparison of pristine lithium anode and surface-treated lithium anode.

Dendrite Growth Prevention with a Surface Lamination. The team continues developing and testing new lithium surface coatings. The surface modification aims for dynamic dendrite growth suppression. Figure 34 shows an example of such modifications. In this example, dendritic lithium reacts with the face layer forming a lithium alloy, due to a small potential differential between the metal lithium and the coating material. The lithium in the alloy can be oxidized during a discharge at the similar potential to that of a metallic lithium. In comparison with a pristine lithium anode, no lithium dendrite can be seen after five cycles. The modified lithium demonstrated much longer cycle life than that of a pristine anode in a symmetric cell.

Patents/Publications/Presentations

Publication

- Ji, W., H. Huang, D. Zheng, X. Zhang, T. Ding, T. H. Lambert, and D. Qu. “A Redox-Active Organic Cation for Safer Metallic Lithium-Based Batteries.” *Energy Storage Material* 32 (2020):185–190.

Task 1.13 – Molecular Ionic Composites: A New Class of Polymer Electrolytes to Enable All-Solid-State and High-Voltage Lithium Batteries
(Louis Madsen, Virginia Polytechnic Institute and State University)

Project Objective. Based on a newly discovered class of solid PE materials, that is, MICs, the overall objective is to develop solid-state lithium conductors targeted for use in transportation applications. MICs form a mechanically stiff, electrochemically stable, and thermally stable matrix. Specific objectives include the following: (1) development of robust MIC electrolyte thin films (~ 20 µm) to serve as simultaneous nonflammable separators and dendrite-blocking Li^+ conductors, (2) electrochemical quantification of key performance metrics including electrolyte stability, interfacial reactions, and suitability/compatibility with a range of electrode materials, and (3) comprehensive investigation of ion transport mechanisms and electrode-electrolyte interfacial reactivity under practical operating conditions using NMR and synchrotron X-ray analyses.

Project Impact. Commercialization of Li-metal SSBs is hampered by lack of a functional nonflammable SE that can provide high ionic conductivity, wide electrochemical window, favorable mechanical properties to inhibit lithium dendritic growth, and low interfacial resistance. The tunable MIC materials platform has potential to fulfill these requirements with relatively simple fabrication techniques, and thus shows promise for enabling nonflammable SSBs that can be optimized for low cost and high energy density.

Approach. MICs rely on a unique polymer that is similar to Kevlar® in its strength, stiffness, and thermal stability, but with densely spaced ionic groups that serve to form an electrostatic network that permeates mobile ions in the MIC. The team can tailor the ion concentrations and types to yield MIC electrolyte films that are electrochemically compatible with Li-metal anode as well as a range of high-voltage layered cathodes. They are searching the composition space of lithium salts, electrochemically compatible ionic liquids, and polymer (PBDT) molecular weight to determine best composition windows for MIC electrolytes. The team is also investigating best methods for casting thin films in terms of temperature, solvent/evaporation conditions, and control over the initial liquid crystalline gel formation point. Concurrently, they are testing MIC films in various electrochemical cells, quantifying transport and structural/morphology parameters with NMR and X-ray techniques, and measuring key mechanical (dynamic mechanical thermal analysis, stress-strain) and thermal [differential scanning calorimetry (DSC), TGA] properties.

Out-Year Goals. This year, the team is focused on understanding evolution of structure and morphology during the film casting process to optimize this process and obtain thin MIC electrolyte films. As part of the team's electrolyte optimization, they are determining the composition windows that yield fast Li^+ conduction, mechanical stability, and electrochemical compatibility with lithium metal and selected cathode materials. They will develop robust electrolyte films and an array of testing schemes (that is, electrochemical, thermal, mechanical, NMR, and X-ray) to sensibly feedback on film composition and fabrication.

Collaborations. The team is beginning collaboration with T. J. Dingemans' group at University of North Carolina (UNC) Chapel Hill in which they are forming composites based on PBDT polymer and carbon materials such as graphene oxide, and are beginning to develop charged rigid-rod polymers building on PBDT. The team is exploring shear rheology and broadband dielectric spectroscopy collaboration with R. H. Colby at Pennsylvania State University (PSU). They are starting collaboration with D. Nordlund at SLAC National Accelerator Laboratory (SLAC) to conduct synchrotron X-ray studies on MIC films.

Milestones

1. Determine synthetic conditions for 100-µm thick electrolyte. (Q1, FY 2020; Completed)
2. Develop baseline Li-ion loading and chemical composition. (Q2, FY 2020; Completed)

3. Establish basic electrochemical, thermal, and mechanical testing protocols for SEs and battery cells. (Q3, FY 2020; Completed)
4. Down-select film fabrication method (drop casting or spray deposition). (Q3/Q4, FY 2020; In progress)
5. Determine optimal synthetic conditions, Li-ion loading, and chemical composition. (Q3/Q4, FY 2020; In progress)
6. Determine the parameter spaces for film formation and develop a design capable of meeting performance requirements for film casting process. (Q4, FY 2020; In progress)

Progress Report

This quarter, the team further studied Li-ion transport properties in MIC electrolytes and their compatibility with lithium metal over a wide temperature range through lithium symmetric cell cycling (Figure 35). When cycled at 23°C, the observed voltage increases slowly during the lithium stripping process, corresponding to establishment of a salt concentration gradient across the cell. The maximum voltage reached during one cycle increases monotonically with increasing current density. When the current density is increased to 0.2 mA/cm^2, the voltage increases drastically to above 5 V, suggesting the concentration of lithium ion at the anode surface is approaching zero and the current density has approached the limiting current density. Since ionic conductivity increases with temperature, the maximum current density obtained from lithium symmetric cell cycling also increases with temperature. At 60°C, the symmetric cell can be cycled steadily using a current density of 0.35 mA/cm^2. The current density can be further raised to 0.6 and 1.8 mA/cm^2 at 100 and 150°C, respectively. It is encouraging that the symmetric cell can be cycled at 150°C for 150 hours (Figure 35b), further demonstrating the thermal and electrochemical stability of the MIC electrolyte at an extreme temperature.

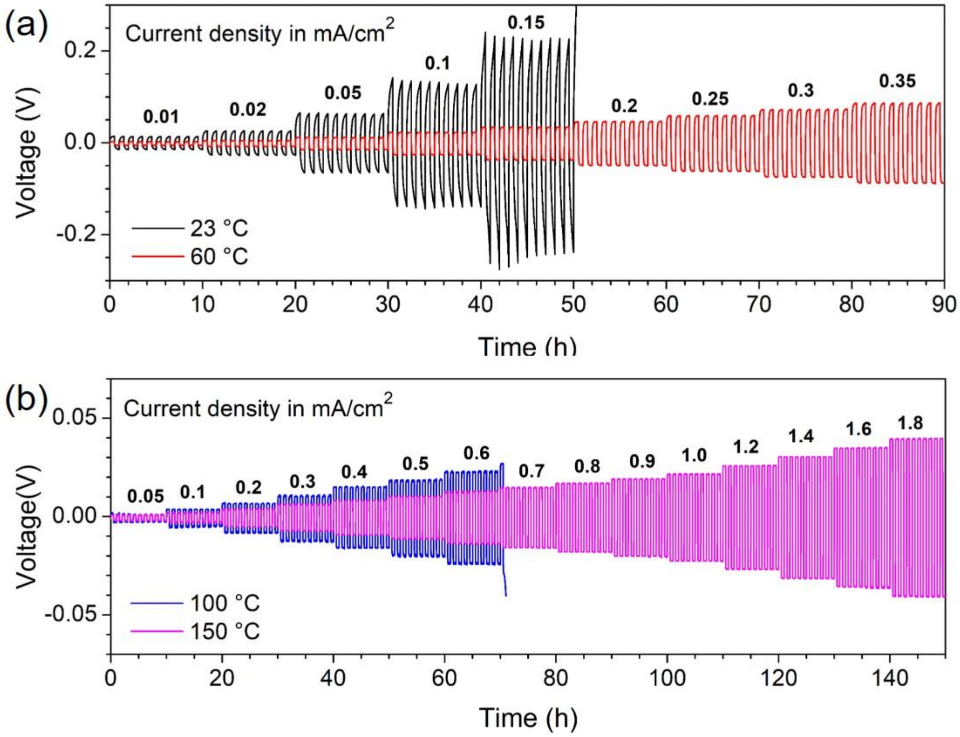

Figure 35. Voltage profiles of lithium symmetric cells cycled at (a) 23°C and 60°C, and (b) 100°C and 150°C in increasing steps of current density. The deposition and stripping time is 0.5 hours, respectively, and the current density (labeled above each step in mA cm^{-2}) is changed every 10 cycles.

In addition to the lithium symmetric cell tests, the team also studied long-term cycling stability of the MIC electrolyte membrane in a Li/MIC/$LiFePO_4$ cell at 23°C using a C/10 charge/discharge rate (Figure 36). The specific capacity increases during the initial few cycles, probably resulting from improved contact between the cathode and electrolyte. The team continues to investigate this mechanism. The CE is above 99.5% in general during cycling, demonstrating that the MIC electrolyte is electrochemically stable. The team is working to further improve CE. The specific discharge capacity reaches a maximum of 150 mAh g^{-1}, with a high retention of 94% after 400 cycles, again signifying the strong stability of the MIC membrane. The charge/discharge profile during cycling shows negligible change except for an increase in ohmic resistance at a high state of charge, which is likely caused by accumulation of side reaction products.

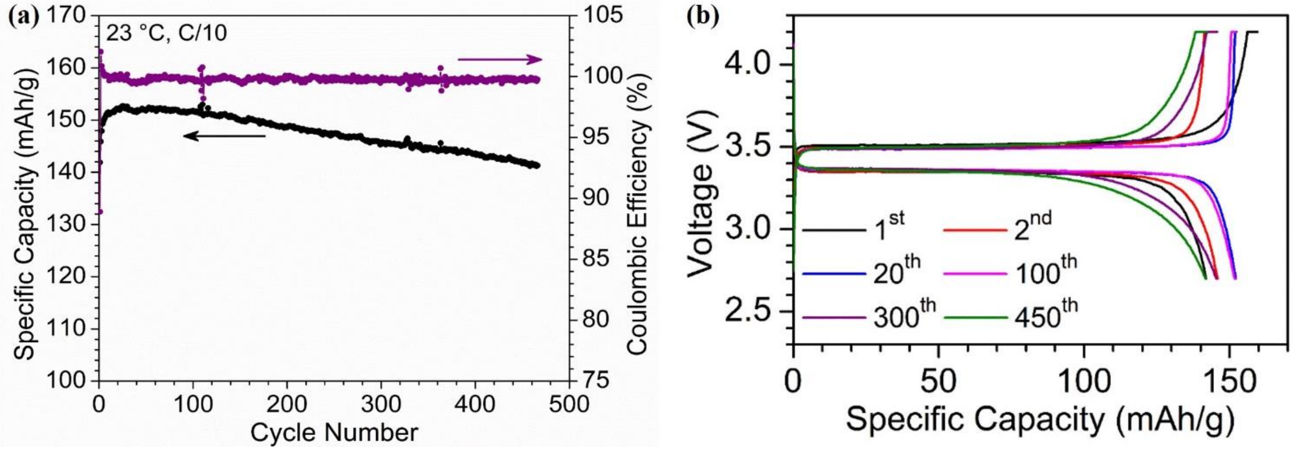

Figure 36. Specific discharge capacity and Coulombic efficiency of Li/MIC/$LiFePO_4$ over 470 cycles (a) and the charge/discharge profile during given cycle numbers (b).

In addition to using $LiFePO_4$ cathode material, the performance of the MIC electrolyte using other cathode materials, such as layered oxides, was also investigated this quarter. Through systematic experiments, the team found that it is necessary to include MIC electrolyte in the cathode formulation to obtain battery cycling (Figure 37b inset, Li/MIC/NMC-811 catholyte cell). Essentially, the MIC electrolyte in the cathode, that is, catholyte, facilitates ion transport in the cathode. In the team's previous report, they showed that the MIC electrolyte is stable with layered cathodes. This quarter, they discovered that the conventional polyvinylidene difluoride (PVDF) / N-methyl-pyrrolidone (NMP) combination can be replaced by the MIC precursor solution during the cathode formulation process, so that cathode particles are embedded in the ionically conductive polymer matrix. Initial assessment has shown that the mechanical properties of the composite cathode are not impacted by building such a catholyte. The preliminary performance of the solid-state cell is shown in Figure 37. When cycled at 23°C using a C/20 charge/discharge rate, the solid-state cells with various cathode mass loadings all exhibit comparable specific capacity. This experiment shows: (1) the MIC electrolyte can replace PVDF in the cathode and improve ion transport in the cathode, and (2) the MIC electrolyte shows stability against layered oxide cathodes. Next, the team will modulate the cathode mass loading and investigate the relationship between mass loading and battery performance. The target is to obtain practically meaningful loadings. Due to the added catholyte in the design, the team expects to achieve a high cathode areal loading capacity. They will also perform battery testing at different temperatures to further evaluate thermal stability and cell kinetics.

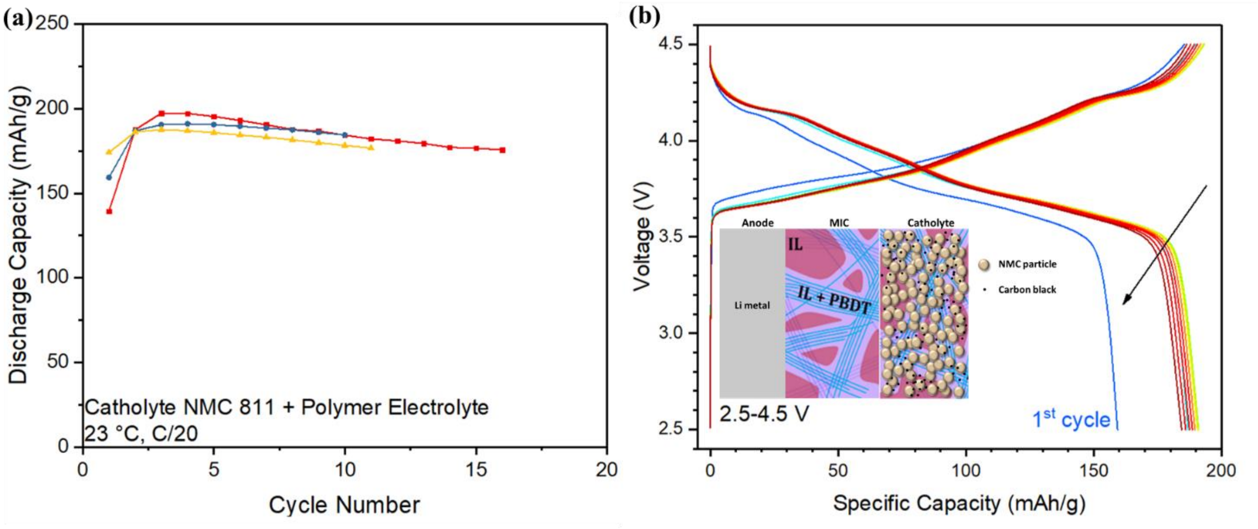

Figure 37. (a) Three repetitions of specific discharge capacity testing of the Li/MIC/NMC-811 catholyte cell cycled at 2.5–4.5 V. (b) Corresponding charge–discharge profiles for 10 cycles at C/20 at room temperature, where the arrows indicate gradual capacity fading. The voltage profile of the first cycle is labeled. The voltage profiles are similar to those for the liquid electrolyte.

Patents/Publications/Presentations

Presentations

- Binghamton University, Department of Chemistry, Binghamton, New York (September 11, 2020): “Investigating Solid-Liquid Interfaces and Defect Chemistry in Electrochemical Energy Systems”; F. Lin. Invited seminar.
- ACS Fall 2020 National Meeting (August 17, 2020): “Solid-State Electrolytes Self-Assembled from a Rigid-Rod Polyelectrolyte, Ionic Liquids, and Metal Salts”; D. Yu, X. Pan, C. J. Zanelotti, F. Lin, and L. A. Madsen.
- ACS Fall 2020 National Meeting (August 17, 2020): “Combining a Double Helix Polyelectrolyte and Ionic Fluids for Tunable Solid Electrolytes”; L. A. Madsen. Invited.

Task 1.14 – All-Solid-State Batteries Enabled by Multifunctional Electrolyte Materials (Pu Zhang, Solid Power Inc)

Project Objective. The project objective is to develop Li-metal SSBs enabled by multifunctional SSEs for EV application. The ultimate goal is scalable production of large-format ASSBs able to deliver ≥ 350 Wh/kg specific energy, ≥ 1000 cycle life, and ≤ $100/kWh cost.

Project Impact. The project impact is enabling scalable production of large format all-solid batteries required by the vehicle market and building domestic battery manufacturers as leaders in the global vehicle ASSB production. The proposed technology will address key limitations of state-of-the-art lithium batteries to meet DOE EV battery targets and accelerate their adoption as large-format EV batteries for sustainable transportation technology.

Approach. The project will develop a high-performance Li-metal solid-state cell enabled by a multifunctional SSE. The new SSE will: (1) have high conductivity (up to 10 mS/cm), (2) be stable against lithium metal and high-voltage cathode (0-4.5 V), (3) promote uniform lithium plating (enabling > 2C charge rate), and (4) be compatible with large-scale manufacturing processes. The specific cell chemistry to be demonstrated will be the SSE with Li-metal anode and high-nickel-content Li-metal oxide cathode. The solid-state cell will be assembled by scalable roll-to-roll processes developed by Solid Power.

Out-Year Goals. In Year 1, multifunctional SSE will be developed with lithium ionic conductivity of ≥ 3 x 10^{-3} S/cm. CCD of ≥ 6 mA/cm^2 will be achieved in a symmetric lithium cell. The SSE design concept will be proven by demonstrating cycle life of ≥ 200 in a full cell. In Year 2, SSE material will be optimized with lithium ionic conductivity of ≥ 5 x 10^{-3} S/cm. Scalable cell assembly processes will be developed. Cycle life of ≥ 500 will be demonstrated in a full cell. In Year 3, large-format solid-state cells (> 2Ah) will be assembled/tested to meet the final goal: ≥ 350 Wh/kg, ≥ 1000 cycles, and ≤ $100/kWh cost.

Collaborations. The proposed team consists of Solid Power and subcontractor UCSD. Solid Power (PI: P. Zhang) will develop the multifunctional SSE and other cell components, assemble cells, and conduct cell tests. UCSD (PI: S. Meng) will carry out material characterization by using advanced techniques such as XPS, cryo-STEM imaging, cryo-STEM energy dispersive X-ray spectroscopy (EDX), electron energy loss spectroscopy (EELS), and cryo-FIB milling. The UCSD team seeks to quantify the kinetics and evolution of each contributing factor and its impact on battery performance.

Milestones

1. Secure precursors and equipment. (Q1, FY 2020; Completed, December 31, 2019)
2. Down-select cathode materials. (Q2, FY 2020; Completed, December 31, 2019)
3. Cathode loading ≥ 3.5 mAh/cm^2. (Q3, FY 2020; Completed, March 31, 2020)
4. SSE ionic conductivity ≥ 3 mS/cm. (Q4, FY 2020; Completed, March 31, 2020)
5. SSE critical current density ≥ 6 mA/cm^2. (Q4, FY 2020; Completed, June 30, 2020)
6. Cell cycle life ≥ 200. (Q4, FY 2020; Completed, July 15, 2020)
7. Charge rate ≥ 0.5C. (Q1, FY 2021; In progress)
8. Pouch cell capacity ≥ 200 mAh. (Q2, FY 2021; In progress)

Progress Report

SSE Powder Development

Solid Power's halogenated LPS material was used as a starting point. Li_2S, P_2S_5, a halogen, and other selected dopants were ball-milled to form GSEs by using a mechanical ball mill. A subsequent heat-treatment was conducted to obtain glass-ceramic SEs. By end of this quarter, Solid Power had developed the multifunctional electrolyte materials meeting Year 1 performance targets on both Li-ion conductivity and CCD against lithium metal.

This quarter, a post-treatment method has been developed to improve purity of the material, which improves the electrolyte CCD (that is, lithium stability) significantly. Figure 38 shows the effect of the post-treatment process on two types of electrolyte materials. It shows more than two times improvement of CCD with both electrolytes, indicating a potential higher charge rate capability in full cells.

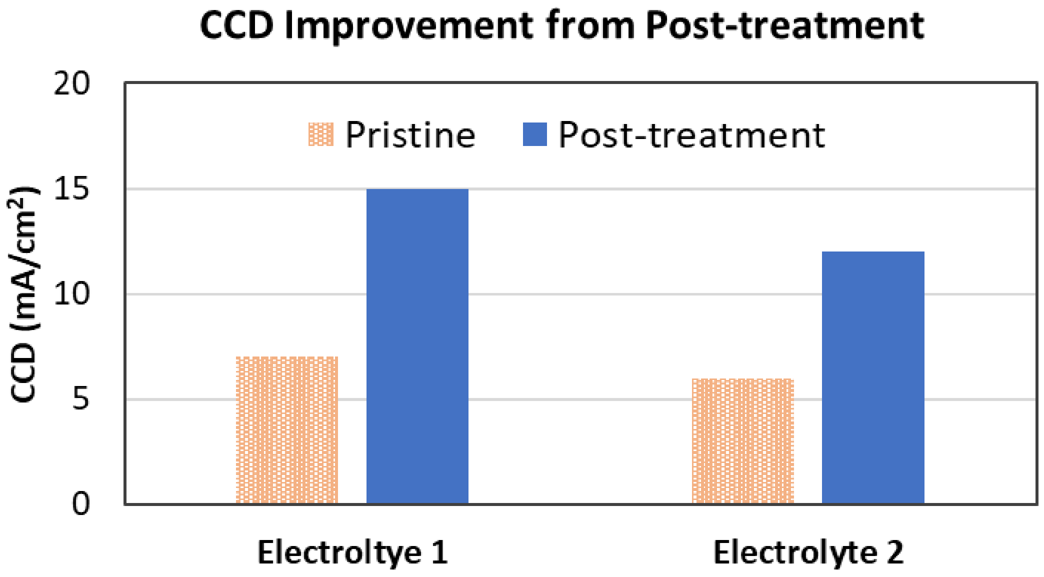

Figure 38. Critical current density improvement with the electrolyte after a post-treatment.

SSE Separator Development

The SSE separator coating process has been developed at pilot scale. A separator slurry was prepared by mixing the SSE powder, a binder, and a solvent by using a Ross high shear mixer. The slurry was then cast on a carrier film on a slot-die coater. Similarly, a NMC-622 cathode was also coated by using the slot-die coater in a roll-to-roll (R2R) mode. Figure 39 shows images of R2R separator coating and R2R cathode coating, respectively. The separator was then laminated to the cathode to form a separator-cathode bi-layer, which was assembled into a solid-state cell by coupling a stand-alone Li-foil anode.

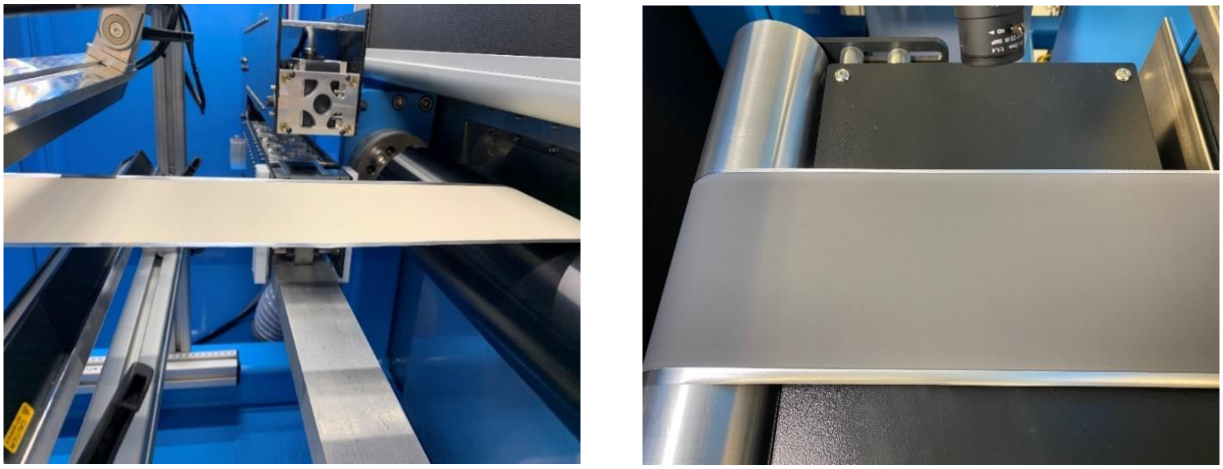

Figure 39. Roll-to-roll coatings from a slot die coater: (left) solid-state electrolyte separator, and (right) NMC cathode.

Full Cell Demonstration

A single-layer pouch cell (at 6 mAh) was assembled for performance demonstration last quarter. The cell contained a NMC-622 composite cathode (at 3 mAh/cm^2), a thin Li-metal foil anode, and a SSE separator. The cell is designed to deliver a specific energy of 300 Wh/kg if scaled to 20 Ah. The cell has been tested at C/5 - C/5, 2.8 - 4.2V, and 70°C since then. To date, the cell demonstrates 250 cycles with 80% capacity retention and 350 cycles with 75% capacity retention (Figure 40). It exceeds the first year goal of 200 cycles.

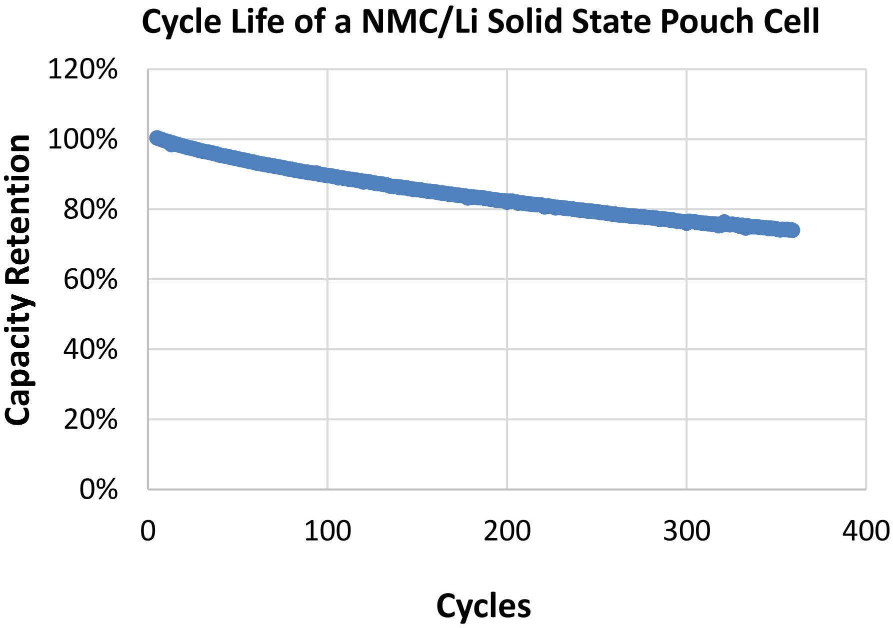

Figure 40. Cycle life of an NMC/Li-metal solid-state pouch cell with the multifunctional solid-state electrolyte.

Patents/Publications/Presentations

The project has no patents, publications, or presentations to report this quarter.

Task 1.15 – Developing Materials for High-Energy-Density Solid-State Lithium-Sulfur Batteries (Donghai Wang, Pennsylvania State University)

Project Objective. The project objectives are to develop materials involving advanced S-C composite materials, solid additives, and sulfide-based SSEs, and to acquire knowledge for Li-S ASSBs. Li-S ASSBs with large areal sulfur loading (≥ 5 mg cm^{-2}) and high sulfur content (≥ 50 wt% in cathode), pairing with lithium or lithium alloy anode, will deliver a high initial specific capacity of over 1200 mAh g^{-1} at high charge/discharge rate (> 0.3 C) for 500 cycles with over 80% capacity retention.

Project Impact. This project aims to develop new materials to enable Li-S ASSBs with high energy density, excellent cycling stability, and good rate performance, and thus to build knowledge for fabrication of prototype Li-S ASSBs. Specifically, the developed new materials will greatly increase the specific capacity of sulfur and sulfur utilization at high areal sulfur loading, alleviate the interfacial problem between S-C composite and SSE within sulfur cathode, boost Li-ion conductivity, and improve moisture stability of glass and glass-ceramic sulfide-based SSE. Meeting the technical targets will potentially promote development of high-energy-density Li-S ASSBs and their practical application in EVs and plug-in hybrid EVs (PHEVs), and reduce petroleum consumption in the transportation sector by helping battery-powered vehicles become more accepted by consumers as a reliable source of transportation.

Approach. The project goal will be accomplished through developing new materials, together with in-depth characterization of sulfur cathode. Specifically, approaches to realize the project objectives include: (1) development of new carbon material with unique structure, high surface area, and large pore volume; (2) development of new S-C materials to facilitate electron/ion transport; (3) development of novel additives to tune interfacial behavior among components in the cathode; (4) development and optimization of new SSE through cation and anion doping with superior properties such as high ionic conductivity, good moisture, and stability; and (5) diagnostics, characterization, and cell tests on the developed new material or advanced sulfur cathode.

Out-Year Goals. The out-year goals are as follows: (1) develop new S-C materials, new cathode additives, and cation-doped SEs (ionic conductivity above 2 mS cm^{-1} at room temperature), (2) conduct characterization and performance tests on both material and electrode levels. The *Go/No-Go Decision* will be demonstration of all-solid-state sulfur cathode with over 1000 mAh g^{-1} discharge capacity at 0.3 C discharge rate and 50 wt% sulfur content for 50 cycles at 60°C.

Collaborations. There are no active collaborations.

Milestones

1. Demonstrate sulfur cathode with above 800 mAh g^{-1} capacity at 0.1 C at 60°C. (Q1, FY 2020; Completed)
2. Demonstrate sulfur cathode > 1000 mAh g^{-1} using new solid additives or developed new electrolyte (> 1 mS cm^{-1}, at 25°C). (Q2, FY 2020; Completed)
3. Demonstrate sulfur cathode with > 1000 mAh g^{-1} using optimized carbon materials. (Q3, FY 2020; Completed)
4. Demonstrate sulfur cathode with >1000 mAh g^{-1} at 0.3 C for 50 cycles at 60°C. (Q4, FY 2020; Completed)

Progress Report

This quarter, the team continued previous work on developing new SE introducing nitrogen and aluminum in the basic Li_2S-P_2S_5 SE system. They have developed a new glass-ceramic SE $65Li_2S$-$65Li_2S$-$26P_2S_5$-$10Li_3N$-$12Al_2S_3$ (LPSNAl-12) with high ionic conductivity of 5.19 mS cm^{-1} at 25ºC and low activation energy of 0.159 eV. Such high ionic conductivity meets the milestone for synthesizing new SE in budget period 1. The team optimized the content of Al_2S_3 ($65Li_2S$-$65Li_2S$-$26P_2S_5$-$10Li_3N$-xAl_2S_3, LPSNAl-x) based on room-temperature ionic conductivity. To synthesize LPSNAl-x SE, precursors including Li_2S, P_2S_5, Li_3N, and Al_2S_3 were ball milled at 500 rpm to form glass-type SE. The detailed XRD spectra of synthesized glass-type SEs with different Al_2S_3 ratio and corresponding ionic conductivity have been reported previously. The synthesized glass-type SE was further heated at 400ºC for 2 hours to obtain glass-ceramic SE. According to XRD results in Figure 41a, thio-LISICON III analog phase is precipitated, and peaks representing Li-Al-S crystals are observed when x is between 1 and 12. The ionic conductivity of synthesized LPSNAl-x SEs at 25ºC is depicted in Figure 41b. Among all synthesized glass-ceramic SEs, LPSNAl-12 demonstrated best ionic conductivity and lowest activation energy; the Arrhenius plot for its measured ionic conductivity is shown in Figure 42.

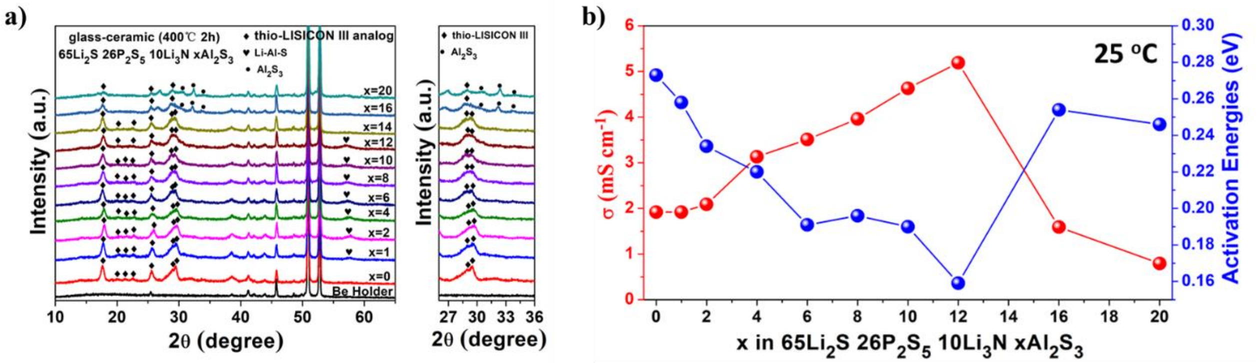

Figure 41. (a) X-ray diffraction spectra and (b) ionic conductivity at 25°C and activation energy of various LPSNAl-x glass-ceramic solid electrolyte (x = 0-20).

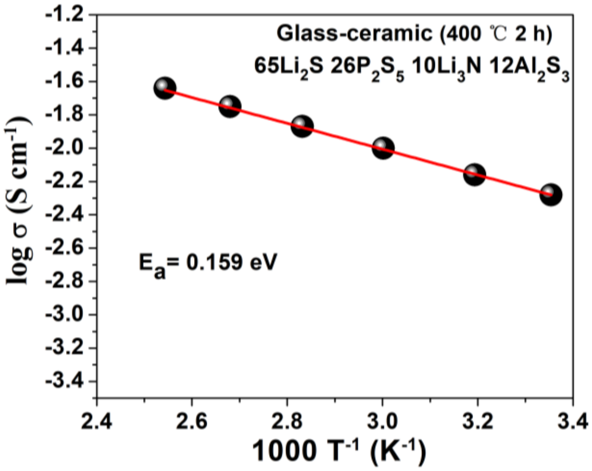

Figure 42. The Arrhenius plot for the measured ionic conductivity of LPSNAl-12 glass-ceramic solid electrolyte.

In addition to the characterization of ionic conductivity and XRD spectra of the material, XPS has also been employed to investigate the surface chemical environment of the synthesized material, as shown in Figure 43. It was observed that nitrogen and aluminum were incorporated into the SE framework by forming Li-Al-S bond, P-N bond, and P=N bond. The formed bonds might contribute to improvement of ionic conductivity of SE.

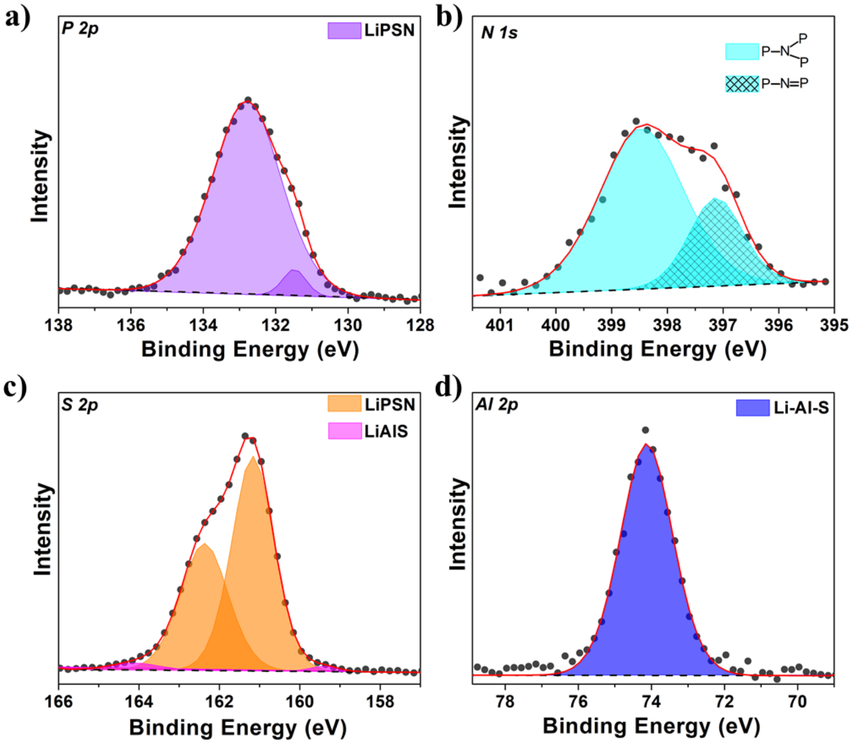

Figure 43. X-ray photoelectron spectra of LPSNAl-12 glass-ceramic solid electrolyte.

Apart from synthesizing SE and evaluating its stability against lithium metal, the team also continued research on EAM additives for all-solid-state Li-S batteries. With less than 5 wt% addition, the sulfur cathode with sulfur content of ~ 50 wt% and areal loading of ~ 1.5 mg cm^{-2} demonstrated high initial discharge capacity of over 1400 mAh g^{-1}; even after 50 cycles, the specific capacity could still retain above 1200 mAh g^{-1} at 0.3 charge/discharge rate at 60°C (Figure 44). Li-In alloy was employed as anode and 75 $Li_2S \cdot 25 P_2S_5$ glass type SSE was employed as SE membrane and electrolyte used in the cathode. Such superior performance fulfilled the EAM additives demonstration milestone as well as the project progress cell demonstration target of *Go/No Go Decision* for budget period 1.

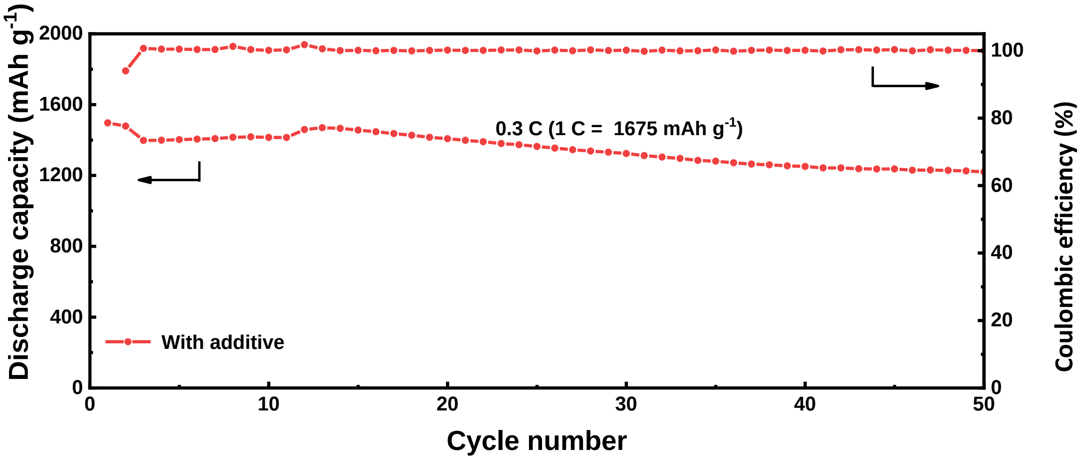

Figure 44. Cycling performance of all-solid-state Li-S battery using electrochemically active molecules additive at 60°C.

Patents/Publications/Presentations

The project has no patents, publications, or presentations to report this quarter.

TASK 2 – DIAGNOSTICS

Summary and Highlights

To meet the goals of the VTO programs on next-generation EVs, low-cost and abuse-tolerant batteries with higher energy density, higher power density, better safety, and longer lifetimes are needed. In pursuit of these goals, high cell operating voltages and demanding cycling conditions are used, which leads to unprecedented chemical and mechanical instabilities in cell components. Successful implementation of promising electrode materials (such as silicon anode and high-voltage cathodes) and new cell chemistry (such as high-energy Li-metal cells combined with SSEs) requires better understanding of fundamental processes, especially those at the interface/interphase of both anode and cathode. Identifying and understanding structure-property-electrochemical performance relationships in materials and various failure modes in cell chemistry are therefore more pressing than ever, not only in guiding battery development activities but also the scale-up efforts needed for commercialization.

Task 2 takes on these challenges by combining model systems, *ex situ*, *in situ*, and *operando* approaches, with an array of state-of-the-art analytical and computational tools. Numerous subtasks are tackling the chemical processes and reactions at the electrode/electrolyte interfaces in Li-metal batteries. Researchers at LBNL use surface- and bulk-sensitive techniques, including FTIR, attenuated total reflectance (ATR)-FTIR, near-field infrared (IR) and Raman spectroscopy/microscopy, and scanning probe microscopy (SPM) to characterize changes in materials and the physio-chemical phenomena occurring at the interface of Li-metal electrode. GM is developing *in situ* diagnostic techniques, including atomic force microscopy (AFM), nano-indentor, dilatometer, and stress-sensor, to be combined with atomic/continuum modeling schemes to investigate the coupled mechanical/chemical degradation of the SEI layer as well as the microstructural evolution at the interface/interphase of Li-metal anode. ANL aims to develop high-conductivity ceramic electrolytes through cation doping and identify mechanistic barriers that limit the chemical/mechanical/electrochemical durability of the solid/solid interfaces. University of Houston (UH) is developing multidimensional diagnostic tools, including FIB-SEM, TOF-SIMS, and in-SEM nanoindentation, to probe structural, chemical, and mechanical evolution at the interfaces of SSLBs. At LBNL, model systems of electrode, SSE, and their interfaces with well-defined physical attributes are being developed and used for advanced diagnostic and mechanistic studies at both bulk and single-particle levels. These controlled studies remove the ambiguity in correlating a material's physical properties and reaction mechanisms to its performance and stability, which is critical for further optimization. Subtasks at BNL and PNNL focus on the understanding of fading mechanisms in electrode materials, with the help of synchrotron-based X-ray techniques (diffraction and hard/soft X-ray absorption) at BNL and HRTEM/STEM and related spectroscopy techniques at PNNL. The final subtask at Stanford/SLAC develops and utilizes an integrated X-ray characterization toolkit to investigate and generate insights on SSBs, by tracking the evolution of nanoscale chemistry as well as structure, microstructure, and transport properties. The diagnostics team not only produces a wealth of knowledge that is key to development of next-generation batteries, it also advances analytical techniques and instrumentation that have a far-reaching effect on material and device development in various fields.

Highlights. The highlights for this quarter are as follows:

- The PNNL (C. Wang) group demonstrated the correlations among lithium deposition conditions, dendrite growth kinetics, and SEI formation mechanisms, offering insights on how to regulate the microstructure and chemical features of electrochemically deposited lithium metal and SEI.
- The ANL (Z. Chen) group revealed that the reactions between Li-metal anode and LLZO electrolyte accelerate with increasing current density. Their study showed micron-sized clustered cracks on flat LLZO pellet surface after repeated lithium stripping/plating, revealing that damages to the electrolyte originate from within instead of from outside.

Task 2.1 – Characterization and Modeling of Li-Metal Batteries: Model-System Synthesis and Advanced Characterization

(Guoying Chen, Lawrence Berkeley National Laboratory)

Project Objective. This project will use a rational, non-empirical approach to design and develop SSE materials and interfaces for next-generation Li-metal batteries. Combining a suite of advanced diagnostic techniques with carefully prepared model-system samples, the project will perform systematic studies to achieve the following goals: (1) obtain understanding on the role of SSE grain and GBs on ion conduction and dendrite formation, (2) obtain fundamental knowledge on rate- and stability-limiting properties and processes in SSEs when used in Li-metal batteries, (3) investigate the reactivities between SSE and electrodes and gain insights on the dynamic evolution of the interfaces, and (4) design and synthesize improved SSE materials and interfaces for safer and more stable high-energy Li-metal batteries.

Impact. The project will focus on fundamental understanding of SSE and relevant interfaces to enable its use in Li-metal batteries. Knowledge gathered from model-system based studies will guide the design and engineering of advanced materials and interfaces. The use of the non-empirical, rational-design approach will develop high-energy battery systems with improved commercial viability.

Approach. The project will combine model-system synthesis and advanced diagnostic studies to investigate ion conduction and interfacial chemistry of SSE in Li-metal batteries. Single crystalline, polycrystalline, and amorphous model SSE samples with various grain and GB properties will be synthesized. Model interfaces between the SSE and electrodes with controlled properties will also be developed. Both bulk-level and single-grain level characterization will be performed. Global properties and performance of the samples will be established from the bulk analyses, while the single-grain-based studies will utilize time- and spatially-resolved analytical techniques to probe the intrinsic redox transformation processes and failure mechanisms under battery operating conditions.

Out-Year Goals. In the out-years, the project will deliver fundamental knowledge on the role of SSE microstructure in Li^+ conduction and lithium dendrite formation/propagation. Insights on performance-limiting physical properties and phase transition mechanisms as well as dynamic evolution of SSE/electrode interfaces will be obtained. Mitigating approaches, such as use of surface coating or “buffer layer” in stabilizing SSE/electrode interfaces, will be evaluated. Further, advanced SSE materials and interfaces for improved high-energy Li-metal batteries will be designed and synthesized.

Collaborations. This project collaborates with the following PIs: G. Ceder, K. Persson, M. Doeff, B. McCloskey, R. Kostecki, and R. Prasher (LBNL); W. Yang (Advanced Light Source, ALS); D. Nordlund and Y. Liu (Stanford Synchrotron Radiation Lightsource, SSRL); C. Wang (PNNL); and J. Nanda (Oak Ridge National Laboratory, ORNL).

`Milestones

1. Develop model systems suitable for studying the impact of SSE grain and GBs in Li-metal based batteries. (Q1, FY 2020; Completed)
2. Synthesize model SSE samples with various grain and GB characteristics. (Q2, FY 2020; Completed)
3. Advanced diagnostic studies of SSE model samples at both particle-level and bulk-sample level. (Q3, FY 2020; Completed)
4. Obtain understanding on SSE grain and GB chemistry, properties, and their effect on ion conduction and dendrite formation. (Q4, FY 2020; On schedule)

Progress Report

This quarter, the team continued to evaluate the properties and electrochemical behavior of halide SSEs with a general formula of Li_3MX_6. Figure 45 shows the Rietveld refinement of XRD patterns collected on the as-synthesized glassy crystalline Li_3YCl_6 (LYC, Figure 45a) and Li_3InCl_6 (LIC, Figure 45b). Structure wise, LYC adopts a hexagonal unit cell with an ABAB stacking anionic sublattice (*P*-3*m*1). While most Y cations are located at the 1*a* and 2*d* sites, a significant fraction of them also share the same sites with lithium at the 6*g* and 6*h* sites. The atomic arrangement based on the refinement is shown in Figure 45a. On the other hand, LIC adopts a monoclinic unit cell with an ABCABC stacking anionic sublattice (*C*2/*m*). Extensive cation mixing is also found between the lithium and indium sites, leading to formation of rocksalt-type phase shown in the XRD pattern and the atomic structural arrangement in Figure 45b.

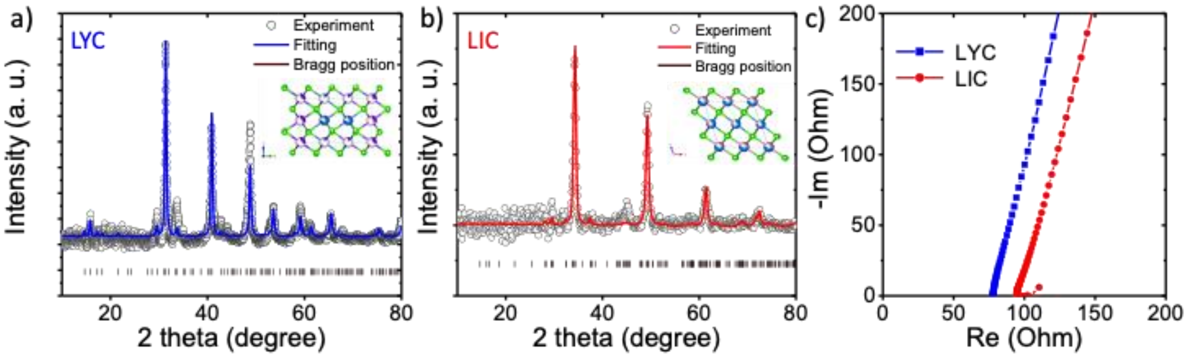

Figure 45. Rietveld refinement of X-ray diffraction patterns: (a) LYC and (b) LIC. The insets show atomic arrangements that highlight the disordering nature of yttrium and indium, respectively. (c) Comparison of electrochemical impedance spectroscopy Nyquist plots of blocking-electrode cells with as-synthesized LYC and LIC.

Room-temperature ionic conductivities were measured by EIS using stainless-steel blocking electrodes (Figure 45c). The obtained values for LYC and LIC were 0.43 and 0.29 mS/cm, respectively, suggesting that bulk LYC is slightly more conductive. EIS measurements were also carried out on symmetrical Li|LYC|Li and Li|LIC|Li cells under the open circuit voltage (OCV) conditions with an AC amplitude of 10 mV. The Nyquist plots in the frequency range of 1 MHz to 0.1 Hz collected on the as-assembled cells are shown in Figure 46a. In general, the depressed semi-circle at the high frequency can be attributed to the interfacial impedance between lithium and SSE. The measured diameters were ~ 2 and 100 Ohms for LYC and LIC, respectively, suggesting a less resistive interface between LYC and lithium metal. Figure 46b-c further compares the evolution of interfacial impedance as a function of time. The EIS measurements were carried out for 10 cycles at an interval of 10 minutes. While the impedance increased continuously in the LIC symmetrical cell (Figure 46b), implying reactivities between LIC and lithium metal, negligible changes were observed on the LYC cell (Figure 46c). The lower initial impedance and higher stability indicate a better interface between LYC and lithium electrode. Although LYC and LIC belong to the same family of halide SSEs with indium and yttrium sharing the same oxidation state of +3, the observed differences on anode reactivity suggest the critical role of metal center in halide SSE behavior. Future work will investigate ion conduction and dendritic activities at the less reactive LYC and Li-metal anode interface.

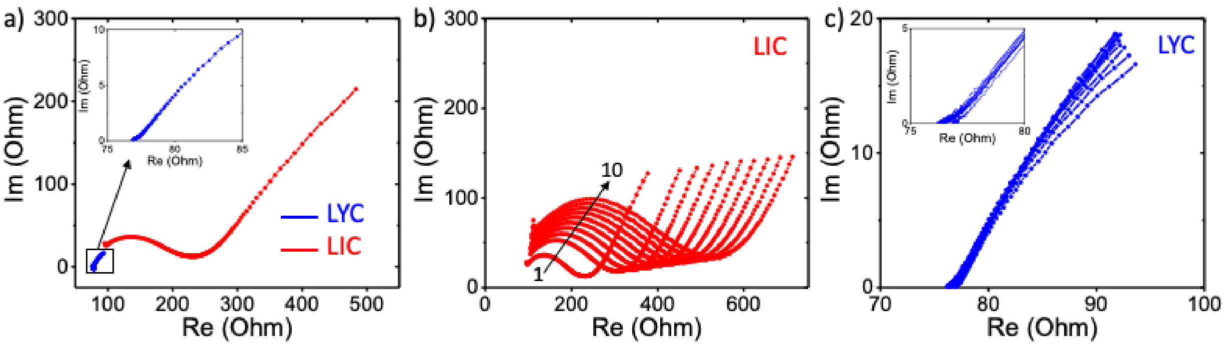

Figure 46. (a) Comparison of electrochemical impedance spectroscopy (EIS) Nyquist plot of as-assembled Li|LYC|Li and Li|LIC|Li symmetrical cells. (b-c) Evolution of EIS as a function of time in Li|LIC|Li and Li|LYC|Li cells, respectively.

Patents/Publications/Presentations

Publications

- Ahn, J., D. Chen, and G. Chen. "A Fluorination Method for Improving Cation-Disordered Rocksalt Cathode Performance." *Advanced Energy Materials* (2020): 2001671. doi: 10.1002/aenm.202001671.
- Chen, D., J. Ahn, E. Self, J. Nanda, and G. Chen. "Design Strategies for Improved Cation-Disordered Rocksalt Cathodes." Submitted (2020).

Task 2.2 – Interfacial Processes – Diagnostics
(Robert Kostecki, Lawrence Berkeley National Laboratory)

Project Objective. The objective of the proposed research is to establish specific design rules toward the next generation of low impedance Li-metal rechargeable batteries that are capable of performing 1000 deep discharge cycles at CE > 99.9% and suppressing lithium dendrite formation at high current densities (> 2 mA/cm^2). This project aims at the following: (1) establishing general rules between Li$^+$ transport properties in novel liquid/solid electrolytes, and (2) determining the mechanism of the SEI layer (re)formation. The other goal is development and application of far- and near-field optical probes and synchrotron-based advanced X-ray techniques to obtain insight into the mechanism of Li$^+$ transport and interfacial reactions in lithium/liquid model systems. Through an integrated synthesis, characterization, and electrochemistry effort, this project aims to develop a better understanding of lithium/LE interface so that rational decisions can be made as to their further development into commercially viable Li-metal cells.

Project Impact. Chemical instability and high impedance at the interface of Li-metal electrodes limits electrochemical performance of high-energy-density batteries. A better understanding of the underlying principles that govern these phenomena is inextricably linked with successful implementation of high-energy-density materials in Li-metal-based cells for PHEVs and EVs. New state-of-the-art techniques to identify, characterize, and monitor changes in materials structure and composition that take place during battery operation and/or storage will be developed and made available to the Program participants. The proposed work constitutes an integral part of the concerted effort within the BMR Program, and it supports development of new electrode materials for high-energy, Li-metal-based rechargeable cells.

Approach. The pristine and cycled composite electrode and model thin-film electrodes will be probed using various surface- and bulk-sensitive techniques, including FTIR, ATR-FTIR, near-field IR and Raman spectroscopy/microscopy, and SPM to identify and characterize changes in materials structure and composition. Novel *in situ / ex situ* far- and near-field optical multi-functional probes in combination with standard electrochemical and analytical techniques are developed to unveil the structure and reactivity at interfaces and interphases that determine materials electrochemical performance and failure modes.

Out-Year Goals. In the out-years, the project aims to achieve the following: (1) understand factors that control performance and degradation processes, (2) unveil structure and reactivity at hidden or buried interfaces and interphases that determine electrochemical performance and failure modes, and (3) propose effective remedies to address inadequate Li-metal-based battery calendar/cycle lifetimes for PHEV and EV applications.

Collaborations. The diagnostic studies will be carried out in sync with other diagnosticians (G. Chen, B. McCloskey, R. Prasher, and L-W. Wang) and theory and computational scientists (G. Ceder and K. Persson).

Milestones

1. Develop novel experimental approach(es) suitable for studying Li/electrolyte interfaces. (Q1, FY 2020; Completed)
2. Manufacture model thin-film lithium model electrodes for *ex situ* and *in situ* fundamental studies of Li/electrolyte interfaces. (Q2, FY 2020; In progress)
3. Characterize chemistry of Li/electrolyte with *ex situ* near-field IR, XAS, and XPS. (Q3, FY 2020; In progress)
4. Gain preliminary insights into SEI composition and reaction pathways for baseline electrolytes. Propose first approximative reaction scheme. (Q4, FY 2020; In progress)

Progress Report

This quarter, the team characterized *in situ* interfaces in a model Li/LiTFSI-PEO/C (graphene) solid-state model battery cell during electrochemical cycling by near-field FTIR nano-spectroscopy (nano-FTIR) in a nitrogen-filled glovebox. A monolayer graphene sheet was used as a working electrode and optical window for nano-FTIR probe characterization. After the lithium plating process, morphological and chemical changes at the graphene/Li-electrolyte (SSE) interface were probed through the graphene window at nanoscale resolution. The dry nitrogen atmosphere prohibited any interference from oxygen and moisture and allowed the team to obtain high-quality nano-FTIR spectra.

(a) 🟩 Lithiated (Plated) Graphene/SSE Interface

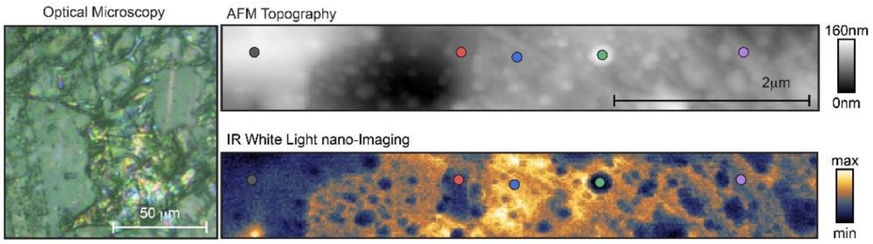

(b) 🟩 Lithiated (Plated) Graphene/SSE Interface

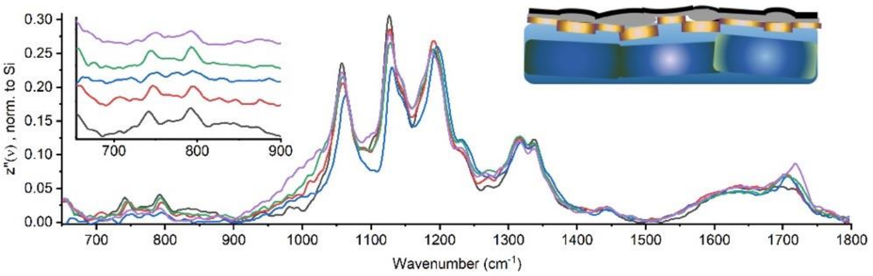

(c) Heated (◆) and Lithiated (🟩) ATR-FTIR

(d) Heated (◆) and Lithiated (🟩) nano-FTIR Mean

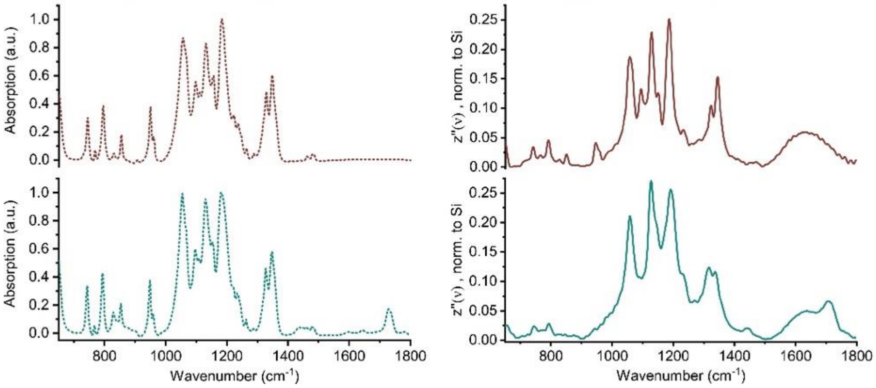

Figure 47. (a) Optical image of the lithium deposited LiTFSI/PEO solid-state battery for 10-hour plating at 25 μA cm^{-2} and a selected area atomic force microscopy topographical image and its corresponding infrared white light nano-image. (b) Nano-FTIR (Fourier transform infrared) spectra of selected five points, and the schematic illustration for the structural changes from graphene to the bulk of solid-state electrolyte (SSE). (c) The attenuated total reflection (ATR)-FTIR mode spectra of SSE at pristine (heated) and after lithiated. (d) The averaged nano-FTIR spectra of SSE at pristine (heated) and after lithiated.

Figure 47a shows an optical image of a selected area of the graphene electrode where lithium plating occurred. The AFM topography image shows inhomogeneous lithium morphology at the graphene/electrolyte interface, whereas the corresponding nano-FTIR image orange-blue contrast reveals the IR chemical contrast at the interface. For the area with a larger amount of lithium deposits, the surface will be more conductive and the

IR nano-image tends to appear in lighter orange colors. The nano-FTIR spectra collected at five locations show quite significant variations. Peaks intensity decreases at < 1000 cm^{-1}; disappearance of PEO peaks and the appearance of new peaks are the most visible indicators of interfacial changes. The peaks intensity reduction is mainly caused by formation of a thin lithium layer at the graphene. The disappearance of PEO peaks is due to the transformation of crystal PEO to amorphous phase. The appearance of new peaks at 1440 cm^{-1} and 1730 cm^{-1} can be assigned to Li_2CO_3 and carbonyl group in organic compounds from SSE decomposition, respectively. The ATR-FTIR spectra indicate that the PEO in a larger and deeper area still stays as a crystalline phase. The crystalline to amorphous phase transformation only occurs in a local region between plated lithium and original SSE. Future work will focus on *in situ* detailed characterization of the SEI in a fully cycled SSB. This work concludes efforts toward this quarter's milestone.

Patents/Publications/Presentations

The project has no patents, publications, or presentations to report this quarter.

Task 2.3 – Advanced *In Situ* Diagnostic Techniques for Battery Materials (Xiao-Qing Yang and Seong-Min Bak, Brookhaven National Laboratory)

Project Objective. The primary objective of this project is to develop new advanced *in situ* material characterization techniques and to apply these techniques to support development of new cathode and anode materials with high energy and power density, low cost, good abuse tolerance, and long calendar and cycle life for beyond Li-ion battery systems to power PHEVs and battery electric vehicles (BEVs). The diagnostic studies will focus on issues relating to capacity retention, thermal stability, cycle life, and rate capability of beyond Li-ion battery systems.

Project Impact. The VTO Multi-Year Program Plan describes the goals for battery: "Specifically, lower-cost, abuse-tolerant batteries with higher energy density, higher power, better low-temperature operation, and longer lifetimes are needed for development of the next-generation of HEVs, PHEVs, and EVs." The knowledge gained from diagnostic studies through this project will help U. S. industries develop new materials and processes for next-generation Li-ion batteries in the effort to reach these VTO goals.

Approach. This project will use the combined synchrotron-based *in situ* X-ray techniques (XRD; and hard and soft XAS) with other imaging and spectroscopic tools such as HRTEM and MS to study the mechanisms governing performance of electrode materials.

Out-Year Goals. In the out years, the project will complete development of diagnostic techniques using X-ray pair distribution function (x-PDF), XRD, and XAS combined with neutron diffraction and neutron PDF (n-PDF), as well as STEM imaging and transmission X-ray microscopy (TXM) for cathode materials studies. It will then apply these techniques to study the structural changes of various new cathode and anode materials.

Collaborations. The BNL team will work closely with material synthesis groups at ANL (Y. Shin and K. Amine) for the high-energy composite, at PNNL for the S-based cathode and Li-metal anode materials, and with ORNL on neutron scatterings. This project will also collaborate with industrial partners at GM and Johnson Controls, as well as with international collaborators.

Milestones

1. Complete the first-stage development of diagnostic techniques to study and improve performance of high-energy-density Li-ion batteries and Li/S batteries. (Q1, FY 2020; Completed)
2. Complete hard X-ray fluorescence (XRF) imaging on the concentration gradient Ni-rich NCM cathode particles in a noninvasive manner with 3D reconstructed images through tomography scans to study the 3D nickel, cobalt, and manganese elemental distribution from surface to the bulk. (Q2, FY 2020; Completed)
3. Complete hard X-ray absorption spectroscopy (hXAS) and soft XAS (sXAS) on the concentration gradient Ni-rich NCM cathode particles to study the valence state changes of nickel, cobalt, and manganese at the surface and bulk. (Q3, FY 2020; Completed)
4. Complete spatially resolved XAS at sulfur K-edge and imaging of sulfur-based chemical species using XRF on the Li-metal anode in a cycled high-energy Li/S pouch cell. (Q4, FY 2020; Completed)

Progress Report

This quarter, the fourth FY 2020 milestone was completed. BNL has been focusing on developing new diagnostic techniques to study high-energy-density Li-ion batteries and Li/S batteries to provide valuable information for improving their performance. The BNL team carried out spatially resolved XAS at sulfur K-edge and imaging studies of sulfur-based chemical species using XRF on the Li-metal anode in a cycled high-energy Li/S pouch cell using electrolyte with $LiNO_3$ (LNO) comparing with electrolytes without LNO additives. The following conclusions were obtained from the results shown in Figure 48:

- After adding LNO, TFSI decomposition was suppressed due to participation of NO_3^- in SEI formation, producing less Li_2S, SO_3^{2-}, and S-S species as confirmed by XAS and XRF results.
- XRF images of Li-metal anode cycled in TFSI-DOL/DME and FSI-DOL/DME electrolytes show different lithium deposition morphology. XAS spectra show that TFSI and FSI salts have almost similar decomposition products, but with different concentration. SO_3^{2-} cannot be detected from Li-metal surface cycled in FSI-based electrolyte.
- Intensity of Li_2S formed in FSI-DX electrolyte is slightly higher than that formed in FSI-DOL/DME, indicating more FSI^- anion decomposed on Li-metal anode.

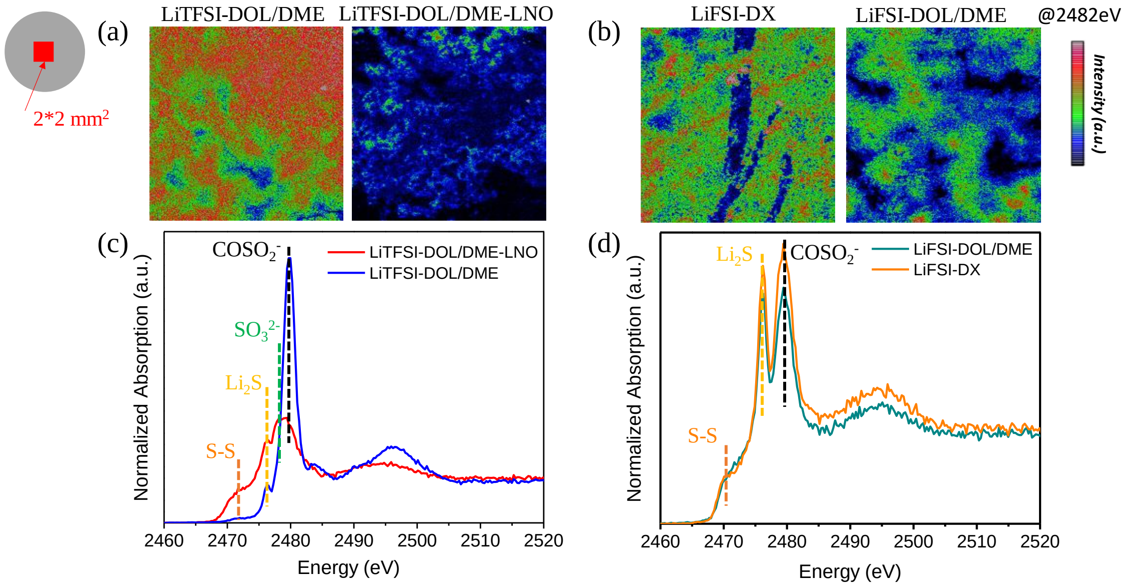

Figure 48. X-ray fluorescence image of Li-metal anodes cycled in (a) LiTFSI-DOL/DME, LiTFSI-DME/DOL-$LiNO_3$, and (b) LiFSI-DX, LiFSI-DME/DOL electrolytes after 10 cycles. Data were measured at an incident beam energy of 2480 eV. (c-d) Normalized sulfur K-edge X-ray absorption spectra measured from the selected area in (a-b).

Patents/Publications/Presentations

Publication

- Shi, L., S-M. Bak, Z. Shadike, C. Wang, C. Niu, P. Northrup, H. Lee, A. Y. Baranovskiy, C. S. Anderson, J. Qin, S. Feng, X. Ren, D. Liu, X-Q. Yang, F. Gao, D. Lu,* J. Xiao,* and Jun Liu.* "Reaction Heterogeneity in Practical High-Energy Lithium–Sulfur Pouch Cells." *Energy & Environmental Science* (2020). doi: 10.1039/d0ee02088e. Publication Date (Web): September 4, 2020.

Task 2.4 – Probing Interfacial Processes Controlled Electrode Stability in Rechargeable Batteries (Chongmin Wang, Pacific Northwest National Laboratory)

Project Objective. The main objective of the proposed research is to explore interfacial phenomena in rechargeable Li-ion batteries of both solid-state and LE configuration, to identify the critical parameters that control the stability of interface and electrodes as well as SE. The outcome will be establishing correlations between structural-chemical evolution of active components of batteries and their properties. These correlations will provide insight and guidance to battery materials development groups for developing high-performance battery materials.

Project Impact. The proposed characterization work focuses on atomic-level structural and chemical analysis and direct correlation with battery fading properties. The work can be directly used to guide design of electrode materials with tailored microstructure and chemistry for enhanced properties of increasing the energy density of Li-ion batteries and to accelerate market acceptance of EVs, especially for PHEVs as required by the EV Everywhere Grand Challenge.

Approach. The project will use integrated advanced microscopic and spectroscopic techniques, including *in situ* S/TEM and *ex situ* S/TEM, environmental S/TEM, cryo-electron microscopy, and *in situ* liquid SIMS to directly probe the structural and chemical information during lithium deposition and stripping. Cryo-S/TEM with analytical tools, such as EDX and EELS, will be used to gain chemical and electronic structural information at the interface between lithium metal and electrolyte of both solid-state and liquid configuration, which will allow direct correlation between the morphology and chemistry. STEM – high-angle annular dark-field (HAADF) atomic-level imaging and EDX/EELS will be used to probe the interface and bulk lattice stability. The work will be in close collaboration with the battery development group within the BMR and U. S.–Germany Collaboration on Energy Storage.

Out-Year-Goals. This project has the following out-year goals:

- Atomic-level multi-scale *ex situ* / *in situ* and *operando* TEM and cryo-TEM investigation of failure mechanisms of energy-storage materials and devices; develop fundamental understanding of electrochemical energy-storage processes and kinetics of electrodes.
- Develop new *in situ* TEM capability for probing challenging questions related to energy storage technology.

Collaborations. This project collaborates with G. Chen (LBNL); J. Nanda (ORNL); K. Amine (ANL); D. Wang (PSU); A. Manthiram (UT Austin); W. Tong (LBNL); Y. Cui (Stanford University); J. Zhang (PNNL); J. Liu (PNNL); W. Xu (PNNL); X. Jie (PNNL); D. Lu (PNNL); X. Xiao (GM); S. Meng (UCSD); and M. S. Whittingham [State University of New York (SUNY) at Binghamton].

Milestones

1. Integrate AFM cantilever into TEM column to *in situ* measure lithium dendrite growth force. (Q1, FY 2020; Completed)
2. Identify correlation of SEI structure and chemistry with electrolyte composition and electrochemical operating condition. (Q2, FY 2020; Completed)
3. Establish molecular signature of SEI formation process. (Q3, FY 2020; Completed)
4. Establish cathode stability in solid-state configuration. (Q4, FY 2020)

Progress Report

Current density has been perceived to play a critical role for controlling lithium deposition morphology and SEI. However, the atomic-level mechanism of current density on lithium deposition and the SEI remains unclear. In this study, the team explores the fundamental mechanism behind the current density effect on electrochemically deposited lithium metal (EDLi) and SEI.

By applying high-resolution cryo-TEM, EDX, and EELS techniques, the team characterizes the detailed structure and chemical distribution of EDLi and SEI layers with systematic control of current density, to establish the correlation between electrochemical performance (interfacial impedance) and current density induced structure and chemical evolution. The morphologies of EDLi and SEI are characterized in the electrolyte of 1.2 M $LiPF_6$/EC-EMC with vinylene carbonate (VC) additive under a systematically controlled variation of current density.

The team found that both lithium growth and SEI morphology/structure depend on the current density. As shown in Figure 49, the EDLi whiskers that formed at a very low current density (0.1 mA cm^{-2}) exhibit nonuniform distribution with various diameters. The EDLi formed at current densities of 2 to 9 mA cm^{-2} shows whisker-like configurations, but with different density numbers, especially at high current density of 9 mA cm^{-2}. All whiskers are crystalline lithium metal, as indicated in Figure 50. The team established that increasing current density leads to increased overpotential for lithium nucleation and growth, leading to the transition from growth-limited to nucleation-limited mode for lithium dendrite.

The present results establish the correlation among lithium deposition condition, dendrite growth kinetics, and SEI formation mechanism, shedding light on the optimization of the lithum morphology and electrode-electrolyte interface. These results offer possible ways of regulating crucial microstructural and chemical features of EDLi and SEI through altering deposit conditions and consequently direct correlation with battery performance.

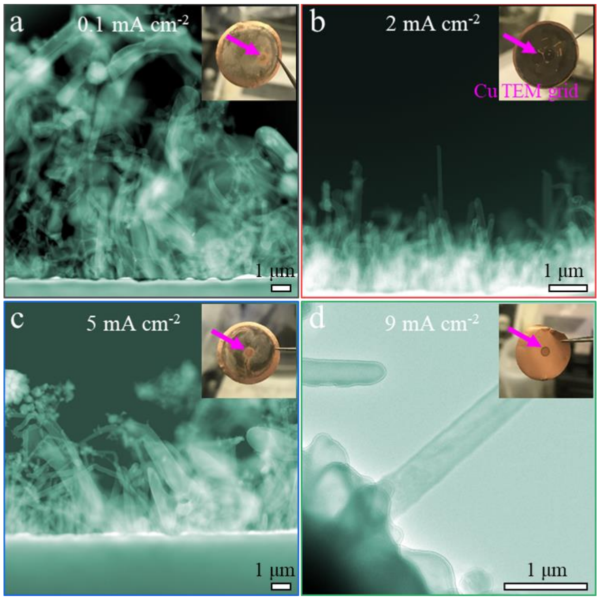

Figure 49. Low magnification transmission electron microscopy images of lithium deposits in 1.2 M $LiPF_6$ in EC-EMC (3:7 by wt) electrolyte with 5% VC under current density of (d) 0.1 mA cm^{-2}, (e) 2 mA cm^{-2}, (f) 5 mA cm^{-2}, and (g) 9 mA cm^{-2} at lower magnification. Insets: Digital photos of deposited lithium.

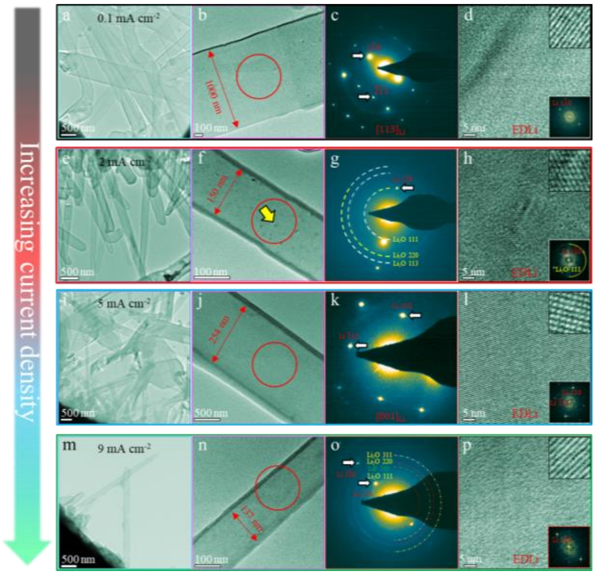

Figure 50. Nanostructure evolution of EDLi as a function of current density. (a-d) Bright field transmission electron microscopy (TEM) images and atomic resolution TEM images of the EDLi at current density of 0.1 mA cm^{-2} for 100 minutes. (e-h) 2 mA cm^{-2} for 5 minutes. (i-l) 5 mA cm^{-2} for 2 minutes. (m-p) 9 mA cm^{-2} for 1.1 minutes. Insets: Corresponding selected area electron diffraction patterns, enlarged area from EDLi, and their corresponding fast Fourier transform patterns.

Patents/Publications/Presentations

Publications

- Unocic, R. R., K. L. Jungjohann, B. L. Mehdi, N. D. Browning, and C. Wang. "*In Situ* Electrochemical Scanning/Transmission Electron Microscopy of Electrode-Electrolyte Interfaces." *MRS Bulletin* 45 (2020): 738-745.
- Jin, Y., Y. Xu, P. M. L. Le, T. D. Vo, Q. Zhou, X. Qi, M. H. Engelhard, B. E. Matthews, H. Jia, Z. Nie, C. Niu, C. Wang, Y. Hu, H. Pan, and J-G. Zhang. "Highly Reversible Sodium Ion Batteries Enabled by Stable Electrolyte-Electrode Interphases." *ACS Energy Letters* 5 (2020): 3212-3220.
- Zhang, X., L. Zou, Y. Xu, X. Cao, M. H. Engelhard, B. E. Matthews, L. Zhong, H. Wu, H. Jia, X. Ren, P. Gao, Z. Chen, Y. Qin, C. Kompella, B. W. Arey, J. Li, D. Wang, C. Wang, J-G. Zhang, and W. Xu. "Advanced Electrolytes for Fast-Charging High-Voltage Lithium-Ion Batteries in Wide-Temperature Range." *Advanced Energy Materials* (2020): 2000368.

Task 2.5 – Integrated Atomic-, Meso-, and Micro-Scale Diagnostics of Solid-State Batteries (Yi Cui, William Chueh, and Michael Toney; Stanford University / SLAC National Accelerator Laboratory)

Project Objective. By developing a characterization toolkit that tackles length scales (Å to mm), cell pressure (1-100 bars), and dynamics (during synthesis, fabrication, and cycling), the project aims to generate insights to engineer SSBs for deployment in EVs. This interdisciplinary team aims to achieve this objective by merging a broad range of characterization approaches as well as modeling to track the evolution of nanoscale chemistry and structure, microstructure, and transport.

Project Impact. The project will have an impact in several areas: (1) accelerate rational design of coatings and artificial SEIs in SSBs; (2) inhibit the root causes leading to cell shorting, and enable high current cycling; (3) accelerate design of cathode coating and composite electrode architectures; and (4) reduce degradation and variability during SSB manufacturing via composition and surface engineering.

Approach. The project has a multi-fold approach that will encompass the following: (1) resolve nanoscale structure and chemistry of SEIs via cryo-TEM; (2) track SE and lithium microstructure evolution in 3D via X-ray micro and diffraction tomography; (3) visualize nanoscale ionic and electronic transport at GBs via conducting AFM; (4) map current distribution in cathodes via scanning transmission X-ray microscopy (STXM); and (5) monitor nanoscale SE evolution with gas impurity via *in situ* environmental TEM (E-TEM).

Out-Year Goals. The project will develop an integrated characterization toolkit to characterize SSBs within a single cycle and over hundreds of cycles, spanning a wide range of relevant length scales.

Collaborations. Project collaborations include work with SSRL, ALS, and Advanced Photon Source (APS) synchrotron light sources.

Milestones

1. Design, build, and test *operando* SSB cell for depth-resolved XAS. (Q1, FY 2020; Completed)
2. Record micro-tomograms of Li/SE/Li half cells for 10 cycling conditions. (Q2, FY 2020; Completed)
3. Record DC conducting AFM map of pristine SEs. (Q3, FY 2020; Completed)
4. Prepare X-ray transparent cathode / SE by cryo-sectioning. (Q4, FY 2020; Completed)

Progress Report

This quarter, the team employed the *operando* X-ray micro-tomography capability developed within the BMR program to understand short-circuiting in Li/LPS/Li cells under both cycling conditions and open-circuit conditions. The *operando* cells employed a 2-mm LPS pellet that is transparent to X-rays. The PEEK cell is hermetically sealed, and the uniaxial pressure is set before measurement. Previous development shows that fracture of cells can be detected at the several microns spatial resolution, though metallic lithium cannot be detected directly due to low absorption contrast. The electrochemistry, including EIS, matches well to larger-formfactor cells, confirming that the team is able to achieve representative performance in the *operando* cell.

In the literature, substantial fracture and microstructure evolution has been reported in sulfide SE. However, none was observed in the team's experiments. In fact, fractures were rare, often only one cycling-induced fracture is detected in the 2-mm cell. The team rationalizes this discrepancy with previous reports by noting a significant difference in the density. In literature, substantial porosity can be detected in tomography even before cycling. In the project's cells, the density is close to theoretical value due to the high compaction pressure during cold pressing and cell assembly. Therefore, the team believes that their results are more indicative of real cell behavior. They speculate that literature results showing substantial fracturing is due to lithium plating within the internal pore, which then subsequently grows to fracture the cell. Their observations suggest that small cracks accompanying narrow lithium dendrites (on the order of microns in diameter) are responsible for shorting and failure.

Sulfides are metastable against lithium, so the team also performed open-circuit experiments to understand the calendar life. They observed that under sufficient mechanical pressure, short-circuiting can occur on the order of tens to hundreds of hours. Using X-ray micro-tomography, they monitor the progression of the short. Under high pressure conditions, they observe direct chemical reaction between lithium and LPS, which produces a product that then fractures the cell near the lithium/LPS interface. The reaction and the fracture then propagate into the center of the SE pellet, eventually causing a short circuit. This product is optically distinct from LPS. Structure and chemical analysis is under way to identify the phase.

Patents/Publications/Presentations

Presentations

- KAIST (formerly the Korea Advanced Institute of Science and Technology) Emerging Materials e-Symposium, Virtual (September 22, 2020): W. C. Chueh.
- ACS National Meeting, Virtual (August 17, 2020): W. C. Chueh. Three presentations.
- Stanford StorageX International Symposium, Stanford University, Stanford, California (July 24, 2020): W. C. Chueh.

Task 2.6 – Investigating the Stability of Solid/Solid Interface (Zonghai Chen, Argonne National Laboratory)

Project Objective. The project objective is to characterize the physical/chemical properties of species at the solid/solid interfaces and to fundamentally understand the critical issues that limit the mechanical, chemical, and electrochemical stability of solid/solid interfaces at the cathode and the anode.

Project Impact. The project will lead to several areas of impact: (1) to generate knowledge that supports the rational design of materials and process development; (2) to establish structure-properties relationship of the interface; and (3) to understand the formation mechanism of lithium dendrite and to predict potential solutions.

Approach. The project approach is multi-fold: (1) understanding the physics behind the transformation between the low conductivity phase and the high conductivity phase; (2) investigating the bonding strength of the cathode/electrolyte interface using model systems; and (3) developing electrolytes with high ionic conductivity and good bonding to cathodes through cation doping.

Out-Year Goals. The project has the following out-year goals:

- Developing synchrotron-based diagnosis tools to investigate physical/chemical properties of solid/solid interface.
- Identifying mechanistic barriers that limit the chemical/mechanical/electrochemical durability of solid/solid interface.
- Developing model systems to validate the failure mechanism of solid/solid interface.

Collaborations. The project collaborates with A. Ngo (ANL), L. A. Curtiss (ANL), V. Srinivasan (ANL), Y. Ren (ANL), J. Libera (ANL), T. Li (Northern Illinois University), F. Wang (BNL), X. H. Xiao (BNL), and D. Chen (UH).

Milestones

1. Forming model Ta-LLZO/NMC-622 interface for physical diagnosis. (Q1, FY 2020; Completed)
2. Investigating the interaction between Ta-LLZO and NMC-622 at the interface on cycling. (Q2, FY 2020; Completed)
3. Investigating the chemical reactions of Ta-LLZO at the reducing environment. (Q3, FY 2020; Completed)
4. Investigating the chemical/mechanical stability of Li/Ta-LLZO interface. (Q4, FY 2020; In progress)

Progress Report

Last quarter, efforts were focused on the interaction between LLZO powder and the processing environment during hot press. The team found the cubic LLZO, regardless of the doping chemistry, can be hot pressed into a condensed pellet, the surface layer (~ 50 microns in thickness) decomposed during hot press, and then converted into ionic isolator $La_2Zr_2O_7$. An aggressive polishing process was adopted to remove the surface layer before assembling symmetric Li/LLZO/Li cells.

Figure 51a shows that the voltage profile of a symmetric cell with repeated lithium stripping/plating for 1000 hours cycles with a constant current of 1 mA/cm^2. Figure 51a clearly shows the voltage profile continuously increases with the testing time, suggesting a slow reaction between the lithium metal and LLZO electrolyte that results in a continuous increase of interfacial impedance. To accelerate this degradation process, another symmetric cell was assembled and tested at a higher current density of 2 mA/cm^2. Figure 51b shows that the reaction between lithium metal and LLZO was significantly accelerated at higher current density. After about 23 hours, the cell showed a substantial increase on the overpotential. At this point, the cell was opened in the glovebox, and the LLZO pellet was recovered from the cell. Visually, the LLZO pellet maintained shining flat surfaces. However, the SEM images of the electrolyte pellet clearly showed big damage on the surface of the electrolyte (see Figure 52). Clustered cracks at micron scale were observed all over the surface of the electrolyte pellet. The SEM images in Figure 52 show that the electrolyte pellet still maintains a flat surface, even after the crack. It appears that the damage was caused from inside out, instead of pinning outside in. From here, an *in situ* SEM experiment will be conducted to observe the lithium plating and identify the mechanism of the surface damage.

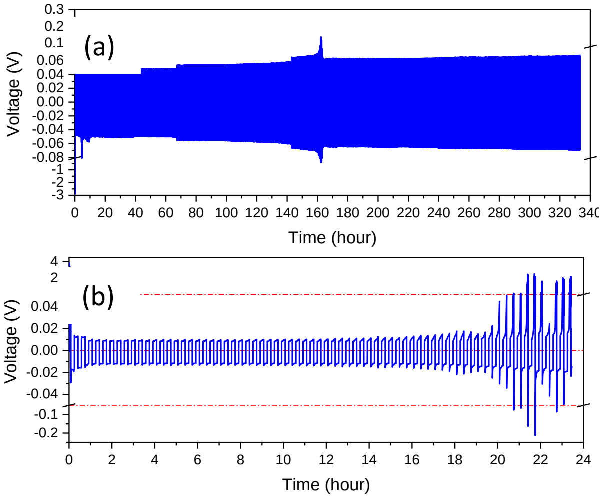

Figure 51. The voltage profile of Li/La-LLZO/Li symmetric cell for repeating lithium stripping/plating at (a) 1 mA/cm^2 and (b) 2 mA/cm^2.

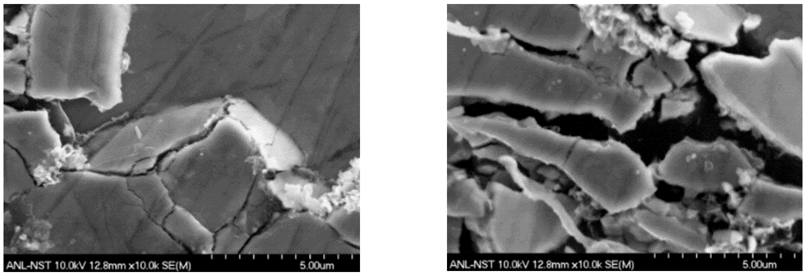

Figure 52. Scanning electron microscopy images of the surface of LLZO pellet after repeating lithium stripping/platting at 2 mA/cm^2.

Patents/Publications/Presentations

The project has no patents, publications, or presentations to report this quarter.

Task 2.7 – Fundamental Understanding of Interfacial Phenomena in Solid-State Batteries (Xingcheng Xiao, General Motors)

Project Objective. The project objective is to develop a comprehensive set of *in situ* diagnostic techniques combined with atomic/continuum modeling schemes to investigate and understand the coupled mechanical/chemical degradation associated with dynamic interfacial phenomena in SSBs. Specifically, *in situ* observations and characterizations of lithium plating-stripping processes, lithium dendrite formation, interphase formation, and the induced interfacial stresses, as well as the mechanical and electrochemical properties of interfaces and interphases, are paramount. The study will provide useful guidelines for optimizing cell structure design and engineering interfaces and interphases to enable SSBs.

Project Impact. The project will provide fundamental understanding of the dynamic interfacial phenomena and the coupled mechanical and chemical degradation. In addition, it will establish a critical guideline to design safe and durable SSBs with energy density > 500 wh/kg for EV applications.

Approach. The multiscale *in situ* diagnostic tools, including AFM, nanoindentation, dilatometer, stress sensors, and pressure cells, will be used to investigate mechanical behavior and microstructure evolution at interface/interphase during lithium plating and stripping. The information (along with Li-ion transport properties and microstructure evolution obtained using the advanced spectroscopic ellipsometry, and *in situ* TEM) will be correlated with electrochemical performance toward high cycle efficiency and dendrite-free SSBs. The goal of this understanding is to develop strategies for surface and interface engineering, apply them to commercially available SEs (including powder, pellets, and foils), and assemble SSBs for further validation and optimization, eventually extending cycle life for EV application.

Out-Year Goals. The project seeks to develop SSB model systems to capture critical mechanical properties and probe the coupled mechanical-chemical degradation by further developing comprehensive *in situ* diagnostic tools. All results obtained from these *in situ* studies, combined with advanced postmortem analysis and modeling, will be correlated with the cycling stability of SSBs. The *in situ* tools developed will be applied to the following two periods to deeply understand the coupled mechanical and chemical degradation of interface/interphase.

Collaborations. The co-PIs involved in experiments and simulation will be as follows: B. W. Sheldon (Brown University), Y-T. Cheng and A. Seo (University of Kentucky), Y. Qi (Michigan State), and Q. Zhang (GM).

Milestones

1. Thin-film electrode system for different *in situ* electrochemical tests developed. (Q1, FY 2020; Completed)
2. Thin-film SE system established with the comparable ionic conductivity reported in the literature. (Q2, FY 2020; Completed)
3. *In situ* electrochemical-mechanical tools established. (Q3, FY 2020; Completed)
4. A rank of the interfacial adhesion between SE and electrodes determined. (Q4, FY 2020; Ongoing with no cost extension)

Progress Report

Interface Design Based on the Electronic Origin of Coating Materials

Since the limiting stripping current density J_C is interface sensitive, it will be insightful to determine which energy barrier is the most effective to allow lithium vacancy to diffuse into the bulk faster. Apparently, based on the project's study, this is not the lithium bulk diffusion. In the kinetic Monte Carlo (KMC) test at Li/LiF interface (Figure 53a), the forward interfacial lithium hopping barrier ($\Delta E_{2\rightarrow1}$) is reduced from 0.332 and 0.561 to 0.05 eV (Figure 53b), and the backward interfacial lithium hopping barrier ($\Delta E_{1\rightarrow2}$) is increased from 0.0 to 0.6 eV for both bonding and non-bonding atoms at the interfaces (Figure 53c). Apparently, the reduction in $\Delta E_{2\rightarrow1}$ plays the main role in facilitating the void filling at the interface, since more vacancies migrated toward the bulk region after the reduction of $\Delta E_{2\rightarrow1}$.

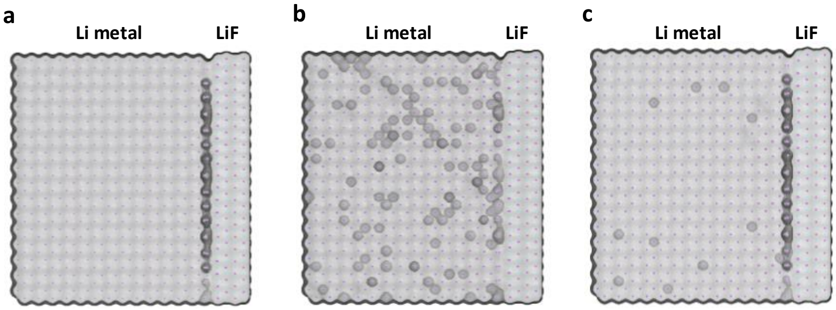

Figure 53. Factors affecting vacancies evolution.

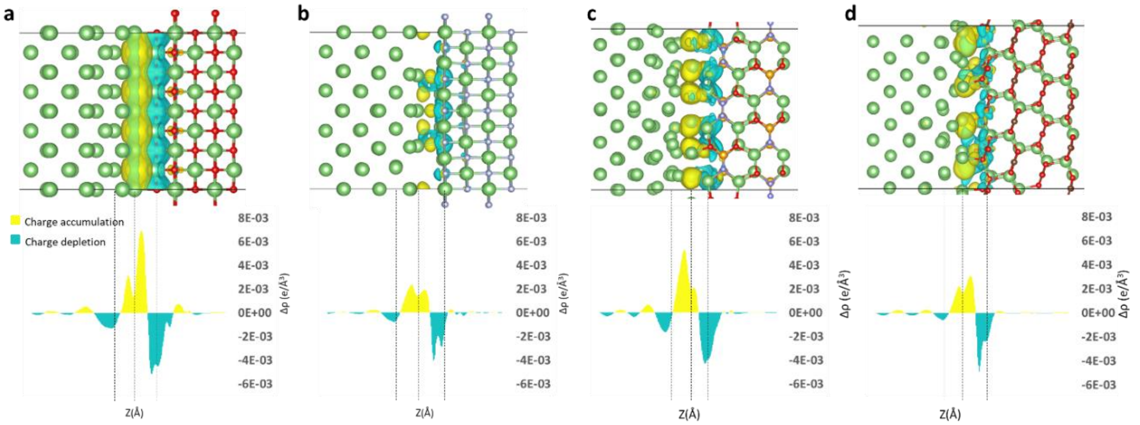

Figure 54. Charge density difference (upper panel) and planar-averaged charge density difference (lower panel).

Therefore, it is important to find coating materials that repel lithium vacancy away from the interface and reduce the energy barrier for lithium to move toward the interface, which can be evaluated based on density function theory (DFT) computable interfacial properties. The work of separation of Li(001)/Li_2O (110) is 1.11 J/m^2, and is 0.28 J/m^2 for Li/LiF. Therefore, Li/Li_2O is lithiophilic and Li/LiF is lithiophobic. Understanding bonding nature and the electronic structures of these interfaces will help to guide coating material design to maintain a smooth lithium surface with high CCD. A simple rationalization to explain the difference of Li/Li_2O and Li/LiF interface is that the Li_2O(110) surface exposes two-lithium under-coordinated oxygen atoms, and LiF(001) surface exposes one-Li under-coordinated fluorine atoms. Although both have developed direct Li-O and Li-F bonds after interface relaxation, some oxygen atoms of Li_2O(110) are still undercoordinated, so it can attract more lithium, and thus is lithiophilic. To quantify the bonding characteristics, the electronic structure origin of the lithiophilic and lithiophobic surfaces was analyzed. The (planar) charge density difference (CDD) was studied (Figure 54). It can be seen that the electron density transferred from SEI materials to the interfaces, and more electron density accumulates at the Li/Li_2O interface than that at the Li/LiF interface. This enhanced electron density can attract more lithium toward the interface, making the Li/Li_2O interface lithiophilic, as well as creating a stronger interfacial adhesion.

Both interfacial adhesion and accumulation of electron density at the interface indicate they are features for lithiophilic interfaces. This observation can be used to guide the coating design and predict lithium morphology during delithiation based on work of separation and interfacial electron charge transfer plot for Li/LiPON and Li/Li_2CO_3 interfaces. LiPON is a SSE with outstanding electrochemical performance, and in this work was represented by Li_2PO_2N with the stable (100) surface. The work of separation of Li/LiPON interface is 0.64 J/m^2, and the (planar) CDD (Figure 54c) is comparable to that of Li/Li_2O (Figure 54a). Li/LiPON interface is likely lithophilic and is predicted to maintain a smooth lithium surface during stripping. Li_2CO_3 is not only a common SEI material, it also appears on LLZO surfaces after exposing to air. Li/Li_2CO_3(001) has been experimentally reported to be lithiophobic, and the computed work of separation is 0.30 J/m^2 and the (planar) CDD (Figure 54d) shows comparable magnitude, with Li/LiF, suggesting lithium surface to be rough during delithiation and that a slower critical current is necessary to maintain a smooth surface to avoid lithium dendrite growth in the next cycle, consistent with the experiment that removing Li_2CO_3 layer on LLZO surface can help to avoid lithium dendrite growth.

Interfacial Design. With the help of interfacial coating, the above problems can be eliminated, and performance can be improved. Here, a mixture composed of three materials is used to coat lithium metal, including $LiNO_3$, 1,2-dimethoxy-ethane (DME), and trimethyl phosphate (TMP). $LiNO_3$ is a well-known additive in LE, and TMP promotes the solubility of $LiNO_3$ in DME. Li_3PO_4 is formed by reduction reaction between lithium metal and TMP. As a result, the coating layer composed of Li_3PO_4 and $LiNO_3$ is formed, and the interfacial properties are improved when utilizing the coated lithium metal with SSE. LAGP is short for $Li_{1.5}Al_{0.5}Ge_{1.5}(PO_4)_3$, and it possesses a Li-ion conductivity of 5 x 10^{-4} S/cm at room temperature. However, the germanium is easily reduced by lithium metal, and this reaction is not self-limiting since the side-reaction product is a mixed electronic and ionic conductive phase. The impedance and cycle performance are shown in Figure 55. Reference LAGP has an initial high impedance of 1*10^6Ω, and the impedance is increased by 4 times after 3 hours of rest, indicating an instant chemical side reaction when LAGP contacts with lithium metal. Due to the high impedance, the 1V cut-off voltage is reached instantly after 5µA current is applied. 1hr_Sample has an initial low

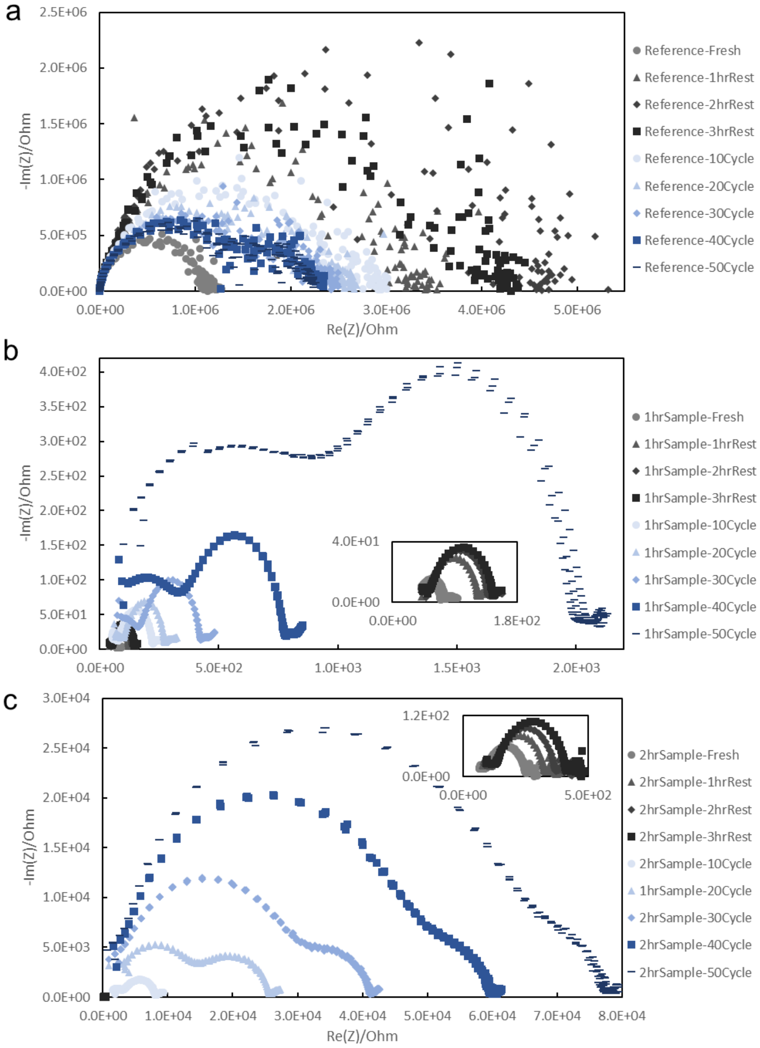

Figure 55. Impedance and cycle performance of reference, 1hr_Sample and 2hr_Sample. (a-c) Impedance increase during 3hr_Rest and 50_Cycle.

impedance of 70 Ω, which is a substantial improvement compared with the reference. During the 3-hour rest, impedance is increased into 146 Ω. After 50 cycles, impedance is increased to 2,000 Ω, and the overpotential is less than 0.15 V. 2hr_Sample has an initial impedance of 250 Ω, which is also an improvement compared with the reference. During the 3-hour rest, impedance is increased into 410 Ω. After 50 cycles, impedance is increased to 78,000 Ω, and the overpotential is around 0.45 V. Among 1hr_Sample and 2hr_Sample, 1hr_Sample has the best protection and significantly improved the cycle stability between lithium metal and LAGP.

Patents/Publications/Presentations

Patent

- Xiao, X., M. Chen, Q. Zhang, and M. Cai. A Solution-Based Approach to Protect Lithium Metal Electrode. P053352.

Publication

- Yang, C-T., Y. Lin, B. Li, X. Xiao, and Y. Qi. “The Bonding Nature and Adhesion of Polyacrylic Acid (PAA) Coating on Li-Metal for Li Dendrite Prevention.” *ACS Applied Materials & Interfaces*. Accepted.

Task 2.8 – Multidimensional Diagnostics of the Interface Evolutions in Solid-State Lithium Batteries (Yan Yao, University of Houston)

Project Objective. The project objective is to develop a platform combining FIB-SEM tomography, TOF-SIMS, and in-SEM nanoindentation-based stiffness mapping for structural, chemical, and mechanical characterizations in SSLBs. Assessment of the influence of cell design and testing conditions (external pressure, current density, temperature) on the evolutions of interfaces will be performed.

Project Impact. The consolidated *in situ* structural–chemical–mechanical diagnostic platform established in this project will provide unprecedented insights into the failure mechanisms of SSLBs.

Approach. Space- and time-resolved structural, chemical, and mechanical characterizations of the cathode–electrolyte and anode–electrolyte interfaces will be performed on all-solid-state lithium batteries using FIB-SEM, TOF-SIMS, and in-SEM nanoindentation. Tasks include the following: (1) development of solid-state cell thin stacks and test-cell configurations that are suitable for *in situ* characterizations; (2) quantitative characterization and *in situ* tracking of interfacial voids formation within composite cathode and electrolyte layer; (3) identification and *in situ* tracking of the chemical composition, spatial distribution, and mechanical properties of electrolyte decomposition products at the lithium- and cathode-electrolyte interfaces; and (4) visualization, chemo-mechanical properties detection, and *in situ* tracking of lithium dendrites grown within the SE layer.

Out-Year Goals. In the out years, the project will develop thin-stack solid-state cells, micro-cells, in-SEM nanoindentation, and testing protocols. The correlation between structural evolution, electrolyte decomposition, and interfacial resistance increase will be investigated.

Collaborations. The UH team (Y. Yao, Z. Fan, and Y. Liang) works closely with the Rice University team (J. Lou and H. Guo).

Milestones

1. Thin-cell stack development. (Q2, FY 2020; Completed)
2. Micro-cell development. (Q3, FY 2020; Completed)
3. Nano-cell development. (Q4, FY 2020; In progress, 6-month no-cost extension requested)
4. Cell optimization and electrochemical benchmarking. (Q4, FY 2020; 6-month no-cost extension requested)

Progress Report

The fabrication of tape-cast electrolyte thin films has been systematically studied. Traditional tape-casting focuses on a variety of methods to improve the resulting films that share a common theme of maximizing the solids content in the casting slurry as part of the development process. The solids content or loading is typically taken to a maximum value to obtain the best quality before the casting slurry becomes too viscous for the art. The team has therefore focused on solid content to improve the quality of the cast films.

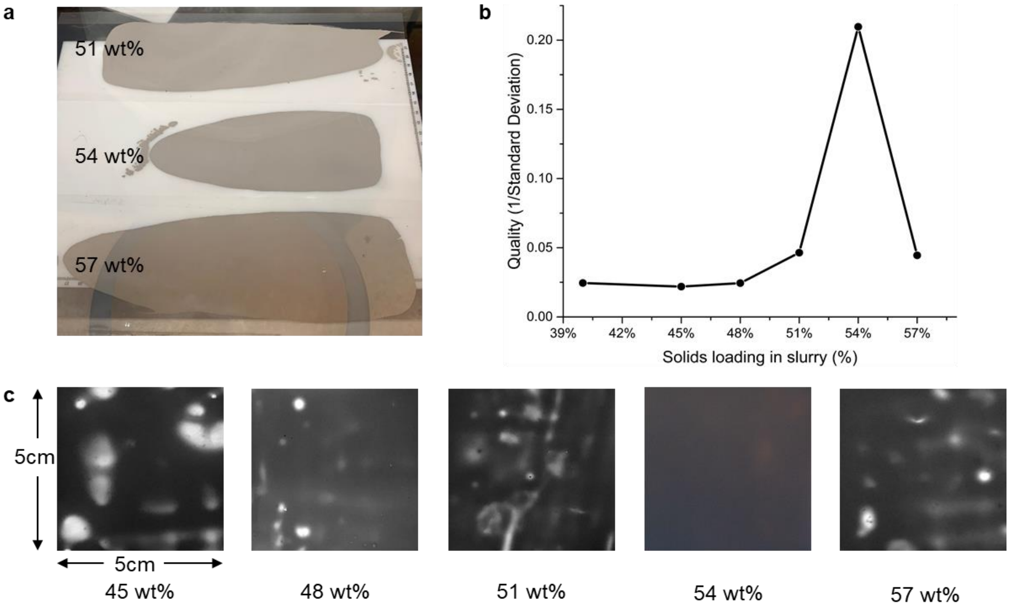

Figure 56. Quality assessment of LPSCl thin films. (a) Optical images of films cast with slurry containing 51–57 wt% of solid content. (b) Correlation of film quality with solid content in the casting slurry. (c) Optical images of back-illuminated films cast with slurry containing 45–57 wt% of solid content.

The team's initial study includes visually looking at the films prepared with different solid contents. When the solid content of the casting slurry of LPSCl is 45 wt% or less, very obvious defects occur on the surface of the films, some of which are at the centimeter scale. Starting from 51 wt%, it is difficult to see the defects under normal lighting conditions (Figure 56a). Therefore, the team has visualized the films with backside illumination. Films cast with slurries containing 45–57 wt% have been visualized at a 5 × 5 cm^2 scale (Figure 56c). Notable defects are observed even for those apparently defect-free films (that is, films cast from slurries with 51–57 wt% solid content). The quality of the film may be quantified by the grayscale deviation of the images, which reflects the uniformity of the films. A large standard deviation of the grayscale of an image indicates poor film uniformity. Therefore, the film quality can be described by the reciprocal of the standard deviation of the grayscale. Figure 56b shows that at a solid content of 54 wt%, the slurry gives the most uniform films.

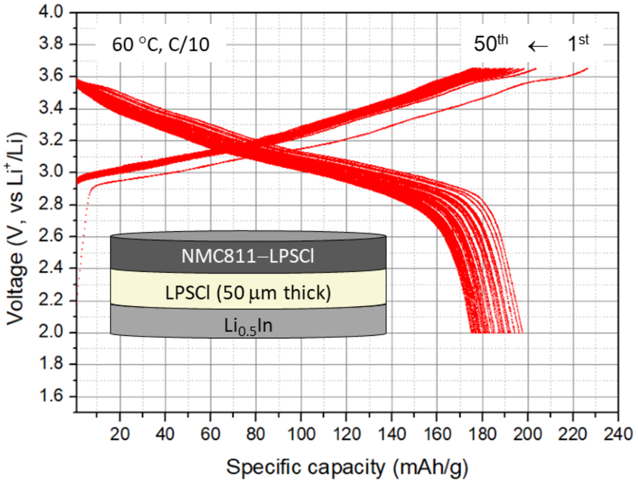

Figure 57. Voltage profile of an NMC–LPSCl/LPSCl/$Li_{0.5}In$ thin cell (total thickness 100 μm).

The optimized electrolyte thin films have enabled highly reproducible thin cells. The performance of a thin cell based on the optimized electrolyte film is shown in Figure 57. The cell has an areal capacity of 1 mAh cm^{-2}. An initial capacity of 198 mAh g^{-1} is achieved, and 89% of the capacity is preserved after 50 cycles at C/10 at 60°C. This performance is on par with that observed for bulk-type solid-state cells. Therefore, diagnostics based on the optimized thin cell will be representative of the behavior of NMC observed from typical studies.

Patents/Publications/Presentations

Presentations

- ECS PRiME 2020, Virtual (October 4–9, 2020): "Solution-Processable All-Solid-State Batteries: Insight to Uniform Electrolyte Layer": B. Emley, Y. Liang, C. Wu, J. Zhang, Z. Chen, Z. Fan, and Y. Yao.
- ECS PRiME 2020, Virtual (October 4–9, 2020): "Accelerated Modeling of Lithium Diffusion in Solid State Electrolytes Using Artificial Neural Networks"; K. K. Rao, Y. Yao, and L. C. Grabow.

TASK 3 – MODELING

Summary and Highlights

Achieving the performance, life, and cost targets outlined by VTO will require moving to next-generation chemistries, such as higher capacity Li-ion intercalation cathodes, silicon and other alloy-based anodes, Li-metal anode, and sulfur cathodes. However, numerous problems plague development of these systems, from material-level challenges in ensuring reversibility to electrode-level issues in accommodating volume changes, to cell-level challenges in preventing cross talk between the electrodes. In this task, a mathematical perspective is applied to these challenges to provide an understanding of the underlying phenomenon and to suggest solutions that can be implemented by the material synthesis and electrode architecture groups.

The effort spans multiple length scales, from *ab initio* methods to continuum-scale techniques. Models are combined with experiments, and extensive collaborations are established with experimental groups to ensure that the predictions match reality. Efforts also focus on obtaining parameters needed for the models, either from lower-length scale methods or from experiments. Projects also emphasize pushing the boundaries of the modeling techniques used to ensure that the task stays at the cutting edge.

A major focus of the effort is around Li-metal-based SSBs. While these chemistries hold promise, numerous challenges such as reactivity, conductivity, and mechanical stability prevent their commercialization. Mathematical models are ideal to provide the guidance and insights needed to solve these issues.

In the area of Li-metal anodes, the focus is on understanding how materials can be designed to prevent dendrite growth using continuum modeling approaches, combined with calculations on mobility in solid conductors. The results are used to guide materials development by providing the properties needed to prevent dendrites, while also achieving the energy and power goals. Models examine the role of the SEI on the morphology of the dendrite and describe the mechanical-electrochemical coupled effects that are critical for dendrite formation. Finally, efforts are focused on discovery of new solid ion conductors with properties that far exceed existing materials. The focus is on using these models as a guide before embarking on extensive experimentation.

Lithium metal with SEs will be paired with cathode materials, often intercalative in nature. Models are being developed to examine the solid-cathode interface in Li-metal based systems, where side reactions and interface debonding issues are known to limit cycling. These models are being used to understand how to prevent chemo-mechanical failure at the interface. Coatings, an effective strategy for high-voltage operation, are being explored with the aim of providing a rational design approach for new coating materials. In addition, focus is paid to porous electrodes with cathode particles to predict the impact of heterogeneities on electrode behavior.

Highlight. Lithium argyrodite with the composition Li-P-S-X (X = Cl, Br, or I) shows superionic conductivity for lithium ions at room temperature. However, the sodium conductivity in these materials has not yet been studied. G. Ceder's team uses DFT-based methods to calculate phase stability, electrochemical stability, and ionic conductivity of 48 types of sodium argyrodites. The prediction provides rules for this class of materials, such as importance of site occupancy on the conductivity of the sulfide classes. Results suggest that sodium argyrodites within the Na-P-Se-X (X = Cl, Br, or I) chemical space may form a good compromise among ionic conductivity, phase stability, and synthesizability.

Task 3.1 – Characterization and Modeling of Li-Metal Batteries: First-Principles Modeling and Machine Learning
(Kristin Persson, Lawrence Berkeley National Laboratory)

Project Objective. This project supports VTO programmatic goals by developing next-generation, high-energy cathode materials and enabling stable cathode operation at high voltages through target particle morphology design, functional coatings, and rational design of electrolytes. The end-of-project goals include the following: (1) understanding of the factors that govern charge transport in nonaqueous, superconcentrated LEs, (2) critical surface and coating design and optimization strategies that will improve cycling of Li-ion battery cathodes by reducing cathode degradation from oxygen loss, and (3) simulation and machine learning (ML) of the early formation of the SEI on Li-metal electrodes.

Project Impact. This project is aimed at providing fundamental insights into the atomistic mechanisms underlying surface reactivity and performance of Li-ion cathode materials and electrolytes with the ultimate goal to suggest improvement strategies, such as coatings, surface protection, novel electrolyte formulations, and particle morphology design. Transport modes as a function of solvent and salt concentrations will be clarified, and a data-driven reaction network framework will be designed and implemented to predict early SEI formation on lithium metal.

Approach. First-principles calculations, both static and dynamic approaches, are used to model SSE material thermodynamics and kinetics. LEs are modeled through coupled classical MD and first-principles methods to accurately capture solvation structure as well as reactivity of the liquid system. The reaction network is built on large-scale first-principles data, using graph theory and ML models.

Out-Year Goals. Electrolyte work will be aimed toward understanding the atomistic interactions underlying performance of lithium electrolytes, specifically elucidating conductivity (as a function of salt concentration) and impact on the charge transport mechanisms at play. Amorphous coatings will be evaluated based on ionic transport metrics and thermodynamic stability. The reaction network will be tested against known interfacial species forming on lithium metal in $LiPF_6$/EC electrolytes.

Collaborations. This project is highly collaborative between BMR PIs G. Chen (LBNL), G. Ceder (UC Berkeley), and R. Kostecki (ANL). Improved coating formulations will be examined by Chen and Ceder, and interfacial reactivity insights corroborated by Kostecki.

Milestones

1. Obtain desirable chemical and structural traits of amorphous cathode coatings. (Q1, FY 2020; Completed, December 2019)
2. Identify the lithium diffusion bottlenecks in two known coating materials. (Q2, FY 2020; Completed)
3. Quantify the conduction mechanisms in superconcentrated $LiPF_6$/PC. (Q3, FY 2020; Completed)
4. Preliminary insights into the SEI composition and reaction pathways for baseline electrolytes. First approximative reaction scheme proposed. (Q4, FY 2020; In progress)

Progress Report

The current BMR project is aimed toward using a data-driven reaction network approach to identify reaction pathways responsible for the formation of important SEI component species on lithium metal. To that end, the team has developed the HT framework capable of simulating arbitrary molecules, including charged, open shell, solvated, and metal coordinated species with calculations completing successfully over 97% of the time. They leveraged these computational workflows to perform tens of thousands of calculations to construct a chemical reaction network describing $LiPF_6$/EC SEI formation on lithium metal, including nearly 6000 species and 4.5 million reactions, orders of magnitude larger than any previously reported reaction network. They further developed a novel chemically consistent graph architecture to allow optimized pathfinding algorithms to be applied to general reaction networks for the first time to be able to tractably analyze such a massive network.

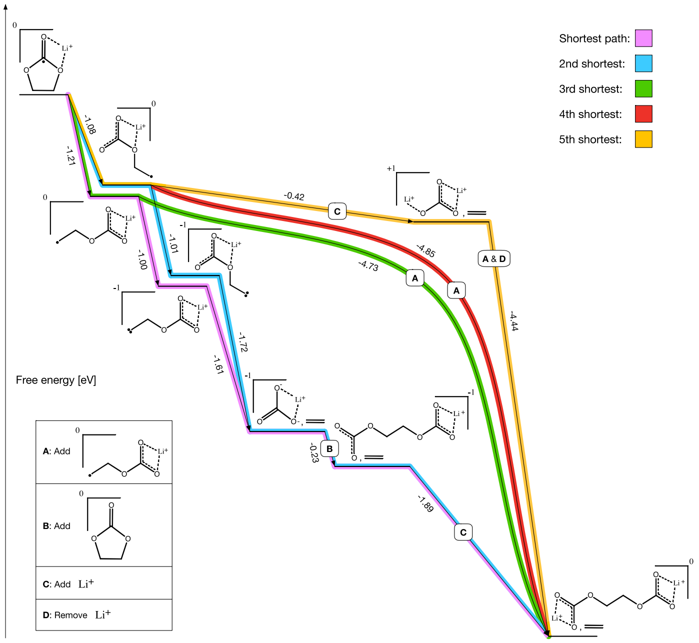

Figure 58. LEDC five shortest paths autonomously identified from a reaction network with nearly 6000 species and 4.5 million reactions.

Lithium ethylene dicarbonate (LEDC) is thought to be a majority organic component that the early SEI formed in $LiPF_6$/EC electrolytes, and its formation pathways have been studied in depth for nearly two decades, making it an ideal candidate with which to test the project's approach. By applying optimized pathfinding algorithms to identify the shortest path to LEDC in their chemical reaction network, the team autonomously identified the five low-cost formation pathways shown in Figure 58. A key validation of the approach is that both previous prominent mechanisms, originally proposed through manual investigations—the two-electron path (purple) and the one-electron path (green)—are recovered as the shortest and 3rd shortest paths, respectively. The 2nd and 4th shortest paths (blue and red) are nearly equivalent to the shortest and 3rd shortest paths, respectively, with the blue path being another two-electron mechanism and the red path being another one-electron mechanism. However, both include a counterintuitive ring-opening step that has not been previously considered because it is slightly less thermodynamically favorable than the conventional ring-opening mechanism (-1.08 eV versus -1.21 eV). Intuitively, a chemist would select the more favorable route at a given step, but in this case, non-intuitive reactions could meaningfully contribute, and the team's reaction network approach will capture such mechanisms.

The 5th shortest path (gold) is entirely novel and leverages a transient lithium ion to decompose ring-opened Li^+EC^- exergonically. Note that decomposing ring-opened Li^+EC^- in isolation is slightly endergonic according to the team's calculations (+0.25 eV), which explains why it has not previously been reported. However, their procedure autonomously identified that the coordination of an additional lithium ion simultaneous with the decomposition yields a much more thermodynamically favorable reaction (-0.42 eV), perhaps making it competitive with the other mechanisms emerging from the network. The additional lithium ion can then dissociate simultaneously with the addition of another ring-opened Li^+EC^- to form LEDC (-4.44 eV), making it a transient participant in the gold pathway. This unexpected mechanism further demonstrates the ability of the team's approach to identify new and unintuitive reaction paths that may participate in SEI formation.

Patents/Publications/Presentations

Publications

- Blau, S. M., H. D. Patel, E. W. C. Spotte-Smith, X. Xie, S. Dwaraknath, and K. A. Persson. "A Chemically Consistent Graph Architecture for Massive Reaction Networks Applied to Solid-Electrolyte Interphase Formation." *ACS Central Science*. Submitted.
- Wen, M., S. M. Blau, E. W. C. Spotte-Smith, S. Dwaraknath, and K. A. Persson. "BonDNet: A Graph Neural Network for the Prediction of Bond Dissociation Energies for Charged Molecules." *Chemical Science*. Submitted.

Task 3.2 – Understanding and Strategies for Controlled Interfacial Phenomena in Lithium-Ion Batteries and Beyond
(Perla Balbuena and Jorge Seminario, Texas A&M University; Partha Mukherjee, Purdue University)

Project Objective. The project objective is to evaluate and characterize interfacial phenomena in lithiated silicon and Li-metal anodes and to develop guidelines for potential solutions leading to controlled reactivity at electrode/electrolyte interfaces of rechargeable batteries using advanced modeling techniques based on first principles.

Project Impact. Understanding SEI growth on constantly evolving silicon surfaces and on highly reactive Li-metal surfaces is expected to allow definition of the electrolyte properties required in high-performance cells. Strategies to control the silicon anode instability and pulverization issues and the well-known safety and short effective lifetimes of Li-metal anodes will be developed by tuning the electrolyte composition, structure, dynamic, and stability, as well as that of the electrode morphology and interactions with the electrolyte, based on multiple characterizations of interfacial phenomena.

Approach. A comprehensive multi-scale modeling approach, including first-principles *ab initio* static and dynamics, classical MD, and coarse-grained mesoscopic models, will focus on the roles of the electrolyte's chemical, structural, and dynamical properties and of the electrode micro- and nano- structure on the formation and evolution of the SEI layer and the associated electrochemical performance on silicon and on Li-metal anodes.

Out-Year Goals. Work will progress toward characterizing lithiation and SEI formation at silicon surfaces as well as the subsequent cracking and reforming events under the most realistic modeling conditions. Similarly, the project will investigate electrolyte effects on reactivity and dendrite formation in Li-metal surfaces. The project aims to capture how the chemistry of the various electrolyte components (mainly liquids, but also solid polymers and gels) affects the main issues that influence electrode performance.

Collaborations. This project funds work at Texas A&M University (TAMU) and Purdue University. The team has collaborated with G. Somorjai (UC Berkeley), S. Yassar (University of Illinois at Chicago, or UIC), and V. Murugesan (PNNL).

Milestones

1. Complete thermal and chemical/electrochemical analysis of dendrite growth. (Q1, FY 2020; Completed)
2. Complete analysis regarding SEI formation and electrodeposition processes. (Q2, FY 2020; Competed)
3. Complete studies on cationic additive effect on electrodeposition. (Q3, FY 2020; Completed)
4. Complete mesoscale investigation on external field effects on electrodeposition. (Q4, FY 2020; Completed)

Progress Report

Effect of External Thermal Field on Electrodeposition Morphology. The temperature of the cell is a controllable design parameter that can tailor the electrodeposition stability of the Li-metal anode. To investigate underlying electrochemical-thermal interactions, the team developed a coarse-grained mesoscale model that incorporates mechanisms of ion transport, electrochemical reaction, and surface self-diffusion. Electrochemical reaction rate is quantified in terms of an electrochemical Biot number (Bi), which denotes the ratio of electrochemical reaction rate and ion transport rate in the electrolyte (at 25°C). A Bi of 1000, corresponding to a transport-limited regime at 25°C, is chosen for the present analysis. Figure 59 illustrates the main results, suggesting a change in the electrodeposition morphology that gradually evolves toward smoother deposition as T increases. It should be pointed out that the effect of temperature on degradation reactions is not included here. The transitions observed from (a) to (d) in Figure 59 are in part due to the enhanced surface migration capability of the deposited atoms, enabling them to descend from sharper tips to lower terraces. Enhanced ion transport at the metal-electrolyte interface also results in significant relaxation of the morphological front and compensates for the depletion of ions due to a higher reaction rate.

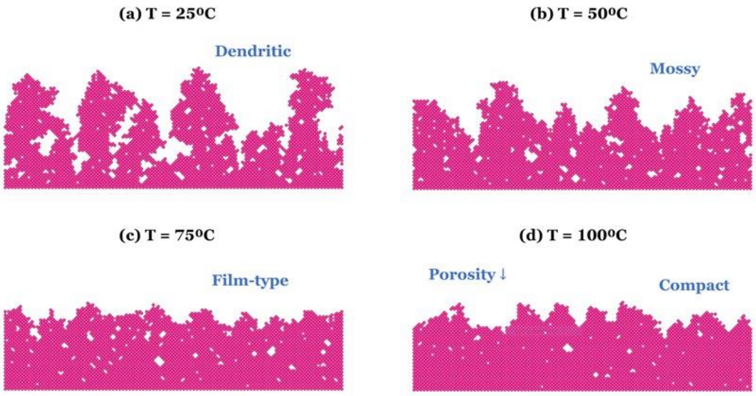

Figure 59. Electrodeposition morphologies obtained at Bi = 1000, indicating electrochemical reaction rate >> transport rate.

Evaluating Barriers for Ion Transport during Electrodeposition Events. The team studied the lithium cation diffusion pathway as well as its deposition in several environments using atomistic first-principles methods. Variations in the electrolyte included changes in the chemistry and structure of solvents and salts as well as the use of diluents or nucleating SEI. The solvation shell created around lithium cation has a great influence on the ability of the cation to diffuse as well as the electron environment that surrounds it. Whenever the Li^+ is solvated by DME, the cation can be reduced by the Li-metal slab, the electrons are transferred from the lithium surface and then transferred to the lithium cation that is reduced. However, if the solvent used is EC-based, the strong solvation shell and its electron affinity will prompt the reduction of the EC molecules instead of Li^+. If the solvation shell is difficult to break due to higher salt concentration or closer anion-cation interaction, the mobility of the cation is limited, and its deposition is shown to be difficult.

To quantify the barriers for transport and electrodeposition, the team used a slow growth *ab initio* constrained MD approach. The method allowed them to study the free energy diffusion pathway and deposition of the cation under specified collective variables leading it to leave its initial solvation shell and reaching the Li-metal surface. Therefore, energetic barriers for desolvation, diffusion, and deposition were characterized. It was concluded that DME solvation does not impose a large energy penalty to Li^+ diffusion. In contrast, large barriers are found in presence of anion decomposition, because of the formation of negatively charged species that tend to retain the cation in solution. In addition, it is clear that breaking the ion-pair represents a high energetic cost that may diminish as the ion pair moves to the surface where the anion usually reduces first. With respect to the nature of the electrode, cation deposition on copper surfaces occurs in a two-step mechanism; the first step is driven by desolvation and transport kinetics in solution, in a similar form as on lithium surfaces. Thus, sufficiently far from the electrode, the ion solvation shell would behave similarly because diffusion through the bulk electrolyte should not change much, even with structural and electronic differences in the electrode surface. However, in regions closer to the electrode surface, the second step involving the desolvation and deposition barriers will be affected differently depending on the nature of the electrode. These ideas and results were summarized in the team's recent publication [*Physical Chemistry Chemical Physics* 22 (2020): 21369–21382].

Patents/Publications/Presentations

Publications

- Tewari, D., and P. P. Mukherjee. "Energetics Dictates Deposition at Metal/Solid Electrolyte Interfaces." *The Journal of Physical Chemistry C* (2020). doi: 10.1021/acs.jpcc.0c05873.
- Galvez-Aranda, D. E., and J. M. Seminario. "Li-Metal Anode in Dilute Electrolyte LiFSI/TMP: Electrochemical Stability Using *Ab Initio* Molecular Dynamics." *The Journal of Physical Chemistry C* 124, No. 40 (2020): 21919–21934.
- Angarita-Gomez, S., and P. B. Balbuena. "Insights into Lithium Ion Deposition on Lithium Metal Anode Surfaces." *Physical Chemistry Chemical Physics* 22 (2020): 21369–21382.

Presentation

- Center for Nanophase Materials Science (CNMS) Annual Users Group Meeting, ORNL, Oak Ridge, Tennessee, Virtual (August 2020): "Mesoscale Physics and Stochastics in Energy Storage"; P. P. Mukherjee.

Task 3.3 – Electrode Materials Design and Failure Prediction (Venkat Srinivasan, Argonne National Laboratory)

Project Objective. The main project objective is to develop computational models for understanding the various degradation mechanisms for next-generation Li-ion batteries. This year's goal is to use the continuum-based mathematical model to (1) investigate interfacial stability between electrodes and ceramic-based SSEs, and (2) experimentally measure and understand the impedance observed at the cathode/SSE interface. Ceramic-based SSEs are expected to enable high-energy-density and liquid-free, safe, next-generation Li-ion batteries. Li-metal anodes should be incorporated due to their substantially larger specific capacity, as compared to present day graphite-based anodes. During deposition, lithium dendrite growth through the SSEs, and subsequent short circuit, has been a major issue, limiting successful implementation of SSEs. Similarly, on the cathode side, diffusion of TMs into the SSEs, along with delamination between cathode and SSE, leads to increased interfacial resistance. The developed computational model will be used to investigate the impact of microstructural (grain size), physical (mechanical stiffness), and transport (conductivity) properties of the SSE on the overall interfacial degradation observed at both the cathode and anode sides. Due to the SOC-dependent electrochemical and mechanical properties of the cathode, an attempt will be made to experimentally measure the SOC-dependent impedance at the cathode/SSE interface. The main focus will be to elucidate interfacial issues, observed at both anode and cathode sides, and to devise strategies to enable successful implementation of SSE in next-generation Li-ion batteries.

Project Impact. Findings from this research will give a better understanding of the factors, at the cathode/SSE interface, limiting the cycle life of SE-based Li-ion batteries. These results will help to enable incorporation of cathode particles within SSEs.

Project Approach. The approach used here is to develop mesoscale models, based on continuum modeling, to describe the critical processes in the materials, and combining them with electrochemical, microscopic, and spectroscopic data to ensure parameter estimation and model validation. The model is then used to provide insights on impact of material properties on performance and life and as guidance for design of new materials.

Out-Year Goals. At the end of this project, a computational framework will be presented that is capable of estimating delamination and impedance at cathode/SSE interface.

Collaborations. This project collaborates with L. A. Curtiss, A. T. Ngo, and C. M. Phatak at ANL.

Milestones

1. Elucidate the difference in delamination mechanisms for NMC/LLZO- and LCO/LLZO- type cathode/SEIs. (Q1, FY 2019; Completed)
2. *Go/No-Go Decision:* Investigate impact of exchange current density on delamination-induced capacity fade. If effect is minor, use experimentally observed exchange current values. Otherwise, use value obtained from DFT calculations. (Q2, FY 2020; Completed)
3. Develop continuum model for charge transport and mechanical degradation incorporating an interphase layer between LLZO electrolyte and NMC cathode. (Q3, FY 2020; Completed)
4. Gain understanding of growth rate of electrodepositing lithium nuclei. (Q4, FY 2020; In progress)

Progress Report

Previous studies have shown that any nonuniformity at the lithium surface can trigger irregular unstable growth. When lithium is electrodeposited on lithium covered with a surface film or on another substrate, it does not immediately grow as a planar front. Such fresh deposition requires forming new contacts between fresh lithium and preexisting surface, and in turn, it follows nucleation and growth dynamics. The depositing interface is nonuniform during this process, and the team describes dynamics using the classical nucleation theory and nonequilibrium thermodynamics for electrodeposition reaction.

The electrode averaged current contributes to (i) nucleation – formation of new nucleation sites and (ii) growth – of the activated sites. For the current densities of interest and representative site density, N_0, values for substrates in contact with LEs, all sites are activated almost instantaneously. At subsequent times, these sites grow via electrodeposition. Figure 60a plots overpotential evolution for galvanostatic deposition. Initially high overpotential is needed to activate the nucleation sites, and subsequently, the overpotential decays as growth progresses. Corresponding size evolution for each nucleus is shown in Figure 60b.

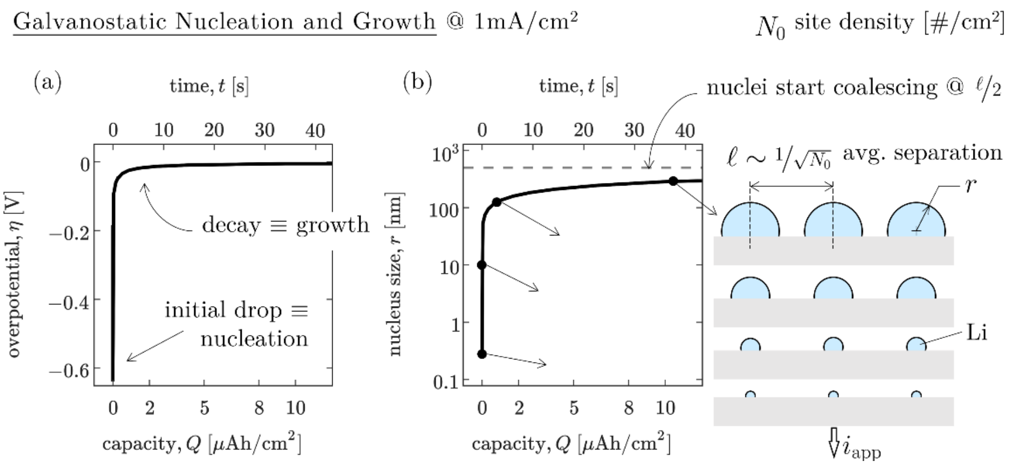

Figure 60. Short-time electrodeposition is due to nucleation and growth. Accordingly, time evolution of (a) overpotential and (b) nucleus size are interrelated. The nuclei coalesce and form a film at late times.

If the growth remains reaction-limited, these individual nuclei will coalesce once they become large enough (comparable to the average separation between nucleation sites) and eventually form a uniform film. Note that the nucleation and growth dynamics play out at very early times, ~ seconds, as shown in Figure 60.

For the same electrode average current, the current per nucleus scales with the site density. Hence, the nuclei grow faster and larger at smaller site densities, as shown in Figure 61a. The nucleus size for different site density and the same amount of deposition (10 μAh/cm^2) is shown in Figure 61b. Even if these initial stages represent fundamentally nonuniform growth, if the growth is reaction limited, the nuclei coalesce and transition to a uniform film (= stable growth). The nuclei need to grow more to coalesce at smaller site densities (Figure 61b). This would indirectly allow more time for electrolyte concentration gradients to manifest, which may cause unstable growth if mass transport becomes limiting. Thus, smaller site densities are more prone to unstable growth before the transition to the film growth can take place.

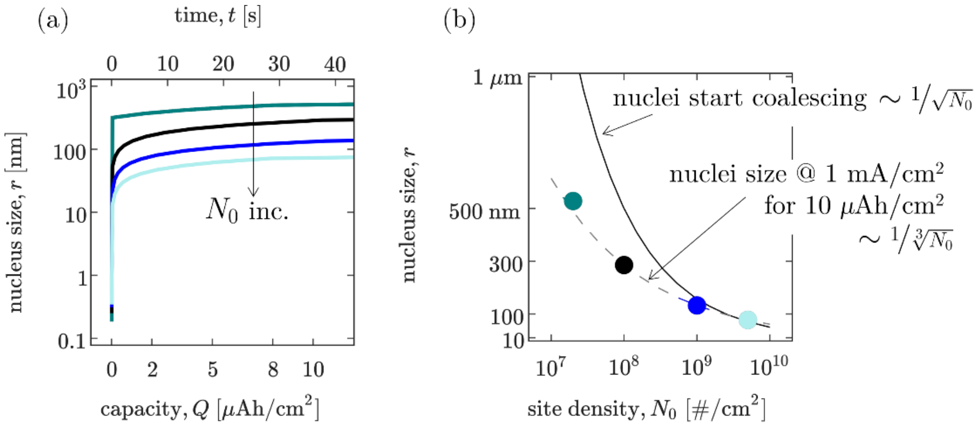

Figure 61. When deposited at the same electrode averaged current density, the current per nucleus scales with the site density. (a) The size evolves faster at smaller site density. (b) Hence, at the same deposition capacity, larger nuclei form at smaller site densities.

Patents/Publications/Presentations

The project has no patents, publications, or presentations to report this quarter.

Task 3.4 – Modeling of Amorphous Solid-State Conductors (Gerbrand Ceder, University of California Berkeley)

Project Objective. SSBs are promising to achieve high energy density. The project objective is to determine the design principles needed to create SSEs with high Li-ion conductivity, while also achieving stability against common Li-ion cathodes and Li-metal anodes.

Project Impact. The project will lead to understanding the factors that control Li-ion motion in crystalline and amorphous solids and will develop strategies to create stable interfaces against lithium metal and high-voltage cathode materials. The understanding of such processes is necessary to determine design principles to develop reliable ASSBs.

Approach. HT computation is used to screen suitable SE with high electrochemical stability and high ionic conductivity, by incorporating Nudged Elastic Band (NEB) and an *ab initio* molecular dynamics (AIMD) method. Meanwhile, DFT is used to calculate bulk elastic constants of materials, surface energies, and interface decohesion energies of GBs. Thermodynamic interface stability is assessed from *ab initio* computed grand potential phase diagrams in which the lithium voltage can be controlled. Kinetic limits for SE decomposition are assessed by topotactic lithium insertion and removal from the SE.

Out-Year Goals. Future goals include the following: (1) gain insight into what creates high Li-ion conduction in sulfide and oxide solids, and (2) develop stable, processable solid-state conductors that can be applied in ASSBs.

Collaborations. There are no collaborative activities this quarter.

Milestones

1. Modeling of the Li_2S-P_2S_5 ground state phase diagram for SSEs: solid phases correctly modeled. (Q1, FY 2020; Completed)
2. Modeling of LPS lithium mobility in amorphous state with variations of PS_4 structural units. (Q2, FY 2020; Completed)
3. Develop model for the lithium conductivity in amorphous sulfide solids. (Q3, FY 2020; Completed)
4. Modeling of the full finite temperature L-S-P phase diagram to understand metastability of the highly conducting solids. (Q4, FY 2020; Completed)

Progress Report

Lithium argyrodite with the composition Li-P-S-X (X = Cl, Br, or I) is a class of well-known superionic conductors with a high room temperature ionic conductivity up to 14.8 mS/cm. However, to date, there have been no studies on the possibility of using this framework for conducting sodium. In the team's recent work, first-principles computational techniques were applied to evaluate the potential of sodium argyrodites for fast Na-ion transport. The team studied different pnictogen (P or Sb), chalcogen (S or Se), and halogen (Cl, Br, or I) combinations and investigated the effect of varying site occupancies on the halogen site. Phase stability, electrochemical stability, and ionic conductivity of 48 types of sodium argyrodites were investigated, allowing the team to identify promising sodium argyrodites with reasonable stability and ionic conductivity.

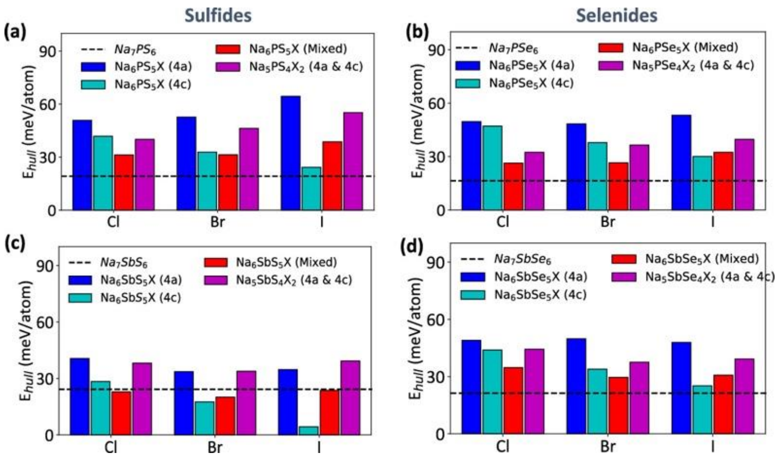

Figure 62. Phase stability (energy above the hull, E_{hull}) of sodium argyrodites in the (a) Na−P−S−X, (b) Na−P−Se−X, (c) Na−Sb−S−X, and (d) Na Sb−Se−X compositional spaces.

The thermodynamic stability of the possible sodium argyrodites was evaluated by constructing the convex hull of the DFT total energy for all phases in the relevant chemical space. The calculated E_{hull} values for all the studied sodium argyrodites are shown in Figure 62. Given that reported lithium argyrodites typically have E_{hull} values of 20 meV/atom, the team proposes that many of the sodium argyrodites considered here may be synthetically accessible.

Electrochemical phase stability is evaluated from grand canonical phase diagrams. By computing the electro-chemical stability window of all argyrodites, the team finds that the type of halogen X does not greatly affect the electrochemical stability or decomposition phases, considering that the stability limits are set by the polyanion and the chalcogen. Sodium argyrodites are generally electrochemically stable within the voltage range of 1-2 V. Higher voltage is predicted to oxidize the chalcogen atom, and voltage below the stability window reduces the pnictogen atom from +5 to +3 or even to negative valence.

AIMD was used to investigate the ionic conductivity. Activation energies and estimated room-temperature conductivities are obtained from an Arrhenius fit to the T-dependent data. Two major trends can be extracted from the distribution of conductivities. First, for all four chemical spaces, the $Na_5AB_4X_2$-type argyrodites generally exhibit higher conductivity than all the configurations with the Na_6AB_5X composition. Second, there is a significant variation in the ionic conductivity with the site occupancy in the sulfide systems. For selenide-based systems, the conductivities do not show a strong dependence on the halogen occupancy.

In summary, sodium argyrodites within the Na-P-Se-X (X = Cl, Br, or I) chemical space may form a good compromise between ionic conductivity, phase stability, and synthesizability. The rules the team found in this study can be extended to lithium argyrodite system, which will help them design new sulfide-type LIC with improved conductivity and stability.

Reference

[1] Ouyang, B., Y. Wang, Y. Sun, and G. Ceder. "Computational Investigation of Halogen-Substituted Na Argyrodites as Solid-State Superionic Conductors." *Chemistry of Materials* 32, No. 5 (2020): 1896–1903.

Patents/Publications/Presentations

Publications

- Kwon, D. H., J. Lee, N. Artrith, H. Kim, L. Wu, Z. Lun ... and G. Ceder. “The Impact of Surface Structure Transformations on the Performance of Li-Excess Cation-Disordered Rocksalt Cathodes.” *Cell Reports Physical Science* (2020): 100187.
- Jadidi, Z., T. Chen, P. Xiao, A. Urban, and G. Ceder. “Effect of Fluorination and Li-Excess on the Li Migration Barrier in Mn-Based Cathode Materials.” *Journal of Materials Chemistry A* (2020).
- Shi, T., Y. Q. Zhang, Q. Tu, Y. Wang, M. C. Scott, and G. Ceder. “Characterization of Mechanical Degradation in an All-Solid-State Battery Cathode.” *Journal of Materials Chemistry A* 8, No. 34 (2020): 17399–17404.

Task 3.5 – Characterization and Modeling of Li-Metal Batteries: Force Field Theory and Lithium-Sulfur Battery Simulations
(Lin-Wang Wang, Lawrence Berkeley National Laboratory)

Project Objective. The project objective is to develop force field (FF) based on *ab initio* calculations to study Li-S cathode and lithium LE. It also includes designs for Li-S cathode systems for high gravimetric and volumetric capacities. Lithium diffusion in both LE in a confined space and in Li-S cathode systems is a main focus of this subtask. To enable calculation of large systems, machine learning force field (ML-FF) trained on *ab initio* calculation data will also be developed. The success of this new approach will greatly expand the capability of theoretical simulation for battery systems. ML-FF can also be used in combination with traditional classical FF to deal with the nonreactive parts of the system.

Project Impact. Making the Li-S battery a commercial reality will have a major impact on society and also help to realize the VTO goal of 500 km per charge for EV. However, the nature of chemical reaction makes it different from the traditional intercalation-based Li-ion battery. The molecular nature of Li_2S_n also allows solvation in the electrolyte. To address these problems, it is essential to have fundamental studies and understandings of the underlying mechanisms. Theoretical simulations can play an important role in discovering and designing new cathode materials. However, traditional *ab initio* calculations are limited by their computational size, while the classical FF simulations are limited by their accuracy and the lack of adequate FF. The development of ML-FF can overcome these problems by bridging the size gap between the *ab initio* simulation and the real systems that need to be studied.

Approach. ML-FF will be developed by first running *ab initio* simulations, which can generate hundreds of thousands of datasets. The project has a unique capability of decomposing the total energy of a DFT calculation into the energy of each atom. Compared to conventional DFT calculations, this increases the number of data by hundreds of times, an important requirement for ML model training. The dependence of the atomic energy to the local atomic bonding environment will be captured using ML methods. Three ML approaches will be: linear fitting, neural network (NN) model, and Gaussian process regression (GPR) model. The team will compare the efficacies of these models. Meanwhile, they will also deal with the long-range Coulomb interactions existing in the electrolyte system and the ionic species in LE. The idea is to first fit the charge density of the system, and remove the long-range electrostatic energy before the fitting of the local energy on each atom. The team will also design new Li-S and Na-S cathode materials. In particular, they will design an amorphous Li-S mixture, with other materials such as CNT, black carbon, or electric conductive 2D materials.

Out-Year Goals. In outgoing years, the project will further develop computational methods for more accurate entropy and interaction energy calculations for the electrolyte, as well as for Li-S cathode systems.

Collaborations. The project will collaborate with G. Liu and Y. Cui for cathode design. It has also collaborated with F. Pan of Beijing University for lithium battery research in general.

Milestones

1. New Li-S design, mixing Li-S with CNT for an ultrafine mixture. (Q1, FY 2020; Partially completed)
2. Lithium charge density fitting in electrolyte, to fit the long-range Coulomb interaction. (Q2, FY 2020; Initiated)
3. Incorporation of Coulomb interaction in the local energy calculation; ML-FF fitting. (Q3, FY 2020; In progress)
4. Further study of Li-S cathode with polymer, to study electric conductivity in such a system. (Q4, FY 2020; In progress)

Progress Report

Time dependent density functional theory (TDDFT) is a powerful first-principle tool to study the material dynamics under the excitation of external fields (for example, light and electric field). Unfortunately, such dynamics simulations are extremely time-consuming, and existing TDDFT tools are restricted to study relatively small systems. The team has developed a new time-evolution algorithm based on a plane-wave adiabatic state basis set. This new method significantly increases the time step for integration. This allows the team to apply the TDDFT method to study the possible charge transfer bottleneck in the Li^+ ion reduction process when the Li^+ ion in the electrolyte becomes attached to electrode while one electron flows from the electrode to neutralize the Li^+ ion. They would like to know whether the electron flow can become a bottleneck.

This quarter, the team has investigated different Li-S systems for the appropriateness of this study. The goal is to investigate whether the electron flow is a bottleneck due to the insulating feature of the sulfur or LiS system. Answering this question can help the team to understand where the lithiation step happens; for example, can it happen far away from the conducting electrode with a sulfur chain? Or it can only happen near the end of the chain close to the electrode? They found that if the reaction happens near the electrode, for example, on the sulfur directly attached to the substrate, the electron flow is not a bottleneck. Thus, they study this effect and have chosen a system where long sulfur chain exists. They have selected the candidate cathode materials (Cu@graphene) based on initial screening. The pathway of Li^+ transfer from electrolyte (EC) to end of sulfur chain is shown in Figure 63. They have finished calculation of its transition barrier under adiabatic ground state calculation using the NEB method. Next quarter, the team will set up the initial velocities for the ground-state Born-Oppenheimer MD, as well as the non-adiabatic real-time TDDFT simulation. They will compare the difference and find out the role of non-adiabatic effect in this transfer process.

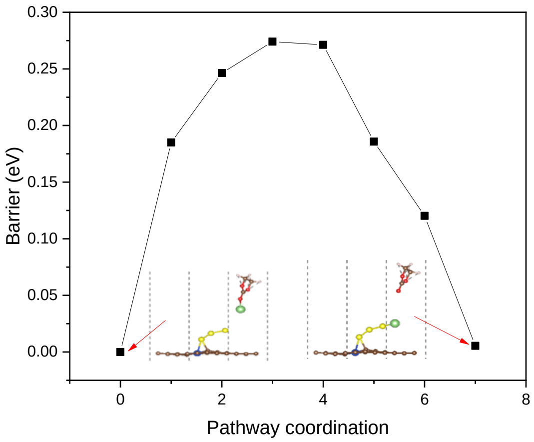

Figure 63. The pathway of lithium transfer from ethylene carbonate to the end of sulfur chain. The current barrier height is calculated in ground state with nudged elastic band method. The goal of the project is to calculate the barrier under time-dependent density functional theory with electron flow effect included.

Patents/Publications/Presentations

Publication

- Gao, G., X. Sun, and W. Wang. “Inverse Vulcanized Conductive Polymer for Li-S Battery Cathode.” (2020). doi:10.1039/D0TA06537D.

Task 3.6 – *In Situ* and *Operando* Thermal Diagnostics of Buried Interfaces in Beyond Lithium-Ion Cells
(Ravi Prasher, Lawrence Berkeley National Laboratory)

Project Objective. Transport at various interfaces in *beyond lithium ion* cells will play a major role in electrochemical performance and reliability. It has not yet been possible to thermally profile a Li-metal cell during operation to provide a spatially resolved map of thermal transport properties throughout the cell. The objective of this research is to create a metrology capable of spatially resolved *in operando* thermal property profiling, and then to relate thermal property to the quality of electrodes and interfaces, and to use the developed thermal metrology to understand electrochemical processes in Li-metal batteries, such as dendrite growth, interface kinetics, and ionic transport.

Project Impact. Characterizing electrochemical processes in Li-metal cells such as lithium deposition and dendrite growth at interfaces is of great significance for understanding and enhancing their electrochemical performance and reliability. *In situ* and *operando* 3-omega micro thermal sensors can provide significant information regarding the impact of buried interfaces as a function of time, material, voltage, current, temperature, etc. Therefore, it is important to develop *operando* 3-omega micro thermal sensors and develop models relating those signals to electrochemical performance for *beyond lithium ion* cells. The physics-based model relating thermal and electrochemical properties based on these measurements can facilitate future design of Li-metal batteries.

Approach. To accomplish project goals, the team will utilize an in-house adapted 3-omega technique to probe thermal properties of a Li-metal cell while it is in operation, without affecting the operation of the cell. The 3-omega sensors will be deposited and fabricated on Li-metal cells based on previous learning on 3-omega sensor fabrication. The characteristic depth of the thermally probed region is defined by the wave's "thermal penetration depth," $\delta_p = \sqrt{D/2\omega}$, where D is the sample's thermal diffusivity, and 2ω is the heating frequency of the thermal wave. By depositing the project's 3ω sensors on the battery's outer surface and adjusting ω, the team controls δ_p to span the full range from the top to the bottom layer, thereby noninvasively probing the thermal transport in subsurface layers and interfaces within the bulk of the battery. Thermal transport can be related to quality of the interface. By doing concurrent thermal transport and electrochemical performance measurements, the team plans to relate thermal transport to electrochemical performance. As frequency based thermal measurement techniques provide excellent spatial resolution within the cell, the team also plans to study heat generation at the electrolyte – Li-metal interface and relate the thermal signals to the interface kinetics and ionic transport. The frequency dependence of heat generated due to transport resistance is different from that due to kinetic resistance. The team plans to utilize this difference to separate the contributions of kinetic and transport resistance at the interface, which will enable understanding of interface kinetics and transport at the Li-metal – SSE interface.

Out-Year Goals. In outgoing years, the project will design, build, and implement the adapted 3-omega metrology to examine thermal properties and a general frequency-dependent thermal metrology to examine heat generation. This will involve developing and testing the metrology itself along with accompanying theory, designing compatible battery samples, and applying the technique to live cells. The team will measure thermal transport properties of battery materials provided by collaborators. Combined with the electrochemical performance measurement, this will provide significant information relating the thermal signal to the electrochemical process.

Collaborations. This project collaborates with two LBNL groups: V. Battaglia's for cell assembly for 3-omega studies, and R. Kostecki's for pristine battery active material growths for studies of thermal signals related to electrochemical process.

Milestones

1. Design pristine samples to be compatible with 3-omega and ambient environments. (Q1, FY 2020; Completed)
2. Perform sensitivity analysis and pristine sample design optimization to maximize measurement sensitivity to thermal interfaces. (Q2, FY 2020; Completed)
3. Fabrication of bi-layer pristine samples to experimentally isolate different kinds of interfaces. (Q3, FY 2020; Completed)
4. Thermal measurements of battery composites made from various materials. (Q4, FY 2020; In progress)

Progress Report

The Prasher group is developing an *operando* frequency-based thermal metrology capable of relating thermal signals to electrochemical properties and performance for *beyond lithium ion* cells. They have developed 3ω sensors to probe thermal properties of Li-metal anodes and related interfaces. Additionally, they are designing a new frequency-dependent heat generation technique to study electrochemical processes related to the charge transport and reaction kinetics at electrode-electrolyte interfaces.

This quarter, they completed the theoretical analysis, experimental design, and experimental setup for the frequency-dependent thermal metrology. From their theoretical analysis, they have identified heat generation terms at different harmonics of the frequency of the current passed to the cell and have quantitatively related these to important electrochemical parameters, including the ionic conductivity of the SSE, transport resistance of the electrolyte – Li-metal interface, and exchange current density for the lithium oxidation/reduction reaction at the electrode. Based on the fact that the technique utilizes the thermal signatures of the heat generated at multiple harmonics of the excitation current to extract the electrochemical properties, the team has named this method multi-harmonic electrothermal spectroscopy (METS). To verify the METS technique, they have designed an experiment to simultaneously measure the electrolyte transport resistance and the exchange current density in a symmetric cell using METS and EIS and then to compare the results. The experimental cell setup for the verification consists of a redox coupled electrolyte Fc1N112-TFSI with symmetric platinum electrodes. It is expected that the electrolyte will not react with platinum, therefore eliminating any SEI–like compounds at the electrode. By doing so, the team will eliminate any SEI resistance, and the interface resistance obtained from EIS can purely be attributed to the charge transfer resistance or the exchange current density. Then, they can directly compare the exchange current density and the electrolyte transport resistance obtained from EIS and METS to verify the METS technique. Figure 64 shows a fabricated METS sensor the team has designed to be used in the Pt-Fc1N112-TFSI-Pt cell for the verification experiment. The METS sensor also incorporates a 3ω sensor in the middle to extract the thermal properties of the layers and the interfaces, as those properties are essential in relating the heat generation with the temperature rise.

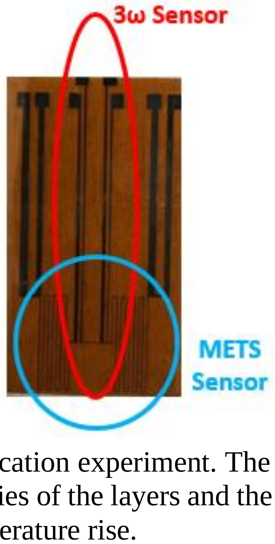

Figure 64. A multi-harmonic electro-thermal spectroscopy (METS) sensor with an integrated 3ω sensor. A 3ω measurement is performed first to extract the thermal properties, which are then used to relate the temperature rise detected by the METS sensor with the spatially resolved heat generation signatures of the separated-out electrochemical properties.

The team has also completed the experimental setup for data acquisition. Shown in Figure 65 is the setup for the METS experiment. It consists of a lock-in amplifier for frequency selective detection of the voltage (which corresponds to the temperature rise) from the METS sensor. The lock-in amplifier also provides an AC voltage/current source, which is used to generate the thermal signatures in the battery. The setup also consists of a custom-built circuit for signal conditioning and a current source to provide a DC sensing current through the METS sensor. The same setup can also work as a 3ω-system to acquire 3ω signals for the thermal properties of the cell.

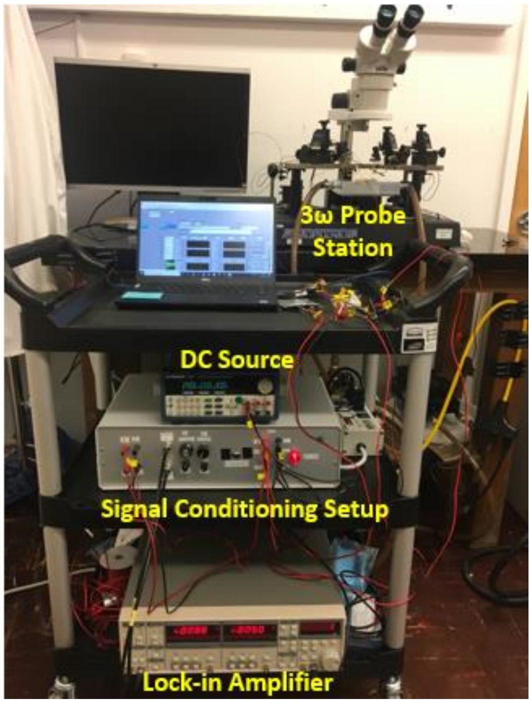

Figure 65. A hybrid multi-harmonic electrothermal spectroscopy (METS) and 3ω data acquisition system.

Patents/Publications/Presentations

The project has no patents, publications, or presentations to report this quarter.

Task 3.7 – Multi-Scale Modeling of Solid-State Electrolytes for Next-Generation Lithium Batteries (Anh Ngo, Larry A. Curtiss, and Venkat Srinivasan, Argonne National Laboratory)

Project Objective. This project is part of a multi-scale modeling effort to obtain an in-depth understanding of the interaction of the electrode and the SE aimed at developing highly efficient SSE batteries for vehicle applications. Input parameters needed for mesoscale (continuum) level calculations are being obtained from atomistic calculations including DFT and classical MD simulations. This atomistic input will enable a multi-scale computational procedure for SSEs that is capable of successfully capturing the physicochemical aspects during charge and discharge process, including lithium transport mechanisms, interfacial phenomena during the insertion and extraction of lithium ions, and mechanical deformation of SSE.

Project Impact. A major safety concern experienced with commercially available Li-ion batteries under some scenarios is leakage of the LE, which can potentially catch fire. Replacement of the LE is necessary to decrease the fire hazard and improve safety associated with present-day Li-ion batteries. In addition, use of SEs provides a path to prevent dendrites in Li-metal anodes, thereby leading to batteries with significantly higher energy density. The impact of this project will be to help in development of good SSEs as a replacement for the commercially used organic LEs to improve safety and energy density in Li-ion batteries.

Approach. Parameters needed for mesoscale modeling of grain interior (GI), GB, and electrode-electrolyte interface will be calculated by DFT-based calculations along with Monte Carlo (MC) and MD simulations. The calculations will be used to determine properties of the electrode with the SE as well as in GB regions of the SE. This will include calculations of structure, stability, ionic conductivity, Young’s modulus, fracture toughness, exchange current density, and other properties.

Out-Year Goals. The out-year goals of this work are to calculate other properties such as fracture toughness and include other SSEs and coatings in the multi-scale modeling.

Collaborations. This project collaborates with Y. Cui at Stanford University.

Milestones

1. Determine the most stable interface between LLZO SE and lithium borate carbonate (LBCO) coating material. Calculate the activation energy barrier between LLZO and LBCO coating materials. (Q1, FY 2020; Completed)
2. Determine the most stable interface between NMC cathode and LBCO coating material, and calculate the activation energy barrier. (Q2, FY 2020; Completed)
3. Evaluate the exchange current density associated with charge transfer from LBCO coating to NMC cathode and LLZO SE. (Q3, FY 2020; Completed)
4. Incorporate the information obtained from the atomistic calculations into the mesoscale model, and predict the impact of coating on performance. (Q4, FY 2020; Completed)

Progress Report

Incorporate the Information Obtained from the Atomistic Calculations into the Mesoscale Model, and Predict the Impact of Coating on Performance. Interphase layers, in terms of LBCO, have been invoked to minimize the extent of interfacial delamination between the NMC cathode and LLZO SEs. In the earlier quarters, several interfacial properties of the LBCO interphase layer were determined with LLZO electrolyte and NMC cathodes. This quarter, those properties estimated from the atomistic calculations have been incorporated within the continuum-based mesoscale model to elucidate the extent of delamination experienced by the LLZO/LBCO/NMC interface. Charge balance equations have been solved within both LLZO electrolyte and NMC solid phase to capture the current distribution within the domain. The reaction currents at the LLZO/LBCO interface and at the LBCO/NMC interface have been estimated from a Butler-Volmer equation, where the reaction rate parameters, or the exchange current densities, have been estimated from the atomistic calculations. Diffusion of lithum atoms within the NMC cathode has also been taken into account. Propensity of fracture has been estimated by solving the mechanical stress equilibrium equations.

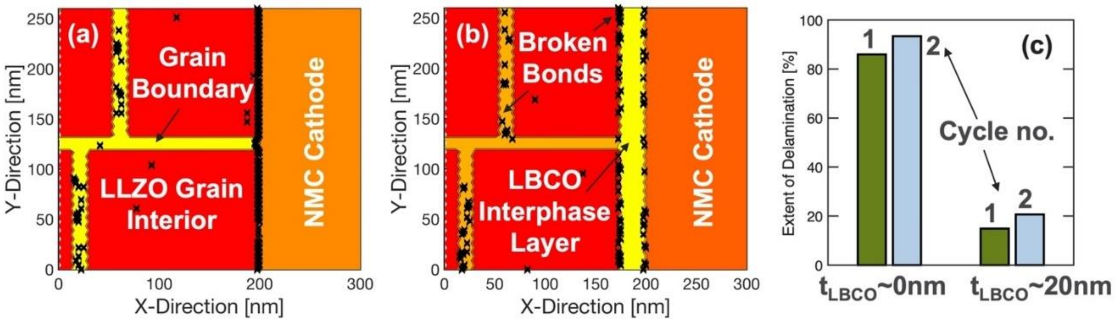

Figure 66. NMC/LBCO/LLZO microstructure with distinct grain-interior/grain-boundary domains. (a) Distribution of broken elements at the interface without any LBCO interphase layer. (b) With the LBCO interphase, extent of delamination decreases. (c) Bar chart showing comparison between delamination with/without LBCO layer over 2 consecutive cycles.

Figure 66a shows the extent of delamination experienced by the NMC/LLZO interface without the LBCO interphase layer. However, incorporation of a 20-nm thick LBCO layer in between LLZO and NMC helps to minimize the extent of delamination, which has been clearly depicted in Figure 66b. The extent of delamination with and without the interphase layer over two consecutive cycles has been clearly shown in Figure 66c. It is evident that the addition of LBCO interphase layer helps to minimize the interfacial detachment to a certain extent. Exchange current densities at the NMC/LBCO interface have been shown in Figure 67a. The charge/discharge curves with and without LBCO interphase layers and corresponding discharge capacity over two cycles are shown in Figure 67b-c, respectively. It is evident that addition of an interphase layer helps to minimize the extent of interfacial delamination and subsequent capacity fade. These analyses with the interphase layer successfully complete the milestone for this quarter.

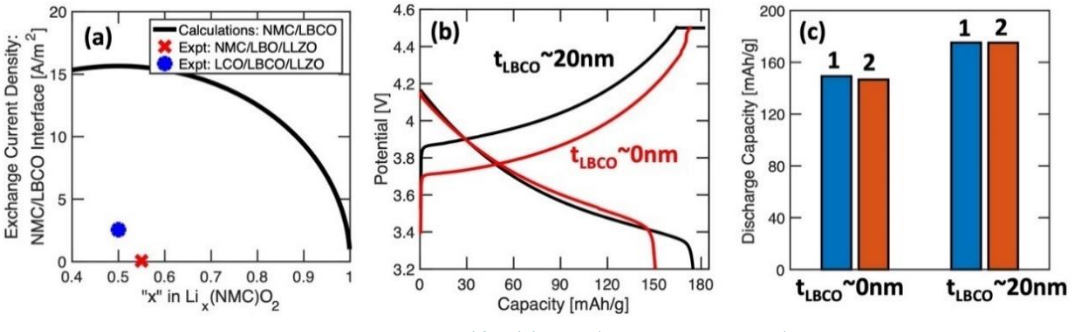

Figure 67. (a) Exchange current density at the NMC/LBCO interface as estimated from the atomistic calculations. (b) Potential versus capacity charge/discharge curves with/without the LBCO interphase layers. (c) Discharge capacity over 2 cycles as observed with/without a 20-nm-thick LBCO interphase layer.

Patents/Publications/Presentations

The project has no patents, publications, or presentations to report this quarter.

Task 3.8 – Integrated Multi-Scale Modeling for Design of Robust 3D Solid-State Lithium Batteries (Brandon Wood, Lawence Livermore National Laboratory)

Project Objective. This project will develop a multi-scale, multi-physics modeling framework for probing the effects of materials microstructure and device architecture on ion transport within 3D ceramic SSB materials, with the goal of enhancing performance and reliability. The project has three primary objectives: (1) integrate multi-physics and multi-scale model components; (2) understand interface- and microstructure-derived limitations on ion transport; and (3) derive key structure-performance relations for enabling future optimization.

Project Impact. This project will lead to understanding interfacial losses and instabilities that impede performance and promote failure of SSBs. The multi-scale and multi-physics modeling framework developed in this work will address shortcomings of existing modeling strategies that either lack coupling of the multi-physics nature of various processes active in 3D batteries or fail to incorporate processes at different length scales to understand function. Ultimately, the tools and understanding generated by this project can be utilized to realize optimization of interface-dominated 3D batteries.

Approach. The project approach integrates simulations at three scales to predict ion transport limitations within the ceramic SSE LLZO, as well as across the interface between LLZO and $LiCoO_2$ (LCO) cathodes. A particular focus is on understanding the effects of microstructures and architectures resulting from processing of 3D SSBs as well as their mechanical and chemical evolution at different stages of cycling. First-principles and classical MD simulations are used to compute fundamental Li-ion diffusion within bulk SE and cathode materials, along/across GBs of the electrolyte, and along/across electrolyte/cathode interfaces. Next, phase-field simulations are used to generate digital representation of realistic microstructures of the materials, which are combined with the atomistic simulation results to parameterize mesoscale effective property calculations and to establish microstructure-property relationships for ion transport. Finally, these relationships inform a cell-level macroscopic electro-chemo-mechanical modeling framework, which can be used to optimize performance of ceramic 3D SSLBs based on LLZO SEs.

Out-Year Goals. Future activities will focus on applying potentials capable of scaling the atomistic interface diffusion models to longer timescales. The team will also work with collaboration partners to reconstruct microstructures of 3D-printed materials and apply them to determine effective stresses and ion transport through the polycrystalline materials. They will also further develop and validate the EIS models for connection to macroscale observables, including implementation of space-charge contributions near interfaces.

Collaborations. This project collaborates with N. Adelstein from San Francisco State University (SFSU) on atomistic diffusion modeling, and J. Ye from LLNL on 3D printing of SSB materials. They also partner with T. Danner and A. Latz from Deutsches Zentrum für Luft- und Raumfaurt (DLR) on impedance modeling and electrochemomechanical interface models, with P. Zapol from ANL on modeling of interfaces in LLZO, and with D. Fattakhova-Rohlfing from Forschungszentrum Jülich (FZJ) and E. Wachsman from UMD on properties of LLZO with varying densities and microstructures as part of the U. S.–Germany partnership on SSB research.

Milestones

1. Construct models of solid-solid LCO/LLZO interface. (Q1, FY 2020; Completed)
2. Perform phase-field simulation to reproduce 3D-printed microstructure of LLZO and LCO. (Q2, FY 2020; Completed)
3. Perform AIMD of LCO/LLZO interface model to determine interdiffusion. (Q3, FY 2020; Completed)
4. Quantify threshold grain/pore size that eliminates Griffith-criterion hot spots based on computed internal stress in polycrystalline LLZO. (Q4, FY 2020; Completed)

Progress Report

Atomistic Simulations of Li-Ion Diffusion at the LLZO/LCO Interface. The team continued efforts to probe the structural and chemical evolution at the LLZO/LCO electrolyte/cathode interface using high-temperature AIMD. Figure 68 shows a snapshot of the LLZO/LCO interfacial structure during the AIMD run. The black dots indicate the positions of lithium vacancies, which were used to identify interfacial diffusion pathways for neighboring Li$^+$ ions migrating into these vacancy sites. The activation energies for diffusion along these pathways were computed using the NEB method and are plotted as a histogram in Figure 68. It was found that the activation energies for lithium diffusion in this specific LLZO/LCO interfacial model span a broad range from 0.03 to 1.74 eV, with an average of 0.63 eV, which is significantly higher than the activation energies for Li$^+$ diffusion (~ 0.3 eV) in bulk LLZO and LCO. In addition, cobalt interdiffusion into the lithium layers is observed. As shown in Figure 69, the presence of cobalt at the lithium layer further blocks lithium diffusion from the surface of LCO to LLZO. The team speculates that the structural instability of the LCO surface caused by cobalt diffusion into adjacent lithium layer is one of the factors that contributes to the sluggish Li-ion diffusion at the LLZO/LCO interfaces. They are sampling additional lithium diffusion pathways at the LLZO/LCO interfaces, the results of which will be reported next quarter.

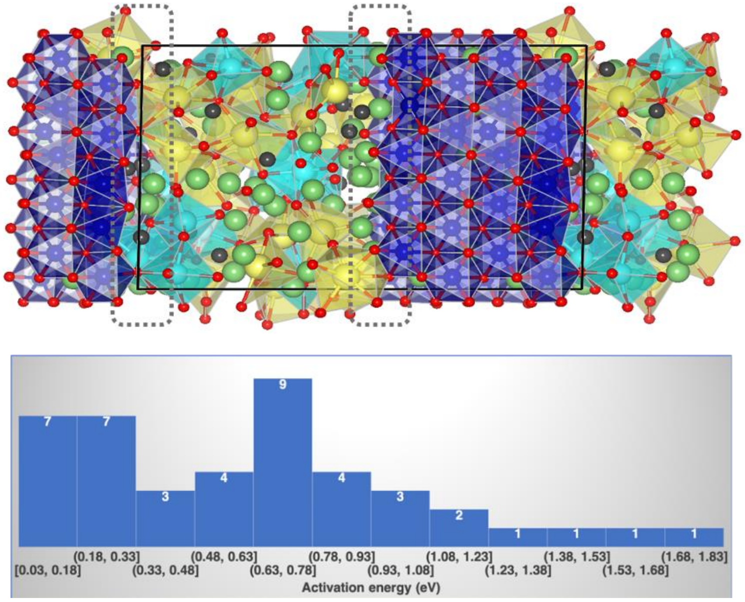

Figure 68. Calculated activation energies for Li-ion diffusion across the LLZO/LCO interfaces (grey dashed box). Lithium, lanthanum, zirconium, cobalt, and oxygen atoms are shown as green, yellow, cyan, blue, and red spheres in the structure representation of the LLZO/LCO interfacial model. The black dots indicate lithium vacancy sites, from which the activation energies are computed for nearby lithium atom migrating into these vacancy sites in the interfacial regions.

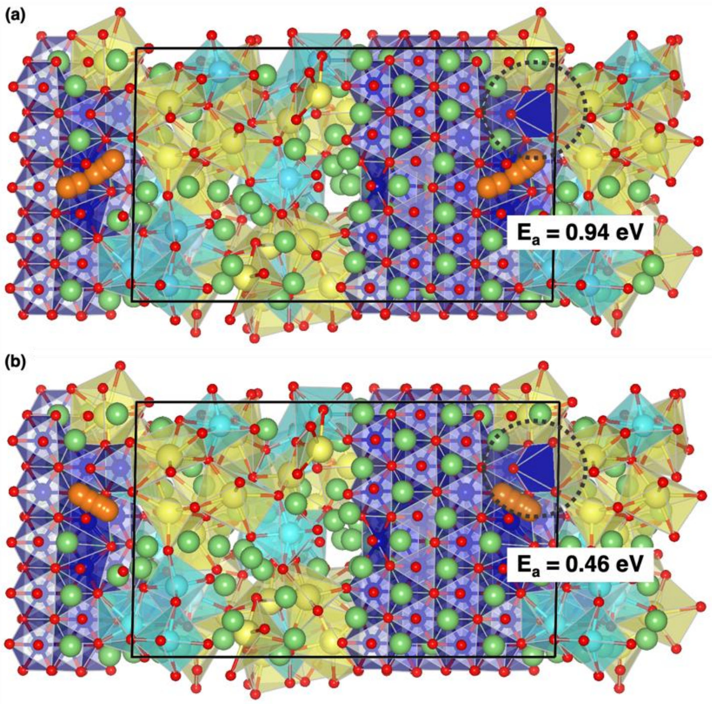

Figure 69. Calculated activation energies and corresponding diffusion pathways (highlighted in orange) for Li-ion diffusion across the LLZO/LCO interface in the presence of an interdiffusing cobalt atom. The dashed circle highlights the cobalt atom, which migrated from the cobalt layer into the lithium layer. The activation energies are computed along the Li-ion diffusion pathways (highlighted in orange) near this migrated cobalt atom.

Atomistic Simulations of the Elastic Properties of Disordered LLZO. As part of an ongoing effort to understand the effects of SE microstructure, the team began investigating how internal stresses induced during operation affect ion transport in GBs. They generated disordered LLZO structures using the AIMD melt-and-quench technique to represent generic high-angle GBs. The elastic constants were calculated for these disordered structures, and the results are summarized in Table 3 alongside the analogous results for the crystalline phase. It was found that the disordered LLZO lattices are much softer compared to the crystalline grains, and that their elastic properties are very sensitive to atomic density. The team expects similar elastic behavior at LLZO GBs, which will be used to parameterize the mesoscale chemomechanical models.

Table 3. Calculated elastic constants for pseudo-cubic LLZO. The disordered LLZO structures were modeled at two different unit-cell volumes: at the optimized volume at 0K (2349.12 Å3), and at the equilibrium volume for the crystalline phase (2203.17 Å3).

$Li_7La_3Zr_2O_{12}$ (LLZO) structure	c11 (GPa)	c12 (GPa)	c44 (GPa)
Crystalline	184	77.3	72.8
Disordered at 0K optimized volume	129	49.2	38.0
Disordered at the equilibrium volume of the crystalline phase	169	77.8	42.3

Mesoscale Modeling of Internal Stress Distribution in LLZO. Based on the computed elastic constants, the team investigated the internal stress distribution and its evolution in polycrystalline LLZO under exerted mechanical loading during cycling. For input microstructures, they generated digital representations of LLZO microstructures using phase-field simulations (see Figure 70 for two examples with different grain sizes). The team then parameterized the site-specific elastic moduli within those polycrystalline microstructures. In this iteration, only the orientation-dependent elastic moduli of individual grains were considered, ignoring the

GB contributions. In coming quarters, the GB elastic modulus will also be incorporated into the model using the results of the atomistic simulations. By numerically solving the mechanical equilibrium equation with the microstructure-informed elastic modulus, the equivalent von Mises stress (σ_v) profile was obtained under the applied loading condition (see Figure 70b for spatial distributions and corresponding statistics). The results show the sensitivity of the internal stress profile to the grain size, with larger grains exhibiting stress distributions skewed towards lower σ_v. The stress distribution was then used to define hot spots surpassing a critical failure criterion $\sigma_v > \sigma_Y$, where σ_Y is the yield strength of LLZO. Figure 70c shows the spatial distribution of hot spots for two different grain sizes, illustrating the potential crack formation sites. The hot spot fraction was also monitored under increasing applied strain. For small grains, the hot spot fraction is more sensitive to increasing strain, indicating that controlling grain size could be effective for reducing possible sites for mechanical failure. This analysis completes the annual progress milestone for the project.

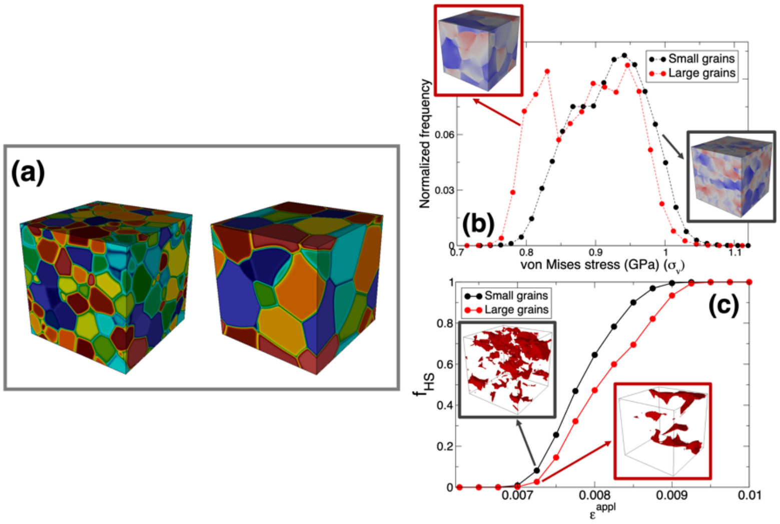

Figure 70. (a) Digital representations of LLZO microstructures with different grain sizes. (b) Computed von Mises stress profiles and statistics for the two microstructures. (c) Stress hot spot evolution with increasing applied strain for the two different grain sizes.

Modeling of Microstructural Effects on EIS. Last quarter, the team completed a parametric study to quantitatively identify the influence of ionic conductivity, permittivity, and grain structures of SEs on EIS. This modeling framework has been extended to include transport limitations at GB regions to increase the physical accuracy of the predicted EIS curve. Specifically, the phase-field method was used to compute the heterogeneity in Li^+ concentration across the GB. The GB segregation was first considered in a 1D domain, then in two grains separated by a GB, and finally for a 2D polycrystal (Figure 71). This model is being coupled to the EIS simulation framework being developed. Results will be exchanged with collaborators for macroscale validation through the U.S.-Germany SSB collaboration.

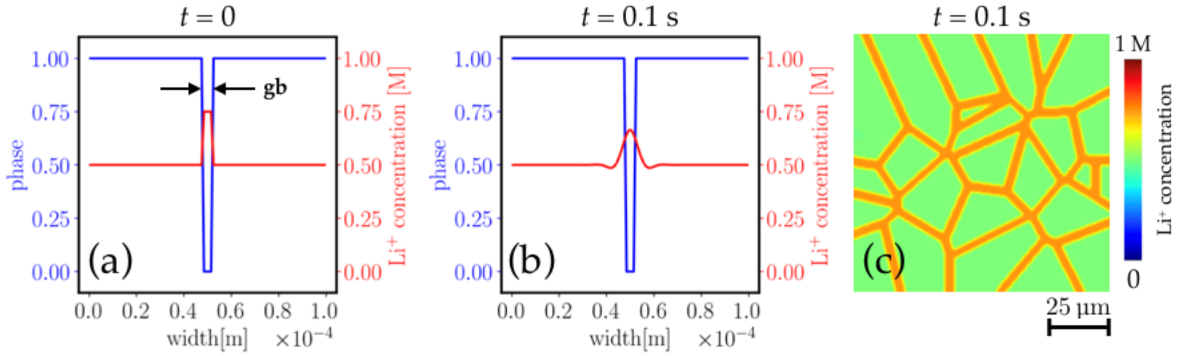

Figure 71. Grain boundary segregation of Li^+ ions in an example solid electrolyte. The variable "phase" in insets (a) and (b) represents the grain (= 1) and grain boundary (= 0) regions. The initial Li^+ concentration is 0.5 and 0.75 M in the grain and the grain boundary, respectively, as shown in (a). The steady-state concentration distribution shows grain boundary segregation and nearby depletion of Li^+ ions, in (b). This effect is reproduced for a polycrystalline sample in (c).

Patents/Publications/Presentations

Publication

- Heo, T. W., A. Grieder, B. Wang, S. A. Akhade, L. F. Wan, L-Q. Chen, N. Adelstein, and B. C. Wood. "Microstructural Impacts on the Ionic Conductivity of Garnet Solid Electrolytes: A Combined Atomistic-Mesoscale Approach." In review.

Presentation

- ACS Fall 2020 National Meeting, Virtual (August 2020): "Microstructural Effects on Electrochemical Impedance Spectroscopy"; A. Jana, T. W. Heo, M. Wood, J. Ye, L. Wan, and B. C. Wood.

Task 3.9 – First-Principles Modeling of Cluster-Based Solid Electrolytes
(Puru Jena, Virginia Commonwealth University)

Project Objective. The objective of the project is to use cluster-ions, which are stable atomic clusters that mimic the chemistry of individual atoms, as the building blocks of new SEs for Li-ion batteries and the corresponding battery system. The advantages of using cluster-ions to replace elemental ions is that the size, shape, and composition of the former can be tailored to achieve higher superionic conductivity, electrochemical stability, and charge transfer across the solid-solid interfaces than the conventional materials. More specifically, the goal is to develop superior SEs based on cluster-ions and to model these SEs and their interfaces with electrodes, especially with the Li-metal anode, for successful integration into high-performance SSBs for EVs. The team will model and screen cluster-based SEs that, compared to conventional SEs, have low activation energies, practical room-temperature ionic conductivities, wide electrochemical stability windows, and desired mechanical properties that, for example, can inhibit the Li-metal anode dendrite growth. They will provide a fundamental understanding of the ionic conduction mechanism in the newly developed, cluster-based SEs and identify means to further improve property metrics via chemical and defect engineering. The team will model the interfacial properties, such as the structural, chemical, electrochemical, and ion/charge transfer properties, between the cluster-based SEs and electrodes at the atomic level, as well as find the interfacial coating materials with desired properties. Based on accumulated data from modeling, they will establish links between the basic parameters of the cluster-ions and the bulk/interface properties, which can directly guide experiments. Meanwhile, the team will work closely with experimentalists in the BMR Program to complement the project's theoretical efforts and to guide them in focused development of the predicted cluster-based SEs and the interfaces.

Project Impact. The proposed project will open a new avenue for guiding experiments in the synthesis of SSBs equipped with cluster-based SEs and capable of operating over a wide temperature range. Modeling and understanding of the ionic conduction of cluster-based electrolytes and their interfacial properties with electrodes, especially with Li-metal anode, will enrich current battery science and also train the future workforce in SSB development for next-generation EVs by supporting postdoctoral fellows.

Approach. This project will employ multi-scale theoretical methods and computational techniques.

Out-Year Goals. The out-year goals involve modeling development of new cluster-based SE materials and database.

Collaborations. The team is working with J. Nanda of ORNL on antiperovskite-based SSEs.

Milestones

1. Structural studies of the designed cluster-based SE materials with selected cluster-ions. (Q1, FY 2020; Completed)
2. Property characterizations of stable cluster-based SE materials. (Q2, FY 2020; Completed)
3. Ionic conductivity characterization for cluster-based SE materials and the ionic conduction mechanism. (Q3-Q4, FY 2020; Completed, September 30, 2020)
4. Complete development of new cluster-based SE materials with a database. (Q4, FY 2021; In progress)

Progress Report

The technique milestone this quarter is: "Ionic conductivities characterization of the cluster-based solid electrolyte materials." Research toward this milestone is complete. The team covered 10 SE materials this quarter, following the 15 SE materials studied last quarter. They conducted the MD simulations and data analysis for ionic conductivities on these newly developed cluster-based SE materials. For each material, they studied the ionic diffusion and conductivities at different temperatures. The diffusivity of the SE at room temperature and the activation energy are obtained by extrapolation or direct calculation using the Arrhenius relationship.

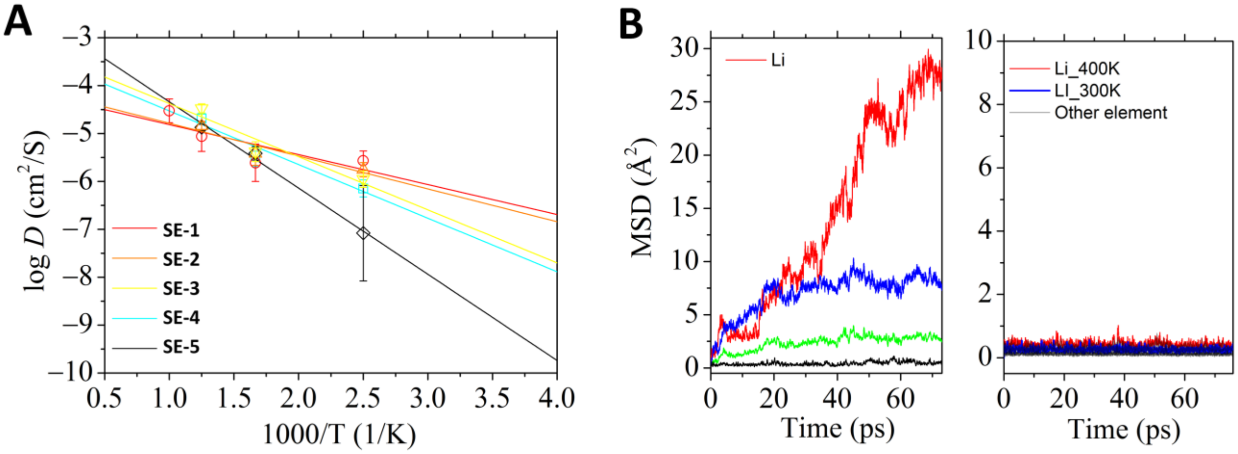

Figure 72. (a) Calculated diffusivities of the newly developed cluster-based solid electrolytes (SEs) fitted by the Arrhenius relationship. These new SE materials exhibit relatively high diffusivities. The corresponding ionic conductivities at room temperature on the order of 10^{-4}-10^{-2} S/cm with activation energies between 0.12-0.36 eV. In particular, the calculated room-temperature conductivity of "SE-1" reaches 0.079 S/cm with a low activation energy of 0.124 eV. (b) One typical SE only exhibits fast-ion conduction at high simulation temperatures over 500 K, as shown by the calculated mean squared displacements (MSD) for different atomic species in the lattice (left panel) with partial melting (blue and green lines). At simulation temperatures of 300 and 400 K, the SE exhibits no superionic conductivity (right panel).

Out of the studied new SE materials, five exhibit high ionic conductivities and low activation energies, as shown in Figure 72a. The major findings are given here. (1) Five SE materials exhibit room-temperature ionic conductivities in the range of 10^{-4}-10^{-2} S/cm and activation energies in the range of 0.12-0.36 eV. Among them, the highest ionic conductivity reaches 0.079 S/cm, with the lowest activation energy of 0.124 eV. (2) Four out of the ten studied SEs only start to exhibit fast-ion conduction at high simulated temperatures in the range of 500-800 K, accompanied by diffusive phase transition or partial melting, as demonstrated in Figure 72b. The calculated Li^+ conductivities at these high temperatures are in the range of 0.1-1.0 S/cm. (3) The remaining SE exhibits no superionic conductivity at the simulated temperatures. (4) Certain types of cluster-ions in the studied SEs show severe distortions from their gas-phase configurations, suggesting poor stabilities at high temperatures. (5) The studied SEs are prototypes of materials. Based on them, new SE candidates can be further developed by chemical (for example, with group element substitutions) or defect engineering.

For each studied SE, AIMD simulations are carried out using a large supercell containing hundreds of atoms. In each case, AIMDs are performed at 3 to 5 different temperatures. A typical AIMD lasts around 100 ps with a 2 fs time step, where 10 ps is allowed for the system to reach thermal equilibrium before the data are collected to calculate the mean squared displacements (MSD) for all the atomic species in the system. The diffusivity at each temperature is then calculated by linear fitting to the MSD. For the SEs that exhibit fast-ion conduction at room temperature, the data points of the diffusivity will be discarded if phase transition or partial melting is found from the analysis. The remaining points are then applied to the Arrhenius relationship to extrapolate to the room temperature and extract the activation energy.

Patents/Publications/Presentations

Publications

- Fang, H., and P. Jena. "Solid Electrolytes Based on Polyatomic Units with Liquid Ionic Conductivity." In preparation, 2020.
- Fang, H., and P. Jena. "Argyrodite-Based Solid Electrolyte Materials Containing Multiple Clusters." In preparation, 2020.
- Fang, H., and P. Jena. "Boranes-Based Materials as Argyrodite Electrolytes." In preparation, 2020.
- Collaboration with ORNL group. "Synthesis and Design Rules for Protiated Antiperovskites." In preparation, 2020.

Presentation

- EERE Progress Meeting (August 25, 2020): Progress Update Presentation: First-Principles Modeling of Cluster-Based Solid Electrolytes.

Task 3.10 – Predictive Engineering of Interfaces and Cathodes for High-Performance All-Solid-State Lithium-Sulfur Batteries
(Badri Narayanan, University of Louisville)

Project Objective. The primary goal of this project is to leverage data-driven methods and ML strategies to develop accurate multi-physics models for all-solid-state Li-S battery materials that can capture electrochemical and transport phenomena over atomic-to-mesoscopic length/timescales; these models will be rigorously validated by synthesis and advanced characterization experiments. The team will leverage the predictive power of these models, alongside synthesis/characterization experiments and battery fabrication to address longstanding issues at the electrode/electrolyte interfaces in all-solid-state Li-S batteries. The project's proposed technology involves the following: (1) halide-doped solid sulfide electrolytes that can concurrently provide high Li^+ ion conductivity and suppress dendrite growth; (2) novel mesoporous cathode composed of interconnected carbon nano-cages co-infiltrated with sulfur and sulfide electrolyte, which hold potential to allow high sulfur loading and optimal ion/electron pathways; and (3) functionalization of sulfide electrolyte with ionic liquids to improve physical contact and minimize impedance at the cathode/electrolyte interface.

Project Impact. All-solid-state Li-S batteries remain far from commercialization due to poor understanding of fundamental electrochemical/chemical and transport processes that occur at the interfaces, especially at atomic to mesoscopic scales. Successful development of proposed predictive models (at multiple scales) will bridge this knowledge gap and will advance fundamental understanding of reaction chemistry, kinetics, charge transfer, and dendrite growth at electrified solid-solid interfaces. This, in turn, will enable predictive design of effective strategies to mitigate interfacial problems in all-solid-state Li-S batteries, including poor interfacial contact, interfacial impedance to Li^+ ion transport, and poor electron/ion conduction within cathodes. Ultimately, the fundamental knowledge gained by this work will lead to development of high-performance all-solid-state Li-S batteries that meet DOE targets of specific energy (350 Wh/kg @C/3), sulfur loading (> 6 mg/cm^2), and high cycle life (1000).

Approach. The project brings together innovative solutions in multi-scale materials modeling, electrolyte synthesis, fabrication of cathode architecture, and electrolyte functionalization to overcome the issues at electrode/electrolyte interfaces in all-solid-state Li-S batteries. The central idea is to employ a data-driven and ML-based approach to develop accurate multi-physics battery models at atomic-to-mesoscopic scales. This approach overcomes critical problems with existing model development methods by foregoing the need for pre-defined functional forms, introducing deep-learning technique to describe reactivity, and employing optimization methods that do not require human intuition. Multi-scale simulations based on the newly developed models will provide insights into electrochemical phenomena at electrode/electrolyte interfaces.

Out-Year Goals. In Year 1, the goal is to optimize electrolyte composition and to develop accurate reactive atomic-scale interaction models of representative SSE system and ionic liquids.

Collaborations. The team collaborates with the groups under A. Ngo and L. A. Curtiss at ANL for quantum simulations of battery systems; they plan to collaborate with J. Nanda at ORNL for advanced spectroscopic *in situ* characterization of interfaces.

Milestones

1. Demonstrate scalable electrolyte synthesis with precise composition control. (Q1, FY 2020; Completed)
2. Computationally optimize electrolyte composition for high Li+ conductivity (10^{-3} S/cm) and good electrochemical stability. (Q2, FY 2020; Completed)

3. Synthesize cathode architectures based on interconnected carbon nano-cages with co-infiltrated sulfur and SSE; obtain baseline for battery performance. (Q3, FY 2020; Completed)
4. Develop reactive models for electrolyte, and ionic liquid. (Q4, FY 2020; Completed)

Progress Report

This quarter, the team made good progress in (a) developing reactive models based on a Tersoff+Qeq formalism for sulfide electrolytes (Li-P-S) that can be employed to investigate electrochemical processes in bulk electrolytes and interfaces via classical MD simulations, (b) experimental characterization of stability of fluorine containing sulfide electrolytes, and (c) fabrication and electrochemical testing of preliminary coin-cell batteries with the project's synthesized cathodes and halide-doped sulfide electrolyte.

Development of Reactive Models for Representative Sulfide Electrolyte (Li-P-S) System. The team used the large quantity of datasets derived from DFT calculations this fiscal year to develop the first reactive atomic interaction potential model (FF) for solid sulfide electrolyte. The FF is capable of providing insights into atomic-scale processes underlying formation of SEI, ion-transport, chemical reactions, and structure-chemistry-property relationships. Since the team's optimized electrolyte compositions (Q1 and Q2) with a desirable combination of Li^+ conductivity and interface stability are derivatives of Li_7PS_6 prototype, they use Li-P-S ternary system as a representative system to develop the reactive FF.

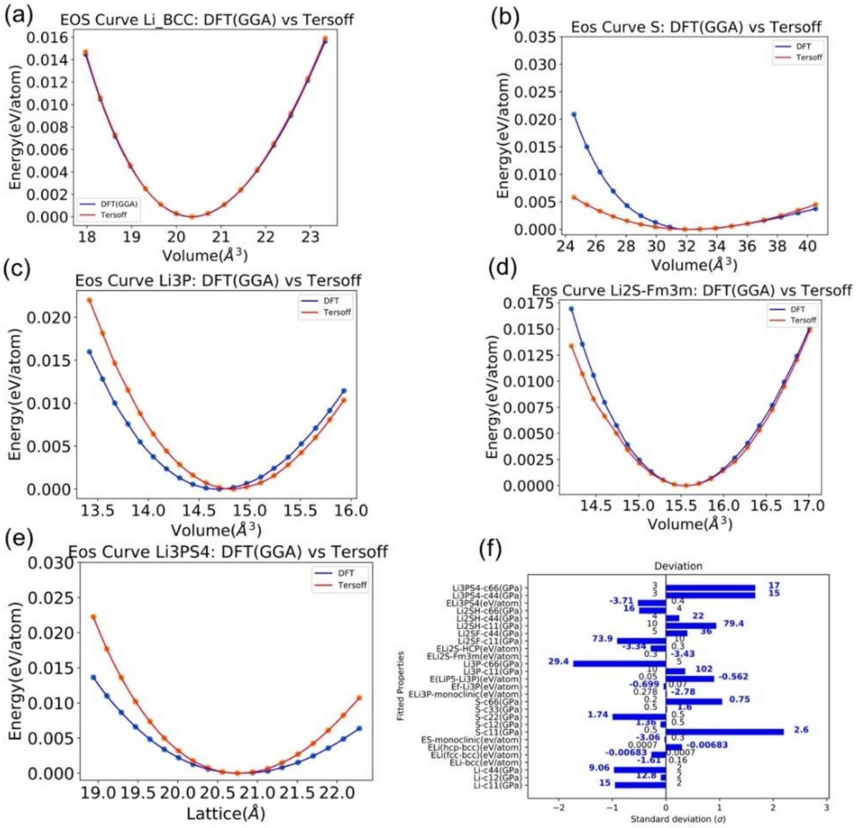

Figure 73. Predictive power of the newly developed Q-BOP potential for Li-P-S system. Comparison of the equation of state (EOS) between density functional theory and fitted Tersoff potential for (a) lithium, (b) sulfur, (c) Li-P, (d) LiS, and (e) Li-P-S systems. (f) Errors in the prediction of Q-BOP for various materials properties. The energies (eV/atom) in panels (a-e) are relative to the energy corresponding to equilibrium volume at a given level of theory.

They employ a Tersoff-type bond-order potential (BOP), which is well known to capture the energetics and dynamics of a wide range of atomic configurations (from the team's previous works, including *Nature Communications* 10, (2019): 379; *Nanoscale* 9 (2017): 18229, and *Journal of Physical Chemistry C* 120 (2016): 13787). To account for the charge transfer between atoms at the interfaces, the team employs the well-established electronegativity equalization (QeQ) scheme to determine redistribution of atomic charges with changes in local atomic configurations. They call this potential Q-BOP. Additonally, accurate Tersoff-type FFs are already available for molecular systems containing carbon and nitrogen atoms (such as ionic liquids) and mesoporous carbon structures. This would enable extending FFs to investigate electrochemical processes at the interfaces between mesoporous carbon cathodes and solid sulfide electrolytes when the interfacial wetting is enhanced by ionic liquids.

To provide a brief desciption of the potential form, the total energy of a system in the framework of Q-BOP can be written as sum of contributions from a short-range Tersoff potential and long-range shielded electrostatic interactions

$$E = \sum_{i=1}^{N} \sum_{j=i+1}^{N} \left[V_{ij}^{SR} + C_{ij} \frac{q_i q_j}{\left(r_{ij}^3 + 1/\gamma_{ij}^3\right)^{1/3}} \right] \tag{1}$$

where V_{ij}^{SR} is the short-ranged Tersoff contribution arising from a pair of atoms *i* and *j* that are r_{ij} apart, C_{ij} is a Taper constant, q_i and q_j are the instantaneous atomic charges whose values are provided by QeQ, and γ_{ij} is a shielding parameter.

The short-ranged Tersoff contribution for each atom pair *i-j* can be written as:

$$V_{ij}^{SR} = f_c(r_{ij})\left[f_R(r_{ij}) + b_{ij} f_A(r_{ij})\right] \tag{2}$$

where $f_c(r_{ij})$, $f_R(r_{ij})$ and $f_A(r_{ij})$ are the cut-off function, repulsive and attractive interaction terms, respectively, between atoms *i* and *j* that are separated by a distance r_{ij}. The cut-off function limits the range of interaction to nearest neighbors for computational efficiency, and is given by:

$$f_c(r) = \begin{cases} 1, & r < R - D \\ \frac{1}{2} - \frac{1}{2}\sin\left(\frac{\pi(r-R)}{2D}\right) & R - D \le r < R + D \\ 0, & r \ge R + D \end{cases}, \tag{3}$$

where *R* and *D* are adjustable parameters. In this work, *D* is set to 0.2 Å following the team's previous works. The repulsive and attractive contributions to bond energy between a pair of atoms are defined to decay exponentially with separation distance:

$$f_R(r) = Ae^{-\lambda_1 r}, \tag{4}$$

$$f_A(r) = -Be^{-\lambda_2 r}, \tag{5}$$

where *A*, *B*, λ_1, and λ_2 are free parameters. The term b_{ij} in Eq. 2 describes the bond-order around a pair of atoms *i-j*, which is dependent on three-body interactions given by Eqs. 6-8:

$$b_{ij} = \left(1 + \beta^n \zeta_{ij}^n\right)^{\frac{-1}{2n}}, \tag{6}$$

$$\zeta_{ij} = \sum_{k \ne i,j} f_c(r_{ik})\, g_{ik}(\theta_{ijk})\, e^{\left[\lambda_3 (r_{ij} - r_{ik})\right]}, \tag{7}$$

$$g(\theta) = \gamma\left(1 + \frac{c^2}{d^2} - \frac{c^2}{d^2 + (\cos\theta + h)^2}\right). \tag{8}$$

In Eqs. 6-8, the parameters β, *n*, λ_3, γ, *c*, *d*, and *h* are adjustable. In all for Li-P-S system, 80 independent parameters need to be optimized.

The team leverages their established ML framework, a large dataset of DFT-properties (~ 1000) including energies of representative clusters, heat of formation of several known compounds in the Li-P-S ternary space at different stoichiometry, elastic constants, and atomic charges in a wide variety of assures following the hierarchy starting from the individual unary systems to all possible binaries; finally, they fit the ternary structures. Following this pattern, the team is not losing the coherency of the potential when the final ternary FF is built. Figure 73 compares predictions of the newly developed potential with DFT values and configurations to develop the FF. Equations of state (energy-volume dependence) predicted by Q-BOP for the unary system are in remarkable agreement with DFT (< 1 meV/atom; Figure 73a-c). For the binary and ternary compounds, the difference between the Q-BOP and DFT values is within 10 meV/atom, which is still within the typical errors of DFT, let alone a classical potential such as Q-BOP. Figure 73f summarizes the errors in the predictions of Q-BOP for a variety of properties. All the predicted energy (or heat of formation) values are within 10 meV/atom of DFT, elastic constants within 20%, and structural properties (for example, equilibrium volume) within 3%. These errors are on par with the most accurate classical interatomic potentials. Note that few shear elastic constants are associated with somewhat higher error; the team is improving these predictions by adding more data on anisotropic distortion of the solid sulfide electrolyte crystals. Finally, the Q-BOP predicted atomic charges are in good agreement with the Bader charges derived from DFT.

Experimental Characterization of Stability of Fluorine Containing Solid Sulfide Electrolyte against Lithium Metal. This quarter, the team employed symmetric cell cycling to determine long-term stability of Li_6PS_5F, Li_6PS_5Cl, and $Li_6PS_5F_{0.5}Cl_{0.5}$ SEs with metal lithium anodes. The symmetric cells were cycled under different current densities (0.05 mA cm^{-2}, 0.1 mA cm^{-2}, and 0.05 mA cm^{-2}), as shown in Figure 74. They recently employed such symmetric cell cycling experiments to demonstrate interfacial stability of Li_6PS_5Cl against lithium metal [*Electrochimica Acta* 363 (2020): 137128]. Under low current density of 0.05 mA cm^{-2}, all symmetric cells showed flat voltage profiles (Figure 74a) and exhibited good stability between three types of SEs with lithium anode. However, the polarization voltage values follow the trend of $Li_6PS_5F_{0.5}Cl_{0.5} < Li_6PS_5Cl < Li_6PS_5F$, suggesting the smallest resistance in $Li_6PS_5F_{0.5}Cl_{0.5}$-based symmetric cell. On increasing current density, the symmetric cell with Li_6PS_5F died via short at 0.1 mA/cm^2, as shown in Figure 74b. The Li_6PS_5Cl-based cell showed good stability at the current density of 0.1 mA/cm^2, but experienced voltage drop and internal short at 0.2 mAcm^{-2} (Figure 74c). In contrast, the symmetric cell with $Li_6PS_5F_{0.5}Cl_{0.5}$ SE showed polarization voltage at 0.2 V after formation of SEI layer to stabilize the interface (Figure 74d). This indicates that $Li_6PS_5F_{0.5}Cl_{0.5}$ SE has higher stability toward lithium metal than Li_6PS_5Cl and Li_6PS_5F. This finding is consistent with the project's AIMD simulations last quarter, which showed that the P-S bonds (that is, PS_4^{3-} structural units) remain more intact near the Li/$Li_6PS_5F_{0.5}Cl_{0.5}$ interface as compared to that with the other two SEs. To further understand interfacial reactions between lithium metal and $Li_6PS_5F_{0.5}Cl_{0.5}$ SE and to validate findings of AIMD simulations, XPS will be carried out for interface studies.

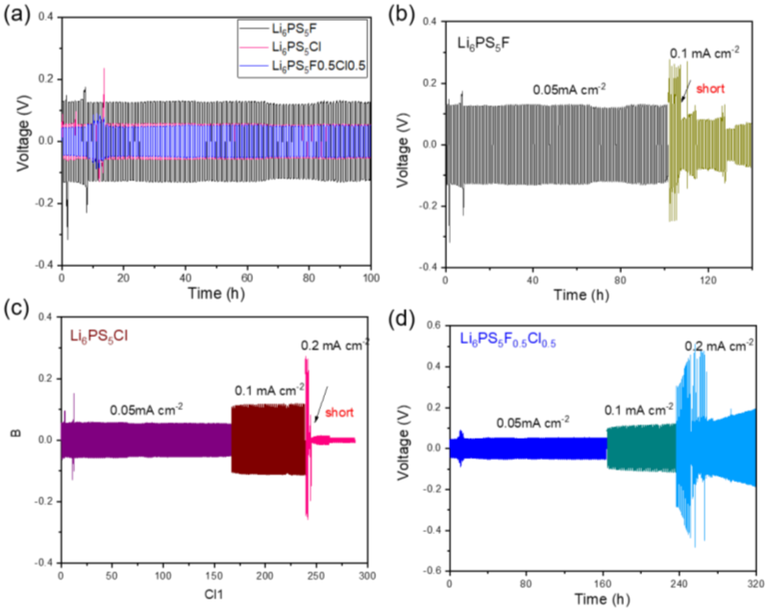

Figure 74. Electrochemical characterization of stability of halide-doped solid-state electrolyte against lithium metal. (a) Electrochemical cycling for Li/SE/Li symmetric cells with solid electrolytes (SEs) of Li_6PS_5F, Li_6PS_5Cl, and $Li_6PS_5F_{0.5}Cl_{0.5}$. Current density of 0.05 mA cm^{-2}; symmetric cell cycling under different current densities with (b) Li_6PS_5F, (c) Li_6PS_5Cl, and (d) $Li_6PS_5F_{0.5}Cl_{0.5}$ as SEs, respectively.

Battery Fabrication and Characterization of Cathode-Electrolyte Interface (CEI). The team fabricated several SSBs with different combinations of binders, wetting agents, SE compositions, and mesoporous cathode architectures. Here, they report the electrochemical performance of five representative batteries (namely, Batteries #1-5) consisting of different SSEs, binders, and wetting agents between cathode and SE (Figure 75). In all cases, they used the same cathode material of C:S (carbon nanotube/sulfur) with 1 mg/cm^2 loading. Lithium was used as the anode material, and all the batteries were run at 0.05 C rate. For Battery #1, they used NMP (as process solvent) in combination with PVDF as the binder, while for all other batteries, they used a water-based binder [carboxy-methyl cellulose/Styrene-Butadiene rubber 5 wt% in DI water (with AB)]. Similarly, for Batteries #1-3, they used an organic (1 M LiTFSI in 1:1 DOL:DME) wetting agent to improve contact between cathode and SE, while for Batteries #4 and 5, they used an ionic liquid made up of N-methyl-N-alkylpyrrolidinium (or piperidinium, PYR) cations and TFSI anions to achieve intimate contact between cathode and SE. They find that the combination of electrolyte composition and the wetting agent has a significant impact on the cycle life of the battery. Battery #1 featuring Li_6PS_5Cl-LiCl electrolyte with DOL-DME-LiTFSI wetting agent showed reasonable cyclability up to 100 cycles (capacity retention ~ 100 mAh/g), as shown by Figure 75a. Although the organic wetting agent provides reasonable cycling for

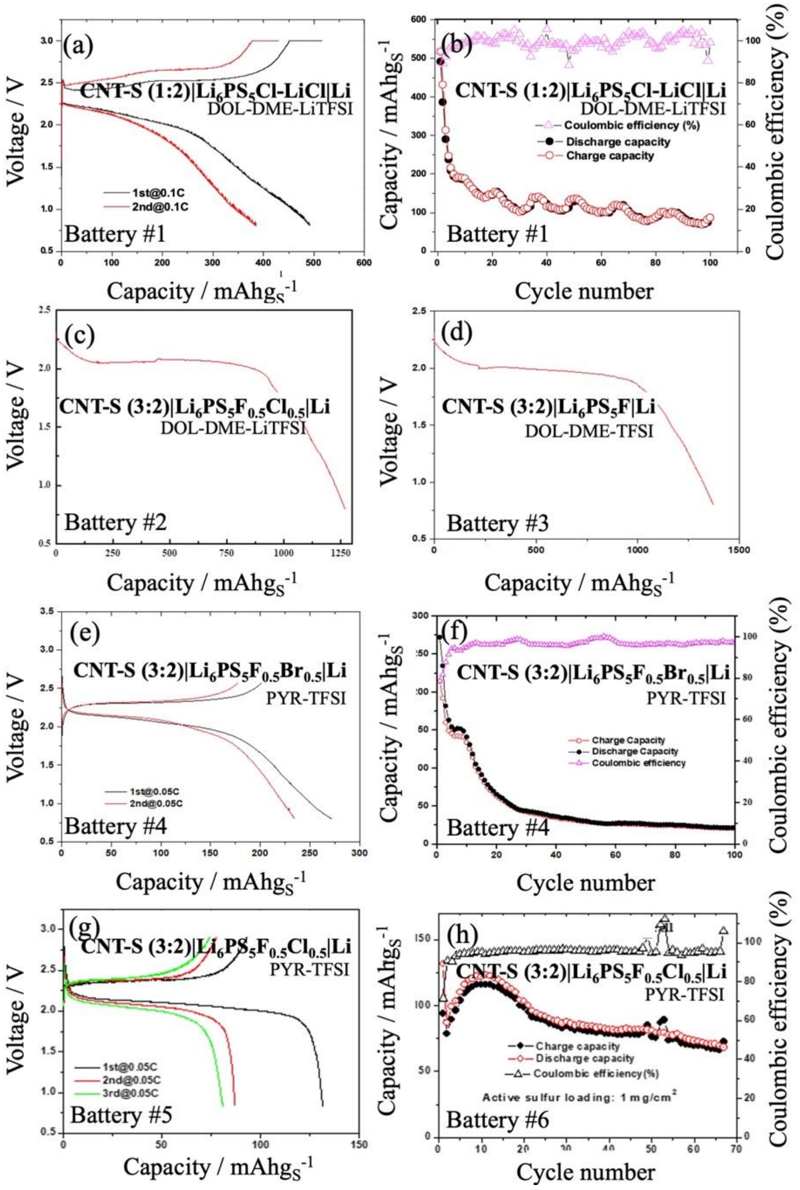

Figure 75. Electrochemical performance of solid-state Li-S batteries. The figure shows charge-discharge characteristics of five representative batteries fabricated this quarter (Batteries #1-5). The electrolyte used in each battery is noted within the panel. For Batteries #1-3, the team uses an organic solvent (1 M LiTFSI in 1:1 vol DOL:DME) as wetting agent, while they use PYR-TFSI ionic liquid in Batteries #4-5. Charge-discharge curves for Batteries #1-5 are shown in panels (a-g), respectively. The capacity of the battery and Coulombic efficiency of Batteries #1/4/5 are shown in panels (b/f/h). Batteries #2-3 employing a combination of F-doped solid-state electrolytes and organic solvent (DOL-DME-LiTFSI) wetting agent failed to charge. See text for a detailed description of batteries.

batteries with Cl-doped electrolytes, these wetting agents render the batteries irreversible (unchargeable) if F-doped electrolytes are employed (Figure 75b-c). For instance, batteries with $Li_6PS_5F_{0.5}Cl_{0.5}$ (Battery #2) and Li_6PS_5F (Battery #3) fail to charge after showing a promising first cycle with a large flat plateau at ~ 2.1 V and high discharge capacities (1271 mAh/g and 1365 mAh/g for $Li_6PS_5F_{0.5}Cl_{0.5}$ and Li_6PS_5F, respectively). The cycle life of batteries containing F-doped SSEs can be improved by using ionic liquid wetting agents (Figure 75d-e). Preliminary batteries with PYR-TFSI ionic liquid wetting agents show excellent cyclability using $Li_6PS_5F_{0.5}Br_{0.5}$ (Battery #4: 100 cycles) and $Li_6PS_5F_{0.5}Cl_{0.5}$ (Battery #5: > 70 cycles). However, the capacities for these batteries using PYR ionic liquid (IL) are quite low (< 100 mAh/g); this is likely related to the high viscosity of the PYR-TFSI ILs. Experiments with low viscosity ILs (such as emim-Cl) are under way.

After the battery cycling tests, the team performed post-mortem characterization using XPS, SEM, and EDX spectroscopy. Each battery was opened carefully under inert atmosphere before characterization. High-resolution spectra were collected for all the elements. The C-C peak of the adventitious carbon, at the binding energy (BE) of 284.5eV, was used for the BE calibration. Figure 76 shows high-resolution S 2*p* spectra from the CEI of each battery, which are grouped into two separate regions, one between 160-164 eV and the other between 166-175 eV. The peaks of the first group originate from lithium sulfide and lithium polysulfides. The spectrum analysis yields three components, namely the lithium sulfide sulfur peak at ~ 162.4 eV, and the peaks of terminal sulfur and bridging sulfur of lithium polysulfide (Li_2S_x with x > 1) at 161.6 and 163.3 eV, respectively. The analysis of the other group yields the S 2*p* peaks at ~ 166.5, 168.5, and 169.1 eV, which are typical BEs for sulfite (S^{4+}) and sulfate (S^{6+}) groups (sulfur-oxygen bonds), respectively. This energy range is also typical of the sulfur present in LiTFSI.

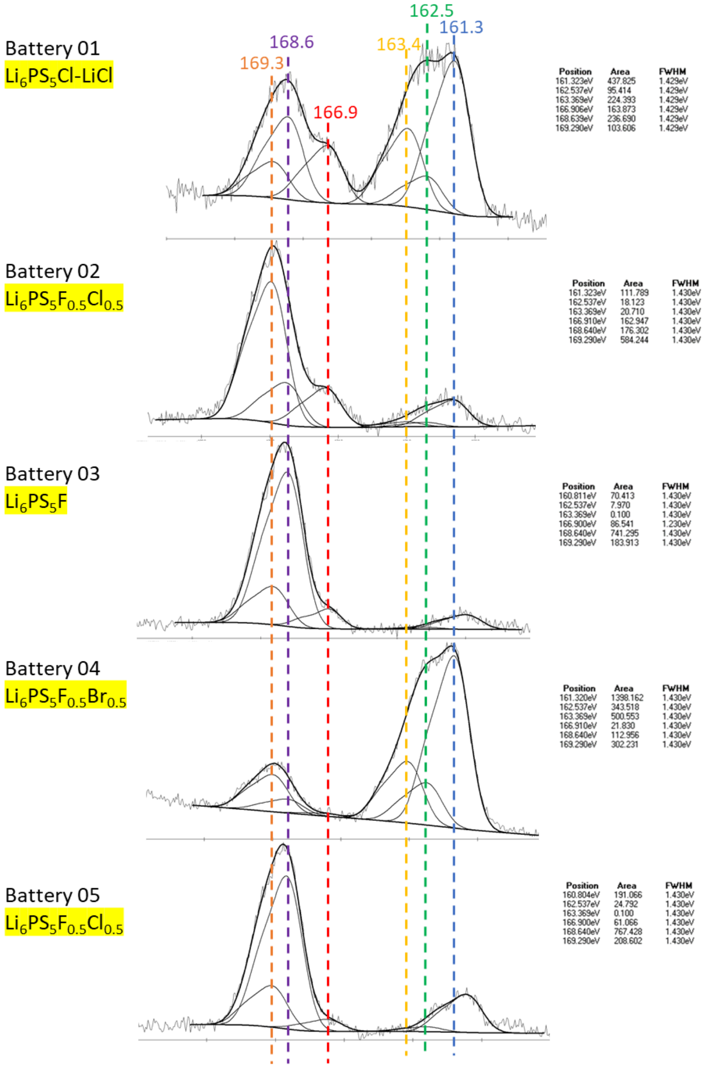

Position	Area	FWHM
161.323eV	437.825	1.429eV
162.537eV	95.414	1.429eV
163.369eV	224.393	1.429eV
166.906eV	163.873	1.429eV
168.639eV	236.690	1.429eV
169.290eV	103.606	1.429eV

Position	Area	FWHM
161.323eV	111.789	1.430eV
162.537eV	18.123	1.430eV
163.369eV	20.710	1.430eV
166.910eV	162.947	1.430eV
168.640eV	176.302	1.430eV
169.290eV	584.244	1.430eV

Position	Area	FWHM
160.811eV	70.413	1.430eV
162.537eV	7.970	1.430eV
163.369eV	0.100	1.430eV
166.900eV	86.541	1.230eV
168.640eV	741.295	1.430eV
169.290eV	183.913	1.430eV

Position	Area	FWHM
161.320eV	1398.162	1.430eV
162.537eV	343.518	1.430eV
163.369eV	500.553	1.430eV
166.910eV	21.830	1.430eV
168.640eV	112.956	1.430eV
169.290eV	302.231	1.430eV

Position	Area	FWHM
160.804eV	191.066	1.430eV
162.537eV	24.792	1.430eV
163.369eV	0.100	1.430eV
166.900eV	61.066	1.430eV
168.640eV	767.428	1.430eV
169.290eV	208.602	1.430eV

Figure 76. X-ray photoelectron spectra from the cathode – solid electrolyte (SE) interface. Details of S *2p* peak arising from the cathode-SE interface for five different batteries shown in Figure 75 are shown. All spectra were de-convoluted consistently for 6 peaks.

CEIs in Batteries #1 and #4 that exhibit reasonable cyclability show strong peaks corresponding to polysulfides. In contrast, the polysulfide peaks are weak for the CE in Batteries #2 and #3 that fail to charge. From these observations, it is reasonable to assume that better cycling batteries show stronger S 2*p* peaks from polysulfides compared to sulfates and sulfites. However, the XPS spectrum from highly cyclable Battery #5 (with $Li_6PS_5F_{0.5}Cl_{0.5}$ electrolyte and PYR-TFSI IL wetting agent) shows stronger peaks in the sulfate/sulfite region, as compared to the polysulfide zone. This is mainly due to the overlapping contributions from sulfur in the IL, which are also expected to appear in the sulfate/sulfite region. The team plans to perform additional studies using ILs that are free of sulfur or fluorine to avoid overlapping signals and investigate interfacial behavior at different state-of-charge. Furthermore, AIMD simulations are under way to understand the effect of IL and organic solvent based wetting agents on the cathode/SSE interface.

Patents/Publications/Presentations

Publication

- Li, Y., W. Arnold, J. Jasinski, A. Thapa, G. Sumanasekera, M. Sunkara, B. Narayanan, T. Druffel, and H. Wang. "Interface Stability of LiCl-Rich Argyrodite Li_6PS_5Cl with Propylene Carbonate Boosts High-Performance Lithium Batteries." *Electrochimica Acta* 363 (2020): 137128.

Task 3.11 – Predicting the Nucleation and Evolution of Interphases in All-Solid-State Lithium Batteries
(Sabrina (Liwen) Wan, Lawrence Livermore National Laboratory)

Project Objective. The goal of this project is to develop and apply a suite of new computational tools to predict early-stage formation of metastable interphases in SSBs. To achieve this goal, this project focuses on meeting three primary objectives corresponding to different regimes within the early-stage interphase formation: (1) identify chemical motifs for pre-nucleation; (2) predict possible interphase structures; and (3) model the kinetics of interphase formation.

Project Impact. Degradation of SSE and formation of undesired secondary interphases at the solid electrolyte / electrode interfaces are some of the key issues that limit SSB technology from practical applications. The computational tools developed in this project will allow modeling of nucleation and formation of interphases with quantum-level accuracy and significantly improved efficiency compared to currently available methods. Completion of this project will also provide valuable insights into the correlation between local chemistry and interphase formation, which can be used to inform the design of interfacial structures to lower interfacial resistance and to extend the cycling life of SSBs.

Approach. The project approach centers on close integration of *ab initio* simulations, ML, and stochastic methods to probe chemistry and nucleation across broad ranges of time and length scales. First, the team will identify chemical motif, which acts as chemical precursor for pre-nucleation based on ML and large-scale AIMD simulations. Second, they will predict possible interphase structures based on stochastic minimizations of population-weighted chemical motifs identified from the MD simulations. Third, they will model the kinetics of interphase formation and evolution using kinetic MC. To test the general applicability of the proposed computational methods, the team considers a variety of commercially viable SE and cathode materials, including cubic LLZO and LiPON SEs and $LiCoO_2$ (LCO) and $LiFePO_4$ (LFP) cathodes. These materials also represent a range of degrees of stability arising from their intrinsic properties—in particular, LiPON|LCO, LLZO|LCO, and LLZO|LFP are expected to form stable, less stable, and reactive interfaces, respectively.

Out-Year Goals. The future goal is to predict practical strategies to either facilitate the formation of desired interphase that allows for fast Li^+ diffusion and is stable on cycling or suppress the formation of undesired interphase to reduce interfacial impedance of ASSBs.

Collaborations. There are no collaborative activities this quarter.

Milestones

1. Construct initial interfacial models for LiPON|LCO, LLZO|LCO, and LLZO|LFP. (Q1 FY 2020; Completed)
2. Perform AIMD simulations for these interfaces. (Q2, FY 2020; Completed)
3. Train and validate ML potentials. (Q3, FY 2020; In progress)
4. Apply ML potentials to sample interfacial chemistry. (Q4, FY 2020; In progress)

Progress Report

Large-Scale *Ab Initio* Simulations of Interfaces. This quarter, the team continued efforts to sample interfacial structures of LiPON|LCO, LLZO|LCO, and LLZO|LFP from high-temperature AIMD simulations. Figure 77 shows example atomic configurations obtained from the AIMD trajectories for various LLZO|LCO interfaces that are initially prepared under different crystallographic orientations of LLZO and LCO. Severe structure degradations are observed at all LLZO|LCO interfaces as cobalt atoms (shown as blue polyhedra with oxygen coordination environment in Figure 77) migrate from the cobalt layer in LCO into the lithium layer and eventually into LLZO. Lanthanum atoms (shown in yellow in Figure 77) also show propensities to migrate toward the surface of LLZO and form La-Co-O clusters at the LLZO|LCO interface. The team is analyzing the structure of such La-Co-O clusters obtained from the AIMD trajectories and comparing the results with simulations performed using the basin hopping algorithm for smaller interfacial models as well as structures sampled using well-trained ML potentials on much larger interfacial models.

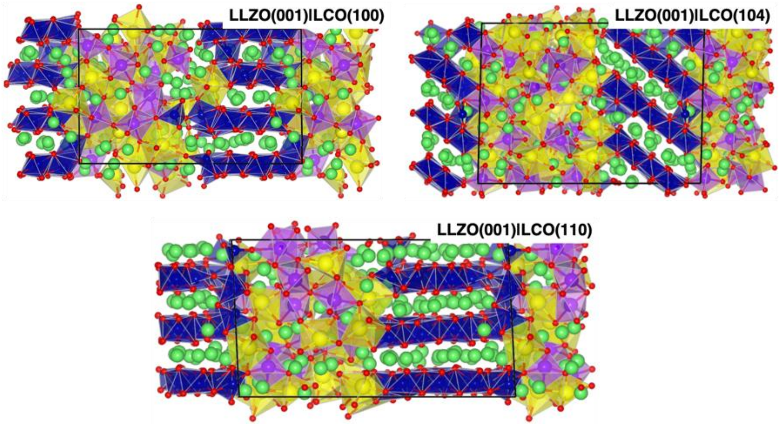

Figure 77. Snapshots of LLZO|LCO interfacial structures from *ab initio* molecular dynamics simulations. The lithium, lanthanum, zirconium, cobalt, and oxygen atoms are represented as green, yellow, purple, blue, and red spheres; the La-O, Zr-O, and Co-O coordination environments are shown as yellow, purple, and blue polyhedra, respectively.

Development of ML Interatomic Potentials. This quarter, the team has tested different ML algorithms and architectures based on artificial neural-network (ANN) to describe the interatomic interactions in bulk LLZO. The training dataset was generated from *ab initio* simulations with certain structural/chemical variations, including strain, vacancies, atomic displacements, and random snapshots from AIMD simulations at various temperatures for crystalline and amorphous LLZO. The first ML model was trained solely on energies with the Chebyshev polynomial representations of radial and angular distribution functions to describe atomic configurations. By performing a series of tests on the architecture of this ML algorithm, the team found that the 30-20 architecture (two hidden layers with 30 and 20 nodes in each layer) gives the lowest training and cross-validation error. The interatomic potentials developed using this ML model also show promising predictions of energies and atomic forces with root mean squared errors (RMSE) of 7.8 meV/atom and 0.89 eV/Å, respectively (see Table 4 below) for a separate testing dataset compared to the *ab initio* results. They are collecting training datasets for various LiPON|LCO, LLZO|LCO, and LLZO|LFP interfaces from *ab initio* simulations and applying the same ML algorithm to develop interaction potentials, which will allow the team to sample the evolution of interfacial structure and chemistry more efficiently. In the meantime, they are testing a different ML algorithm that is trained on both energies and atomic forces for a given structure. They are also exploring different descriptors such as Gaussian, Zernike, and Bispectrum for the definition of local atomic environment. The accuracy and computational efficiency of these different descriptors will be compared and discussed in the next quarterly report.

Table 4. Mean absolute error (MAE) and root mean squared error (RMSE) from machine-learning potentials compared with density functional theory calculations.

Energy MAE (meV/atom)	6.2
Energy RMSE (meV/atom)	7.8
Atomic force MAE (eV/Å)	0.69
Atomic force RMSE (eV/Å)	0.89

Patents/Publications/Presentations

The project has no patents, publications, or presentations to report this quarter.

Task 3.12 – Design of Strain Free Cathode – Solid-State Electrolyte Interfaces Using Chemistry-Informed Deep Learning

(Hakim Iddir, Argonne National Laboratory)

Project Objective. The main objective of this project is to use state-of-the-art ML techniques and high-performance computing to model complex oxide materials that will allow the team to develop cathode – SE interfaces that exhibit minimal or no strain as well as provide the chemical stability at the interface between the cathode material and the SSE. A deep understanding and control of the cathode/SSE interface (including its chemical and mechanical stability) is needed to develop an effective SSB. The active cathode material changes volume during cycling, particularly at high SOC.[1] This volume change leads to strained interfaces triggering loss of contact and delamination, and hence reduction/elimination of electron and ion transport pathways. The increased strain could also generate cracks within the SSE, creating new paths for lithium dendrite growth channels. These structural changes degrade the electrochemical performance of the battery. Several strategies have had limited success in alleviating these drawbacks, including mixed SSE, buffer layers between the cathode and the SSE, and dopants to improve chemical stability of the interface.[2] These approaches, although promising, could not solve both the chemical and mechanical stability of the interface. In this project, the team proposes a new approach that takes advantage of well-established ML techniques and high-performance computing (HPC) to screen for candidate dopants of high-Ni-content NMC cathodes that would both reduce the volume expansion and the chemical reactivity (mixing) at the interface, with minimum impact on the electrochemical performance and energy density of the cathode.

Project Impact. Structure-property relationships are at the heart of most fundamental scientific approaches. However, the link between structure and property remains a challenge in the materials science of complex systems, such as the oxides that form battery components. In particular, the chemical and mechanical stability of the cathode-SSE interface presents a challenge to development of SSBs. High-performance DFT calculations provide the necessary framework to understand such systems. Unfortunately, given the limited number of atoms and time scales accessible by the method along with the myriad calculations required to achieve satisfactory results, the computational cost of simulating all the possible configurations of a multicomponent oxide is prohibitive. In this work, the team augments the DFT data with ML—especially deep learning—techniques that allow them to access large system sizes and longer time scales necessary to build thermodynamic models. They focus on understanding the nature of benchmark $Li_{1-\alpha}Ni_{1-x-y-z}Mn_xCo_yM_zO_2$ structures (M dopant, $\alpha,x,y,z < 1$), their volume change with lithium content, the nature and concentration of the dopants, and the chemical stability of the SSE-cathode interface. The DFT and ML approach will provide new cathode compositions that will reduce the strain of the SSE-cathode interface and hence improve its mechanical and chemical stabilities

In this project, the team aims at developing a methodology that will allow them to explore and expand the configurational space using HPC approaches in a systematic and efficient way. The methodology will encompass DFT, AIMD, MD, and ML. The methodology will also take advantage of various software already developed at ANL and at other DOE laboratories (for example, Balsam) to automate, manage, and control the large number of calculations needed to achieve the project goal.

Approach. All calculations will be performed by spin-polarized DFT as implemented in the Vienna *Ab Initio* Simulation Package (VASP).[3-4] After geometry optimization within the DFT+U framework, electronic relaxation will be performed using a single-point calculation with the hybrid functional HSE06.[5] For production calculations, they will use the message-passing interface (MPI) parallelized version of VASP.

Exploration of the potential energy surface (PES) is needed to predict the structure of solid materials and interfaces. Such calculations are infeasible using MD or DFT calculations alone. Thankfully, the PES of a system can be represented by the sum of the energies of the local neighborhoods surrounding each atom. This enables the use of ML surrogate models trained with DFT calculations to capture the energies in local neighborhoods. The input to the ML surrogate must be a unique representation of the system under study.

Consequently, the local environment of each ion is described using a local environment descriptor that renders the atomic configuration invariant to rotations, translations, and permutations of the atoms. In recent years, several different descriptors have come to prominence with advantages and disadvantages. Once the ML surrogate is trained, the total energy and forces over all the ions of any structural configuration can be determined. Such information can be used for atomistic simulations, namely, MD and MC.

In this project, the team proposes to use the open-source DeepMDkit python/C++ package to construct the ML PES and FFs. The promise of DeepMDkit in this work is to provide near-DFT accuracy at orders of magnitude lower computational expense, comparable to traditional MD simulations. Efficiency in training is facilitated through integration with TensorFlow and MPI/GPU support.

One of the challenges of developing ML PES is achieving accurate predicted forces and energies across the entire configurational space, while minimizing the total number of calculations required for training. In recent years, active learning has been highlighted for its ability to target training examples most likely to improve the model quality or to achieve some other objective (that is, maximizing a predicted material property). DP-GEN, an open source python package based on DeepMDkit, implements a similar active learning scheme with HPC support, and has been employed to construct ML PES with accuracy approaching DFT and sometimes exceeding embedded atom potential for experimentally measured properties of interest.[6] In this work, the team proposes to leverage DeepMDkit and DP-GEN to efficiently generate ML-PESs for cathode-electrolyte systems including a variety of dopants.

Out-Year Goals. One out-year goal involves developing a DFT-trained ML model on NMC/LLZO interface, ready to use for large screening of new cathodes, SSE compositions, and cathodes/SSE interfaces. A second is to provide fundamental understanding on critical parameters limiting performance and stability of the cathode/SSE interface and hence of the SSB

Collaborations. Collaborations in this project include J. Croy, C. Johnson, and E. Lee from ANL Chemical Sciences and Engineering Division for the synthesis phase of the project

Milestones

1. Develop a DFT-trained ML model to determine the low energy configurations for NMC-811. (Q1, FY2020; Completed)
2. Implementation of the ML models to NMC-based oxides. (Q2, FY2020; Completed)
3. DFT-trained ML model for delithiated $LiNiO_2$ and NMC-811. (Q3, FY2020; In progress)
4. ML model based on NMC/LLZO interfaces data. (Q4, FY2020; In progress)

Progress Report

The volume decrease of Li_xNiO_2 during charging causes significant stress and damage to $LiNiO_2$ during cycling. Understanding the volume change in the cathode is paramount for the design of cathode solid electrolyte interfaces. However, the physics of this volume change caused some controversy. The more conventional theory attributes the change in oxygen stacking sequence to the collapse of the spacing between layers.[1] However, more recent evidence points to the electronic depletion around oxygen ions as the main cause of the decrease in the c-lattice parameter.[2] According to previous results for Li_xNiO_2, there are no stable lithium distributions when $x < 0.25$.[3] Hence, for the region of interest in this project ($x < 0.25$), completely delithiated regions are thought to be formed at high SOC, which might trigger a change in the oxygen stacking sequence (O3 to O1, that is, H-2 to H-3). However, since the calculated energies for these two oxygens stacking sequences (O1 versus O3) are very similar, both stacking sequences could be present within the material. To mimic those local composition heterogeneities, a "hybrid" supercell was designed to accommodate different stacking sequences in the delithiated regions. Figure 78a shows a schematic representation of the supercell used for the DFT calculations. The optB86-vdw functional was used to account for non-local interactions.[4] Figure 78b shows the experimental and simulated c lattice parameters at high SOC in each region of the simulated domains. At x = 0.25 the simulated value underestimates the experimental value by about 0.2 Å. Furthermore, the experiment shows some H-3 phase already present at that composition. For even lower lithium content, the simulations predict a collapse in the c lattice parameter that mimics the experimental results. However, there is not a clear difference between the regions with and without lithium and the different stacking sequences. Further investigation of this issue is under way (SCAN+rVV10 and RPA).

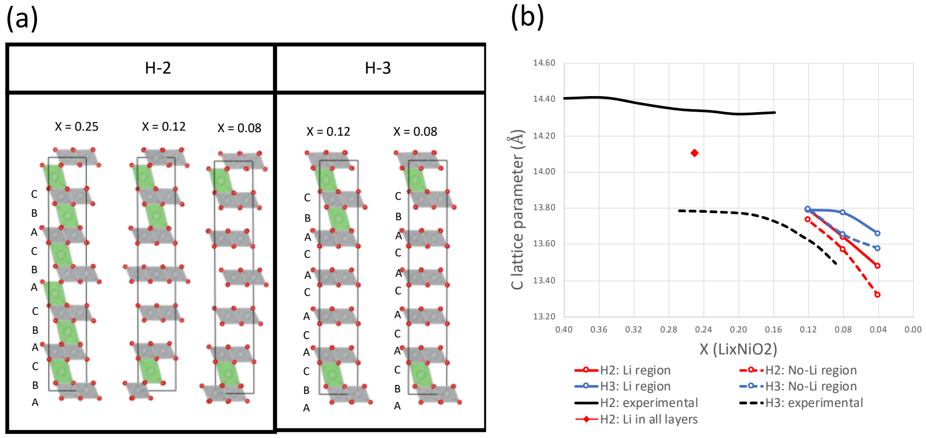

Figure 78. (a) Schematic representation of the Li_xNiO_2 structures used to model a "hybrid" cell where part of the cell can be lithiated, while some layers are completely delithiated. Two different hexagonal structures were represented with different stacking sequences for the delithiated regions. Grey octahedrons represent nickel sites, green octahedrons represent lithium sites, and red spheres represent oxygen ions. (b) Simulated c lattice parameter changes with lithium content for Li_xNiO_2. For compositions with less than x = 0.25, some lithium layers are completely empty (labeled as No-Li region) while other layers have the same amount of lithium as the x = 0.25 composition (labeled as lithium region). All the density functional theory computed values used the optB86b-vdW functional.

Standard DFT does not include van der Waals' forces (VDW). Hence, it does not correctly estimate the interaction between layers of NiO_2 in NiO_2 or the strong correlation of the nickel d electrons. The team has tested several DFT functionals to discard spurious results given by the DFT methodology. The SCAN meta-functional has been shown to account for the strong correlation in $LiNiO_2$.[5] With the addition of VDW in the SCAN+rVV10 functional,[6] it is possible to account for strong correlation and VDW with no empirical terms. Issacs and Wolverton have shown that SCAN+rVV10 yields more accurate predictions of lithium intercalation voltages in rechargeable battery cathode materials than PBE, optPBE-vdw, SCAN or SCAN+rVV10.[7] The team has optimized the geometry of NiO_2 with PBE+U, SCAN, and SCAN+rVV10 functional to demonstrate that VDW is indeed required to model the crystal structure of NiO_2. In going from PBE to SCAN and SCAN+rVV10, one increases the amount of VDW terms in the functional. PBE has no VDW terms. SCAN includes some VDW terms, and SCAN+rVV10 includes all VDW terms. The c lattice constant, which is equivalent to three times interlayer spacing, decreases as VDW terms are added. This is true for both O3 and O1 stacking of the layers of NiO_2. Note that the predicted c lattice constant of 13.33 Å compares well to the experimentally determined value of 13.039 Å for the H4 (O1 stacking) NiO_2 phase.[8] However, the predicted lattice constant for O3 stacking is 13.17, which is lower than the same distance in the predicted geometry for O1 stacking and experimentally measured distance for O3 (R3-NiO_2) stacking of 13.472 Å.[8] The team believes that this difference is largely due to the presence of Ni(II) between the NiO_2 layers in R3-NiO_2, which has stoichiometry of $Ni_{1.07}O_2$ in the experimental sample. A comparison of the binding energies O1 and O3 stacking relative to separated NiO_2 layers (large c distances) is shown in Figure 79. They find the interlayer distances and binding energies for O1 and O3 stacking to be very similar. Although they are predicting that O3 stacking is a kJ/mol lower than O1 stacking, O1 could still have a lower energy than O3 stacking in reality because kJ/mol is likely to be less than the expected error in this calculation. The team plans to conduct RPA calculations for NiO_2 to get a more accurate estimate of the relative energy of O1 and O3 stacking in NiO_2.[9]

They also explored elemental segregation to surfaces. The TM configuration in the material might change with the presence of a surface or an interface. The appropriate description of the cathode solid electrolyte interfaces requires an accurate local composition to estimate interfacial properties. The team followed the same procedure explained in the previous report to explore the potential energy surface using DFT and Bayesian optimization and propose the best candidates in a stepwise manner. Figure 80 shows the energies of different configurations for the first and second round of calculations. The Bayesian optimization procedures found some lower configuration energies in the second round. Continuing this procedure, in the next quarter a "final" optimal configuration will be found.

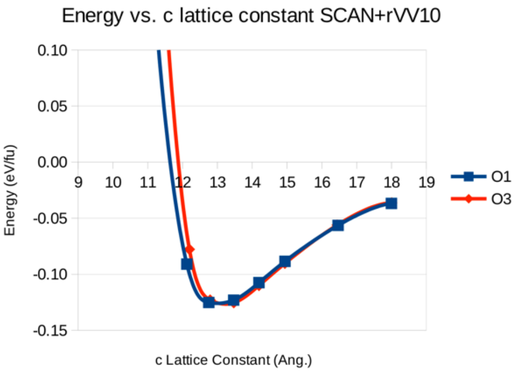

Figure 79. Comparison of the binding energy of O1 and O3 stacking in NiO_2.

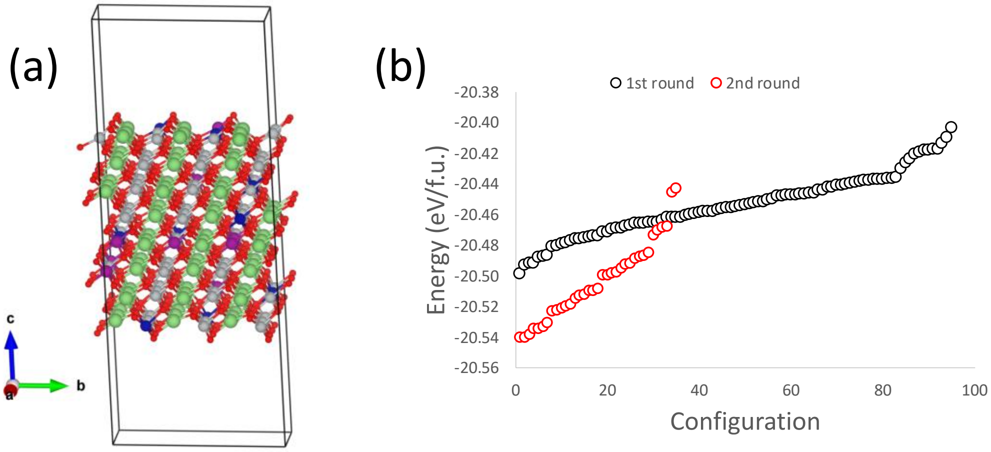

Figure 80. (a) Schematic representation of the NMC-811 surface slab model. Green spheres represent lithium, grey spheres represent nickel, blue spheres represent cobalt, purple spheres represent manganese, and red spheres represent oxygen. (b) Density functional theory calculated energies for 98 configurations (round 1) where transition metals (TMs) are positioned randomly in the TM layers and energies after Bayesian optimization (round 2).

This quarter, the Argonne team began a transition from the open-source AMP Atomistic python package to DeepMDkit and DP-GEN ecosystem. AMP is a foundational package for ML fitting of atomistic potentials with flexibility in both ML modeling and local atomic environment descriptors. Unfortunately, as newer approaches have been developed and packages released, AMP has not received frequent updates and the user community does not appear to be large. Furthermore, the Argonne team had difficulties with force training in AMP. In contrast, DeepMDkit is a more recently developed package with active support and demonstrated successes on both energy and force predictions in multicomponent systems. The Argonne team has some promising preliminary results in fitting FFs for diverse Li_xNiO_2 and NMC-111 structures with high R^2 on the force and energy predictions. Example results for Li_xNiO_2 and NMC-111 are shown in Figure 81. The team plans to add more training geometries from Artrith et al. considering substituents for nickel.[10, 11] DeepMDkit and related software will be a strong choice moving forward, as it will be well suited to run at scale on a variety of HPC resources and shows signs of a rapidly growing user community. In one recent publication, DeepMDkit was shown to scale to a 113,246,208 atom copper system at 1ns per day with a peak performance of 86 PFLOPS.[12]

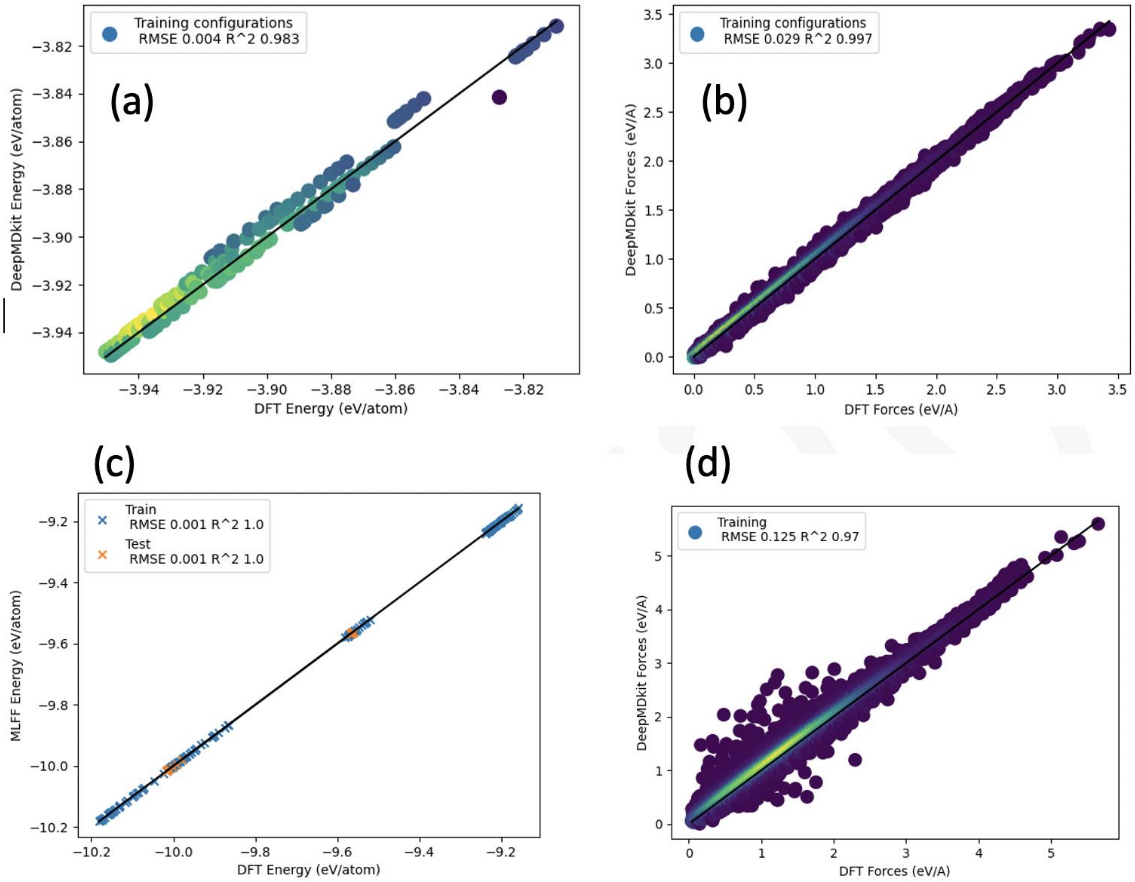

Figure 81. DeepMDkit training (a) energy predictions and (b) force predictions for Li_xNiO_2 structures compared with density functional theory (DFT) training data. (c) Training and test energy predictions and (d) training force predictions for NMC-111 structures compared with DFT training data.

DFT calculations are a powerful tool for predicting the electronic structure of elements and compounds at 0K. However, taking these predictions to finite temperatures is challenging, primarily due to difficulties in evaluating entropy. It was demonstrated by both experiments and computations that the free energy, which includes a temperature times entropy term, can change the relative stability of various phases at room or higher temperatures. In some cases, mixtures can be more stable than individual phases. The thermodynamics of $LiNiO_2$–NiO_2 pseudo-binary sub-system have been studied using the Calculation of Phase Diagram (CALPHAD) approach coupled with *ab initio* calculations and sublattice models of the O1, H1-3, and other

O3 ordered and disordered phases.[13] The study concluded that $LiNiO_2$ and NiO_2 form an ideal solution. However, this result was obtained based on the calculated 0K enthalpy of mixing and the assumption that the entropy consists of an ideal configurational term. It is not surprising that the prediction was an ideal solution. Similarly, the relative stability of the O1, H1-3, and O3 phases was based on 0K results. In this project, the team is evaluating all entropy terms (configurational, vibrational, and electronic) and using the Gibbs free energy to predict finite temperature properties and stability of various phases. To that end, they are examining temperature effects using state-of-the-art thermodynamic modeling that incorporates DFT, AIMD, and ML results, for the particular case of the Li-Ni-M-O system, where M is a metal. The approach was developed by members of the team and was successfully applied to complex, non-stoichiometric oxides.[14] They estimate obtaining significant results during the next two quarters.

References

[1] Bianchini, M., M. Roca-Ayats, P. Hartmann, T. Brezesinski, and J. Janek. "There and Back Again—The Journey of $LiNiO_2$ as a Cathode Active Material." *Angewandte Chemie International Edition* 58 (2019): 10434–10458.

[2] Kondrakov, A. O., H. Geßwein, K. Galdina, L. de Biasi, V. Meded, E. O. Filatova, G. Schumacher, W. Wenzel, P. Hartmann, T. Brezesinski, and J. Janek. "Charge-Transfer-Induced Lattice Collapse in Ni-Rich NCM Cathode Materials during Delithiation." *Journal of Physical Chemistry C* 121 (2017): 24381–24388.

[3] Arroyo y de Dompablo, M. E., A. Van der Ven, and G. Ceder. "First-Principles Calculations of Lithium Ordering and Phase Stability on Li_xNiO_2." *Physical Review B* 66 (2002): 064112.

[4] Klimeš, J., D. R. Bowler, and A. Michaelides. "Chemical Accuracy for the Van Der Waals Density Functional." *Journal of Physics: Condensed Matter* 22 (2009): 022201.

[5] Chakraborty, A., M. Dixit, D. Aurbach, and D. T. Major. "Predicting Accurate Cathode Properties of Layered Oxide Materials using the SCAN Meta-GGA Density Functional." *npj Computational Materials* 4 (2018): 1–9.

[6] Peng, H., Z.-H. Yang, J. P. Perdew, and J. Sun. "Versatile Van Der Waals Density Functional Based on a Meta-Generalized Gradient Approximation." *Physical Review X* 6 (2016): 041005.

[7] Isaacs, E. B., S. Patel, and C. Wolverton. "Prediction of Li Intercalation Voltages in Rechargeable Battery Cathode Materials: Effects of Exchange-Correlation Functional, van der Waals Interactions, and Hubbard U." *Physical Review Materials* 4 (2020): 065405.

[8] Croguennec, L., C. Pouillerie, and C. Delmas. "NiO_2 Obtained by Electrochemical Lithium Deintercalation from Lithium Nickelate: Structural Modifications." *Journal of the Electrochemical Society* 147 (2000): 1314.

[9] Harl, J., L. Schimka, and G. Kresse. "Assessing the Quality of the Random Phase Approximation for Lattice Constants and Atomization Energies of Solids." *Physical Review B* 81 (2010): 115126.

[10] Artrith, N., and A. Urban. "An Implementation of Artificial Neural-Network Potentials for Atomistic Materials Simulations: Performance for TiO_2." *Computational Materials Science* 114 (2016): 135–150.

[11] Cooper, A. M., J. Kästner, A. Urban, and N. Artrith. "Efficient Training of ANN Potentials by Including Atomic Forces via Taylor Expansion and Application to Water and a Transition-Metal Oxide." *npj Computational Materials* 6 (2020): 1–14.

[12] Lu, D., H. Wang, M. Chen, L. Lin, R. Car, W. E, W. Jia, and L. Zhang. "86 PFLOPS Deep Potential Molecular Dynamics Simulation of 100 Million Atoms with *Ab Initio* Accuracy." *Computer Physics Communications* 259 (2021): 107624.

[13] Chang, K., B. Hallstedt, and D. Music. "Thermodynamic Description of the $LiNiO_2$–NiO_2 Pseudo-Binary System and Extrapolation to the $Li(Co,Ni)O_2$–$(Co,Ni)O_2$ System." *Calphad* 37 (2012): 100–107.

[14] Mei, Z-G., and M. Stan. "Pressure-Induced Phase Transitions in UN: A Density Functional Theory Study." *Journal of Alloys and Compounds* 588 (2014): 648–653.

Patents/Publications/Presentations

Presentations

- Northwestern University (July 20, 2020): “Intelligent Material and Process Design”; M. Stan, N. Paulson, J. Libera, D. Dasgupta, J. Gabriel, J. Low, J. Garcia, and H. Iddir. Invited.
- Atomistic Simulations for Industrial Needs (August 5–7, 2020): “Machine Learning Force Fields for Li-Ion Cathodes”; J. Gabriel, J. Garcia Sanchez, N. Paulson, J. Low, M. Stan, and H. Iddir.

Task 3.13 – Tackling Solid-State Electrochemical Interfaces from Structure to Function Utilizing High-Performance Computing and Machine Learning Tools

(Shinjae Yoo, Feng Wang, and Deyu Lu, Brookhaven National Laboratory; Nongnuch Artrith and Alexander Urban, Columbia University)

Project Objective. This project aims at elucidating the structural evolution and other dynamic properties of the interphases at the solid-solid interfaces (SSIs) in SSBs under processing and electrochemical cycling conditions that strongly impact the cell performance. By leveraging synergies of first-principles theory, HPC, ML, and computational/experimental spectroscopy, this project involves a comprehensive investigation of SE systems and SSIs that may enable the practical use of lithium anodes and high-nickel NMC cathodes in SSBs. Specific project objectives are as follows: (1) develop realistic atomic-scale structure models of the SSIs, (2) develop SSB systems designed for integrated experimental spectroscopy and computational modeling of SSIs, (3) determine the impact of structural evolution on the stability and transport properties of the SSIs, and (4) identify the coating/doping chemistry that may stabilize SSIs during formation and electrochemical cycling.

Project Impact. Interfacial properties and the dynamical evolution of interphase structures are crucial for the stability and performance of SSBs. This project will lead to fundamental understanding of current materials limits and will identify key materials parameters for optimizing the performance of SSBs. By corroborating atomic-scale theory with experiment, the project will identify structure–property relationships of the heterostructural SSIs in SSB systems that are relevant for EVs. The outcomes of this project will therefore accelerate development of high-energy-density, safe SSBs for EVs.

Approach. Accurate ML potentials will be trained on an extensive database from DFT calculations to simulate the structure evolution and electrochemical properties of the SSIs. Using a second ML model, key physical descriptors will be extracted from EELS and XAS measurements. This spectral fingerprinting will enable automated interpretation of spectroscopy measurements, thereby bridging between atomistic modeling and experiment. In combination, the two ML models and the spectroscopic data will facilitate the construction of a physics-based model to unravel the structure–property relationships of the SSIs.

Out-Year Goals. The project will progress toward establishing dynamic composition-structure-property relationships for interface stability and transport within and across the electrochemical SSIs in SSBs. The ML approach will be further developed to a general model for thermodynamic and transport properties of dynamic hetero-structural electrochemical interfaces and will eventually be applied to the practical SSB systems.

Collaborations. There are no collaborative activities this quarter.

Milestones

1. Complete experimental measurements of the XAS reference data for NMC cathodes. (Q1, FY 2020; Completed)
2. Benchmark the performance of computational spectroscopy methods against reference experimental nickel K-edge XAS spectra. (Q2, FY 2020; Completed)
3. Complete compiling the extensive reference database of NMC/Al-LLZO DFT calculations needed for the development of ML models. (Q3, FY 2020; Completed).
4. Develop accurate machine-learning potentials (MLPs) for large-scale modeling of $LiTMO_2$ and LLZO, and validate by comparison with DFT. (Q4, FY 2020; Completed)

Progress Report

Last quarter, the team reported development of MLPs for large-scale modeling of LLZO. This quarter, they further refined the ML models for lithiated and delithiated NMC-811 and applied the models to investigate temperature effects by thermally equilibrating (nickel, manganese, and cobalt) distributions. They have also made progress toward the computational interpretation of experimental XAS measurements.

Impact of Temperature on the Cation Order in NMC-811. Last quarter, the team detailed an atomic structure model of NMC-811 obtained from 0 Kelvin structure enumeration. At 0 Kelvin, the nickel, manganese, and cobalt atoms in NMC-811 exhibit a long-range ordering that is not observed in experiments at finite temperatures. The degradation of NMC-811 during battery cycling may involve the migration of TM ions, especially Ni.[1] Segregation may additionally alter the TM distribution at the cathode surface and at interfaces.[2] Therefore, room-temperature structure models are needed that exhibit long-range disordered TM planes and realistic short-range order including segregation effects.

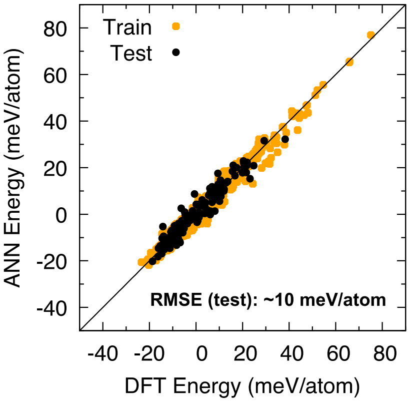

Figure 82. Comparison of structural energies predicted by the artificial neural network (ANN) machine-learning model and the corresponding density functional theory references. The root mean squared error (RMSE) obtained on an independent test set is ~ 10 meV/atom.

The team refined their ML model of NMC-811, which has now been trained on, in total, around 2,000 atomic configurations: ~ 250 lithiated NMC-811 configurations with different (nickel, manganese, and cobalt) orderings, ~ 1,000 partially and fully delithiated NMC-811 configurations, and ~ 700 NMC configurations with composition LiNi$_{1/3}$Mn$_{1/3}$Co$_{1/3}$O$_2$. The ML model accurately reproduces DFT energies and achieves a RMSE of ~ 10 meV/atom, as determined using an independent test set (Figure 82). The ML model can be used in place of DFT to enable modeling of larger structure models and more extensive sampling than would be possible directly with DFT. A manuscript detailing the results is in preparation.

To obtain atomic configurations with thermally equilibrated (nickel, manganese, and cobalt) distributions, the ML model was used to perform Metropolis MC simulations of the TM ordering in NMC-811 structure models with 320 atoms. Annealing from high initial temperatures (1,000–5,000 K) to room temperature (300 K) was simulated, resulting in a database of room-temperature atomic configurations.

Three representative (nickel, manganese, and cobalt) configurations obtained from simulated annealing are shown in Figure 83. As shown, both manganese (magenta) and cobalt (blue) atoms are generally surrounded by nickel (grey), giving rise to hexagonal local motifs of six nickel atoms surrounding either manganese or cobalt. A second-nearest neighbor ordering is also seen, in which manganese atoms prefer linear (stripe) motifs, and cobalt atoms tend to form triangular motifs (Figure 83).

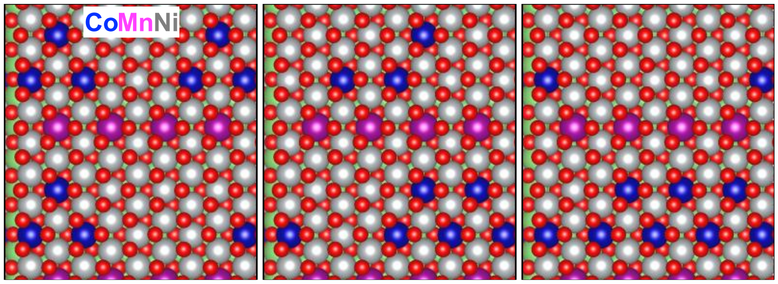

Figure 83. Representative transition-metal (TM) orderings in the TM plane of NMC-811 obtained from simulated annealing with the machine-learning model. Cobalt is blue, manganese is magenta, nickel is grey, and oxygen atoms are red.

The team is analyzing how the TM short-range ordering affects the redox mechanism in NMC-811.

Electronic Structure and Redox Reaction of NMC-811. For the reliable interpretation of XAS measurements of NMC-811 degradation in contact with oxide coatings and SEs with computational tools, the accuracy of the approach first needs to be established. Therefore, electronic structure predictions from calculations were validated (i) by comparison of computational results from a hierarchy of electronic structure theory methods with increasing accuracy and (ii) by comparison with measured XAS spectra under controlled conditions, that is, in the absence of degradation.

Figure shows an example of the *d*-band projected electronic density of states of a nickel atom in NMC-811, as predicted by three levels of DFT. The accuracy is expected to increase from PBE+U[3] to SCAN+U[4] and HSE,[5] respectively. As can be expected, the three methods predict significantly different band gaps, but the partially occupied e_g states predicted by each method are all consistent with a nickel oxidation state of Ni^{3+}. The team confirmed that the three DFT methods predict the same oxidation states for all TM ions and at all SOC (lithium contents), showing that even the computationally most efficient method (PBE+U) already predicts the correct redox mechanism.

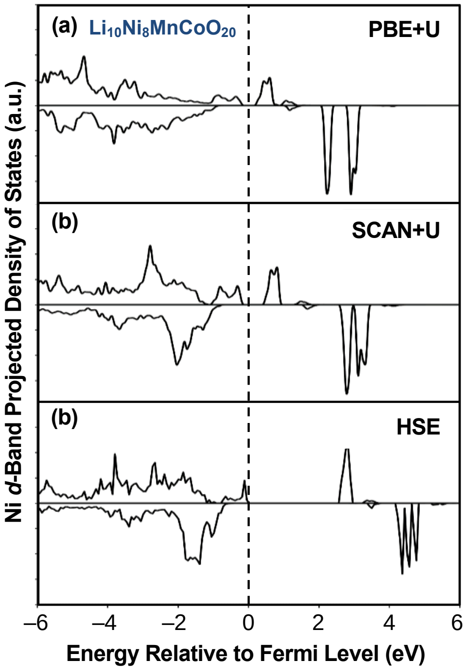

Figure 84. Example NMC-811 nickel *d*-band projected density of states as predicted by three levels of theory (PBE+U, SCAN+U, and HSE). The dashed line indicates the Fermi level.

While the results from theory are consistent, agreement with experiment also needs to be confirmed. The team performed nickel K-edge X-ray absorption near-edge spectroscopy (XANES) measurements for NMC-811 using transmission mode from the pristine and fully charged states. They also performed corresponding spectral simulations using the OCEAN code,[6] which treats the important final state effects using many-body perturbation theory.

Figure 85 shows a comparison of the measured and simulated nickel K-edge XANES spectra. As shown, the simulations are in good quantitative agreement with the measurements, and both the relative peak positions and the shift of the edge during charge are accurately reproduced. This confirms that the project's computational approach is quantitative and suitable for the interpretation of experimental XANES measurements of NMC-811.

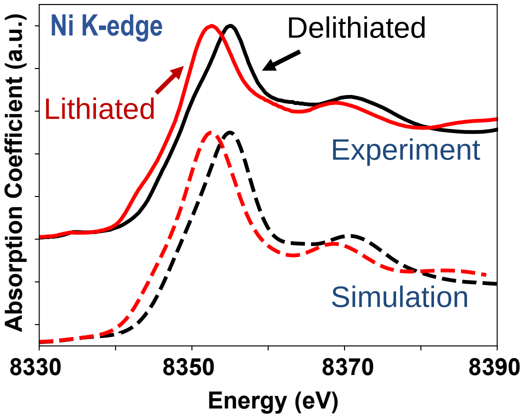

Figure 85. Comparison of measured and calculated nickel K-edge near-edge X-ray absorption spectra of NMC-811 in its pristine (red) and fully charged (delithiated; black) states. The simulated spectra correctly capture the shift of the nickel edge and the main features of the spectra. The simulated spectrum of the delithiated NMC-811 was aligned to the experimental spectrum at the main edge.

References

[1] Kim, J., J. Cho, et al. *Advanced Energy Materials* 8 (2017): 1702028.

[2] Lin, F., M. M. Doeff, et al. *Nature Energy* 1 (2016): 15004.

[3] Jain, A., G. Ceder, et al. *Physical Review B* 84 (2011): 045115.

[4] Long, O. Y., E. A. Carter, et al. *Physical Review Materials* 4 (2020): 045401.

[5] Seo, D-H., G. Ceder, et al. *Physical Review B* 92 (2015): 115118.

[6] Vinson, J., J. J. Rehr, J. J. Kas, and E. L. Shirley. *Physical Review B* 83 (2011): 115106.

Patents/Publications/Presentations

The project has no patents, publications, or presentations to report this quarter.

TASK 4 – METALLIC LITHIUM

Summary and Highlights

The use of a metallic lithium anode is required for advanced battery chemistries like Li-ion, Li-air, and Li-S to realize dramatic improvements in energy density, vehicle range, cost requirements, and safety. However, use of metallic lithium with liquid and solid polymer or ceramic electrolytes has so far been limited due to parasitic SEI reactions and dendrite formation that eventually short circuit the battery. Adding excess lithium to compensate for such losses negates the high-energy-density advantage of a Li-metal anode and leads to further concern for battery safety. For a long lifetime and safe anode, it is essential that no lithium capacity is lost either (1) to physical isolation by roughening, dendrites, or delamination processes, or (2) to chemical isolation from side reactions. The key risk, and current limitation, for this technology is the gradual loss of lithium over the cycle life of the battery.

BMR, Battery500, and other DOE programs are addressing this challenge with many innovative and diverse approaches. Key to all is the need for a much deeper analysis of the degradation processes and new strategies to maintain a dense, fully connected lithium and a dendrite-free electrolyte so that materials can be engineered to fulfill the target performance metrics for EV application, namely 1000 cycles and a 15-year lifetime, with adequate pulse power. Projecting the performance required in terms of just the lithium anode, this requires a high rate of lithium deposition and stripping reactions, specifically about 30 µm of lithium per cycle, with pulse rates up to 10 and 20 nm/s (15 mA/cm^2) charge and discharge, respectively, with little or no excess lithium inventory. This is daunting in the total mass and rate of material transport that must be achieved without failures.

The efficient and safe use of metallic lithium for rechargeable batteries is then a great challenge, and one that has eluded R&D efforts for years. This project takes a broad look at this challenge for both SSBs and batteries continuing to use LEs. Electrolytes reported here include nonflammable liquid solutions, gel type polymer-in-a-salt, composites of ceramic polymer phases, common and novel PEs, and both oxide and sulfide ceramic electrolytes. In most studies, the electrolyte phases were modified by addition of plasticizers or interface coatings to improve transport, stability, and ease of manufacturing. Researchers are typically working toward cycling of full cells with relevant and balanced capacities for the lithium anode and cathode using measures of CE, interface resistance, and post-cycling observation of the disassembled cell components to assess stability of the Li-metal anode and chosen electrolyte.

Highlights. The highlights for this quarter are described below. The projects cover different battery component research directed toward Li-metal or Li-alloy batteries.

For batteries using LEs, two projects are investigating Li-alloy anodes, one as Li-Mg and one as prelithiated Li-Si. Researchers led by W. Xu at PNNL (Task 4.1) have preliminary extended cycling results for Li-Mg alloys in a high-capacity (4.2 mAh/cm^2) cell with 811 NMC cathodes. The anode with 5 wt% magnesium is more stable over 170 cycles than pure lithium; interestingly, however, an alloy with 10 wt% magnesium fails rapidly at 80 cycles. This promising result will be studied further. Y. Cui's team at Stanford (Task 4.6) is investigating prelithiation of silicon anode as a way to eliminate the typical loss measured by the initial Coulombic efficiency (ICE). For the highest concentration of the lithiation reagent, the ICE could be tuned to near 100%. Residual graphene also formed a protective film to further stabilize the silicon anode for a few cycles.

Several programs have reported on single-phase and composite SEs. PNNL (Task 4.1) reports a new gel PE that is non-flammable. Cycling at 60°C was shown for Li//Cu cells and for NMC-622 batteries and appears to be promising. The program at ANL led by N. Markovic (Task 4.3) continues in-depth investigations of the cubic garnet LLZO, doped with tantalum and undoped. The MD work this quarter examined internal GBs by modeling an amorphous layer (~ 2nm) between crystalline plates. The amorphous layer reduced the Li-ion transport for temperatures below 800°C, but conductivity was still higher than for the tetragonal LLZO phase.

They also find that the cubic to tetragonal transition is suppressed for crystallites of small dimensions, ~ 3.6nm. This may explain the stability of the cubic phase for ultrafine-grained nanofibers.

Two programs continue investigation of ceramic-polymer composite electrolytes. J. Nanda's team at ORNL (Task 4.5) furthers their investigation of β-Li_3PS_4 compared to amorphous Li_3PS_4 fabricated with 1 wt% PEO binder. Using Raman spectroscopy and XPS, the team probed the bond coordination of P-S as a function of annealing temperatures to 250°C. There are important transformations of the PS_4^{3-}, $P_2S_6^{2-}$, and $P_2S_7^{4-}$ polyanions, which impacts electrochemical performance of the composite electrolyte. A second program at ORNL (Task 4.2), led by N. Dudney, continued study where both the ceramic and polymer phases are themselves electrolytes. Using LLZO powders from the Materials Engineering Research Facility (MERF) at ANL, a porous ceramic body was sintered at low temperature with improved crystallinity of the cubic phase. Ongoing investigations will examine filling the pores with different PEs. The Li^+ ion transport was further investigated by Li//Li polarization tests and compared to predictions from models for the different relative ceramic loading.

The program led by J. Ye at LLNL (Task 4.4) is addressing fabrication of co-sintered composites of an NMC-622 cathode with Ta-doped LLZO. Sintering at different temperatures in air and argon is mapping conditions where the desired phases and dense bodies can be achieved. Different coatings were applied to the LLZO particles, which improved sintering. In addition, 3D architectures of an NMC cathode covered by LLZO were printed and co-sintered. Several sintered examples of ~ 1-mm-scale mesh patterns were shown.

Task 4.1 – Lithium Dendrite Prevention for Lithium Batteries
(Wu Xu and Ji-Guang Zhang, Pacific Northwest National Laboratory)

Project Objective. The objective of this project is to enable lithium metal to be used as an effective anode in rechargeable Li-metal batteries with good stability and high safety. The investigation this fiscal year will focus on two aspects. First, develop nonflammable PEs and investigate effects of various flame-retardant solvents and polymers on ionic conductivity, lithium CE, Li-anode morphology, flammability, and battery performances in terms of long-term cycling stability and rate capability at various temperatures. Second, establish correlation of morphologies of SEI layer and deposited lithium with electrolyte formulation, current density, and lithium deposition/stripping cycling.

Project Impact. Lithium metal is an ideal anode material for rechargeable batteries, but the application of Li-metal anode is hindered by lithium dendrites and low CE. Although much progress has been achieved in suppressing lithium dendrites and increasing lithium CE in LEs, most of the LEs are flammable and may pose a safety hazard in case of extreme conditions. Therefore, development of electrolytes with improved safety for advanced battery chemistry is imperative. An ideal electrolyte for Li-metal anode should not only suppress lithium dendrite growth and have high CE, but also be intrinsically nonflammable. This fiscal year, the team will develop low flammable or nonflammable hybrid polymeric composite electrolytes (NHPCEs) that have high lithium CE, suppress lithium dendrites, and are stable with high-voltage cathodes. The success of this project will increase safety of Li-metal and Li-ion batteries and accelerate market acceptance of EVs, especially for PEVs as required by the EV Everywhere Grand Challenge.

Approach. The approach will encompass several areas: (1) develop appropriate high-concentration phosphate LEs (HCEs) that have high lithium CE over 98% and can suppress lithium dendrites, (2) add flame-retardant phosphate monomers into the HCEs and utilize radical polymerization to form crosslinked polymer gel electrolyte, and (3) investigate ionic conductivity, electrochemical window, flammability, lithium CE, and morphology. Battery performance of HCEs and NHPCEs will also be investigated.

Out-Year Goals. The long-term goal of the proposed work is to enable Li-metal and Li-ion batteries with a specific energy of > 350 Wh/kg (in cell level), 1000 deep-discharge cycles, 15-year calendar life, and less than 20% capacity fade over a 10-year span to meet the goal of EV everywhere.

Collaborations. This project collaborates with C. Wang of PNNL on characterization by TEM/SEM; K. Xu and M. Ding of U. S. Army Research Laboratory (ARL) on solvent purification and DSC measurements; and B. Polzin at ANL on coated electrode sampling.

Milestones

1. Develop polymerization method to achieve nonflammable PEs with lithium CE > 98%. (Q1, FY 2020; Completed, February 19, 2020)
2. Characterize morphologies of SEI layers and deposited lithium films at different current densities and deposition capacities. (Q2, FY 2020; Completed, March 31, 2020)
3. Investigate lithium CE, deposited lithium morphology, and flammability of hybrid polymer composite electrolytes. (Q3, FY 2020; Completed, August 15, 2020)
4. Achieve over 100 cycles for Li||NMC-622 batteries with nonflammable hybrid polymer composite electrolytes. Characterize compositions of SEI layers and deposited lithium films at different current densities and deposition capacities. (Q4, FY 2020; In progress, expected December 31, 2020)

Progress Report

This quarter, the cycling performance of two Li-Mg alloys with magnesium of 5 and 10 wt% was continually evaluated with comparison of pure Li-metal anode in Li-metal batteries with NMC-811 cathode, but under a stringent condition of high-voltage (4.4 V), high cathode loading (4.2 mAh cm^{-2}), and lean electrolyte (E/C ratio of 3 g $(Ah)^{-1}$). As shown in Figure 86, the Li-Mg5||NMC-811 cell has demonstrated the best performance among three anode materials, with a capacity retention of 80% after 171 cycles. However, the Li-Mg10||NMC-811 cell shows the shortest cycle life, which is quite different from the performance tested in the condition of low cathode loading and flooded electrolyte last quarter. More cell testing is under way to verify the results.

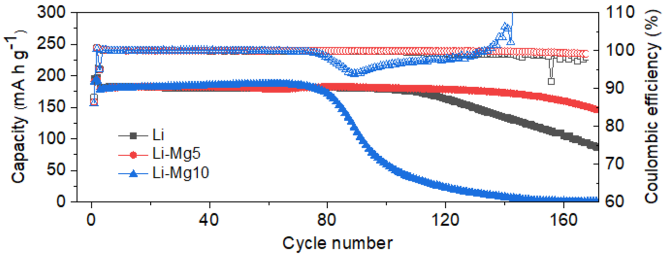

Figure 86. Room-temperature cycling performance of Li||NMC-811 cell and Li-Mg||NMC-811 cells with two Mg-doped lithium anodes (Li-Mg5 and Li-Mg10), 4.2 mAh cm^{-2} NMC-811 cathode, and lean electrolyte at 14 μL comprising flooded electrolyte of LiFSI-1.2DME-3TTE at C/3 charge and discharge rate after two formation cycles at C/10 rate in the voltage range of 2.8-4.4 V.

Furthermore, a phosphonate-based monomer (dimethyl-p-vinylbenzyl phosphonate, hereinafter, DMVP) was successfully synthesized for the fabrication of non-flammable gel polymer electrolytes (GPEs). [^{1}H NMR: (δ 7.25 (d, J = 8.0 Hz, 2H), 7.15 (dd, J = 8.4, 2.6 Hz, 2H), 6.57 (dd, J = 17.6, 10.9 Hz, 1H), 5.62 (d, J = 17.6 Hz, 1H), 5.12 (d, J = 10.9 Hz, 1H), 3.55 (d, J = 10.8 Hz, 6H), 3.04 (d, J = 21.8 Hz, 2H)]. Based on the DMVP monomer, a self-standing GPE membrane was successfully synthesized by *in situ* polymerization (Figure 87a).

The flammability of the GPE was evaluated by ignition test. A butane flame was directly applied to the GPE under ambient condition. As shown in Figure 87b, the GPE exhibits non-flammability, even under constant butane flame blazing. Therefore, this GPE exhibits excellent flame resistivity.

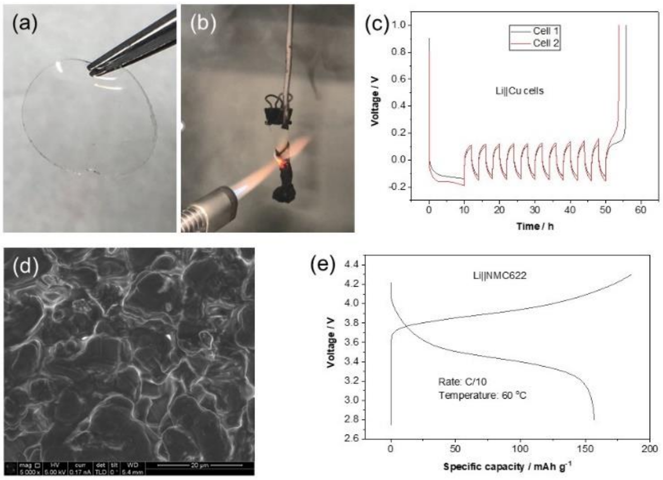

Figure 87. (a) Photo of *in situ* polymerized GPE. (b) Flammability test on the gel polymer electrolyte (GPE). (c) Voltage profile of Li||Cu cells using the GPE during the average lithium Coulombic efficiency measurement. (d) Morphology of deposited lithium in the GPE. (e) Voltage profiles of Li||NMC-622 cell using the GPE at 60°C.

The lithium CE of the flame-resistive GPE was measured in Li||Cu cells at 60°C. Figure 87c shows the voltage profiles of two parallel cells. The average lithium CE was determined to be 81.3%. The deposition morphology of lithium on copper substrate was also evaluated, which shows a granular morphology of lithium (Figure 87d). Figure 87e shows the voltage profile of a Li||NMC-622 cell using the GPE at C/10 rate in the first charge/discharge cycle. The discharge capacity of the cell amounts to 157.1 mAh g^{-1} under such a condition. The long-term cycling performance of the Li||NMC-622 cells is being tested; results will be reported next quarter.

In addition to this experiment work, recent progress in understanding SEI on Li-metal anode was systematically reviewed, especially on the understanding of structures, properties, and influencing factors of SEI as well as efficient strategies of tailoring SEI to elucidate the mechanisms of SEI formation and evolution and to understand how SEI influences lithium deposition morphology and cycle life of Li-metal batteries. The results of this review have been submitted for publication.

Patents/Publications/Presentations

Publication

- Wu, H., H. Jia, C. Wang, J-G. Zhang, and W. Xu. "Recent Progresses in Understanding Solid Electrolyte Interphase on Lithium Metal Anode." Submitted for publication.

Task 4.2 – Composite Electrolytes to Stabilize Metallic Lithium Anodes (Nancy Dudney and X. Chelsea Chen, Oak Ridge National Laboratory)

Project Objective. The project has several objectives: (1) prepare novel polymer and ceramic electrolyte materials that can work together to achieve thin membranes that have the unique combination of electrochemical and mechanical properties required for practical manufacturing and to stabilize the metallic lithium anode for good power performance and long cycle life, (2) identify key features of the composite composition, architecture, and fabrication that optimize performance, and (3) fabricate thin electrolyte membranes to use with a thin metallic lithium anode that provides good power performance and long cycle life.

Project Impact. A stable lithium anode is critical to achieve high energy density with excellent safety, lifetime, and cycling efficiency. This study will identify key design strategies that should be used to prepare composite electrolytes to meet the challenging combination of physical, chemical, and manufacturing requirements to protect and stabilize the Li-metal anode for advanced batteries. By utilizing well characterized and controlled component phases, design rules developed for composite structures will be generally applicable toward substitution of alternative and improved SE component phases as they become available. Success will enable DOE technical targets: 500-700 Wh/kg, 3000-5000 deep discharge cycles, and robust operation.

Approach. This project seeks to develop practical SEs to provide stable, long-lived protection for Li-metal anode. Current electrolytes have serious challenges when used alone; oxide ceramics are brittle, sulfide ceramics are air sensitive, polymers are too resistive and soft, and many electrolytes react with lithium. Composites provide a clear route to address these issues. While work continues to emphasize study of ceramic electrolyte / PE interfaces, this effort has expanded to address the following: (1) practical processing routes to fabricate full batteries using better composite electrolytes with a composite cathode and thin Li-metal anode, and (2) introduction of alternative polymer and ceramic phases to replace well-known model materials and develop improved composite electrolytes. In addition to solid-state devices, hybrid batteries are investigated using a fluid or gel catholyte within the porous cathode. Coatings have also been employed to stabilize electrode interfaces. These directions increase complexity of the studies, but are needed to improve cycling stability and rate performance and to advance practical implementation of the SE and Li-anode technology.

Out-Year Goal. The goal is to use advanced manufacturing processes where the architecture of the composite membrane can be developed and tailored to maximize performance and cost-effective manufacturing.

Collaborations. Work is conducted by Y. Zhang and X. Chen. Ceramic electrolyte powders (LICGC^{TM}) are obtained from Ohara Corporation. ORNL internal collaborators include B. Armstrong and S. Kalnaus. For the single ion conducting (SIC) polymers, the team partnered with J. L. Schaefer at University of Notre Dame. Joseph Libera from Argonne National Lab provided large quantity of LLZO powders.

Milestones

1. Develop methods to minimize interconnected composite electrolytes' interfacial resistance with lithium by varying polymer chemistry. (Q1, FY 2020; Completed)
2. Fabricate interconnected ceramic network with different ceramic chemistry and particle size to increase strength of the composite. (Q2, FY 2020; Completed)
3. Investigate the trade-off between Li^+ transference number and ionic conductivity of the gel composite electrolytes, and optimize it. (Q3, FY 2020; Completed)

4. Fabricate full batteries using NMC cathode, composite electrolyte, and Li-metal anode. Identify cell failure mode. (Q4, FY 2020; Completed)
5. Create chemical/physical bonding between polymer and interconnected ceramic network that leads to optimized interface to improve mechanical modulus and ionic conductivity. (Annual stretch milestone).

Progress Report

This quarter, the team completed the second quarter's pending milestone using LLZO powders provided by MERF. So far, the program has mainly focused on LICGC^{TM} (an LATP type ceramic) in terms of ceramic processing. LICGC^{TM} powders can form necks without significant GB resistance, which is the advantage of a glass-ceramic. However, LICGC^{TM} reacts fiercely with lithium and cannot be used with lithium anode without extra protection. The purpose of this milestone is to evaluate an alternative ceramic, that is, LLZO, which is chemically stable with lithium metal and potentially has higher ionic conductivity.

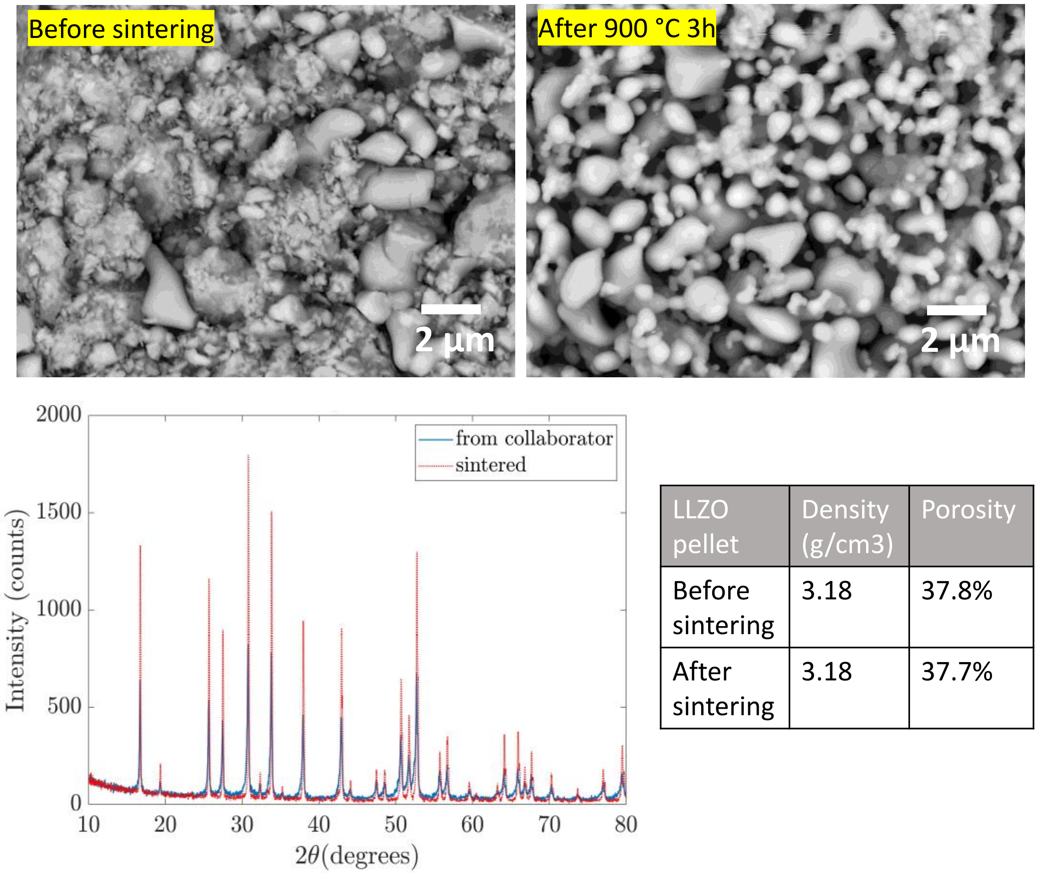

LLZO pellet	Density (g/cm3)	Porosity
Before sintering	3.18	37.8%
After sintering	3.18	37.7%

Figure 88. (top left) Scanning electron microscopy (SEM) image of LLZO pellet before sintering. (top right) SEM image of LLZO pellet after sintering at 900°C for 3 hours. (bottom left) X-ray diffraction pattern of as-received and sintered LLZO, showing the majority is cubic phase LLZO. (bottom right) Density and porosity of LLZO pellet before and after sintering.

LLZO powders were synthesized and milled at MERF and transferred to ORNL. To evaluate the powders, 0.5 g of LLZO was pressed into a .5-inch diameter pellet in an Ar-filled glovebox and sintered at 900°C in dry air for 3 hours. The morphology of the pellet before and after sintering is shown in Figure 88. As the SEM images show, densely packed LLZO powders formed interconnected necked structure after sintering. X-ray diffraction

(XRD) indicates that after sintering, LLZO remained cubic phase. Compared to the XRD of as-received powders, the crystallinity of LLZO improved after sintering. The sintered pellet also lacks a slight shoulder that is observed in the as-received powders on multiple peaks.

The density and porosity of the pressed pellet before and after sintering were estimated by measuring the dimension and weight of two pellets (Figure 88, bottom right). The density is estimated to be 3.18 g/cm^3, corresponding to a porosity of 37.8%, assuming the fully dense LLZO density to be 5.12 g/cm^3.

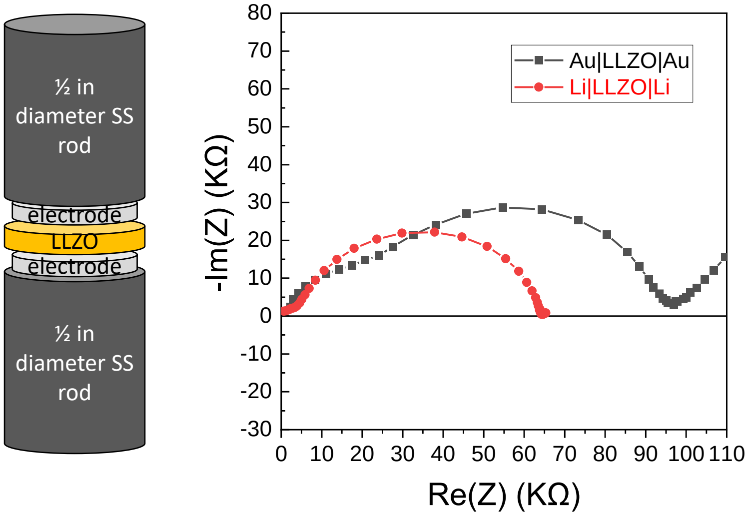

Cell	Au|LLZO|Au	Li|LLZO|Li
Frequency at the top (1st) (Hz)	12 x 10^3	2.0 x 10^3
Resistance (1st) (KΩ)	31	3.4
Frequency at the top (2nd) (Hz)	59 x 10^3	34 x 10^3
Resistance (2nd) (KΩ)	65	61

Figure 89. (left) LLZO symmetric cell with lithium contacts or, alternately, gold-blocking contacts. Impedance results are shown (center and right).

The sintered LLZO pellet was made into a symmetric cell, with either gold or lithium as the electrode. Cell geometry is shown in Figure 89, left panel. The whole cell was sealed with two layers of heat shrink tubing and measured in a AA battery holder. The impedance spectra of Au|LLZO|Au and Li|LLZO|Li are shown in Figure 89, with the analysis tabulated (center and right). Both cells showed two semicircles. The resistance of the first semicircle was 31 KΩ for the gold symmetric cell and 3.4 KΩ for the lithium symmetric cell. This corresponds to a bulk conductivity of 5.1×10^{-6} S/cm and 3.6×10^{-5} S/cm, respectively. The discrepancy between the two cells may come from deformation of the soft lithium against the porous LLZO pellet, as the lithium cell was assembled on a 180°C hot plate. The second semicircle of the gold and lithium cells was very comparable in resistance, both ~ 60 KΩ. This semicircle may originate from the GB resistance between LLZO particles; this will be further investigated in FY 2021.

The team continues investigating full-cell cycling (Milestone 4) using a gel composite electrolyte membrane containing crosslinked PEO (XPEO), dispersed ceramic particles of LICGC^{TM} from Ohara Corporation, and TEGDME as the plasticizer. The full cell was assembled using NMC-622 cathode and a thick Li-metal anode. Because the cathode does not include SE, 20 µl of LE, in this case Gen2, is added as the catholyte. In earlier studies, the amount of Ohara powder in the CEM was varied from 0 to 70 wt%. The highest conductivity was observed for 50 wt% ceramic loading, CEM-50. Batteries made with this gel composite electrolyte cycle reasonably well, here with the LiTFSI and TEGDME and earlier with the Gen 2 salt and plasticizer. The charge and discharge curves with cycling and rate performance are shown in Figure 90a-b. The cell was cycled at 100 µA/cm^2 (C/10) for 10 cycles, followed by 200 µA/cm^2 (C/5) and 300 µA/cm^2 (C/3.3). Capacity fades rapidly after ~ 20 cycles. Interestingly, batteries with other composite gel electrolytes, including XPEO, CEM 30, and CEM-70, cycled poorly for reasons that are not yet understood but may be related to their lower Li$^+$ ion transference number.

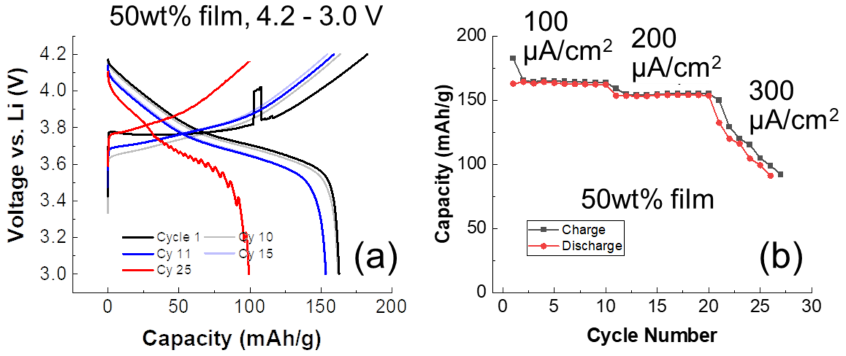

Figure 90. (left) Selected cycles for full cell NMC-622|CEM-50|Li using the gel electrolyte with 50 wt% ceramic particles. (right) Cycling and rate performance of the same cell.

This quarter, the team again reports the current relaxation response of a gel composite electrolyte at 30°C with different LICGC™ content. Compared to initial results in the third quarter, these new cells have a much lower resistance, resulting in less noise in the measured current (see Figure 91). This trend remains the same for the third- and fourth- quarter data sets, where the steady current under 10 mV bias followed the order of CEM-50 > CEM-30 > XPEO > CEM-70, as does the normalized current. The later indicates an uncorrected estimate of the Li^+ ion transference in the gel polymer ceramic composite.

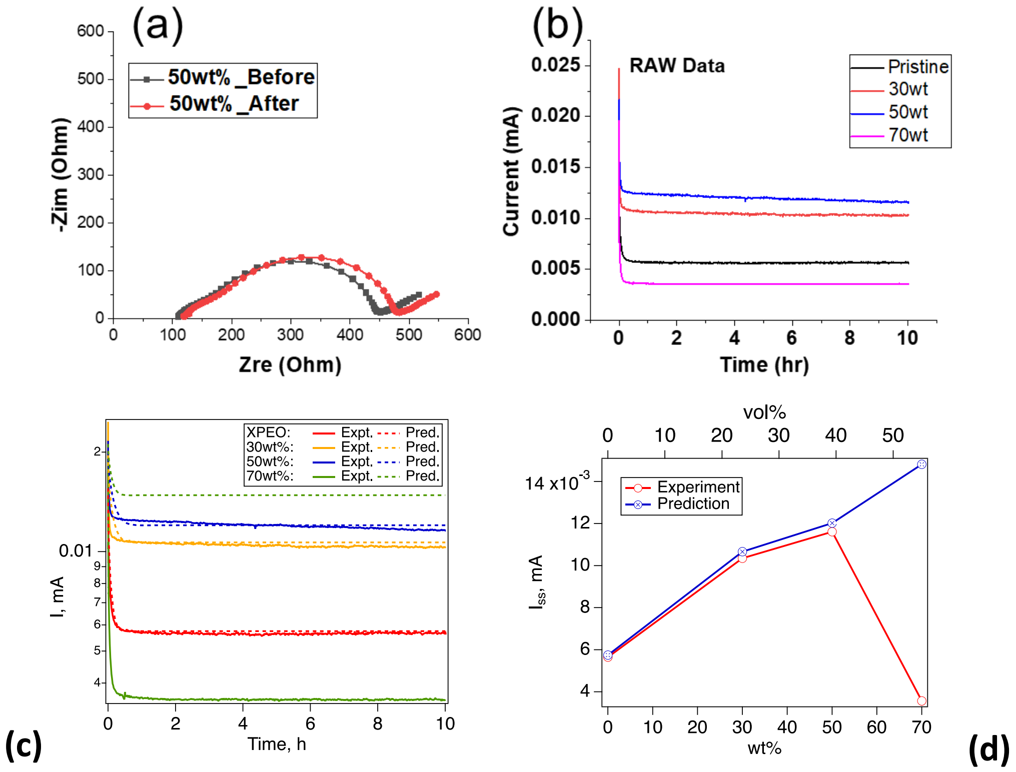

Figure 91. Experiment (a-b) and model (c-d) for chronoamperometry polarization of gel polymer composites in Li//Li cells by 10 mV at 30°C. Four gel polymer XPEO electrolytes were examined with 0 to 70 wt% LiCGC™ dispersed particles. (a) Impedance evaluation for Li/CEM-50/Li cell before and after bias for 10 hours. (b) Current as a function of relaxation time for each of the four electrolytes. (c) Current relaxation to steady state compared to numerical prediction. (d) Steady state current from experiments compared to numerical prediction.

Numerical modeling to predict the transient behavior and relaxation to steady state current under 10 mV bias was also conducted this quarter. Instead of applying electrolyte theory based on effective ionic conductivity and transference number, the team uses Nernst-Plank equations to directly trace the fluxes of anions and cations in the electrolyte due to diffusion and mobility in electric field. The comparison between experimentally measured and predicted chronoamperometry curves is shown in Figure 91c. In the model, the ion diffusivity was taken as an average of the diffusivities in the polymer, ceramic, and gel components of the composite using the corresponding volume fractions. The same approach was done to set initial concentrations of Li^+ and $TFSI^-$. As can be seen, the model significantly overpredicts the current in the case of 70 wt% loading of LICGC^{TM} in the composite. This is further illustrated in Figure 91d, where the steady state current from experiments is compared to that from numerical prediction. To obtain the steady state current, the raw experimental data was passed through binomial smoothing[1] followed by taking central-difference numerical time derivative of the *I-t* data and averaging the values of the points where $dI/dt < 2{\cdot}10^{-05}$ mA/h (considered as "close to zero"). As can be seen, the case where the composite contains a very high amount of LICGC^{TM} does not correspond to the numerical prediction (Figure 91d). A model where the two phases are explicitly resolved, as opposed to being represented by averaged values, is being developed; progress will be reported in the next report.

Reference

[1] Marchand, P., and L. Marmet. "Binomial Smoothing Filter: A Way to Avoid Some Pitfalls of Least-Squares Polynomial Smoothing." *Review of Scientific Instruments* 54 (1983): 1034.

Patents/Publications/Presentations

Publications

- Merrill, L. C., X. C. Chen,* Y. Zhang, H. O. Ford, J. L. Schaefer, and N. J. Dudney. "Polymer-Ceramic Composite Electrolytes for Lithium Batteries: A Comparison Between Single Ion Conducting Polymer Matrix and Its Counterpart." *ACS Applied Energy Materials* 3, No. 9 (2020): 8871–8881.
- Chen, X. C.,* Y. Zhang, L. C. Merrill, C. Soulen, M. L. Lehmann, J. L. Schaefer, Z. Du, T. Saito, and N. J. Dudney. "A Cation Dissociated, Anion Immobilized Gel Composite Electrolyte for Lithium Batteries." In revision.

Task 4.3 – Enabling Solid-State Batteries through Characterization and Modeling (Nenad M. Markovic and Larry A. Curtiss, Argonne National Laboratory)

Project Objective. The project objectives are multi-faceted, including development of a new mechanically and chemically stable and Li-ion conductive ($\geq 2 \times 10^{-4}$ S/cm at 298 K) crystalline/amorphous SE for SSB. The anode and cathode are composed of lithium metal and a Li-based oxide, respectively, allowing operation at cathode potentials > 5 V (denoted as a S_{Li}-S_{EL}-S_C system).

Project Impact. Protective organic and inorganic compounds can enhance stability of the interface, improve Li-ion interfacial transport, minimize dendrite formation, and increase safety in Li-ion batteries.

Approach. The project proposes to develop and use interdisciplinary, atomic-/molecular-level insight obtained from integrating both experimental- and computational- based methodologies to define the landscape of parameters that control interfacial properties for a new generation of the Li-ion solid-solid battery systems. The strategy will involve transferring knowledge gained from well-characterized thin-film materials to real-world materials. This strategy forms a closed loop wherein the knowledge gained from model systems is used to design more complex, real-world materials, and vice versa. The work will focus on utilizing existing in-house synthesis and characterization methods to enable rapid transition from fundamental science to realistic cells.

Out-Year Goals. The out-year goals are to use and develop the physical and chemical synthesis methods for design of solid-solid interfaces with unique chemical/mechanical/conductivity properties. The proposed work will develop and exploit a variety of *ex situ* and *in situ* experimental optical and surface sensitive techniques and electrochemical methods to explore and explain bulk and interfacial properties of the selected materials. The results will serve to unravel many puzzling bulk and interfacial properties of S_{Li}-S_{EL}-S_C systems, including various types of ceramic and glass materials.

Collaborations. This project funds work at ANL and collaboration with J. Sakamoto at UM.

Milestones

1. Chemical stability, evaluation, and correlation with interfacial and bulk chemical reactivity for Li/PEO interfaces. (Q1, FY 2020; Completed)
2. Characterization of lithium / $Li_{0.33}La_{0.55}TiO_3$ (LLTO) interfaces: effect of crystallinity on surface and bulk reactivity and electrochemical stability. (Q2, FY 2020; Completed)
3. Characterization of LCO/electrolyte interfaces: effect of crystallinity and orientation on surface and bulk reactivity. (Q3, FY 2020; Completed)
4. Characterization of lithium interfaces with doped and undoped LLZO, with modeling and experimental study. (Q4, FY 2020; Completed)

Progress Report

MD Modeling of Interfaces in Undoped and Ta-Doped LLZO. Dopant and lithium distribution in the interfacial regions of LLZO play a critical role in stabilization of the high-temperature (T > 630° C) cubic crystal phase (c-LLZO) and determine properties of lithium interactions with the material, including development of inhomogeneous metal distribution. The baseline MD results validate use of Buckingham and Coulomb interatomic potentials by confirming that Li-ion conductivity in cubic phase is orders of magnitude larger than the tetragonal phase, and Ta-doped LLZO (LLZT) retains cubic phase at room temperature.

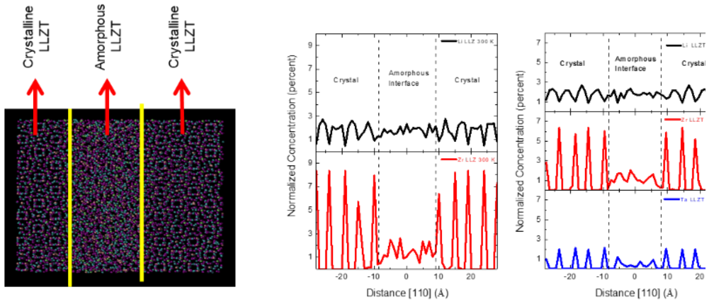

Figure 92. (left) Amorphous interface was created using molecular dynamics with NPT simulation after bringing together two partially melted LLZT surfaces. Amorphous region is ~ 2 nm in width; distribution of lithium (black) and zirconium (red) across internal interfaces in LLZO (center) and LLZT (left). Tantalum distribution is in blue (left).

Tantalum Distribution across Internal Interfaces on Doped LLZO. MD simulations for internal interfaces in LLZO and LLZT were performed using NPT ensemble to equilibrate interface structures obtained by bringing together LLZO or LLZT surfaces initially terminated with lithium, lanthanum, and oxygen in (110) orientation that annealed at high temperature. The resulting structure was further simulated using NVT ensemble and resulted in a formation of about 2-nm-wide disordered region separating crystalline LLZT, as shown in Figure 92 (left). Doped LLZT and undoped LLZO concentration profiles are shown in Figure 92 (right and center, respectively). While structure retains highly organized garnet phase in the crystalline regions, the interfacial region exhibits disorder, which appears to be more pronounced in the case of LLZT. The average atom density ratios in the disordered region are similar to the values for bulk materials. The distribution of tantalum shows higher ordering in the amorphous region close to the interface compared to the middle of the region, in contrast to the zirconium distribution, which does not show such ordering in the amorphous region.

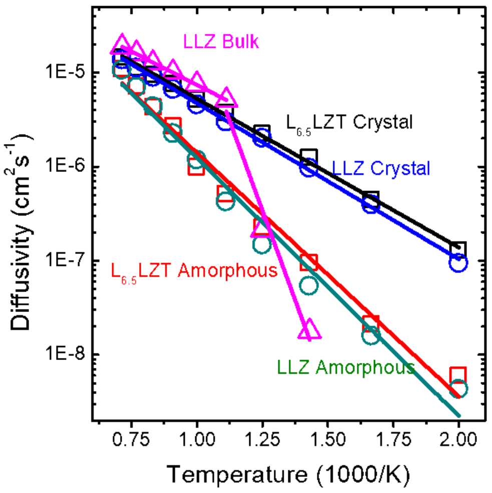

Figure 93. Lithium diffusivities from molecular dynamics calculations of in the interface regions of LLZO and LLZT.

Lithium Diffusivity in the Interface Region of Doped LLZO. While amorphous materials have unique surface and bulk reactivities, the team evaluates how the lithium transport properties are influenced by structure near interfaces. To evaluate these transport properties, they have performed MD simulations at different temperatures for a minimum of 1 ns. The diffusivity was obtained by calculating the MSD at each temperature and applying the Einstein relation, $MSD = 2nDt$, where n is the dimensionality, D is the diffusivity, and t is time. As shown in Figure 93, the crystalline regions of LLZO and LLZT in high-temperature cubic phase show very similar diffusivity to the single crystal LLZO. However, amorphous regions were calculated to have diffusivity lower by more than an order of magnitude compared to crystalline region. The team notes that at lower temperatures, the diffusivity of amorphous LLZO and LLZT is still much higher than bulk tetragonal phase of undoped LLZO. While further investigations are needed, results suggest internal interfaces in cubic phase of these garnets retains favorable lithium transport properties.

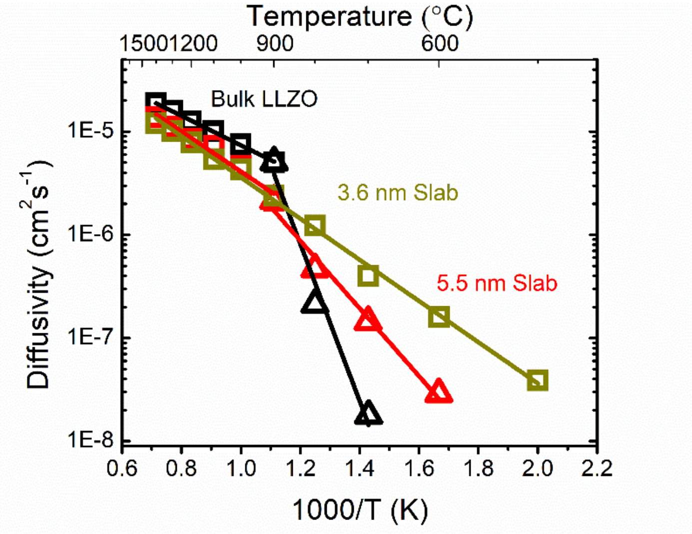

Figure 94. Calculated lithium diffusivity as a function of temperature for bulk LLZO and 2D slabs of thicknesses, 3.6 nm and 5.5 nm.

Size Effect of Lithium Diffusivity in LLZO. On close examination of diffusivities in Figure 93, a surprising result was the absence of the change in diffusivity slope with temperature for crystalline regions of undoped LLZO structure. Since this observation suggests absence of phase transition to tetragonal phase, the team examined several possible reasons using MD simulations. It appears that the size limitation of crystalline regions to several nm with periodic boundary conditions resulted in suppression of the phase transition. They have examined the size effect by calculating temperature dependence of diffusivities of LLZO and LLZT slabs with different thicknesses at 1.8 nm, 3.6 nm, and 5.5 nm bounded by lithium, lanthanum, and oxygen terminated (110) surfaces. Both sides were identical in composition. The diffusivities of two slabs, 3.6 nm and 5.5 nm, are shown in Figure 94. No structural phase transition from cubic phase to tetragonal phase is observed with temperature lowering for 1.8 nm and 3.6 nm slabs. The transition is observed for 5.5-nm thick slab, where diffusivity partially recovers change in slope versus temperature that is associated with the phase transition. The size effect is partially attributed to slight depletion in bulk lithium concentration caused by its migration to the interface in slabs of thickness below 5.5 nm. Characterization of ultrafine grain undoped LLZO nanofibers synthesized using electrospinning method indicate formation of cubic garnet phase in nanoscale grains of undoped LLZO at 600°C and 700°C, by *in situ* wide-angle X-ray scattering at APS 12-ID-B. The cubic phase persists on cooling to room temperature. This experimental evidence is consistent with the team's computational results that indicate suppression of phase transition at small grain size.

The findings from MD simulations on the structure and transport properties of internal interfaces with doped LLZO will help experimental studies on characterization of lithium interfaces with doped LLZO.

Patents/Publications/Presentations

The project has no patents, publications, or presentations to report this quarter.

Task 4.4 – 3D Printing of All-Solid-State Lithium Batteries (Jianchao Ye, Lawrence Livermore National Laboratory)

Project Objective. This project has three objectives: (1) tuning microstructures of 3D-printed SSE separators, (2) determining material and processing compatibilities with cathode printing, and (3) 3D printing of sintering-free SSE separators.

Project Impact. All-solid-state lithium batteries are difficult to process due to the brittleness of ceramic materials, poor solid-solid contact, and electrolyte-electrode stability issues. As a result, the energy and power density and also cycling stability are far from satisfying. This project will address fabrication difficulties by using state-of-the-art 3D-printing techniques that can introduce 3D interfaces and architectures to enhance solid-solid contact and reduce charge transfer resistance. Success will benefit the DOE by establishing the best manufacturing methods for ASSBs to achieve VTO goals on the performance of beyond Li-ion batteries.

Approach. The project employs 3D-printing techniques to manufacture SSEs and related components for ASSBs. The team starts with direct ink writing (DIW) to develop ink recipes with desired rheological properties and explore post-sintering approaches to achieve high densification. In parallel with DIW 3D printing, the team also explores other 3D printing options, such as projection microstereolithography (PuSL). Both sintering and sintering-free approaches can gain benefit from 3D printing and therefore will be investigated.

Out-Year Goals. The team will determine particle sizes and morphologies as well as post-processing conditions that deliver good ionic conductivity and charge transfer properties of LLZTO separators. They will examine co-sintering of LLZTO/cathode and determine the effects of material, particle size, surface coating, and sintering conditions.

Collaborations. Microstructures, ionic conductivities, and mechanical properties will be provided to the LLNL simulation team, led by PI B. Wood, for establishing and validating phase-field modeling methods.

Milestones

1. Atomic layer deposition (ALD) coating on LLZTO/electrode powders. (Q1, FY 2020; Completed)
2. Thermochemical stabilities of electrolyte-electrode-conductive additive mixtures. (Q2, FY 2020; Completed)
3. Down selection of electrolyte-electrode-conductive additive mixtures with good electronic and ionic conductivities. (Q3, FY 2020; In progress)
4. Evaluation of half-cell stability and failure mechanisms. (Q4, FY 2020; In progress)

Progress Report

Co-Sintering Chemical Stability of Cathode/Electrolyte Composite Pellets

LLZTO was ball milled with NMC-622 and co-sintered at three different temperatures (750°C, 900°C, and 1050°C) in different environments (air and argon) to determine the degree of densification and degradation. Three different LLZTO powders were used to explore the effect of sintering aids and coatings on co-sintering outcomes: ball milled LLZTO, ball milled LLZTO with an Al_2O_3 ALD coating, and LLZTO ball milled with 5 wt% lithium borate (LBO). The ball-milled powders were prepared by ball milling LLZTO for 60 minutes with 0.5 mm YSZ beads, and the NMC-622 powder was prepared by ball milling for 60 minutes with 3-mm YSZ beads. The LLZTO and NMC-622 powders were then mixed in a 1:1 wt ratio and ball milled again for 60 minutes with 3-mm YSZ beads before pressing into pellets and co-sintering.

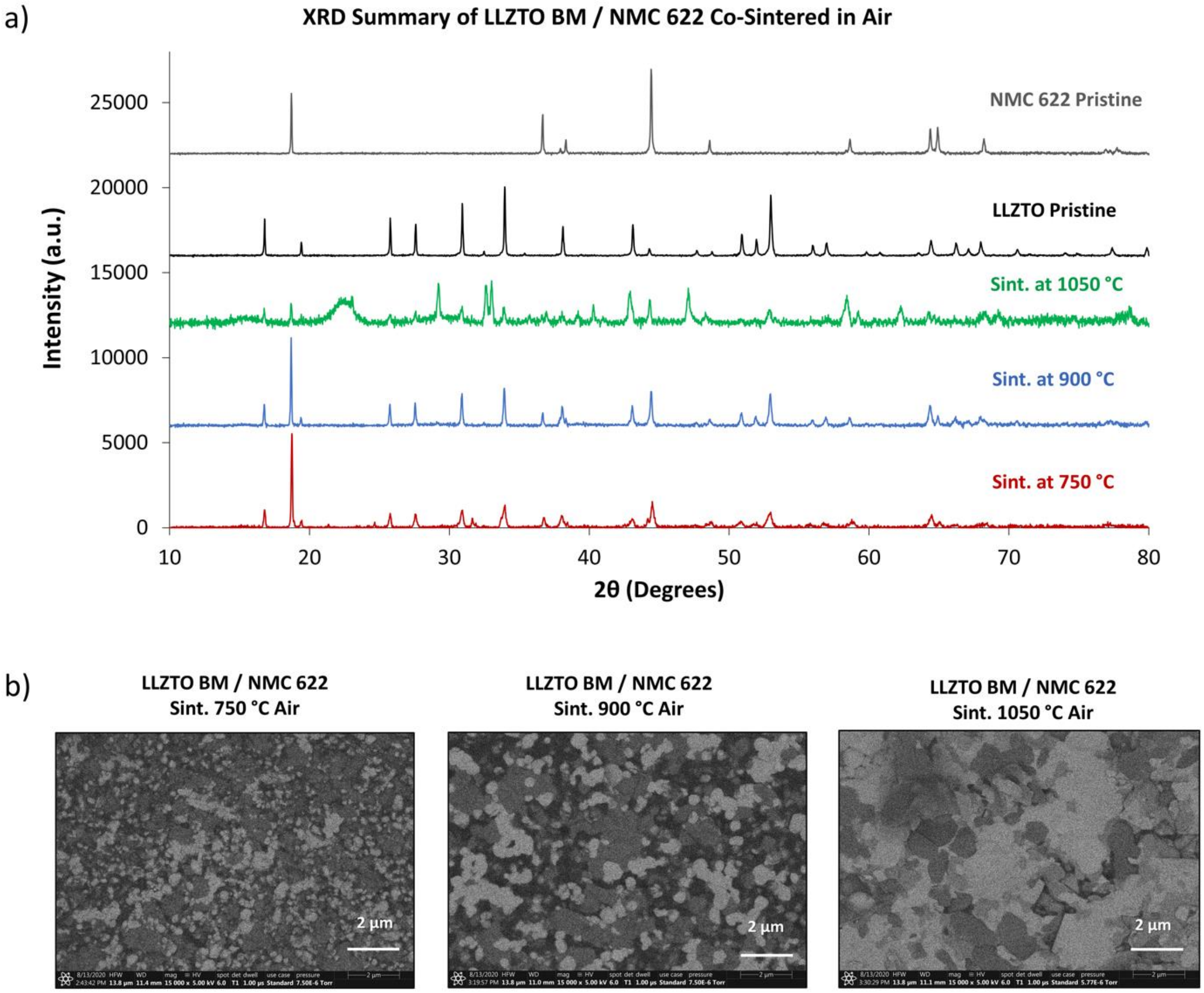

Figure 95. X-ray diffraction (XRD) spectra (a) and backscattered scanning electron microscopy cross-sections (b) of LLZTO (ball milled) / NMC-622 pellets co-sintered at different temperatures for 2 hours with mother powder in air. Pellets were prepared by ball milling LLZTO and NMC-622 (both previously ball milled individually) together in a 1:1 wt ratio for 60 minutes with 3-mm YSZ beads. Note that the broad peak at ~ 22 degrees in the 1050°C XRD spectrum is due to the paper on which the XRD sample was mounted.

Figure 95 shows the XRD spectra and corresponding backscattered SEM cross-sections for ball-milled LLZTO/NMC-622 pellets co-sintered at different temperatures with mother powder for 2 hours in air. The densification and contact between the LLZTO and NMC-622 particles clearly increase with increasing temperature. However, the XRD analysis shows the formation of secondary phases in the 1050°C sample, suggesting interfacial reactions and/or cathode degradation have occurred. While there is a small additional peak at ~ 32 degrees in the 750°C sample (compared to the pristine materials), there are no additional peaks in the 900°C sample, indicating that this temperature does not cause significant degradation, although the sample is still porous.

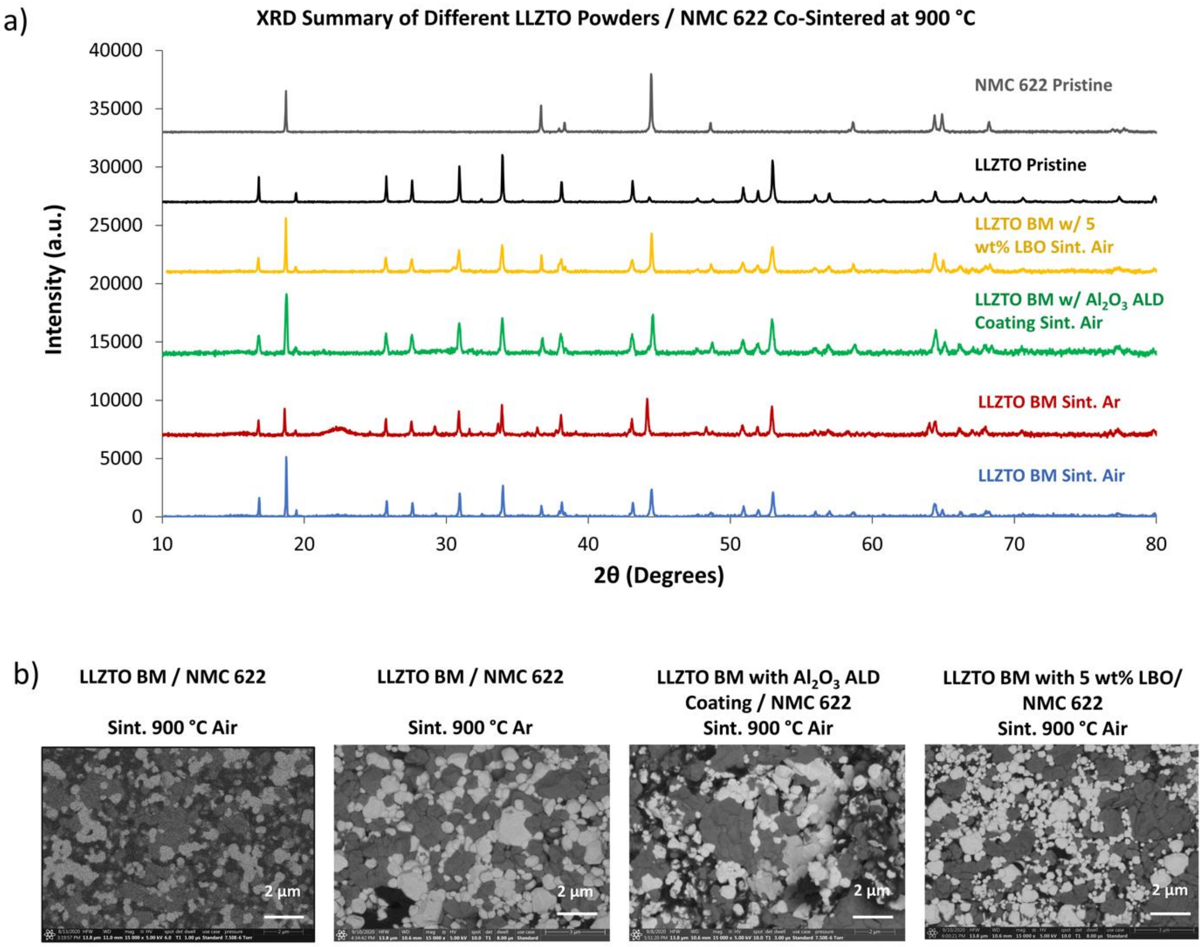

Figure 96. X-ray diffraction (XRD) spectra (a) and backscattered scanning electron microscopy cross-sections (b) of pellets made with different LLZTO powders / NMC-622 co-sintered at 900°C for 2 hours with mother powder in either air or argon. Pellets were prepared by ball milling LLZTO and NMC-622 (both previously ball milled individually) together in a 1:1 wt ratio for 60 minutes with 3-mm YSZ beads. Note that the broad peak at ~ 22 degrees in the XRD spectrum of the sample sintered in argon is due to the paper on which the XRD sample was mounted.

A comparison of the three different LLZTO powders co-sintered with NMC-622 at 900°C for 2 hours is shown in Figure 96. The ball-milled LLZTO/NMC-622 pellet sintered at 900°C in argon densifies much better than the same sample sintered in air. However, the XRD spectrum shows additional peaks that suggest the formation of secondary phases. Therefore, sintering in air seems to be the best environment to preserve the integrity of the materials. The XRD spectra for the three samples made with different LLZTO materials look almost identical, with no additional peaks and no indication of significant degradation. However, the samples made with 5 wt% LBO and the Al_2O_3 ALD coating both sintered better than the sample made just with ball-milled LLZTO, suggesting that the coating and LBO additive facilitate sintering between the electrolyte and cathode particles at lower temperatures.

Co-Printing and Co-Sintering

Several ink recipes for DIW of both LLZTO and NMC-622 layers were investigated. Binders including polyvinyl butyral (PVB), cellulose, poly(ethylene glycol) diacrylate (PEGDA), polypropylene carbonate (PPC), and PEO with corresponding solvent systems have been tested for both raw LLZTO and NMC-622 powders. It was found that although most binders work fine with raw powders (several micrometers size), some may strongly interact with ball-milled powders, leading to accelerated degradation of ink properties. Figure 97a shows a co-printing of a log-pile NMC-622 structure followed by a uniform coating of LLZTO layer based on a solvent recipe with PVB binder. Raw powders worked well for this approach. Co-sintering of the printed bilayer structure was conducted at different temperatures and in either air or argon environment (shown in Figure 97b-d). While possible thermal-induced reactions as indicated from color change are still under investigation, the geometry of the bilayer structure can be well maintained after co-sintering. Very limited shrinkage in addition to 3D interface can be attributed to the structural integrity; albeit, it leads to a porous structure that is highly resistive. It is critically important to develop NMC and LLZTO inks with low-temperature densification capability and synchronized shrinking behavior to avoid thermal-induced strain mismatch. Proper binder systems with optimized solid content are under development to achieve good printability and mechanical and chemical compatibility during co-sintering.

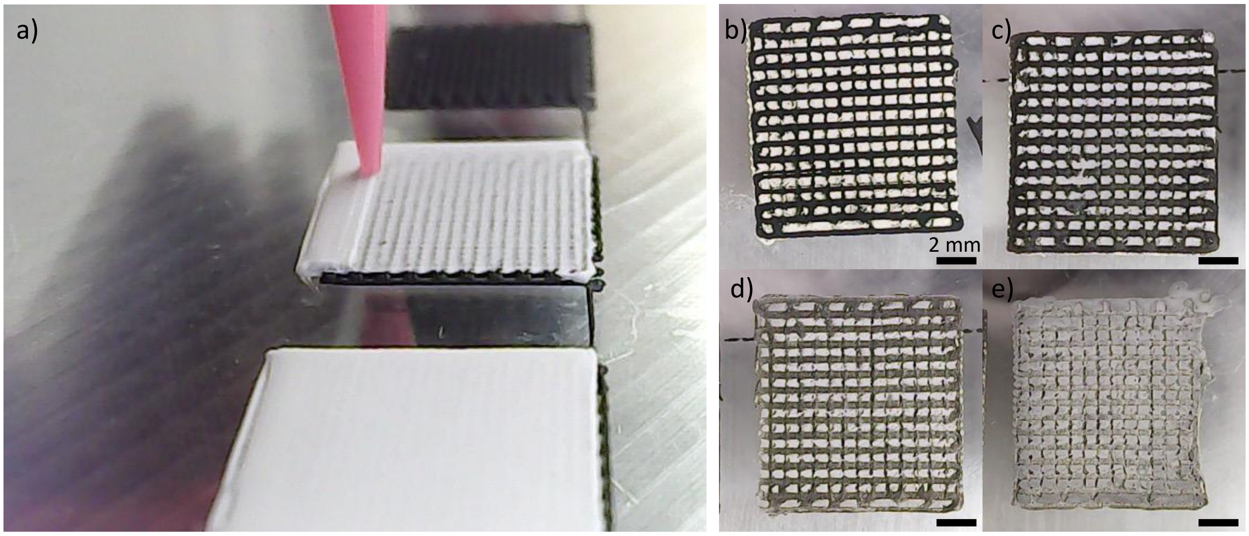

Figure 97. (a) Direct ink writing of a structured NMC-622 cathode followed with a uniform coating of LLZTO layer. (b-e) The NMC/LLZTO bilayer co-sintered at 750°C in air, 750°C in argon, 900°C in argon, and 1050°C in argon, respectively. Note the color change with the increase of temperature, suggesting possible thermal-induced reactions.

Patents/Publications/Presentations

Publication

- Wood, M., X. Gao, R. Shi, J. Espitia, T. W. Heo, J. A. Espitia, E. B. Duoss, and J. Ye. "Exploring the Relationship between Solvent-Assisted Ball Milling, Particle Size, and Sintering/Temperature in Garnet-Type Solid Electrolytes." Under revision.

Task 4.5 – Interfacial Studies on Lithium Thiophosphate Based Solid Electrolytes and Cathodes (Jagjit Nanda, Oak Ridge National Laboratory)

Project Objective. Capacity fading and the underlying interfacial side reactions between thiophosphate SEs and cathode active materials are not well understood. A key project deliverable is to combine EIS measurements with complementary *in situ* and *ex situ* spectroscopy and microscopy to identify decomposition reaction products at the CEI. Ultimately, this work will enable a mechanistic understanding of factors that limit the rate performance and capacity loss of SSBs. The goal here is to combine the information from these techniques to provide a unified overview of the interfacial layer's composition, structure, and morphology. In this multi-year work, the team will investigate a number of SEs [Li_3PS_4 (LPS), $Li_{10}GeP_2S_{12}$ (LGPS), and $Li_{9.54}Si_{1.74}P_{1.44}S_{11.7}Cl_{0.3}$ (LSiPCl)] and cathode compositions belonging to different structural families [$LiFePO_4$ (olivine), FeS_2 (sulfide-based conversion cathode), and $LiNi_{0.6}Mn_{0.2}Co_{0.2}O_2$ (NMC-622, layered oxide)].

Project Impact. SSBs are poised to be the next-generation battery technology for meeting EV goals in terms of energy density, cycle life, and safety. Among other technical barriers, the success of this technology relies on design of stable electrode/electrolyte interfaces. Sulfide-based SEs have high ionic conductivity ($> 10^{-4}$ S/cm) and are mechanically soft, which simplifies processing compared to their oxide counterparts. Furthermore, sulfide SEs are comprised of earth abundant materials (for example, sulfur and phosphorus) and can be easily synthesized using scalable, low-temperature solution-based routes.

Approach. A low-temperature (< 350°C) solution-based synthesis method will be used to synthesize the LPS family of SEs. The structure of these materials is characterized using XRD, Raman spectroscopy, and neutron scattering. Standard AC/DC electrochemical methods are used to characterize ionic conductivity, electrochemical stability, and CCD. The work scope includes using various *in situ* and *ex situ* electrochemical, microscopic, and spectroscopic tools for characterizing the structure, morphology, and kinetics of the interfacial reaction layer formed between thiophosphate SEs and cathodes.

Out-Year Goals. Develop thiophosphate SEs – sulfide cathode interfaces with low ASRs for ASSBs.

Collaborations. This project will collaborate with G. Ceder (UC Berkeley) and P. Jena (Virginia Commonwealth University) on modeling and synthesis guideline, as well as with S. Greenbaum on solid-state NMR to measure ion-diffusivity and local bonding.

Milestones

1. Identify synthesis, doping, and processing conditions to prepare Li_3PS_4-based SEs with Li^+ conductivity exceeding 10^{-4} S/cm. (Q1, FY 2020; Completed, December 31, 2019)
2. Develop binder systems for Li_3PS_4 family of SEs for improving processability and stability at the Li-metal and cathode interfaces. (Q2, FY 2020; Completed)
3. Measure and compare the Li^+ diffusion coefficient for pristine Li_3PS_4 and substituted Li_3PS_4 SEs using solid-state NMR. (Q3, FY 2020; In progress and moved to Q4)
4. Undertake *in situ* Raman and electron microscopy including cryo-TEM for characterizing Li_3PS_4 and cathode-Li_3PS_4 interfaces as part of determining the ASR. (Q4, FY 2020; Completed)

Progress Report

This fiscal year, the team developed solvent-mediated synthesis routes to produce thiophosphate-based SEs including: (i) crystalline ß-Li_3PS_4, and (ii) composites containing amorphous Li_3PS_4 + PEO binder. The Li_3PS_4+PEO polymer/ceramic composites generally exhibit lower conductivity (for example, 8 x 10^{-6} S/cm versus 1 x 10^{-4} S/cm for ß-Li_3PS_4 at room temperature), which is attributed to: *(i)* the negligible conductivity of the polymer phase, which contains no Li-based salt, *(ii)* the intrinsic properties of amorphous Li_3PS_4 that may contain Li-P-S bonding environments with lower Li^+ mobility compared to ß-Li_3PS_4, and *(iii)* the lower Li^+ concentration in amorphous Li_3PS_4 as indicated by the presence of trace Li_2S from the XRD and cryo-TEM measurements (reported in the second quarter). To better understand the near-order structure of the composites and how it changes with thermal treatment, Raman spectroscopy and XPS measurements were performed on ß-Li_3PS_4 and amorphous Li_3PS_4 + 1% PEO composites.

Figure 98 presents Raman spectra of ß-Li_3PS_4 and amorphous Li_3PS_4 + 1% PEO composites after thermal treatments up to 250°C. As expected, the ß-Li_3PS_4 showed a single peak at 427 cm^{-1}, which is assigned to a P-S stretch in the structure's isolated PS_4^{3-} tetrahedra. In comparison, the unheated composite showed several Raman-active bands in the range 100-600 cm^{-1}. The bands at 395 and 435 cm^{-1} are assigned to P-S vibrational modes of the $P_2S_6^{2-}$ and PS_4^{3-} polyanions, respectively. The Raman spectra of Li_3PS_4 + 1 wt% PEO exhibited subtle changes in the range 390-430 cm^{-1} on heating due to rearrangement of the polyanionic network. More specifically, heating at 140-200°C resulted in a new band at 408 cm^{-1} (attributed to formation of $P_2S_7^{4-}$ polyanions) and increased intensity ~ 430 cm^{-1} (attributed to PS_4^{3-}). Compounds with these polyanionic structures (for example, ß-Li_3PS_4 and $Li_7P_3S_{11}$) typically exhibit higher Li^+ conductivity compared to structures containing $P_2S_6^{2-}$ (for example, $Li_2P_2S_6$), which was the predominant moiety in the unheated sample. This finding is consistent with the conductivity measurements reported in the second quarter that showed that annealing Li_3PS_4 + 1% PEO at 140°C increased the material's Li^+ conductivity by several orders of magnitude.

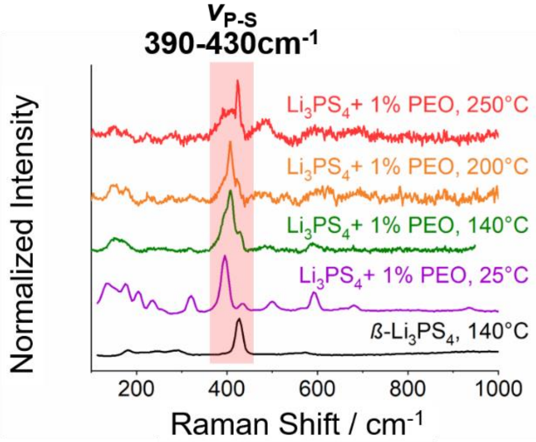

Figure 98. Raman spectra of ß-Li_3PS_4 and amorphous Li_3PS_4 + 1 wt% PEO dried overnight at 25-250°C. Signals near 400 cm^{-1} provide information on how the P-S bonding environment changes with different thermal treatments.

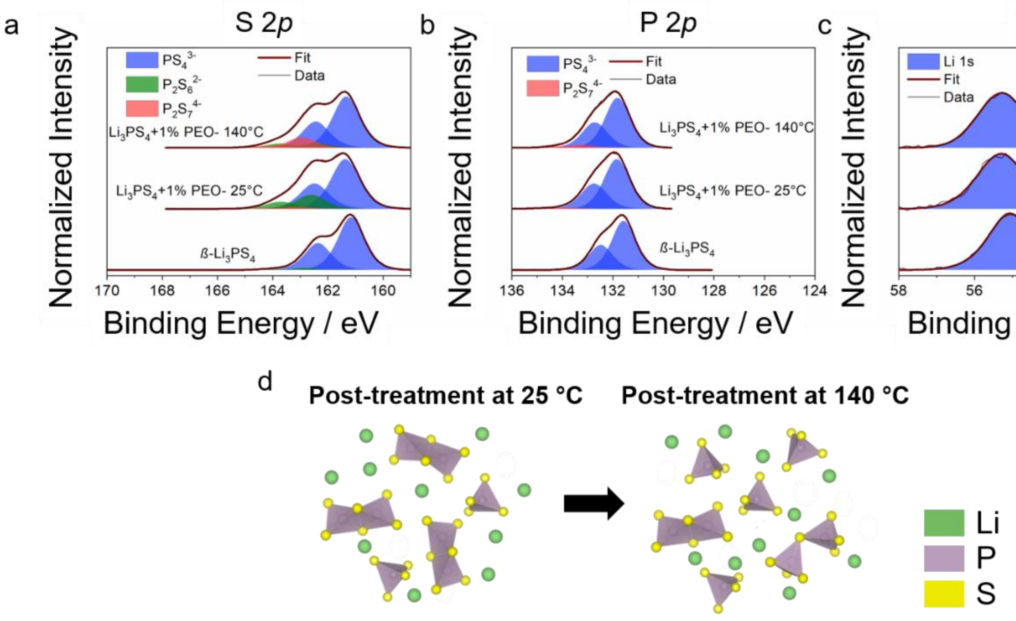

Figure 99. X-ray photoelectron spectroscopy analysis showing core-level scans of (a) S 2p, (b) P 2p, and (c) Li 1s for ß-Li_3PS_4 and amorphous Li_3PS_4 + 1 wt% PEO dried overnight at 25°C and 140°C. Compared to ß-Li_3PS_4, the amorphous composites contained a broad distribution of Li-P-S bonding environments, which resulted in lower Li^+ conductivity (reported in the second quarter). (d) Schematic of structural variation between the PS_4^{3-}, $P_2S_6^{2-}$, and $P_2S_7^{4-}$ polyanions as a function of post-processing temperature.

To complement the Raman measurements in Figure 98, the near-surface structures of Li_3PS_4 + 1% PEO and ß-Li_3PS_4 were studied using XPS, and core-level S 2p, P 2p, and Li 1s spectra are provided in Figure 99a-c, respectively. The S 2p and P 2p spectra of ß-Li_3PS_4 showed doublets due to $2p_{1/2}$ and $2p_{3/2}$ spin-orbit splitting where the components were separated by 1.1 and 0.9 eV for S 2p and P 2p, respectively. These features indicate a single type of P-S bonding environment was present in ß-Li_3PS_4 (that is, isolated PS_4^{3-} tetrahedra). In comparison, the amorphous Li_3PS_4 + 1% PEO samples showed significantly broader signal in the S 2p spectra with additional features at 162.6-163.7 eV, which are assigned to $P_2S_6^{2-}$ and $P_2S_7^{4-}$ polyanion structures that contain bridging sulfur bonds. Notably, the sample annealed at 140°C contained more $P_2S_7^{4-}$ and less $P_2S_6^{2-}$ compared to the unheated sample, which is consistent with the Raman findings. On the other hand, the P 2p spectra of the composites were very similar to that of the ß-Li_3PS_4, which may be due to similar 2p binding energies of phosphorus in different polyanion structures (for example, PS_4^{3-} versus $P_2S_7^{4-}$), thus making it difficult to resolve these subunits. The Li 1s spectra of the composites were broader and shifted by +0.2 eV compared to ß-Li_3PS_4, which indicates the amorphous Li_3PS_4 contained a wider distribution of local Li-P-S bonding environments that led to their lower Li^+ conductivity as reported in the second quarter. The XPS and Raman data show important transformations in the PS_4^{3-}, $P_2S_6^{2-}$, and $P_2S_7^{4-}$ polyanions during annealing, which is presented schematically in Figure 99d. These structural variations have critical implications on the electrochemical performance of the composite SEs.

Experiments in FY 2021 will compare the performance of SSBs containing ß-Li_3PS_4 and composite SEs. The effects of electrolyte composition and key testing parameters (for example, stack pressure) on the cycling performance and electrode/electrolyte interfacial stability will be probed using *in situ* spectroscopic and microscopic techniques.

Patents/Publications/Presentations

Publications

- Self, E. C.,* Z. D. Hood,* T. Brahmbhatt, F. M. Delnick, H. M. Meyer III, G. Yang, J. L. M. Rupp, and J. Nanda. "A New Class of Amorphous Sulfide-Based Solid Electrolytes: Synthesis, Characterization, and Electrochemical Properties." *Chemistry of Materials* (2020). In Press.
- Brahmbhatt, T., G. Yang, E. Self, and J. Nanda. "Cathode-Sulfide Solid Electrolyte Interfacial Instability: Challenges and Solutions." *Frontiers in Energy Research* 8 (2020): 247.

* Denotes co-first authorship

Task 4.6 – Prelithiation of Silicon Anode for High-Energy Lithium-Ion Batteries
(Yi Cui, Stanford University)

Project Objective. Prelithiation of high-capacity electrode materials is an important means to enable those materials in high-energy batteries. This study pursues three main directions: (1) developing facile and practical methods to increase 1st cycle CE of anodes, (2) synthesizing fully lithiated anode to pair with high-capacity Li-free cathode materials, and (3) prelithiation from the cathode side.

Project Impact. Prelithiation of high-capacity electrode materials will enable those materials in next-generation high-energy-density Li-ion batteries. This project's success will make high-energy-density Li-ion batteries for EVs.

Approach. Silicon electrode film will be prepared by coating the slurry of silicon nanoparticles, carbon black, and binder mixture on copper foil through a doctor-blading method. The silicon electrode film will be prelithiated by pressing a Li-metal foil on top of it and heating it in an argon glovebox for a certain time. Then, Li_xSi electrode film can be obtained by removing the redundant lithium foil through a peeling-off approach. The redundant lithium foil is reusable for the next prelithiation. The structure, morphology, and other properties can be analyzed by SEM, TEM, XPS, Raman spectroscopy, XRD, etc. In the first year, the team aims to fabricate Li_xSi freestanding electrode film and improve its air stability. In the second year, the team aims to improve the electrochemical stability in full cells.

Out-Year Goals. Materials containing a large quantity of lithium will be synthesized for pre-storing lithium ions inside batteries. Materials and process will be developed to be compatible with battery electrode and cell fabrication. First-cycle CE of anodes will be improved and optimized by prelithiation materials. Develop materials for prelithiation from the cathode side.

Collaborations. This project engages in collaboration with the following: BMR PIs; SLAC: M. Toney *(in situ* X-ray); and Stanford: W. Nix (mechanics).

Milestones

1. Demonstrate a new solvent-free dry method for anode prelithiation. (Q1, FY 2020; Completed)
2. Demonstrate control of prelithiation amount by adjusting contact duration between thick lithium foil and anode materials. (Q2, FY 2020; Completed)
3. Demonstrate synthesis of thin lithium foil with different thickness (5-20 μ) for use in dry prelithiation method. (Q3, FY 2020; Completed)
4. Demonstrate thin lithium foil with different thicknesses as dry prelithiation reagents for anode materials to pair with different-capacities cathode materials. (Q4, FY 2020; Completed)

Progress Report

Substantial improvements on energy density of Li-ion batteries require development of high-capacity electrodes. Alloy anodes with much higher capacity have been recognized as promising alternatives to graphites. However, low ICE accompanied with alloying chemistry limits full usage of the designed capacity in battery. Silicon, as an example of a typical alloy anode, exhibits a low ICE of 50-80%, indicating 20-50% of capacity will be lost after 1st cycle. Therefore, prelithiation as a strategy to compensate the irreversible capacity loss in the 1st cycle has become critically important for battery performance improvement.

In the previous report, the team presented using a series of graphene-hosted-thin-lithium-foils (Li@eGF) with different thickness as a novel prelithiation reagent for one-step, heat-free, solvent-free prelithiation. Li@eGF with a wide range of thickness (500 nm, 1 µm, 2 µm, 10 µm, and 20 µm) was successfully fabricated, designed to exhibit a wide range of prelithiation capacity from 0.1 mAh/cm^2 to 4 mAh/cm^2. This quarter, the team continued applying Li@eGF to silicon battery system and exploring its prelithiation role on battery performance.

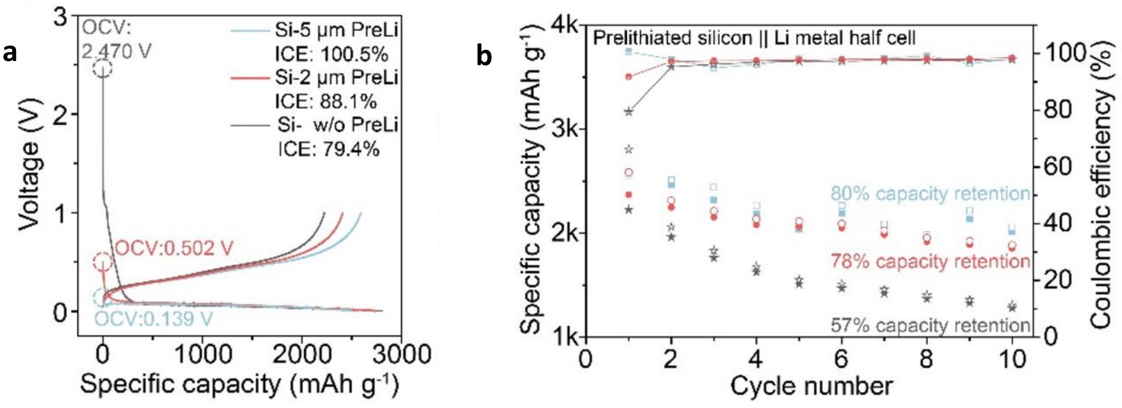

Figure 100. (a) Voltage profiles of silicon electrodes using different thickness of Li@eGF film in the 1st cycle. (b) Galvanostatic cycling of silicon electrodes at 0.05 C using different thickness of Li@eGF films for prelithiation.

Si||Li-metal half cells were fabricated to show that ICE of silicon electrode improved from ~ 80% to ~ 100% with delicate control by using Li@eGF as prelithiation reagent. The mass loading of silicon electrodes was controlled around 1.2 mg/cm^2, with an expected desired prelithiation amount of 0.8-1 mAh/cm^2. 2-µm-thick and 5-µm-thick Li@eGF with designed 0.4 mAh/cm^2 and 1 mAh/cm^2 prelithiation capacity, respectively, were applied for prelithiation. As shown in Figure 100a, pristine silicon anode exhibited low ICE ~ 80%. The 2-µm-thick Li@eGF (0.4 mAh/cm^2) partially compensated the 1st cycle irreversible loss and improved ICE to 88.1%. The 5-µm-thick Li@eGF, which has the well matched stored capacity (1 mAh/cm^2) with the desired prelithiation amount (0.8-1 mAh/cm^2), successfully improved the ICE of silicon anode to 100.5%. This result supports that Li@eGF is capable of finely controllable prelithiation to improve ICE to ~100% by tuning the thickness to match stored capacity with the desired prelithiation amount. Besides ICE improvement, Li@eGF also plays a role to enhance Si-anode cycling ability. With 2-µm-thick and 5-µm-thick Li@eGF prelithiation, ~ 80% capacity retention was achieved after 10 cycles, compared to 57% retention of pristine silicon anode after cycling. As Li@eGF prelithiation will leave a layer of conductive graphene sheet above silicon anode in battery cycling, the graphene film can act as a secondary current collector for active material utilization. Therefore, Li@eGF provides not only tunable prelithiation capability, but also a protection layer for silicon cycling stabilization, making it a promising strategy toward applicable high-energy-density silicon electrodes.

Patents/Publications/Presentations

The project has no patents, publications, or presentations to report this quarter.

TASK 5 – SULFUR ELECTRODES

Summary

The collected work in this Task involves six projects that have focused on the following areas:

- Conducting focused fundamental research on the mechanism of "shuttle effect" inhibition for rechargeable Li-S batteries.
- Developing electrode and electrolyte systems that can mitigate the "shuttle effect" so the low self-discharge and long cycle life can be achieved.
- Synthesizing sulfur composite materials with an emphasis on polymer sulfur composite materials.
- Developing creative electrode-making processes to improve processability and aerial capacity; for example, polymeric sulfur composites may not be suitable for the traditional slurry casting process.
- Developing a novel S_xSe_y cathode material for rechargeable lithium batteries with high energy density and long life, as well as low cost and high safety.
- Delivering an electrochemically responsive self-formed hybrid LIC as a protective layer for Li-metal anodes, enabling Li-metal anodes to cycle with a high efficiency.
- Developing high-energy, low-cost Li-S batteries with long lifespan.

Highlights. The highlights for this quarter are reported below.

- Task 5.1 led by K. Amine's group at ANL this quarter has implemented SEM combined with TOF-SIMS characterization to precisely visualize the impact of the subtle shuttling effect of polysulfides on the morphology and composition of the cycled Se-S cathode and Li-metal anode during cycling utilizing DME-based electrolytes and ANL-developed fluorinated ether based electrolytes. The team has demonstrated that cycling of the cells in DME-based electrolytes shows presence of irregular deposition products of sulfur and selenium on the surface of the cycled lithium. On the other hand, the hydrofluoroether (HFE)-based electrolyte exhibited a uniform and homogeneous morphology with no detectable selenium presence and a weak signal for sulfur, indicating effective elimination of shuttling effect in the HFE-based electrolytes. Presence of fluorine in cycled lithium in the HFE-based electrolyte signals the formation of F-rich SEI absent on the Li-foil surface cycled in DME-based electrolytes. Similarly, on the DME-based electrolyte cycled cathode surface, isolated sulfur and selenium deposits were observed due to polysulfide and polyselenides shuttling, whereas HFE-based electrolyte cycled cathode surface exhibited uniform and homogeneous deposits of sulfur and selenium, indicating absence of shuttling. The results demonstrate the benefit of using fluorinated ether solvents in Li-S systems.
- Task 5.2 led by D. Lu and J. Liu's group at PNNL this quarter demonstrated the cycling ability of dense sulfur electrodes using the optimized integrated Ketjen Black (IKB) cathode materials system in pouch cells. The team focused on achieving a rational design of low-porosity electrodes with high sulfur utilization rate. They show that electrodes with > 70-µm particles exhibit improved performance compared to electrodes using < 20-µm particles. At a porosity of ~ 50%, high sulfur loaded sulfur electrodes (> 4 mg/cm^2) yield a high specific capacity of > 950 mAh/g at 0.1C for 80 cycles at low electrolyte to sulfur (E/S) ratio of 4 µL/mg. At lower porosity of ~ 40%, the high density sulfur cathodes were still able to delivery initial discharge capacity of 1090 mAh/g at an extremely low E/S ratio of 3 µL/g, albeit with slightly elevated cell polarization in the first cycle recovered in the second cycle, demonstrating the challenge of dense electrodes. The dense sulfur electrodes cycled at low E/S ratios nevertheless showed

improved capacity retention (87% after 25 cycles) without the drop in initial capacity seen in porous electrodes. The team has also demonstrated feasibility to scale up the IKB/S system. The results demonstrate the benefit of the IKB/S system for high-energy-density Li-S batteries.

- Task 5.3 led by Y. Cui's group at Stanford this quarter has developed a new strategy of using a thin layered titanium disulfide (TiS_2) as an effective encapsulation to prevent polysulfide dissolution into the solid PEs in all-solid-state Li-S batteries. The team has demonstrated this using Li_2S as the cathode to eliminate structural damage seen in elemental sulfur. The thin (~ 20 nm) layer of TiS_2 effectively traps polysulfide species. They have used SEM and TEM to show the direct formation of TiS_2 on the Li_2S particle by converting 20% of the Li_2S to yield 1-5 micron-sized particles of an average size of 2 microns. They have also used HRTEM to confirm the presence of crystalline TiS_2 layer with lattice spacing of 0.57 nm. The results demonstrate use of Li_2S with TiS_2 as an effective catalyst for polysulfide conversion in an all-solid-state Li-S battery.
- Task 5.4 led by E. Hu and D. Qu's group at UWM has demonstrated this quarter the use of alternative anode materials and the effect of prelithiation along with testing of polymer sulfur in coin cells. The team reported the use of prelithiated red phosphorus as the anode material in a P(Li)-S full cell. The team has also shown the use of tin and SnO_2 as anodes for effective prelithiation to obtain high lithium loadings and prevent loss of active lithium. They demonstrate the use of prelithiated tin and SnO_2 with $LiCoO_2$ cathodes. They have also tested 26 polymer sulfur compounds via heat treatment at ~ 210°C to link the sulfur with ionomer to form conjugated double bonds. The system using dicyclopentadiene monomer seems to exhibit promising electrochemical cycling response of ~ 78% capacity retention after 200 cycles at high current rates of 250 micro amperes. The results show the feasibility of prelithiation and polymeric sulfur compounds in Li-S batteries.
- Task 5.5 led by G. Liu's group at LBNL has focused this quarter on testing their new class of amphiphilic electrolyte additive based on HFEs for feasibility in Li-S battery systems. The team first studied the solubility of lithium salts, LiTFSI in highly fluorinated HFE additives. They observed that diluted form using inert 2,2,2-Trifluoroethyl Ether (TTE) solvent gave acceptable viscosity with a conductivity of 10^{-4} – 10^{-3}S/cm lower than organic electrolytes. Use of smaller HFE molecules of F_4EO_2 and F_3EO_1 gave higher ionic conductivities. They therefore tested two electrolyte compositions of 1.0 M LiTFSI in F_4EO_2/TTE (1:2.5) and 1.0M LiTFSI in F_3EO_1/TTE (1:2.5) in initial Li-S battery configurations. They showed that when using the latter electrolyte system in contrast with the typical DOL/DME electrolyte, the discharge curves show a sloping voltage response devoid of any clear polysulfide dissolution plateau characteristic of DOL/DME electrolyte systems. The profile is representative of sluggish kinetics due to the solid-state nature of the conversion reaction rather than solid-liquid, owing to the inferior solubility of the polysulfides in this electrolyte system. Furthermore, the CE is also above 100% in the first 35 cycles, likely due to higher sulfur utilization. The results indeed show the uniqueness of this new electrolyte system for Li-S batteries.

Task 5.1 – Novel Chemistry: Lithium Selenium and Selenium Sulfur Couple (Khalil Amine, Argonne National Laboratory)

Project Objective. The project objective is to develop a novel S_xSe_y cathode material for rechargeable lithium batteries with high energy density and long life, as well as low cost and high safety.

Project Impact. Development of a new battery chemistry is promising to support the goal of PHEV and EV applications.

Approach. The dissolution of lithium polysulfides in nonaqueous electrolytes has been the major contribution to the low energy efficiency and short life of Li-S batteries. In addition, insulating characteristics of both end members during charge/discharge (sulfur and Li_2S) limit their rate capacity. To overcome this problem, sulfur or Li_2S is generally impregnated in a carbon-conducting matrix for better electronic conductivity. However, this makes it difficult to increase the loading density of practical electrodes. It is proposed to solve these barriers using the following approaches: (1) partially replace sulfur with selenium, (2) nano-confine the S_xSe_y in a nanoporous conductive matrix, and (3) explore advanced electrolytes with suppressed shuttle effect.

Out-Year Goals. This new cathode will be optimized with the following goals:

- A cell with nominal voltage of 2 V and energy density of 600 Wh/kg.
- A battery capable of operating for 500 cycles with low capacity fade.

Collaborations. This project engages in collaboration with the following: Y. Ren and C. Sun of APS at ANL, L. A. Curtiss at ANL, and A. X. Sun at Western University, Canada.

Milestones

1. Synthesize new carbon materials to prepare SeS_x/carbon composites with high sulfur loading in the composite. (Q1, FY 2020; Completed)
2. Optimize cathode structures to increase SeS_x areal loading, and improve battery performance. (Q2, FY 2020; Completed)
3. Gain interface understanding on the cycled SeS_x cathode using TOF-SIMS and XPS. (Q3, FY 2020; Ongoing)
4. Gain interface understanding on the cycled lithium metal using TOF-SIMS and XPS. (Q4, FY 2020; Ongoing)

Progress Report

This quarter, the team used SEM and TOF-SIMS characterization to precisely visualize the impact of subtle shuttle effect on the morphology and composition of cycled Se-S cathode and Li-metal anode during cycling in conventional DME-based electrolytes and ANL-invented fluorinated ether based electrolytes.

As shown in Figure 101a, after cycling in the DME-based electrolyte, many irregular deposition products were found on the surface of the cycled lithium foil. Strikingly, in the case of HFE-based electrolyte, the cycled lithium metal exhibited a uniform and homogeneous morphology (Figure 101b). As further shown in Figure 101c-d, a large amount of sulfur and selenium elements was found on the surface of the cycled lithium foil in the Li-Se/S cell with DME-based electrolyte, corresponding to a severe shuttle effect. In contrast, in the HFE-based electrolyte, only a weak S$^-$ signal was detected, and a Se$^-$ signal could not be detected (Figure 101d), confirming that the shuttle effect had been effectively eliminated. The weak S$^-$ signal was due to the formation of a SEI on the Li-metal anode. As clearly shown in the TOF-SIMS depth profiling of the cycled Li-metal anodes (Figure 101e), high S$^-$ and Se$^-$ intensities were observed on the cycled Li-foil surface in the DME-based electrolyte. Nevertheless, Se$^-$ was not found on the cycled Li-foil surface in the HFE-based electrolyte, further confirming the shuttle-free chemistry of Se/S cathode in this electrolyte. Moreover, the higher F$^-$ intensity on the outermost surface of cycled lithium foil in HFE-based electrolyte confirmed the formation of a robust F-rich SEI layer, which does not appear on the Li-foil surface in DME-based electrolyte. Figure 101f shows the elemental mapping of S$^-$ and Se$^-$ on the cycled cathode surfaces. Several isolated sulfur and selenium species were identified on the cycled cathode in DME-based electrolyte, which can be explained by the dissolution and deposition of LiPSs/LiPSes. In sharp contrast, in HFE-based electrolyte, both S$^-$ and Se$^-$ were uniformly and homogeneously distributed on the cathode, indicating no LiPSs/LiPSes were dissolved in the bulk electrolyte.

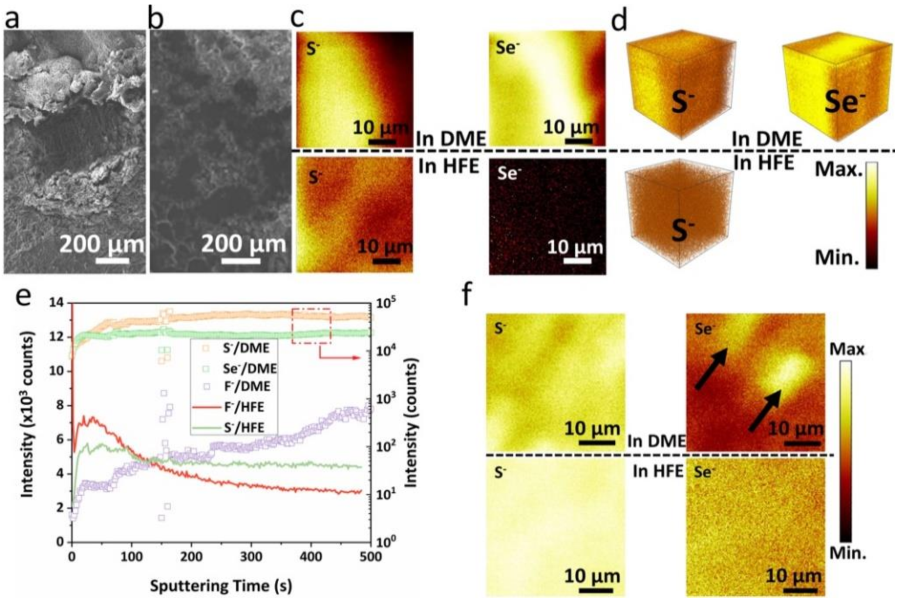

Figure 101. Scanning electron microscopy images of cycled Li-metal anode of Li-Se/S cells in (a) DME-based electrolyte and (b) HFE-based electrolyte. (c) Time-of-flight secondary ion mass spectrometry (TOF-SIMS) mapping. (d) 3D element reconstruction (S$^-$ and Se$^-$). (e) Depth profile of cycled Li-metal anode in Li-Se/S cells with two electrolytes. (f) TOF-SIMS elements mapping (S$^-$ and Se$^-$) of cycled core-shell hollow structured-S/Se-10% cathode in DME-based and HFE-based electrolytes.

Since the fluorinated ether electrolytes can significantly eliminate the shuttle effect and enable reversible lithium stripping/plating, the team will further optimize the structure of fluorinated ether electrolytes in FY 2021 by screening fluorinated ether solvents to improve their performance under higher areal sulfur loading and lean electrolyte conditions. At the same time, the team will design better cathode structures to improve the sulfur redox kinetics when increasing the areal sulfur loading to 5 mg cm^{-2} and under an electrolyte/sulfur ratio of < 10. The team will further test the electrolytes in practical Li/S and Li/Se-S pouch cells.

Patents/Publications/Presentations

Publication

- Zhao, C., G. L. Xu, T. Zhao, and K. Amine. "Beyond Polysulfides Shuttle and Li Dendrite Formation: Addressing the Sluggish S Redox Kinetics for Practical High Energy Li-S Batteries." *Angewandte Chemie International Edition* (2020): 17634–17640.

Task 5.2 – Development of High-Energy Lithium-Sulfur Batteries (Dongping Lu and Jun Liu, Pacific Northwest National Laboratory)

Project Objective. The project objective is to develop high-energy, low-cost Li-S batteries with long lifespan. All proposed work will employ thick sulfur cathode (≥ 2 mAh/cm^2 of sulfur) at a relevant scale for practical applications. The diffusion process of soluble polysulfide out of thick cathode will be revisited to investigate cell failure mechanism at different cycling. The fundamental reaction mechanism of polysulfide under the electrical field will be explored by applying advanced characterization techniques to accelerate development of Li-S battery technology.

Project Impact. The theoretical specific energy of Li-S batteries is ~ 2300 Wh/kg, which is almost three times higher than that of state-of-the-art Li-ion batteries. The proposed work will design novel approaches to enable Li-S battery technology and accelerate market acceptance of long-range EVs required by the EV Everywhere Grand Challenge.

Approach. The project proposes to (1) identify and address key issues of applying high-energy sulfur cathodes including materials, binders, electrode architectures, and functional electrode additives, (2) advance the mechanism study of sulfur cathode and electrolyte by using *in situ* / *ex situ* techniques and custom-designed hybrid cell setup, and (3) verify effectiveness of the new approaches with coin/pouch cells by using high-loading electrodes (> 4 mg/cm^2), limited lithium (< 200% lithium excess), and lean electrolyte (E/S < 4 μL/mg).

Out-Year Goals. This project has the following out-year goals:

- Fabricate Li-S pouch cells with thick electrodes to understand sulfur chemistry/electrochemistry in environments similar to real application.
- Leverage the Li-metal protection project funded by the DOE and PNNL advanced characterization facilities to accelerate development of Li-S battery technology.
- Develop Li-S batteries with a specific energy of 400 Wh/kg at cell level, 1000 deep-discharge cycles, improved abuse tolerance, and less than 20% capacity fade over a 10-year period to accelerate commercialization of EVs.

Collaborations. This project engages in collaboration with the following: X-Q. Yang (BNL), D. Qu (UWM), G. Zhang (University of Alabama), and J. Tao (PNNL).

Milestones

1. Synthesis of IKB with controlled secondary particles from 5 to 100 μm for high-loading sulfur electrodes (> 4 mg S/cm^2). (Q1, FY 2020; Completed)
2. Realize sulfur utilization rate > 1200 mAh/g in dense sulfur electrodes (S > 4 mg/cm^2, porosity ≤ 50%) at an E/S ≤ 4 μL/mg through electrode architecture control. (Q2, FY 2020; Completed)
3. Demonstrate > 80 cycles (80% capacity retention) in dense sulfur electrodes at E/S ≤ 4 μL/mg through the hybrid electrode design. (Q3, FY 2020; Completed)
4. Complete evaluation of high-loading sulfur electrodes at E/S ≤ 3 μL/mg and transfer sufficient materials to Battery500 for high-energy pouch cell demonstration. (Q4, FY 2020; Completed)

Progress Report

This quarter, cycling of highly dense sulfur electrodes at extremely lean electrolyte conditions has been demonstrated, and optimized cathode materials have been delivered to Battery500 consortium for Li-S pouch cell demonstration. At low E/S ratio, conserving a higher proportion of electrolyte is critical to compensate for the electrolyte consumption and, therefore, extend the cycle life of Li-S cell. However, the extremely porous and thick sulfur cathodes used widely in Li-S batteries require a large amount of electrolyte for pore filling. The research efforts of the team focused on rational design of low-porosity electrodes with high sulfur utilization rate. Approaches from materials design to electrode architecture control have been adopted to minimize the electrode porosity, without sacrificing the sulfur utilization rate. It has been identified that electrodes with > 70 µm particles show improved performance compared to those using < 20 µm particles. At a porosity of ~ 50%, the high-loading sulfur electrodes (> 4 mg/cm^2) can deliver a high specific capacity of > 950 mAh/g at 0.1C and last for 80 cycles with a capacity retention of 80% at a very low E/S ratio of 4 µL/mg.

To further push the limit of electrode porosity, dense electrodes with porosity of ~ 40% were fabricated with desired architectures. Figure 102a plots the discharge and charge curves of 1st (grey) and 2nd (red) cycles. At an extremely low E/S ratio of 3 µL/mg, the dense sulfur cathode functions well and can deliver an initial discharge capacity as high as 1090 mAh/g. Although slightly high cell polarization is observed in the 1st cycle, the reaction kinetics can be recovered during the 2nd cycle and subsequent cycling. In the highly porous electrodes, it is hard to obtain a reasonably high discharge capacity if E/S ratio is as low as 3 µL/mg. This suggests that use of dense electrodes is critical to enable cell operation at extremely lean electrolyte conditions. It is important to note that a rational design of electrode architecture is required to enable a uniform and adequate electrolyte wetting in the dense electrodes. Additionally, dense sulfur electrodes with limited electrolyte content (that is, low E/S ratio) also benefit from minimized polysulfides shuttling and the resulting irreversible capacity loss. As shown in Figure 102b, the dense sulfur electrode exhibits significantly improved capacity retention without an obvious capacity drop in the initial cycles, which was often observed in the highly porous electrodes when cycled under flooded electrolyte conditions. This indicates that the polysulfide free diffusion and loss are significantly suppressed, which contributes to improved capacity retention (87% after 25 cycles).

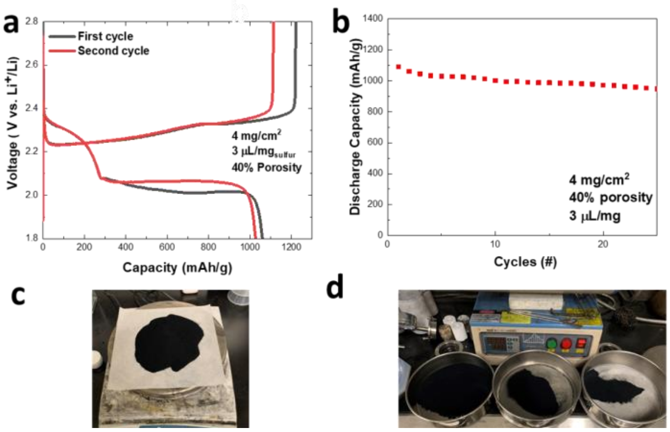

Figure 102. (a) First and second charging/discharging curves and (b) cycling performance of dense sulfur electrodes at extremely lean electrolyte conditions. (Electrode: 4 mg S/cm^2, porosity 40%, and E/S = 3 µL/mg S, 0.1C for cycling, at room temperature). (c-d) Scaling up synthesis of IKB/S composite with different particle sizes.

Given the promising materials performance, another research focus this quarter is to scale up the synthesis of S/C materials and supply to Battery500 Consortium for pouch-cell demonstration. Using an optimized synthesis approach, the IKB system can be synthesized at a scale of 8 g per batch with desired particle size and quality. Figure 102c shows the weight of IKB/S composite cathode materials through one batch synthesis. This synthesis approach is feasible for scaling up production via an amplified reactor design. According to research reported last quarter, the large-sized IKB/S particles exhibit superior electrode performance characteristics over small particle sizes particularly, for low porosity sulfur cathode cycled under lean electrolyte conditions. Accordingly, the IKB/S materials with optimal particle size were prepared through control of synthesis conditions and appropriate precursors. With an additional sieving process, particles were further screened to ensure batch consistency (Figure 102d) and thus achieve acceptable electrode performance repeatability. Such materials have been validated and supplied to Battery500 consortium for practical pouch-cell demonstration.

Patents/Publications/Presentations

Publication

- Shi, L., S-M. Bak, Z. Shadike, C. Wang, C. Niu, P. Northrup, H. Lee, A. Baranovskiy, J. Qin, S. Feng, X. Ren, D. Liu, X. Yang, F. Gao, D. Lu, J. Xiao, and J. Liu. "Reaction Heterogeneity in Practical High-Energy Lithium-Sulfur Pouch Cells." *Energy & Environmental Science*. https://doi.org/10.1039/D0EE02088E.

Presentation

- International Battery Seminar, Virtual (July 28–30, 2020): "Advancing High-Energy Lithium-Sulfur Battery: Challenges from Liquid-Rich, Liquid-Lean, to All-Solid-State"; D. Lu, Z. Yu, J. Xiao, and J. Liu.

Task 5.3 – Nanostructured Design of Sulfur Cathodes for High-Energy Lithium-Sulfur Batteries (Yi Cui, Stanford University)

Project Objective. The charge capacity limitations of conventional TM oxide cathodes are overcome by designing optimized nano-architectured sulfur cathodes. This study aims to enable sulfur cathodes with high capacity and long cycle life by developing sulfur cathodes from the perspective of nanostructured materials design, which will be used to combine with Li-metal anodes to generate high-energy Li-S batteries. Novel sulfur nanostructures as well as multi-functional coatings will be designed and fabricated to overcome issues related to volume expansion, polysulfide dissolution, and the insulating nature of sulfur.

Project Impact. The capacity and cycling stability of sulfur cathode will be dramatically increased. This project's success will make Li-S batteries to power EVs and decrease the high cost of batteries.

Approach. The approach involves three main efforts:

- Advanced nanostructured sulfur cathodes design and synthesis, including (1) engineer empty space into sulfur cathode to solve problem of electrode volume expansion, (2) develop novel sulfur nanostructures with multi-functional coatings for confinement of S/Li polysulfides to address issues of active materials loss and low conductivity, (3) develop/discover optimal nanostructured materials that can capture the polysulfide dissolved in the electrolyte, (4) develop space-efficiently-packed nanostructured sulfur cathode to increase volumetric energy density and rate capability, and (5) identify interaction mechanism between sulfur species and different types of oxides/sulfides, and find optimal material to improve capacity and cycling of sulfur cathode.
- Structure and property characterization, including *ex situ* SEM, XPS analysis, and *in operando* XRD and optical microscopy.
- Electrochemical testing including coin cells and pouch cells as well as a set of electrochemical techniques.

Out-Year Goals. The cycle life, capacity retention, and capacity loading of sulfur cathodes will be greatly improved (200 cycles with 80% capacity retention, > 0.3 mAh/cm^2 capacity loading) by optimizing material design, synthesis, and electrode assembly.

Collaborations. This project collaborates with the following: BMR PIs; SLAC: M. Toney *(in situ* X-ray); and Stanford: W. Nix (mechanics) and Z. Bao (materials).

Milestones

1. Understanding the mechanism of liquid sulfur on the surface of 3D materials. (Q1, FY 2020; Completed)
2. Demonstrate improvement by utilizing liquid sulfur in Li-S batteries. (Q2, FY 2020; Completed)
3. Develop high sulfur loading cathode based on understanding of liquid sulfur. (Q3, FY 2020; Completed)
4. Enable Li-S batteries with high sulfur loading, low E/S ratio, and fast kinetics. (Q4, FY 2020; Completed)

Progress Report

As reported last quarter, the team developed high sulfur loading cathode based on the understanding of liquid sulfur. This quarter, the team reports on designing a new strategy, by using thin-layered titanium disulfide (TiS_2) as an effective encapsulation for preventing polysulfides dissolving into solid PEs in all-solid-state Li-S batteries (Figure 103a-c). Li_2S cathodes are chosen because fully lithiated Li_2S is able to minimize structural damage compared to elemental sulfur, and is compatible with anode-free cells. The TiS_2 encapsulated layer can efficiently trap polysulfides inside its shell because of a strong binding with Li_2S/Li_2S_x species. To test the hypothesis, as shown in Figure 103c, $Li_2S@TiS_2$ particles were synthesized by directly converting 20% of the Li_2S on the surface into TiS_2. SEM image of Li_2S after TiS_2 coating reveals that the typical particle size of as-prepared $Li_2S@TiS_2$ is 1-5 µm, with an average size of 2 µm (Figure 103d). TEM image shows that Li_2S is encapsulated by a uniform layer with a thickness of ~ 20 nm (Figure 103e). HRTEM image shows a spacing of 0.57 nm, which is consistent with the interlayer spacing of TiS_2 and verifies the crystalline structure of the TiS_2 layer (Figure 103f).

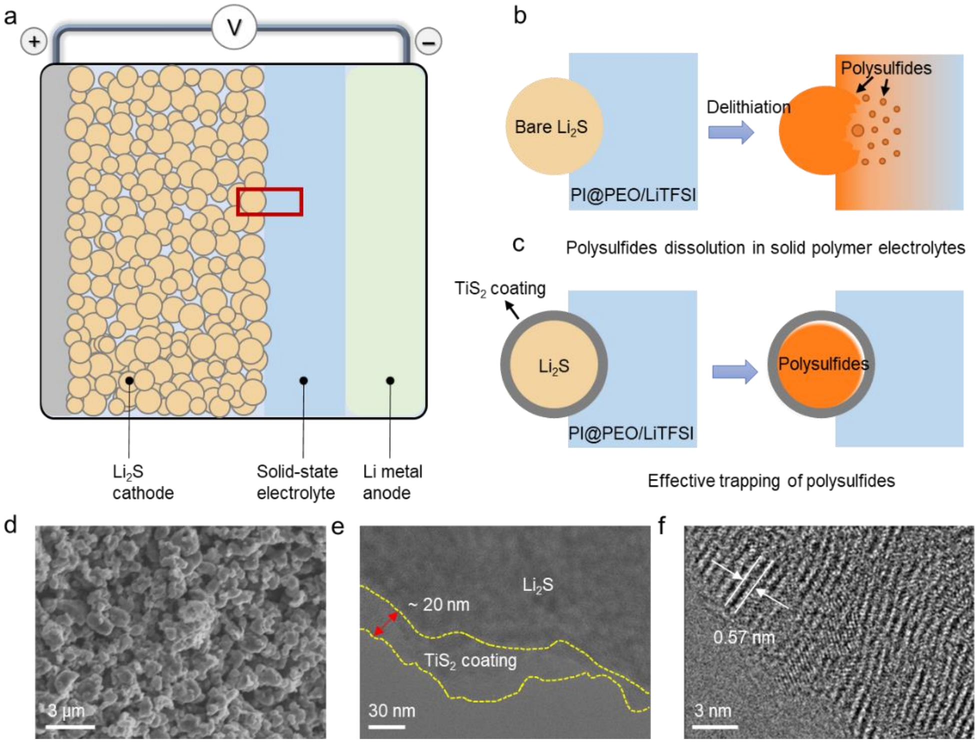

Figure 103. Design of encapsulated Li_2S cathodes for high-energy-density all-solid-state Li-S batteries. (a) Schematic of the all-solid-state Li-S batteries architecture comprising of Li-metal anode, PI@PEO/LiTFSI solid electrolyte, and Li2S composite cathode. Zoomed-in schemes of the red rectangle in (a), to depict the interface between solid-state electrolyte and cathode during delithiation process for (b) bare Li_2S cathode, and (c) $Li_2S@TiS_2$ cathode. Bare Li_2S particles undergo polysulfide dissolution on delithiation, resulting in rapid capacity decay and low Coulombic efficiency. $Li_2S@TiS_2$ core-shell structure provides a structurally intact shell for effectively trapping polysulfides, thereby avoiding the polysulfide dissolution into solid polymer electrolytes. Light yellow: Li_2S particles; orange: polysulfide; grey shell: TiS_2 coating. (d) Scanning electron microscopy and (e) transmission electron microscopy (TEM) image of $Li_2S@TiS_2$. The thickness of TiS_2 coating is about 20 nm. (f) High-resolution TEM image of TiS_2 coating.

Patents/Publications/Presentations

Publications

- Zhou, G., A. Yang, G. Gao, X. Yu, J. Xu, C. Liu, Y. Ye, A. Pei, Y. Wu, Y. Peng, Y. Li, Z. Liang, K. Liu, L-W. Wang, and Y. Cui. “Supercooled Liquid Sulfur Maintained in Three-Dimensional Current Collector for High-Performance Li-S Batteries.” *Science Advances* (2020): doi: 10.1126/sciadv.aay5098.
- Yang, A., G. Zhou, X. Kong, R. A. Vila, A. Pei, Y. Wu, X. Yu, X. Zheng, C-L. Wu, B. Liu, H. Chen, Y. Xu, D. Chen, Y. Li, S. Fakra, H. Y. Hwang, J. Qin, S. Chu, and Y. Cui. “Electrochemical Generation of Liquid and Solid Sulfur on Two-Dimensional Layered Materials with Distinct Areal Capacities.” *Nature Nanotechnology* (2020). doi: 10.1038/s41565-019-0624-6.

Task 5.4 –Investigation of Sulfur Reaction Mechanisms
(Enyuan Hu, Brookhaven National Laboratory; Deyang Qu, University of Wisconsin at Milwaukee)

Project Objective. The primary objectives are as follows:

- To continue conducting focused fundamental research on the mechanism of "shuttle effect" inhibition for rechargeable Li-S batteries.
- To continue developing the polymeric sulfur electrode, adequate anode, and corresponding electrolyte to achieve high-energy-density, long-cycle Li-S batteries.
- To carry out spatially resolved XRF image and sulfur K-edge XAS [including XANES and X-ray absorption fine structure (XAFS)] studies of polymeric sulfur compounds.
- To investigate the alternative anode materials so they will not react with dissolved polysulfide ions.
- To continue developing and optimizing creative electrode-making processes to improve processability and aerial capacity, for example, dry process and thick electrode.

Project Impact. Further understanding of the mechanisms of all reactions in a Li-S cell will lead to mitigation of the "shuttle effect." The project results will thus guide development of sulfur cathode and Li-S designs with significant increase of energy density and of cycle life and with reduction of cost. This will greatly accelerate deployment of EVs and reduce carbon emission associated with fossil fuel consumption.

Approach. This project will use not only *in situ* electrochemical high-performance liquid chromatography (HPLC)/MS, XPS and TXM, but also synchrotron-based *in situ* X-ray diagnostic tools such as XRD and XAS to study sulfur electrodes. The team will continue to develop thicker sulfur electrode with high areal capacity using dry process.

One-Year Goals. The major goal this fiscal year is to extend successful investigation of dissolved polysulfides to the polysulfides in the solid phase. This includes the following actions: (1) synthesize cross-linked polymerized sulfur compounds, (2) explore additives that can rapidly catalyze polysulfide radicals, (3) continue exploring alternative anode materials, and (4) develop *in situ* synchrotronic method to investigate sulfur and polysulfide in the solid phase.

Collaborations. The PI works closely with beamline scientists at synchrotron facilities to develop novel Li-S characterization tools. The PI and co-PI collaborate closely with top scientists at ANL, LBNL, and PNNL, as well as U. S. industrial collaborators at GM, Duracell, Clarios, etc. The PI and co-PI also collaborate with scientists in China, Japan, and South Korea. These collaborations will be strengthened and expanded to give this project a vision on both today's state-of-the-art technology and tomorrow's technology in development, with feedback from the material designer and synthesizers upstream and from industrial end users downstream.

Milestones

1. Test the newly synthesized polymeric sulfur compounds. Conduct spatially resolved XRF image and sulfur K-edge XAS (including XANES and XAFS) studies of polymeric sulfur compounds. (Q1, FY 2020; Completed)
2. Survey alternative anode materials and determine their interaction with dissolved polysulfide ions. Continue synthesis and testing of polymeric sulfur compounds, and optimize electrode-making processes. (Q2, FY 2020; Completed)

3. Investigate radical disproportionation catalyst, and test alternative electrolytes in which the solubility of polysulfide ions is lower than ether-based electrolyte. (Q3, FY 2020; Completed)

4. Complete initial design of the full cell consisting of polymeric sulfur compounds, alternative anode, and adequate additive in either coin-cell or pouch-cell format. (Q4, FY 2020; Completed)

Progress Report

The fourth quarter of FY 2020 has involved several challenges. Due to the pandemic of COVID-19, the PI's research labs in the university were only partially open to maintain social distancing. However, the team managed to complete all milestones of FY 2020. The BNL and UWM teams have (1) completed initial tests of polymeric sulfur compounds; (2) started exploring alternative anodes; and (3) completed initial testing of alternative anode and polymer sulfur in coin cells.

Alternative Anode Materials and Prelithiation. By means of the unique analytical HPLC-MS assays developed in the PI's group, a systematic investigation has been conducted to study the chemical interactions between the alternative anode materials and the dissolved polysulfide ions. The team aims to develop an alternative anode that does not react with polysulfide ions while maintaining decent cell voltage. Thus, the "shuttle effect" can be mitigated without a compromise of much energy density. The team reported using prelithiated red phosphorus as the anode material in a P(Li)-S full cell. They also found tin and SnO_2 can be good candidates. They have successfully prelithiated SnO_2 with high lithium loading and low active lithium loss during cycling. Figure 104 shows the performance of prelithiated Sn(Li) anode with LCO as cathode, demonstrating good electrochemical performance. However, the team is struggling to find an adequate electrolyte that will accommodate both Sn(Li) anode and sulfur / polymeric sulfur cathode. The prelithiated SnO_2/C electrodes were obtained by dipping the pristine SnO_2/C electrode into 1 M Li-Bp/THF solution. The prelithiated SnO_2/C electrodes were then immediately washed with anhydrous THF and dried under vacuum.

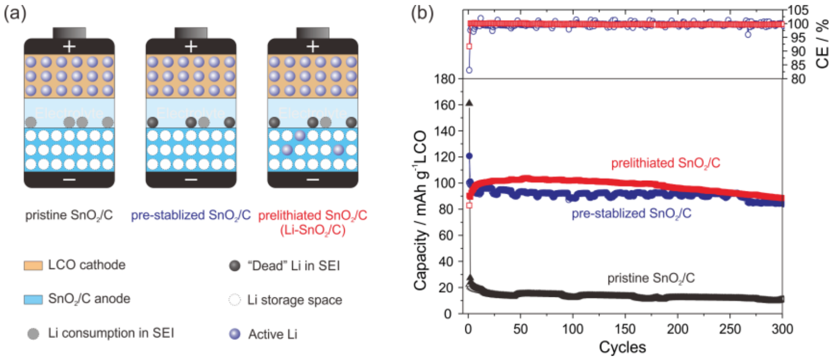

Figure 104. (a) Schematic illustration of the full cells consisting of LCO cathode and different SnO_2/C anodes, respectively. Voltage profiles (b), cycling performance (c), and Coulombic efficiency (d) of the full cells at 1C rate (1C = 140 mA g^{-1} of LCO).

Polymeric Sulfur Compounds. In total, 26 polymeric sulfur compounds were synthesized through a route involving radicals. Various base monomers were selected. Polymeric sulfur compounds were synthesized through a sequence of heat treatment in which the sulfur and the ionomer are linked through a radical assisting mechanism. All the monomers consist of double bonds and are conjugated molecules. Figure 105 shows an example of the monomers and the electrochemical performance of the associated polymeric sulfur compound. The polymeric sulfur compound was synthesized with dicyclopentadiene monomer.

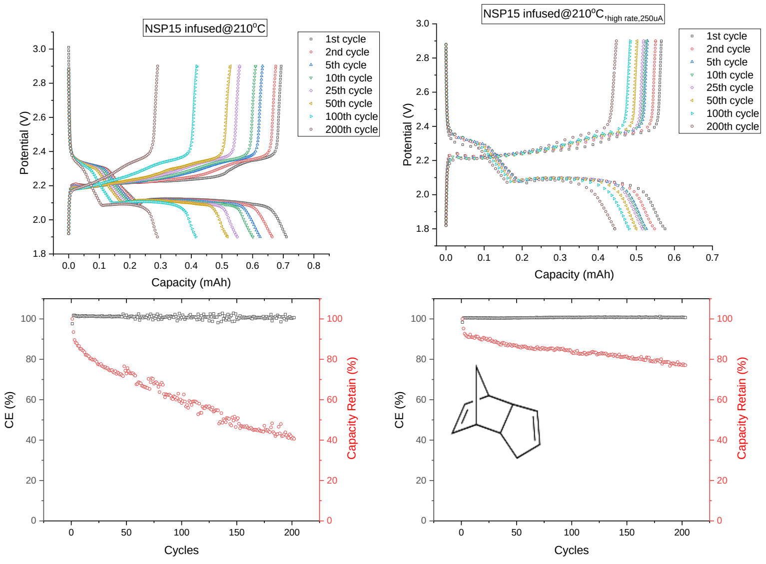

Figure 105. The electrochemical performance of polymeric sulfur compound made with monomer (Dicyclopentadiene DCPC) shown in the inset. Low rate cycling (left graphs) and high rate cycling (right graphs).

Patents/Publications/Presentations

Publication

- Li, F., G. Wang, D. Zheng, X. Zhang, C. J. Abegglen, H. Qu, and D. Qu. “Controlled Prelithiation of SnO_2/Carbon Nanocomposite Anode for Building Full Lithium-Ion Batteries.” *ACS Applied Materials & Interfaces* 12 (2020): 19423–19430. Publication date (Web): April 7, 2020.

Task 5.5 – New Electrolytes for Lithium-Sulfur Battery
(Gao Liu, Lawrence Berkeley National Laboratory)

Project Objective. The project objective is to develop new electrolytes, additives, and electrode compositions for Li-S battery with high ion-conductivity, stable toward polysulfide and promoting the polysulfide affiliation with the electrode substrate to prevent polysulfide dissolution.

Project Impact. This work will address the high cost and low energy density of Li-ion rechargeable batteries. The emerging Li-S batteries could feature both high energy density and low cost. This project enables applications of the low-cost, abundant sulfur element as a major chemical component for electrical energy storage. This project will develop new approaches for electrolytes and electrode compositions of Li-S rechargeable batteries.

Approach. This project aims to develop new electrolytes and additives for Li-S battery. The properties of the ideal electrolyte for sulfur electrode would be high ion conductivity, stable toward polysulfide, and promoting the polysulfide affiliation with the electrode substrate to prevent polysulfide dissolution. The project is designed to first understand the electrode substrate interaction with the polysulfides in different electrolytes. This will lead to better understandings of the polysulfide nucleation and precipitation mechanisms in common electrolytes. The second stage of the project will focus on chemically modifying the structures of the solvent and salt electrolyte molecules to increase electrolyte stability and ionic conductivity and to prevent polysulfide dissolution and promote polysulfides precipitation.

Out-Year Goals. The team will also investigate the contribution of Li-metal electrodes to overall Li-S battery performance and will develop methods to stabilize Li-metal surface.

Collaborations. This project collaborates with J. Guo and W. Yang (ALS/LBNL), A. Minor (National Center for Electron Microscopy at LBNL/UC Berkeley), L-W. Wang (LBNL), and P. B. Balbuena, TAMU.

Milestones

1. Use the synchrotron analyses in studying new electrolytes. (Q1, FY 2020; Completed)
2. Measure and optimize compositions of the new electrolyte for conductivities, Li-ion transference numbers, and amount of polysulfide dissolution. (Q2, FY 2020; Completed)
3. Study cycling properties of lithium metal under new electrolytes. (Q3, FY 2020; Completed)
4. Select two electrolyte compositions to test in Li-S battery. (Q4, FY 2020; Completed)

Progress Report

A new class of amphiphilic electrolyte additive based on HFEs has been synthesized. The HFE amphiphilic additives in combination with lithium salt (such as LiTFSI) and fluorocarbon solvents (such as TTE) form micelle structures. These HFE amphiphilic additives have special structure design: a lithiophilic head [ethyleneoxide (EO) moiety] attached to a lithiophobic tail (hydrofluorocarbons). The lithium salts follow a micelle solvation mechanism on dissolution in the HFE amphiphilic additives. The dissociated Li^+ ions readily coordinate with EO moiety to induce self assembly of the amphiphilic HEF additive into micelle structures (Figure 106).

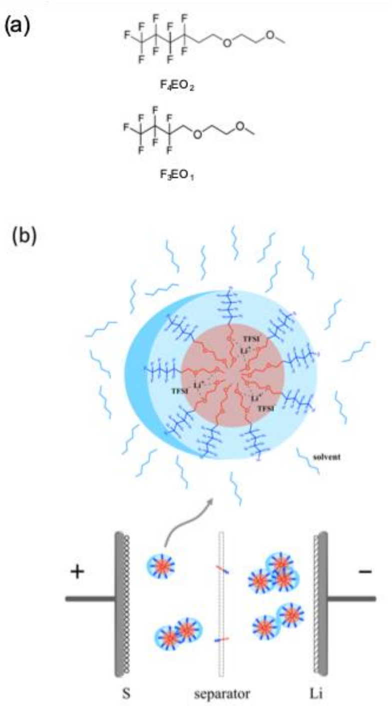

Figure 106. (a) Molecular structures of two selected fluorocarbon ethylene oxides with different chain length denotated as F_4EO_2, and F_3EO_1, respectively. (b) Schematic diagram to show solvation mechanism of LiTFSI with HFE in the electrolyte and formation of micelle complex structure.

Before cell fabrication and cycling test, the solubility of lithium salts LiTFSI in the highly-fluorinated HFE additives developed by the team was initially tested. Results showed that maximum solubility reached was 3.5 M to 4.0 M for both salts in HFE solvents; however, the solutions at that concentration were too viscous for cell application. Therefore, the highly concentrated solutions were diluted with chemically inert TTE. Electrolytes with acceptable viscosity reveal a conductivity at the level of 10^{-4} - 10^{-3} S/cm, which is lower than that of the commercial organic LE. Higher ionic conductivity is achieved with the smallest HFE molecules of F_4EO_2 and F_3EO_1. This is likely due to formation of larger complexes, which reduces overall ion diffusion path and facilitates ion conduction. Another interesting finding is that higher conductivity is favored by the 1:1 dilution ratio because more ion-conducting EO groups are present in the electrolyte. Electrolyte ionic conductivity and the desired wettability associated with appropriate viscosity are the key factors to select 1.0 M LiTFSI concentration for further study, including Li-S cell testing. Two electrolyte compositions were selected based on electrochemical performance for Li-S cell testing: 1.0 M LiTFSI in F_4EO_2/TTE (1:2.5) and 1.0M LiTFSI in F_3EO_1/TTE (1:2.5). Here, the team reports the performance of Li-S battery cycling results based on 1.0 M LiTFSI in F_3EO_1/TTE (1:2.5) in Figure 107. In contrast to the DOL/DME electrolyte, the discharge curve shows a sloping voltage profile without a clear polysulfides (Li_2S_n, $n \geq 6$) dissolution plateau. This behavior is quite common in sparingly solvated electrolytes and indicates sluggish kinetics due to the increasingly solid-state nature of conversion. Because polysulfides barely dissolve, the sulfur on the cathode surfaces will go through solid-solid phase transformations rather than solid-liquid. The other unique feature is the discharge capacity is slightly larger than charge capacity in the first 35 cycles tested here; hence, the CE is above 100%. This may be due to the increasing utilization of the sulfur particles in the electrode.

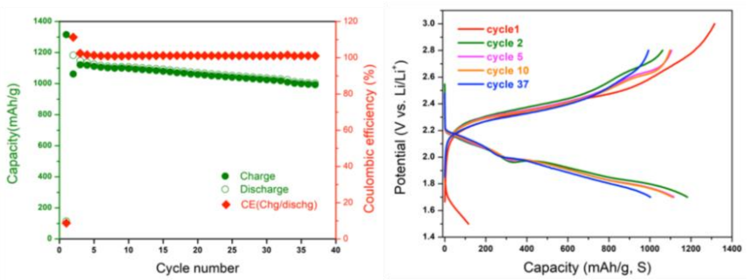

Figure 107. Li-S cell performance using electrolyte 1.0 M LiTFSI in F_3EO_1/TTE (1:2.5) between 1.6-2.8 V: (a) cycle numbers versus sulfur gravimetric specific capacity; and (b) potential versus capacity.

Patents/Publications/Presentations

The project has no patents, publications, or presentations to report this quarter.

TASK 6 – AIR ELECTRODES / ELECTROLYTES

Summary and Highlights

High-density energy storage systems are critical for EVs required by the EV Everywhere Grand Challenge. Conventional Li-ion batteries still cannot fully satisfy the ever-increasing needs because of their limited energy density, high cost, and safety concerns. As an alternative, the rechargeable lithium-oxygen (Li-O_2) battery has potential to be used for long-range EVs. The practical energy density of a Li-O_2 battery is expected to be ~ 800 Wh kg^{-1}. The advantages of Li-O_2 batteries come from their open structure; that is, they can absorb the active cathode material (oxygen) from the surrounding environment instead of carrying it within the batteries. However, the open structure of Li-O_2 batteries also leads to several disadvantages. The energy density of Li-O_2 batteries will be much lower if oxygen must be provided by an onboard container. Although significant progress has been made in recent years on fundamental properties of Li-O_2 batteries, research in this field is still in an early stage, with many barriers to be overcome before practical applications. These barriers include:

- Instability of electrolytes—The superoxide species generated during discharge or O_2 reduction process is highly reactive with electrolyte and other components in the battery. Electrolyte decomposition during charge or O_2 evolution process is also significant due to high over-potentials.
- Instability of air electrode (dominated by carbonaceous materials) and other battery components (such as separators and binders) during charge/discharge processes in an O-rich environment.
- Corrosion of Li-metal anode in an electrolyte saturated with oxygen.
- Low energy efficiency associated with large over-potential and poor cyclability of Li-O_2 batteries.
- Low power rate capability due to electrode blocking by the reaction products.
- Absence of a low-cost, high-efficiency oxygen supply system (such as oxygen selective membrane).

The main goal of this Task is to provide a better understanding on the fundamental reaction mechanisms of Li-O_2 batteries and identify the required components (especially electrolytes and electrodes) for stable operation of Li-O_2 batteries. This task will investigate several new approaches to improve stability of Li-metal anode in Li-O_2 batteries:

- Li-metal anodes will be protected using two approaches: (1) *in situ* formation of a stable SEI layer before Li-O_2 cell operation through various electrolyte formulations and treatment protocols, and (2) *ex situ* formation of stable inorganic/polymeric hybrid electrolyte layers through dip-coating or tape-casting method to coat the inorganic/polymeric hybrid electrolyte layer on Li-metal surface.
- A joint theoretical/experimental approach for design and discovery of new cathode and electrolyte materials will act synergistically to reduce charge overpotentials and increase cycle life. Synthesis methods, in combination with design principles developed from computations, will be used to make new cathode architectures. Computational studies will be used to help understand decomposition mechanisms of electrolytes and how to design electrolytes with improved stability.
- A new cathode will be developed based on high-efficiency catalyst such as 2D TM dichalcogenides (TMDs). These cathode materials will be combined with new electrolyte blends and additives that work in synergy to reduce charge potentials and increase stability of the Li-air system.

State-of-the-art characterization techniques and computational methodologies will be used to understand charge and discharge chemistries. Success of this Task will establish a solid foundation for further development of Li-O_2 batteries toward practical applications for long-range EVs. The fundamental understanding and breakthrough in Li-O_2 batteries may also provide insight on improving performance of Li-S batteries and other energy storage systems based on chemical conversion process.

Highlights. The Task highlights for this quarter are as follows:

- ANL (K. Amine / L. A. Curtiss / J. Lu) reported a simple strategy via tuning the cell chemistry to achieve a reversible LiOH based Li-O_2 battery at a low charge potential of 3.4 V with the use of a cation additive, sodium ions, to the lithium electrolyte. A solution-based reaction route is proposed, showing that the competing solvation environment of the catalyst and Li^+ leads to LiOH precipitation at the cathode.
- ANL (L. A. Curtiss / A. Ngo) and UIC (A. Salehi-Khojin) team revealed the nature of the protective SEI that forms on the lithium anode when InI_3 is used as an additive to an electrolyte in a Li-O_2 battery, in addition to its acting as an effective redox mediator. From analysis of SEM imaging it is found that 25 wt% indium is incorporated into the Li-anode surface, which is responsible for giving the battery a cycle life of more than 200 cycles.
- PNNL (J. Zhang / W. Xu) developed polymer-supported solid electrolyte interphase (PS-SEI) layers by a combination of *ex situ* and *in situ* methods to protect Li-metal surface. A redox mediator (RM) was also used to reduce cell overpotential for the long-term cycling of Li-O_2 batteries.

Task 6.1 – Rechargeable Lithium-Air Batteries (Ji-Guang Zhang and Wu Xu, Pacific Northwest National Laboratory)

Project Objective. The objective of this project is to develop rechargeable Li-O_2 batteries with long-term cycling stability through in-depth research on more stable electrolytes and highly efficient catalysts for air electrodes, protection of Li-metal anodes, and deeper understanding on the oxygen reduction reaction (ORR) and oxygen evolution reaction (OER) mechanisms behind the electrochemical performance of Li-O_2 cells. In FY 2020, the team will further investigate stability of electrodes and electrolytes to build more stable Li-O_2 batteries with long-term cycling capability.

Project Impact. The project will develop rechargeable Li-O_2 batteries with long-term cycling stability through in-depth research on more stable electrolytes and highly efficient catalysts for air electrodes and protection of Li-metal anodes. This fiscal year, the team will further investigate stability of electrodes and electrolytes to build more stable Li-O_2 batteries with long-term cycling capability.

Approach. Develop highly stable electrolytes, including localized high concentration electrolytes (LHCEs) and optimize their compositions to prevent the irreversible parasitic reactions at the electrodes (cathode and anode). The electrochemical test of Li||Li symmetric cell containing above stable electrolyte will be first measured comparatively with typical ether (tetraethylene glycol dimethyl ether, or TEGDME) based electrolyte to evaluate the stability of the electrolyte itself and the SEI layer. Then, the stability of proposed electrolytes at the cathode side with reactive oxygen species during ORR/OER will be further characterized in the Li-O_2 cells. In addition, with comparative measurements for physical properties of electrolytes, the team will find the key parameters of suitable electrolyte in Li-O_2 batteries.

Out-Year-Goals. The long-term goal of the proposed work is to enable rechargeable Li-air batteries with a specific energy of 800 Wh/kg at cell level, 1000 deep-discharge cycles, improved abuse tolerance, and less than 20% capacity fade over a 10-year period to accelerate commercialization of long-range EVs.

Collaborations. This project collaborates with C. Wang of PNNL on characterization of cycled air electrodes by TEM/SEM, with P. Gao of PNNL on computational calculations and simulations, and with J. Read of ARL on oxygen solubility tests.

Milestones

1. Develop stable electrolyte to minimize parasitic reactions at the electrodes. (Q1, FY 2020; Completed, December 31, 2019)
2. Protect anodes to prevent the lithium dendrite and LiOH formation. (Q2, FY 2020; Completed, March 31, 2020)
3. Develop stable additives (solid or soluble) or methods for sustainable catalytic effect. (Q3, FY 2020; Completed, June 30, 2020)
4. Complete evaluation of cycling performance of Li-O_2 batteries with optimized cell components and conditions. (Q4, FY 2020; Completed, September 30, 2020)

Progress Report

This quarter, the PS-SEI layers were generated to protect Li-metal surface by a combination of *ex situ* and *in situ* methods. The RM was also used to reduce cell overpotential for the long-term cycling of Li-O_2 batteries. The characteristics of PS-SEI layer were carefully investigated by XPS, SEM, and EDX. XPS images demonstrated that PEO-based gel polymer (PG) layer promotes a uniform distribution of LiF and Li_2CO_3 components, which enhanced mechanical strength of PEO coating layer during the pre-charging step under O_2 due to the strong coordination chemistry of PEO chains with lithium ions (Figure 108a). SEM analysis revealed that the PS-SEI layer is a continuous film, while the pristine lithium has a brittle mosaic-stacked SEI consisting of particulate inorganic components. Lithium deposition with PS-SEI layer is much thinner (PPG5-O_2, about 18 µm) and more uniform than that of the pre-treated bare lithium anode without PS-PEO layer (PLi-Ar, about 70 µm) after 10 cycles (Figure 108b).

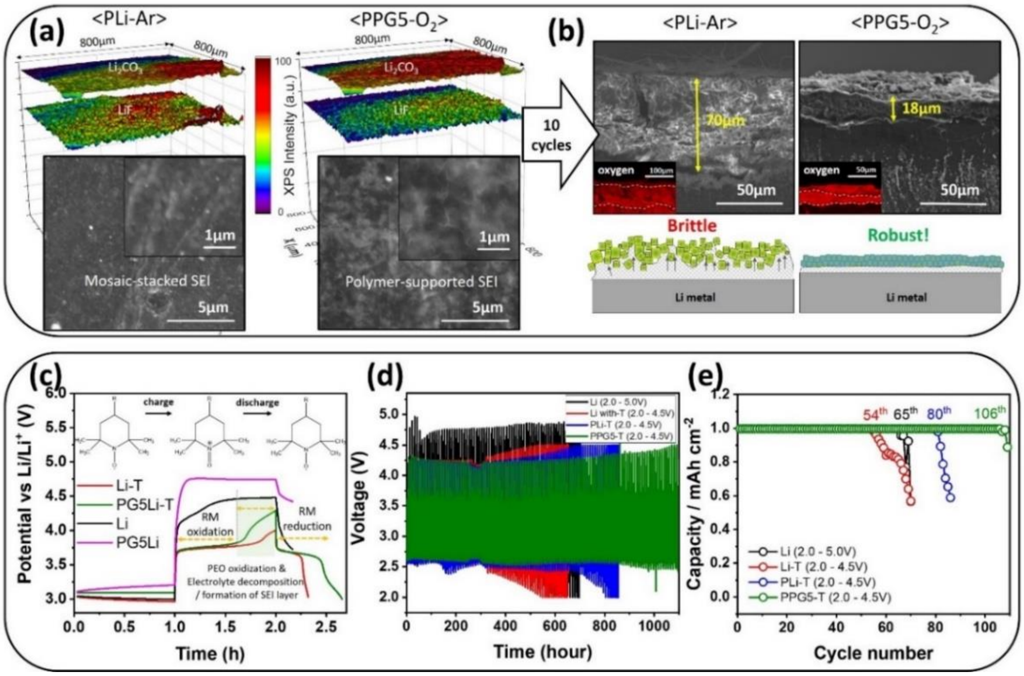

Figure 108. Analysis of SEI layers: (a) X-ray photoelectron spectroscopy and scanning electron microscopy (SEM) images (Li_2CO_3 and LiF) of Li-metal surface with PPG5-O_2 [PEO-based gel polymer (PG) coating and electrochemical pre-treatment under O_2] and with PLi-Ar (without PG coating and electrochemical pretreatment under argon). (b) Cross-sectional images and oxygen – energy dispersive X-ray maps of Li-metal anodes with PLi-Ar or PPG5-O_2 after 10 cycles at a current density of 0.2 mA cm^{-2} under a capacity limited protocol of 1.0 mAh cm^{-2} in operation voltage range of 2.0-5.0 V and corresponding illustrations for each SEM image. Electrochemical Li-O_2 battery performance with redox mediator [(2,2,6,6-tetramethylpiperidin-1-yl) oxidanyl, TEMPO]. (c) Charging profiles of Li-O_2 battery cells including TEMPO for the pretreatment step to generate different SEI layers. (d) Charge/discharge curves and (e) cycling of Li-O_2 battery cells with different SEI layers at a current density of 0.2 mA cm^{-2} under a capacity limited protocol of 1.0 mAh cm^{-2} in the operation voltage range of 2.0-4.5 V.

This work indicated that the PS-SEI layer can effectively prevent side reactions on Li-metal surface with 0.1 M TEMPO as RM (PPG5-T); consequently, prolonged cycle life was obtained even in a narrow cut-off voltage range (2.0-4.5 V). The team designed the pretreatment step to utilize RM molecules even after pretreatment (Figure 108c) for further Li-O_2 battery cycling. As a result, the combination of the PS-SEI layer and the TEMPO RM led to significant improvement of cycling stability (106 cycles) with a relatively low operation charging voltage, while bare lithium (Li-T) and pretreated bare lithium (PLi-T) anodes with TEMPO only reached 54 and 80 cycles under the same testing conditions, respectively (Figure 108d-e). In other words, the PS-SEI layer with uniform distribution of strong inorganic components embedded in the flexible PEO phase is chemically and mechanically robust to stabilize Li-metal anodes effectively against attacks of highly reactive species during Li-O_2 battery operations.

Patents/Publications/Presentations

The project has no patents, publications, or presentations to report this quarter.

Task 6.2 – Lithium-Air Batteries
(Khalil Amine, Larry A. Curtiss, and Jun Lu; Argonne National Laboratory)

Project Objective. This project will develop new cathode materials and electrolytes for Li-air batteries for long cycle life, high capacity, and high efficiency. The goal is to obtain critical insight that will provide information on the charge and discharge processes in Li-air batteries to enable new advances to be made in their performance. This will be done using state-of-the-art characterization techniques combined with state-of-the-art computational methodologies to understand and design new materials and electrolytes for Li-air batteries.

Project Impact. The instability of current nonaqueous electrolytes and degradation of cathode materials limits performance of Li-air batteries. The project impact will be to develop new electrolytes and cathode materials that are stable and can increase energy density of electrical energy storage systems based on lithium.

Approach. The project is using a joint theoretical/experimental approach for design and discovery of new cathode and electrolyte materials that act synergistically to reduce charge overpotentials and increase cycle life. Synthesis methods, in combination with design principles developed from computations, are used to make new cathode architectures. Computational studies are used to help understand decomposition mechanisms of electrolytes and how to design electrolytes with improved stability. The new cathodes and electrolytes are tested in Li-O_2 cells. Characterization, along with theory, is used to understand the performance of materials used in the cell and to make improved materials.

Out-Year Goals. The out-year goals are to find catalysts that promote discharge product morphologies that reduce charge potentials and to find electrolytes for long cycle life through testing and design.

Collaborations. This project engages in collaboration with K. C. Lau (UC at Norridge), Y. Wu (Ohio State University), D. Zhai (China), and R. Shahbazian-Yassar (UIC).

Milestones

1. Investigation of effect of salt modification on discharge product and charge overpotentials. (Q1, FY 2020; Completed)
2. Development of electrolyte blends for Li-anode protection for longer cycle life. (Q2, FY 2020; Completed)
3. Investigation of new alloys for templating LiO_2 discharge products with low charge potentials. (Q3, FY 2020; Completed)
4. Development of novel electrocatalysts for low charge potentials in synergy with new electrolyte blends. (Q4, FY 2020; Completed)

Progress Report

Lithium oxygen (Li-O_2) batteries have attracted extensive research interest due to their high energy density. The high delithiation overpotential associated with the typical discharge product of Li_2O_2 has become a key problem in developing this technology. LiOH is proven to be electrochemically active as an alternative product, and can deliver much lower charge overpotential than Li_2O_2. However, reversible LiOH formation/decomposition requires application of soluable RMs, which would inevitably promote internal shuttling, causing low Coulombic and energy efficiency. This quarter, the team reports a simple strategy to achieve a reversible LiOH-based Li-O_2 battery with use of a cation additive, sodium ions, to the lithium electrolyte. Without RMs in the cell, LiOH is detected as the sole discharge product, and it charges at a low charge potential of 3.4 V.

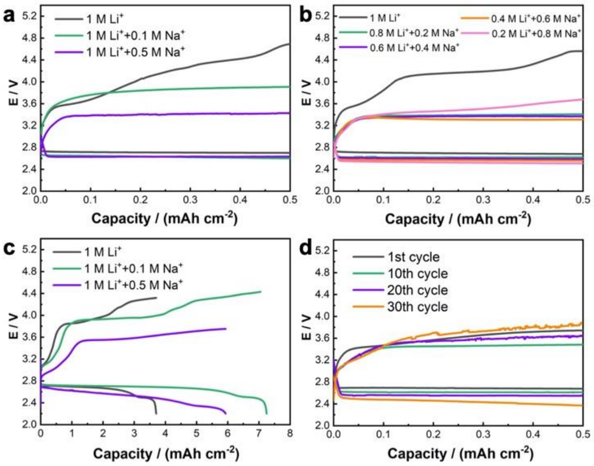

Figure 109. Electrochemical results of Li-O_2 batteries. (a) Voltage profiles and (c) deep cycles in 1 M Li triflate/TEGDME electrolyte with 0, 0.1, and 0.5 M sodium triflate, respectively. (b) Voltage profiles in TEGDME-based electrolyte with a total concentration of 1 M metal triflate. (d) Cycle life in 1 M lithium triflate and 0.5 M sodium triflate. The current density for all the galvanostatic tests is 50 μA·cm^{-2}.

As shown in Figure 109a-b, the addition of Na^+ can considerably reduce the charge potentials: for the electrolyte with 1 M Li^+ and 0.5 M Na^+, charge voltage decreases to 3.4 V, exhibiting a low charge overpotential smaller than 0.5 V. Further, the addition of Na^+ can also increase the discharge capacity and enhance the cyclability: the discharge capacity increases from 2.08 to 7.2 mAh•cm^{-2} (Figure 109c) and a low charge voltage over 30 cycles is maintained (Figure 109d).

To figure out the discharge mechanism, DFT calculation was carried out. The calculated Na-O distance (2.19 Å) is longer than the Li-O distance (1.82 Å) in the complexes with TEGDME (Figure 110b-c), indicating that surrounding the solvent molecules by Na^+ ions near the electrode could create a more gas-phase like environment, compared to Li^+ ions. The presence of Na-ions in the double-layer would enhance the "gas-phase like" environment near the electrode surface via participation of NaO_2 in the formation of H_2O (Figure 110e, pathway B). As C-H activation of TEGDME by NaO_2 (Figure 110d) has a lower barrier of 0.91 eV than that without NaO_2 (1.58 eV), it may be less favorable for LiO_2 to participate in these reactions (Figure 110e, pathway B). Thus, it is NaO_2 that mainly causes formation of H_2O, which plays a critical role in MOH forming during discharge. As NaOH is more soluble than LiOH, any NaOH will remain in solution while LiOH will form a precipitate; thus, the final product MOH should be LiOH. Charge mechanism is also studied via DEMS, as shown in Figure 110a, and the $4e^-/O_2$ process is resulting from oxidation of LiOH.

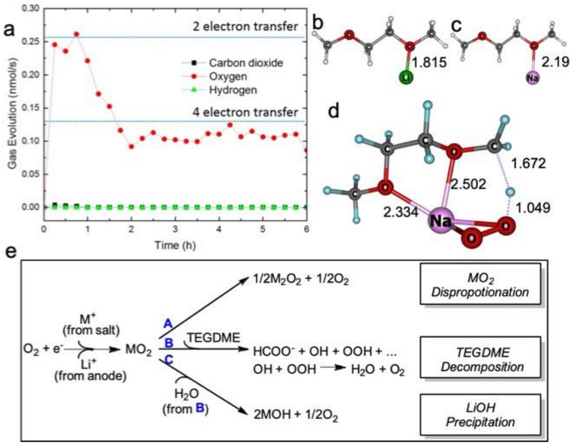

Figure 110. (a) Differential electrochemical mass spectrometer measurement of the charging process of the Li-O_2 battery in 1 M Li^+ + 0.5 M Na^+ electrolyte. (b-c) The indication of the bond length of TEGDME binding to sodium and lithium ions. (d) Optimized geometry of the transition state of C-H activation of TEGDME by NaO_2. (e) Illustration of possible reaction pathways of Li^+ and Na^+ during discharge. "M" denotes either lithium or sodium.

In conclusion, Na^+ plays a critical role in Li-O_2 cells by directly changing of the cell chemistry, and this study also demonstrates the feasibility of using LiOH as an active material in a Li-O_2 battery system.

Patents/Publications/Presentations

Publication

- Bi, X., M. Li, C. Liu, Y. Yuan, H. Wang, B. Key, R. Wang, R. Shahbazian-Yassar, L. A. Curtiss, J. Lu, and K. Amine. "Cation Additive Enabled Rechargeable LiOH Based Lithium-Oxygen Batteries." *Angewandte Chemie International Edition*. (2020). ASAP.

Task 6.3 – Lithium Oxygen Battery Design and Predictions
(Larry A. Curtiss/Anh Ngo, Argonne National Laboratory; Amin Salehi-Khojin, University of Illinois at Chicago)

Project Objective. The objective of this work is to develop new materials for Li-O_2 batteries that give longer cycle life and improved efficiencies in an air environment. New electrolyte blends and additives will be investigated that can reduce clogging and at the same time promote the cathode functionality needed to reduce charge overpotentials. New cathode and anode materials will be investigated that can work in conjunction with the electrolytes to improve cycle life in the presence of air components.

Project Impact. Li-air batteries are considered as a potential alternative to Li-ion batteries for transportation applications due to their high theoretical specific energy. The major issues with the existing Li-O_2 systems include degradation of the anode electrode, reactions with air components, clogging of the cathode, and electrolyte instability. Thus, this project is using a comprehensive approach to improve cycle life and efficiency through developing new materials for electrodes, anodes, and electrolytes that work in synergy.

Approach. The experimental strategy is to use cathode materials based on 2D TMDs that the team has found to be among the best oxygen reduction and evolution catalysts. These cathode materials will be combined with new electrolyte blends and additives that work in synergy to reduce charge potentials and increase stability of the Li-air system. DFT and AIMD simulations are used to gain insight at the electronic structure level of theory of the electrolyte structure, and function both in bulk and at interfaces with the cathode, anode, and discharge product. Classical MD is used to obtain understanding at longer length and time scales of processes occurring in the electrolyte and growth mechanisms of discharge products. The team will also utilize a HT screening strategy based on experiment and theory to develop a large database of properties and outcomes of electrolyte combinations that can be analyzed using ML to predict electrolytes and additives with the best performance.

Out-Year Goals. The out-year goals are to find electrolytes that give high capacities and long cycle life in an air atmosphere using HT screening.

Collaborations. This project engages in collaboration with R. Assary and J. G. Wen of ANL, B. Narayanan of University of Louisville, T. Li of Northern Illinois University, and F. Khalili-Araghi and R. Klie of UIC.

Milestones

1. Investigate various salt combinations for Li-O_2 electrolytes for both lithium anode protection and low charge potentials for the performance of Li-O_2 batteries with use of computations to provide understanding. (Q1, FY 2020; Completed)
2. Investigate bromine-based RMs by experiment and theory for comparison with iodine-based RMs with MoS_2 cathode materials. (Q2, FY 2020; Completed)
3. Perform DFT studies of InX_3 additive mechanisms in Li-O_2 batteries. (Q3, FY 2020; Completed)
4. Investigate mechanisms by how additives can form SEI that can protect the lithium anode. (Q4, FY 2020; Completed)

Progress Report

Li-O_2 batteries are considered as an advanced energy storage system that could provide a much higher specific energy than Li-ion batteries for electrical transportation. However, there are major issues with the existing Li-O_2 systems, including degradation of the anode electrode, poor volumetric energy density, electrolyte instability, and high charge overpotential. The team is focused on finding a combination of electrolytes, additives, and cathode catalysts to enable a Li-O_2 battery that can operate in an air atmosphere with a low charge potential while maintaining a long cycle life. They been investigating two bifunctional additives, with one of the functions being that of RM to reduce the charge potential and the other function being to provide anode protection. Previously, they reported on how additives based on InI_3 and $InBr_3$ can give low charge potentials and cycle life of more than 200 cycles. In this work, the team presents results of the characterization study of the protective SEI that forms on the lithium anode when InI_3 is used. The electrolyte for the Li-O_2 cell was composed of 25 mM InI_3 ($InBr_3$), 0.1 M LiTFSI, and a mixture of 9:1 by volume DMSO/EMIM-BF_4. The catalyst was MoS_2 nanoflakes.

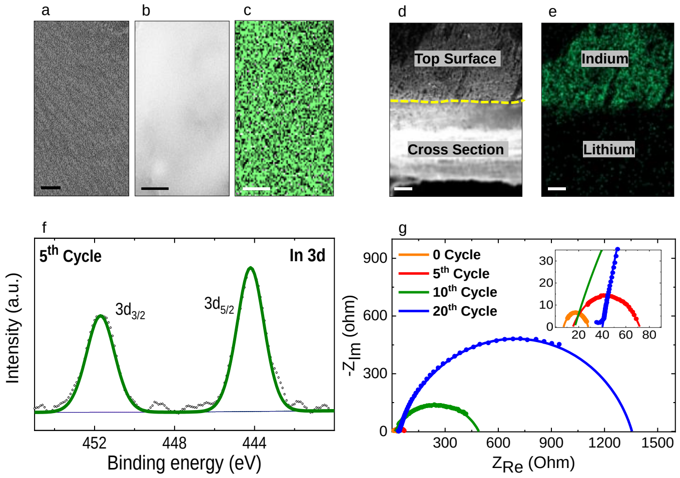

Figure 111. Characterization of lithium anode in the InI_3 system. (a) Top-view scanning electron microscopy (SEM) image of fresh anode (Scale bar: 500 nm). (b) Top-view SEM image of anode after 5th discharge (Scale bar: 500 nm). (c) Top-view SEM – energy dispersive X-ray (EDX) composition mapping of anode for indium (Scale bar: 500 nm). (d) Cross-sectional SEM image of anode after 5th discharge (Scale bar: 10 μm). (e) Cross-sectional SEM-EDX composition mapping of anode after 5th discharge for indium (green) showing it present on surface, but not in the interior. (Scale bar: 10 μm). (f) X-ray photoelectron spectroscopy results of lithium anode showing In 3d after 5th discharge cycle. (g) Electrical impedance spectroscopy measurements and fitted data for fresh and cycled anode surface.

To characterize the SEI formed on the lithium anode from the InI_3, SEM imaging was carried out on the pure lithium anode and the lithium surface after the 5th discharge cycle. The results are shown in Figure 111. Figure 111a-b shows a top-view SEM image of the pristine and cycled anodes. Also, the top-view SEM-EDX composition mapping of the In element is shown in Figure 111c. These results indicate that indium is incorporated into the anode surface. Also, the cross-sectional SEM image of the anode is shown in Figure 111d-e. The cross-sectional SEM-EDX composition mapping of the anode reveals the presence of ~ 26 wt% indium, shown by green color, in the surface region of the lithium. XPS was also carried out on the surface of cycled lithium anode to identify chemical compositions. Figure 111f shows the distinctive peaks of the indium 3d spectrum (at 444.2 eV and 451.7 eV), consistent with EDX characterization results. Moreover, EIS measurements were performed on the fresh and cycled (5, 10, and 20 cycles) anodes to measure charge transfer resistance on battery cycling (Figure 111g). Results indicate an increase in the charge transfer resistance from 21 ohms to 1315 ohms after 20 cycles, which is attributed to the incorporation of the indium on the lithium anode surface on cycling.

The mechanism by which InI_3 forms an SEI is believed to involve dissociation of indium from the InI_3 triiodide when it reacts with and is incorporated into the lithium surface, with the lithium cations reacting with the iodine anions to form LiI species in the electrolyte that can then act as RM at the cathode. When the InI_3 reacts and dissociates on the surface, the In^{3+} picks up electrons from the lithium anode because indium is more electronegative than the lithium. The reaction of InI_3 with the lithium surface is consistent with the mechanism found in computational AIMD studies. Hence, experimental and computational results reveal that while the In^{3+} reacts on the lithium anode side to form a protective layer on the surface, the I_3^- is the source of the RM, LiI at the MoS_2 cathode, thus acting as an effective bifunctional additive in a dry air environment. In addition, $InBr_3$ acts in a similar manner to give a long cycle life with reduced charge potentials in a Li-O_2 battery.

Patents/Publications/Presentations

Publications

Ahmadiparidari, A., S. Fuladi, L. Majidi, S. Plunkett, E. Sarnello, Z. Hemmat, S. Rastegar, S. Misal, P. C. Redfern, J. Wen, T. Li, A. T. Ngo, F. Khalili-Araghi, L. A. Curtiss, and A. Salehi-Kojin. "Lowering Charge Potentials with Negligible Capacity Loss in High Rate Lithium Oxygen Batteries." Submitted.

- Rastegar, S., Z. Hemmat, C. Zhang, S. Plunkett, J. G. Wen, N. Dandu, T. Rojas, L. Majidi, S. Misal, A. T. Ngo, L. A. Curtiss, and A. Salehi-Khojin. "A Lithium-Oxygen Battery that Operates in Dry Air with a Bifunctional InX_3 (X=Br,I) Electrolyte Additive." Submitted.

TASK 7 – SODIUM-ION BATTERIES

Summary

During FY 2019, the BMR added new projects, including several in the area of Na-ion batteries. Four of these projects were continuously funded into FY 2020. Progress on these four projects is described in this report. The Na-ion battery will require investigations to identify optimal electrode materials, electrolytes, separators, and binders to reach full potential. The BMR program will therefore have a limited effort directed toward identifying Na-ion battery materials that have potential value for vehicle applications.

Highlights. The highlights for this quarter are as follows:

- The ANL team conducted experiments to compare Pb@PbO nanoparticles in a carbon composite in both Li- and Na-ion batteries. The lithium cells with 600 mAh/g capacity performed well over 100 cycles with only 10% loss, but the sodium type gives ~ 2 times higher resistance in the sodium electrolyte than lithium with commensurate low capacity. The electrode kinetics are much slower in the Pb@PbO electrode in the Na-ion case, and thus electrolyte/interface improvements are needed.
- The BNL team carried out synchrotron-based spectroscopy studies to understand the anion redox reaction in NaCrSeS cathode, revealing that sulfur anions make important contributions to the capacity by going through reversible S^{2-}/S^{n-} and $S^{2-}/(S_2)^{m-}$ redox reactions during cycling.
- The LBNL team studied a series of lepidocrocite-type $NaxTi_{2-y/4}O_4$ electrodes that were cycled in sodium half-cell configurations and were found to be able to deliver 198-237 mAh/g reversibly, depending on composition. This is in excess of that predicted from interlayer site considerations, implying that vacancies in the TM layers provide extra sites for sodium.
- The PNNL team further investigated the properties of non-flammable electrolyte [NaFSI:TEP:TTE (1:1.5:2 in molar)] in full cells using $NaCu_{1/9}Ni_{2/9}Fe_{1/3}Mn_{1/3}O_2$ (Na-NCFM) as the cathode and pre-sodiated HC as the anode. The cell retained 82.5% capacity after 200 cycles, which is much better than those using baseline electrolyte with 48% capacity retention.

Task 7.1 – Exploratory Studies of Novel Sodium-Ion Battery Systems
(Xiao-Qing Yang and Enyuan Hu, Brookhaven National Laboratory)

Project Objective. The objective of this project is to develop new advanced *in situ* material characterization techniques and apply these techniques to explore the potentials, challenges, and feasibility of new rechargeable battery systems beyond the Li-ion batteries, namely, the Na-ion battery systems for EVs, such as PHEV and BEV. To meet the challenges of powering PHEVs and BEVs, new rechargeable battery systems with high energy and power density, low cost, good abuse tolerance, and long calendar and cycle life need to be developed. This project will use the synchrotron-based *in situ* X-ray diagnostic tools, combined with TEM and STEM imaging techniques developed at BNL, to evaluate the new materials and redox couples to obtain fundamental understanding of the reaction mechanisms of these materials aiming for improvement of and guidance for new material and new technology development regarding Na-ion battery systems.

Project Impact. In the VTO MYPP, the goals for battery were described: "Specifically, lower-cost, abuse-tolerant batteries with higher energy density, higher power, better low-temperature operation, and longer lifetimes are needed for the development of the next-generation of HEVs, PHEVs, and EVs." The knowledge learned from diagnostic studies and collaborations with U. S. industries through this project will help U. S. research institutions and industries to develop new materials and processes for a new generation of rechargeable battery systems, namely, Na-ion battery system, in their efforts to reach these VTO goals.

Approach. This project will use the synchrotron-based *in situ* X-ray diagnostic tools developed at BNL to evaluate the new materials and redox couples to enable a fundamental understanding of the mechanisms governing performance of these materials and provide guidance for new material and new technology development regarding Na-ion battery systems.

Out-Year Goals. Complete the synchrotron-based *ex situ* XRD, PDF, XAS, and XRF studies of novel anion redox-based cathode materials $NaTi_{1/3}Cr_{2/3}S_2$ and NaCrSeS at different SOCs.

Collaborations. The BNL team has been closely working with top scientists on new material synthesis at ANL, LBNL, and PNNL and with U. S. industrial collaborators at GM and Johnson Controls, as well as with international collaborators.

Milestones

1. Complete chromium, titanium, and sulfur K-edge XAS [including XANES and extended X-ray absorption fine structure (EXAFS)] studies of $NaTi_{1/3}Cr_{2/3}S_2$ cathode material at different SOCs. (Q1, FY 2020; Completed)
2. Complete synchrotron-based *ex situ* XRD and PDF analysis of novel anion redox-based cathode material NaCrSeS at different SOCs. (Q2, FY 2020; Completed)
3. Complete the chromium and selenium K-edge XAS study and analysis of NaCrSeS cathode material at different SOCs. (Q3, FY 2020; Completed)
4. Complete the sulfur K-edge XANES and EXAFS studies of NaCrSeS cathode material at different SOCs. (Q4, FY 2020; Completed)

Progress Report

This quarter, the fourth milestone for FY 2020 was completed. BNL has been focusing on synchrotron-based XAS studies for NaCrSeS cathode material at different SOCs. *Ex situ* XAS spectra at sulfur K-edge at different charge/discharge stages are shown in Figure 112a. The relative intensity of peak A at ~ 2470 eV (red area in Figure 112a) varies greatly during cycling, and the evolution of peak B at ~ 2480e V (blue area in Figure 112a) has a similar moving trend as that for selenium K-edge. The peak A could be attributed to the transition of 1s electron to the unoccupied Cr 3d-S 3p hybrid orbitals. During the charge process, the emerging and growing of the shoulder peak located at ~ 2468 eV and addition peak formation at 2470.7 eV are clearly observed, corresponding to formation of the holes of sulfur and the dimerization of S/Se-S/Se, respectively; the process reverses on discharge. These results suggest the reversible valence changes of sulfur anions and the occurrence of S^{2-}/S^{n-} and $S^{2-}/(S_2)^{m-}$ redox couples during cycling. The corresponding FT-EXAFS spectra of sulfur are shown in Figure 112b. Note that the FT-EXAFS spectra have not been phase-corrected so that the actual bond lengths could be ~ 0.4 Å longer. The peak at 2.1 Å for the pristine state in Figure 112b is corresponding to the closest chromium ions to the core sulfur, which shift to 2.0 Å after fully charged. During charge (desodiation), Cr-S/Se bonds shrink, also shown as the decrease in lattice parameters “a” and “b” obtained by XRD, caused by the contraction of the sulfur and selenium anion radii at higher oxidation states. These structural changes are in line with the mechanism of “normal unit cell breathing.”

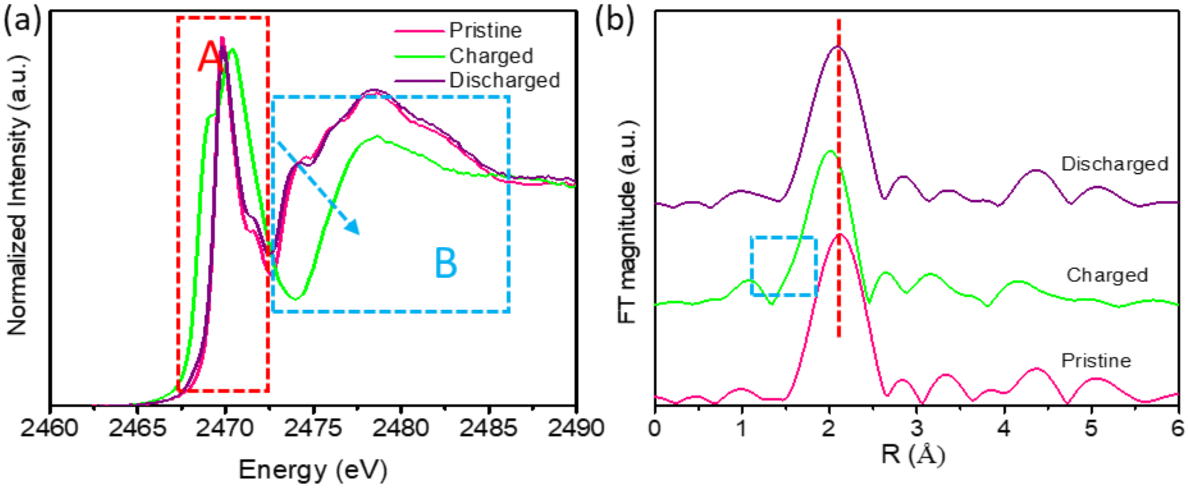

Figure 112. (a) Sulfur K-edge X-ray absorption near-edge structure spectra and (b) corresponding Fourier transform – extended X-ray absorption fine structure spectra of NaCrSSe electrodes at various charge/discharge states, which include pristine, full charged (charged to 3.3 V), and full discharged (discharged to 1.5 V after full charged).

Patents/Publications/Presentations

Publications

- Wang, P-F., T. Jin, J. Zhang, Q-C. Wang, X. Ji, C. Cui, N. Piao, S. Liu, J. Xu, X-Q. Yang, and C. Wang. “Elucidation of the Jahn-Teller Effect in a Pair of Sodium Isomer.” *Nano Energy*. doi: 10.1016/j.nanoen.2020.105167. Publication Date (Web): July 28, 2020.
- Yang, L., J. M. López del Amo, Z. Shadike, S-M. Bak, F. Bonilla, M. Galceran, P. K. Nayak, J. R. Buchheim, X-Q. Yang, T. Rojo, and P. Adelhelm. “A Co- and Ni-Free P_2/O_3 Biphasic Lithium Stabilized Layered Oxide for Sodium-Ion Batteries and its Cycling Behavior.” *Advanced Functional Materials*. doi: 10.1002/adfm.202003364. Publication Date (Web): August 21, 2020.

Task 7.2 – Development of a High-Energy Sodium-Ion Battery with Long Life (Chris Johnson and Khalil Amine, Argonne National Laboratory)

Project Objective. The project objective is to develop a high-energy Na-ion battery with long life. Moreover, the battery chemistry should utilize low-cost materials. The energy density target is 200 Wh/kg and/or 500 Wh/L, wherein the anode and cathode capacity targets are 600 $\mathrm{mAhg^{-1}}$ and 200 $\mathrm{mAhg^{-1}}$, respectively.

Project Impact. A Na-ion battery on par with the energy density of a Li-ion battery can have a high impact in the transportation sector with the assumption that the cost is significantly below $85/kWh and that the battery pack provides a 300-mile range. The consumer is not concerned about the battery chemistry employed if these metrics can be met. Development of these battery chemistries will situate the United States in a strong position as relates to new low-cost energy storage systems beyond lithium ion.

Approach. In a team approach, the Na-ion battery group will create a versatile Na-ion battery chemistry with beneficial advantages such as low cost, safety, recycling, and sustainability of materials used. The team will work synergistically so that the final design is the culmination of advances in phosphorus carbon composites mated with optimized lead or other highly dense metalloids, such as tin and/or antimony and derivatives thereof, for the recyclable anode. Synthesis and optimization of such blended composite anodes will be conducted in parallel to diagnostic characterization of structures, phase formation, and cycling stability. Cathode work will begin at the end of the first year and will involve gradient cathodes consisting of Fe-Mn compositions, as well as intergrowths of layer stacking sequenced oxides. If resources allow, the team also will attempt to stabilize cathode surfaces using ALD methods, particularly for the benefit of staving off dissolution of manganese and iron / electrolyte reactivity. Electrolytes will be partly procured from H. Li at PNNL.

Out-Year Goals. The state-of-the-art Na-ion battery in the literature has now been surpassed by this team, but performance is still too low for commercialization. Thus, the goal is to move forward and continually invent the most superior Na-ion battery chemistry that can compete worldwide through work output from this project.

Collaborations. Researchers from PNNL who are developing electrolytes for Na-ion batteries will provide this project with formulations to test with the various electrode combinations investigated at ANL. The team also exchanges commercial samples with J. Barker of Faradion Ltd. in the United Kingdom.

Milestones

1. Investigate reaction mechanism of P-based and Pb-based anode. (Q1, FY 2020; Completed)
2. Synthesize high-performance layered oxide cathodes using continuous stirred tank reactor (CSTR) method. (Q2, FY 2020; In progress)
3. Optimize the interface of P-based and Pb-based anode for long cycle life and high ICE. (Q3, FY 2020; In progress)
4. Develop composition-gradient oxide cathodes. (Q4, FY 2020; In progress)

Progress Report

In contrast to their excellent electrochemical performances in lithium cells (stable cycling capacity of ~ 600 mAh/g), the newly developed Pb@PbO-C nanocomposite anode has limited electrochemical sodium reaction properties showing moderate capacity and rate performances (Figure 113a). This quarter, the team reports on fundamental differences in the lithium and sodium reaction mechanisms of the Pb-based anode materials and elucidates the main reasons for the limited sodium reaction properties.

To compare the lithium and sodium storage mechanisms of the Pb@PbO-C nanocomposite anode, the lead redox reaction and local structural change were investigated by *ex situ* XAS measurements. The XANES spectrum for the pristine Pb@PbO-C nanocomposite is located at a slightly lower energy than that of the lead(II) oxide reference, reflecting the average valence state of PbO and lead. The XANES spectrum during the initial discharge process shows an edge shift toward lower energy, according to the conversion reaction during which Pb^{2+} (PbO) reduces to zero-valent lead (metallic lead). In the following alloying reaction region, the XANES spectra show a surprisingly large degree of edge shifts toward the lower absorption energy (Figure 113b). This was quite an unexpected observation because it indicates that lead continues to reduce even during the Li-Pb or Na-Pb alloying reaction. The observed change in the half-height edge energy corresponds to the lead valence of approximately Pb^{-4} at the end of the reaction. Such a large degree of edge shift has never been reported in other alloying-reaction-based anode materials (for example, silicon, germanium, and tin). It is evident from the data that lead acts like an anion in the Li-Pb alloying process, and the wide-range lead redox is the basis for the large capacity of the Pb@PbO-C nanocomposite material. A clear distinction between the Li-Pb and Na-Pb alloying reactions was found in the EXAFS analysis. After the dissociation of the Pb-O bond in lead oxide due to the conversion reaction, the Na-Pb data show an evolution of a strong peak at around 3.2 Å. In accordance with the large negative charge of lead in the Na_xPb phases, this intensified new peak likely corresponds to the Pb-Pb cluster in a Zintl phase. However, the EXAFS data for the Li_xPb phases do not show a similar Pb-Pb peak in the alloying region, suggesting different phase transition pathways for Na-Pb and Li-Pb intermediates.

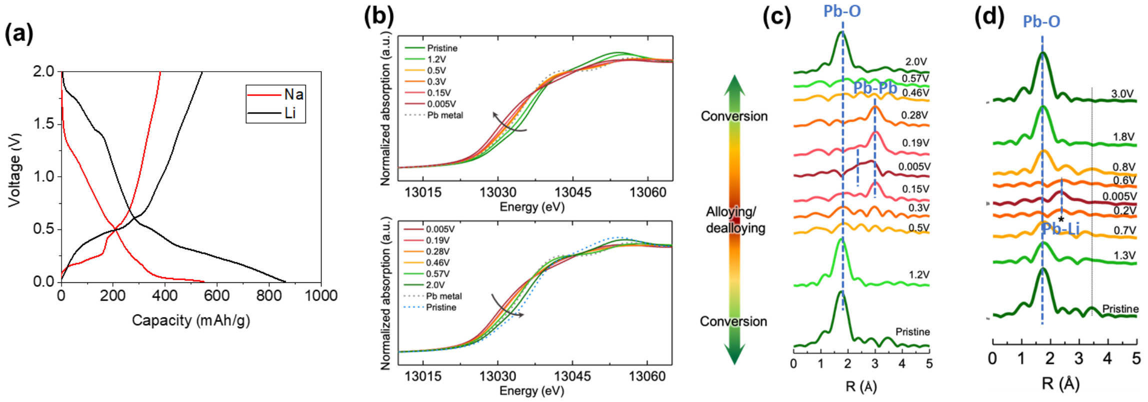

Figure 113. (a) Comparison of the voltage profiles of Pb@PbO-C cycled in lithium and sodium cells. (b) X-ray absorption near-edge spectroscopy and (c-d) extended X-ray absorption fine structure data collected at various states of (b-c) sodium and (d) lithium reactions.

The *operando* XRD analysis was conducted to compare the phase evolutions during the electrochemical sodiation and lithiation processes (Figure 114a). In contrast to the room-temperature lithiation and sodiation of other group 14 metals that exhibit amorphous intermediate phases during the entire (tin and germanium) or significant regions (tin) of the reaction pathways, the Pb@PbO-C follows the thermodynamic equilibrium pathways forming crystalline intermediate structure. Interestingly, the NaPb phase is stabilized as the tetragonal Zintl structure (*$I4_1/acd$*) while LiPb is formed as a cubic phase (*Pm-3m*). The formation of the tetragonal Zintl structure, which comprises tetrahedral Pb_4 clusters, corresponds to the EXAFS data that shows the evolution of the Pb-Pb bond during the sodium reaction. The strong covalent character of the Pb_4 Zintl clusters adversely affect the electronic conductivity (Figure 114c) and thus limit the electrochemical performance of the Pb@PbO-C anode in sodium cells.

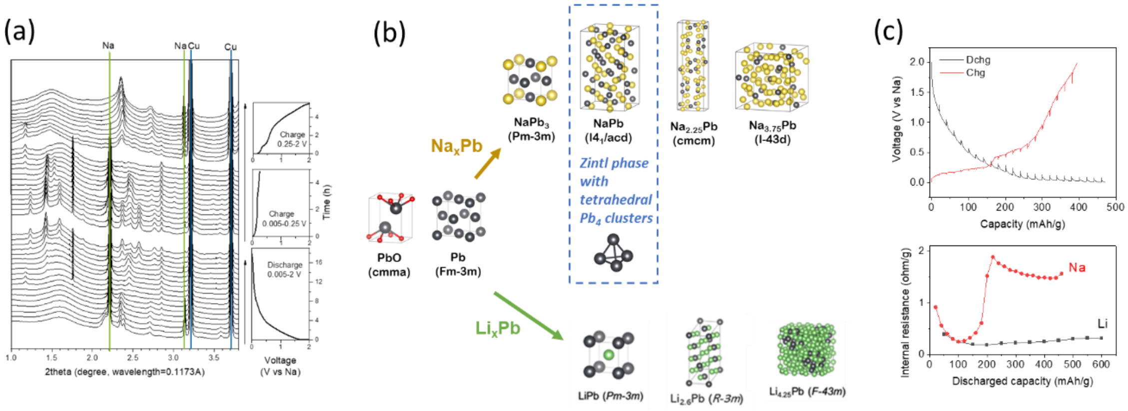

Figure 114. (a) *Operando* X-ray diffraction of the Pb@PbO-C anode during sodium cycling, the comparison of (b) phase evolution, and (c) internal resistance change during the electrochemical sodium and lithium reaction.

Patents/Publications/Presentations

Publication

- Han, J., J. Park, S-M. Bak, S-B. Son, J. Gim, C. Villa, X. Hu, V. P. Dravid, C. C. Su, Y. Kim, C. Johnson, and E. Lee. "New High-Performance Pb-Based Nanocomposite Anode Enabled by Wide-Range Pb Redox and Zintl Phase Transition." *Advanced Functional Materials* (2020): 2005362. doi.org/10.1002/adfm.202005362 and Front Cover Art (John Goodenough, Nobel Prize Issue).

Presentation

- ECS PRiME 2020, Whittingham Symposium, Virtual (October 4–9, 2020): "Performance and (De)Lithiation Mechanism of Lithium-Lead (Pb) Anode for Li Battery"; C. S. Johnson. Invited.

Task 7.3 – High-Capacity, Low-Voltage Titanate Anodes for Sodium-Ion Batteries (Marca Doeff, Lawrence Berkeley National Laboratory)

Project Objective. The objectives are to understand differences in the sodium intercalation mechanism of various sodium titanate anodes through an array of synthetic, electrochemical, and structural characterization techniques, and to overcome practical impediments to their use, such as the high 1st cycle Coulombic inefficiencies that are currently observed. The ultimate goal is to produce a 200-250 mAh/g anode that cycles reversibly.

Project Impact. Although several suitable cathode materials for Na-ion batteries exist, there are few suitable anode materials due to low potential instabilities. Therefore, sodium titanate variations will be synthesized through different routes to develop materials with various morphologies and dopants. Decreasing the 1st cycle inefficiencies and improving cycling performance will allow enabling technology for a practical high-energy Na-ion battery.

Approach. Candidate stepped layered titanates will be synthesized by appropriate routes (hydrothermal, solid-state routes, etc.). Materials will then be characterized electrochemically and physically. Structure-function relationships will be built to correlate the effect of changing structure (for example, step size) on electrochemical properties.

Out-Year Goals. A series of synchrotron characterization techniques will be used to further develop sodium titanate anode materials with stable cycling while delivering high capacities.

Collaborations. TXM is done in collaboration with Y. Liu (SSRL). Synchrotron hard, sXAS, and X-ray Raman efforts are in collaboration with D. Nordlund and D. Sokaras (SSRL). Electrolyte design is done in collaboration with K. Xu (ARL).

Milestones

1. Conduct SEI studies. (Q1, FY 2020; In progress, pending beam time at SSRL)
2. Synthesize lepidocrocite titanates. (Q2, FY 2020; In progress)
3. Select best electrolyte solution. (Q3, FY 2020; In progress)
4. *Go/No-Go Decision*: On sodium nonatitanate, stop if problems are not solved. (Q4, FY 2020; Decision is *Go*; the team is able to cycle 200 mAh/g, a goal of the program)

Progress Report

This quarter, the team electrochemically characterized the lepidocrocite-type $Na_xTi_{2-y/4}O_4$ electrodes (x = 0.74, 0.8, 0.9, and 1.0; 2-y/4 = 1.815, 1.8, 1.775, and 1.75). Their 2nd cycle discharge capacities were plotted in Figure 115 as a function of initial compositions. The second-cycle discharge capacity decreases with decreasing number of both reducible titanium ions and available sites for sodium intercalation. When further comparing to the values calculated based on limitations of either reducible titanium ion or available sites, it is obvious that available sites for sodium accommodation determine the capacities of those titanate electrodes. Surprisingly, all the experimental capacities are higher than the calculated values based only on the number of vacant sodium sites between layers. Possible explanations are as follows: (1) vacant titanium sites are also used for accommodating sodium, (2) the actual initial sodium contents are lower than the values calculated from precursor stoichiometry because of the ion-exchange process, and/or (3) surface sodium storage. More insights might be obtained from solid-state Na23 NMR spectroscopy via studying the intercalated Na^+ environments. The long-term cycling performance of $Na_xTi_{2-y/4}O_4$ electrodes was also evaluated, and typical results are presented in Figure 116. After 38 cycles, 75.3% of the 2nd discharge capacity was obtained with CE of 94.4% in the 2nd cycle and over 99.0% from the 8th cycle onward (Figure 116a). Further analyzing the capacity retention in high-voltage (1.0-2.0 V versus Na^+/Na) and low-voltage (0.1-1.0 V versus Na+/Na) regions reveals that the capacity fading mainly occurs in the high-voltage region (Figure 116b-c). This finding, though maybe counterintuitive at first sight, corroborates with the gas analysis result that shows H2 evolution in the high-voltage region (Figure 117). The team's current hypothesis is that sodium storage in the high-voltage region mainly results from activated surface water and/or hydroxyl groups, and those water/hydroxyl groups are gradually reduced to H_2 on cycling and cause capacity fading. Rate performance test of $Na_xTi_{2-y/4}O_4$ electrodes as a function of compositions is ongoing, and results are expected to be reported next quarter.

Work during the next quarter will include: (1) exploring in more detail whether the surface structure of $Na_xTi_{2-y/4}O_4$ electrodes dominates high-voltage sodium storage; (2) studying the structural evolution of $Na_xTi_{2-y/4}O_4$ electrodes using XRD, and (3) using spectroscopy techniques to study the sodium storage mechanism (depending on the beam time at SSRL).

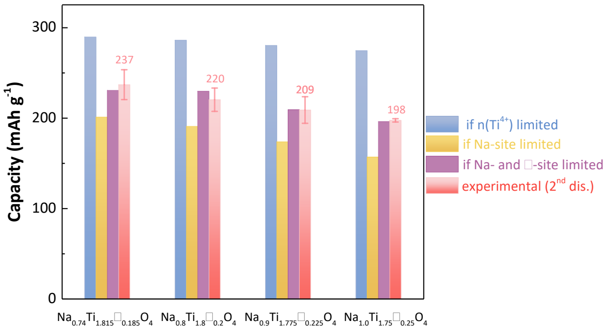

Figure 115. Calculated and experimental capacity of $Na_xTi_{2-y/4}O_4$ electrodes. The calculations considered situations limited by the number of reducible titanium ions and by the number of available interlayer sites for sodium intercalation. For the experimental values, three to five cells were tested with each composition to obtain better statistics. The error bar represents the standard deviation of the average values of 2nd cycle discharge capacity obtained at current rate of C/20 (that is, 8 mA g^{-1}, 0.012 mA cm^{-2}).

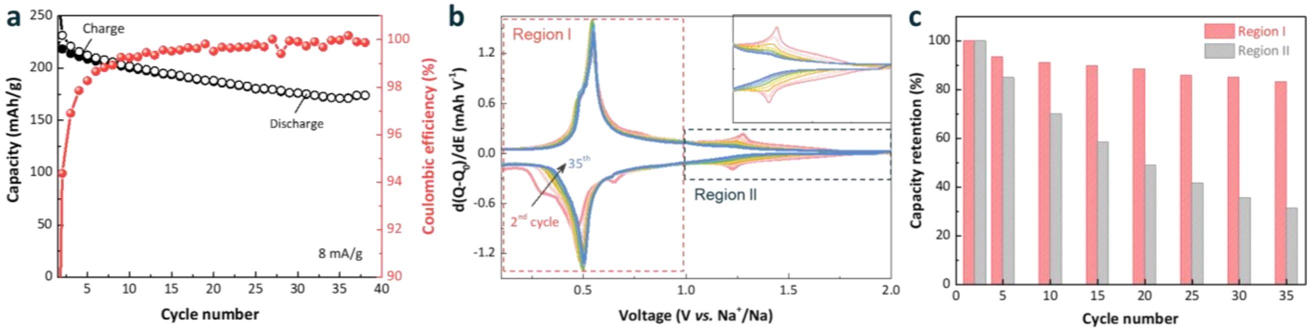

Figure 116. Long-term cycling performance of $Na_{0.74}Ti_{1.815}O_4$ electrode. (a) Discharge/charge capacity retention and Coulombic efficiency of $Na_{0.74}Ti_{1.815}O_4$ electrode. (b) Evolution of dQ/dV plots from 2nd to 35th cycles. (c) The capacity retention of Region I and Region II. Region I: voltage range of 0.1-1.0 V; Region II: voltage range of 1.0-2.0 V. The capacities of Region I and Region II were integrated from their respective surface areas in the dQ/dV plots. The capacity retention (%) of Region I and Region II was obtained by normalizing the capacities relative to the 2nd cycle. The cell was cycled in electrolyte of 0.5 M $NaPhB_4$ in diethylene glycol dimethyl ether (DEGDME) at current rate of C/20 (that is, 8 mA g^{-1}, 0.012 mA cm^{-2}).

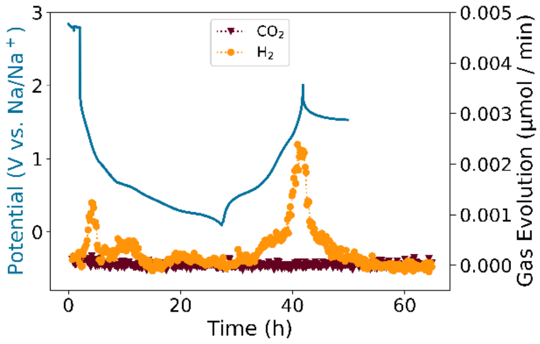

Figure 117. Differential electrochemical mass spectrometry (DEMS) analysis of $Na_{0.74}Ti_{1.815}O_4$ electrode in the first electrochemical cycle. The cell was cycled in electrolyte of 0.5 M $NaPhB_4$ in diethylene glycol dimethyl ether (DEGDME) at current rate of C/10 (that is, 16 mA g^{-1}, 0.024 mA cm^{-2}).

Patents/Publications/Presentations

Publication

- Alvarado, J., G. Barim, C. D. Quilty, E. Yi, K. J. Takeuchi, E. S. Takeuchi, A. C. Marschilok, and M. M. Doeff. "Optimization of Nonatitanate Electrodes for Sodium-ion Batteries." *Journal of Materials Chemistry A* (2020). doi:10.1039/D0TA07561B.

Task 7.4 – Electrolytes and Interfaces for Stable High-Energy Sodium-Ion Batteries (Ji-Guang Zhang, Pacific Northwest National Laboratory)

Project Objective. This project will develop innovative electrolytes and enable fundamental understanding on the interface between electrode and electrolyte for stable operation of high-energy Na-ion batteries. The proposed research will enhance the achievable capacities of both anode and cathode for Na-ion battery and improve the stability of electrodes/electrolyte interface, establish correlation (electrolyte design rule) between electrochemical performances of Na-ion batteries and the electrolyte/interface properties, and enable long cycle life and safe operation of high-energy Na-ion batteries.

Project Impact. Success of this project will provide a solid understanding on the electrolyte/electrode interphase of Na-ion batteries and significantly improve their energy density, cycle life, and safety. It will also accelerate the practical application of Na-ion batteries in both EV and stationary energy storage.

Approach. This project will optimize the electrolyte components and concentrations to develop innovative electrolytes and additives with improved electrochemical and physical properties. *In situ* and *ex situ* spectroscopy methods will be used to unravel the origin of the SEI at the dynamic interface, providing guidance for the electrolyte and interface design and enabling high capacity and long life of Na-ion batteries.

Out-Year Goals. This project will select the electrolyte compounds and identify the formation of interfacial SEI layer on hard carbon and CEI layer-on-layer oxide cathode and its effect on the electrode materials. It will also provide guidance on electrolyte optimization and to improve CE of sodium deposition/stripping to be more than 99%.

Collaborations. This project will collaborate with ANL, LBNL, and other leading scientists in the field of cathode and anode materials for Na-ion batteries. It will also collaborate with C. Wang and M. Engelhard of PNNL for TEM and XPS characterization.

Milestones

1. Optimize electrolyte composition: Na-based LHCE will be developed to improve cycling stability. (Q1, FY 2020; Completed)
2. Develop electrolyte additives to improve stability of SEI on anode and of CEI layer on cathode. (Q2, FY 2020; Completed)
3. Develop compatible polymer separator (or PE) to stabilize long-term cycling and provide a stable/adequate interphase. (Q3, FY 2020; Completed)
4. Apply the new electrolytes and additives in Na-ion batteries to improve CE to more than 99%. (Q4, FY 2020; Completed)

Progress Report

This quarter, Na-ion full cells were tested in non-flammable LHCE [NaFSI-TEP/TTE (1:1.5:2 in mole)] and compared with those tested in baseline electrolyte [BE: 1 M $NaPF_6$/EC+DMC (1:1 in weight)]. The electrochemical performance of full cells using $NaCu_{1/9}Ni_{2/9}Fe_{1/3}Mn_{1/3}O_2$ (Na-NCFM) as the cathode and pre-sodiated HC as the anode is shown in Figure 118. Three formation cycles at 0.1 C were conducted for better electrode-electrolyte interphase formation before long-term cycling at 0.2 C. The HC||Na-NCFM full cells in both electrolytes show similar discharge capacity during the initial formation cycle, that is, 118.2 mAh g^{-1} for the NaFSI-TEP/TTE electrolyte and 117.8 mAh g^{-1} for the baseline carbonate electrolyte (Figure 118a). Note the capacity calculation for the full cell was based on the mass of cathode active material. However, the long-term cycling stability of the HC||Na-NCFM full cells differs significantly in these electrolytes.

In the conventional carbonate electrolyte, the capacity of the full cell decayed quickly, with a low capacity retention of 48.4% after 200 cycles (Figure 118a). The CE of 99.6% (see Figure 118b) corresponds to 44.8% capacity retention in 200 cycles (0.996^200 = 44.8%). Considering the accuracy of Landt battery testing system (less than 0.03%), this projected value was consistent with the capacity retention of 48.4% measured in the experiment. Drastic overpotential increase and capacity decrease during cycling were observed in the Na-ion battery full cells using the baseline electrolyte, as shown in Figure 118a/c. This indicates that unstable electrode-electrolyte interphase reactions result in increased interfacial resistance and quick capacity fade during cycling. In contrast, in the nonflammable NaFSI-TEP/TTE electrolyte, the Na-ion battery full cell shows greatly improved cycling performance with a highly reversible capacity of 97.5 mAh g^{-1} and capacity retention of 82.5% after 200 cycles (Figure 118a/d). The CE of the Na-ion battery full cell reached 99.93% during cycling due to both the high quality CEI layer formed on the Na-NCFM cathode, and the SEI layer formed on the HC anode in the NaFSI-TEP/TTE electrolyte. The charge and discharge curves of the Na-ion battery full cell with NaFSI-TEP/TTE electrolyte exhibit minimal changes over 200 cycles (Figure 118d). Therefore, the electrode-electrolyte interphase formed at both the cathode and anode sides is very stable in NaFSI-TEP/TTE electrolyte during long-term cycling.

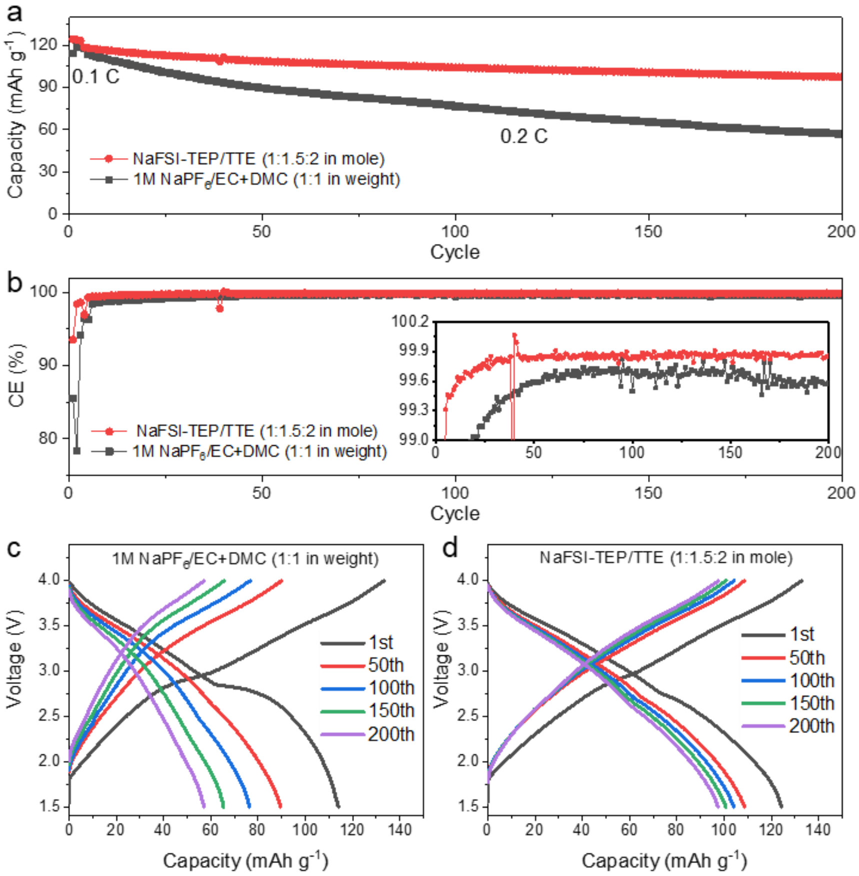

Figure 118. Electrochemical behaviors of HC||Na-CNFM full cells. (a) Cycling performance and (b) Coulombic efficiency of the full cells using nonflammable NaFSI-TEP/TTE (1:1.5:2 in mole) electrolyte and conventional 1 M $NaPF_6$/EC+DMC (1:1 in weight) electrolyte. (c-d) Selected charge–discharge voltage curves for the full cells using 1 M $NaPF_6$/EC+DMC (1:1 in weight) (c) and NaFSI-TEP/TTE (1:1.5:2 in mole) (d) electrolyte.

Patents/Publications/Presentations

Publication

- Jin, Y., Y. Xu, P. M. L. Le, T. D. Vo, Q. Zhou, X. Qi, M. H. Engelhard, B. E. Matthews, H. Jia, Z. Nie, C. Niu, C. Wang, Y. Hu, H. Pan,* and J-G. Zhang.* "Highly Reversible Sodium Ion Batteries Enabled by Stable Electrolyte-Electrode Interphases." *ACS Energy Letters* 5 (2020): 3212−3220.

Innovation Center for Battery500
(Jun Liu, Pacific Northwest National Laboratory; Yi Cui, Stanford University)

Project Objective. The project aims to develop commercially viable lithium battery technologies with a cell-level specific energy of 500 Wh/kg through innovative electrode and cell designs that enable the extraction of the maximum capacity from advanced electrode materials. In addition to achieving high specific energy, the project aims to be able to achieve 1,000 cycles for the developed technologies.

Project Impact. The Battery500 Consortium will develop next-generation lithium battery technologies that will significantly increase energy density, improve cycle life, and reduce cost. This will greatly accelerate deployment of EVs and reduce carbon emission associated with fossil fuel consumption. The consortium will utilize first-class expertise and capabilities in battery research in the United States and develop an integrated and multi-disciplinary approach to accelerate development and deployment of advanced electrode materials in commercially viable high-energy batteries. The advances made in this consortium will also benefit the improvement of current Li-ion battery technologies.

Approach. This project will utilize an assortment of national resources located at the national laboratory level and university level. The lithium anode combined with a compatible electrolyte system and two cathodes—one high-Ni $LiNi_xMn_yCo_zO_2$ and another sulfur—will be studied and developed to reach high energy density. The project focus is to design novel electrode and cell architectures to meet the 500 Wh/kg goal. The consortium will work closely with R&D companies, battery/materials manufacturers, and end users/OEMs to ensure that the developed technologies are aligned with industry needs and can be transitioned to production.

Out-Year Goals. This project aims for the following out-year goals. (1) Fabricate and test a pouch cell capable of 350 Wh/kg and 350 cycles. (2) Fabricate and test a pouch cell capable of 400 Wh/kg and 100 cycles.

Collaborations. Collaboration among consortium team members will be well coordinated by the leadership team, which includes the keystone project leads and co-leads along with PIs at all member institutions. Collaboration with the community outside of this consortium and with industry will be facilitated by the executive committee, the advisory board, and the industry committee.

Milestones

1. Deliver pouch-cell design and pouch-cell parameters for over 400 Wh/kg pouch cells. (Q1, FY 2020; Completed)
2. Develop new 3D anode structures; test and validate such using coin-cell standard protocols. (Q2, FY 2020; Completed)
3. Fabricate and test 350 Wh/kg Li-S pouch cells with over 50 stable cycles. (Q3, FY 2020; Completed)
4. Fabricate and test a pouch cell capable of 400 Wh/kg and 100 cycles. (Q4, FY 2020; Completed)

Progress Report

Keystone Project 1: Materials and Interfaces

The goal of Keystone 1 is to provide the materials and chemistry support for Keystone projects 2 and 3. This quarter, doping and surface coating methods were used to improve the surface and structure properties of NMC cathodes (SUNY Binghamton and UT Austin); an alternative anode was investigated (University of Washington, UW); and novel electrolytes were synthesized (Stanford) and analyzed (PNNL) to enhance the CE and cycling stability of Li||NMC batteries.

The SUNY Binghamton group investigated relative merits of surface modification versus bulk substitution for improved cathode stability. Their previous work showed that a surface coating using a Li-Nb-O solution on NMC-811 meatballs reduces 1st cycle capacity loss and improves rate performance. Surface coating plus surface substitution occurs when the Li-Nb-O/NMC material is fired at 400-500°C; whereas, when the firing occurs at ≥ 700°C, the niobium diffuses into the bulk of the material. Both thermal treatments gave improved capacity retention over the untreated 811, as shown in Figure 119a; however, bulk substitution showed the best performance. It is believed that surface coating protection suppresses the side reactions with electrolyte, and the bulk Nb-substitution enhances the structural stability during cycling. Figure 119b-d shows that both coating and substitution reduce the change in the dQ/dV 4V peaks relative to untreated 811. This may be associated with suppression of the H2 to H3 transition or converting it into a single-phase region. Therefore, there is a need for both a coating to protect the surface and substitution to stabilize the lattice. Phosphate, borate, and Al-O species have been extensively studied for the layered oxides; more work will be done to look at different species for the coating and for substitution, for example, by coating an Al-substituted material. In addition, more investigation will be done to replace NMP in the preparation of NMC-811 electrodes by the greener solvent-Cyrene. However, under ambient conditions it is unable to satisfactorily dissolve the PVDF binder and the coating crumbled in use. Other opportunities for replacing NMP will be studied.

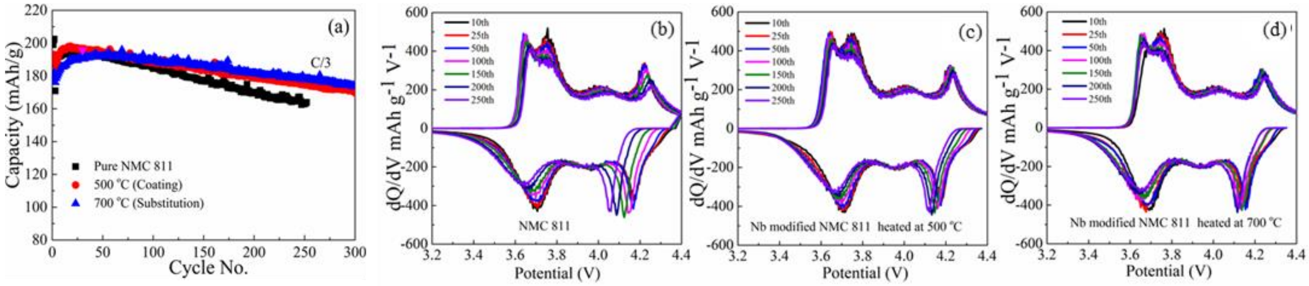

Figure 119. Cycling performance of NMC-811 and Nb-modified NMC-811 at 500°C (mainly coating) and 700°C (mainly substitution). Cycled 2.8 ~ 4.4 V at C/3. dQ/dV versus V curves of (b) NMC-811, (c) Nb-modified NMC-811 at 500°C, and (d) Nb-modified NMC-811 at 700°C for cycles 10, 25, 50, 100, 150, 200, and 250.

The UT Austin group investigated the capacity retention of an array of high-nickel-content compounds in lithium half cells, to validate their use in high-energy-density Li-metal batteries. It was confirmed that layered-oxide cathodes with a nickel content > 90% can achieve > 220 mAh g^{-1} at C/3 rate when paired with lithium anodes, while operated at room temperature and without any constant voltage steps (Figure 120a). However, without extrinsic modifications, the cycle life of these materials does suffer. $LiNi_{0.94}Co_{0.06}O_2$ (NC9406) reaches a maximum capacity of 228 mAh g^{-1} and is projected to reach 80% capacity retention after 95 cycles. $LiNiO_2$ (LNO) reaches a maximum capacity of 223 mAh g^{-1} and reaches 80% capacity retention after 97 cycles. $LiNi_{0.95}Co_{0.02}Mn_{0.015}Al_{0.01}Mg_{0.005}O_2$ (NCMAM95) reaches a maximum capacity of 218 mAh g^{-1}, slightly below 220 mAh g^{-1}, and is projected to reach 80% capacity retention after 121 cycles. $LiNi_{0.9}Mn_{0.05}Co_{0.05}O_2$ (NMC900505) is substantially below 220 mAh g^{-1} at 208 mAh g^{-1}, but is projected to reach 80% capacity retention after 176 cycles. It is worth noting that capacity does not have to directly correlate to nickel content.

By adjusting calcination parameters, such as temperature and oxygen pressure, pure-nickel LNO can give superior capacity retention compared to NC9406, though at the cost of reduced capacity. To improve the stability of the cathodes, a typical LHCE, LiFSI-DME-TTE in a molar ratio 1:1.2:3 (Figure 120b), was investigated. Al-clad cell cases were used to prevent the corrosion of the LiFSI salt. By comparing the normalized capacity of these cells to other cells subjected to the same temperature spike (Figure 120c), it is clear that the capacity retention of the LHCE cells is dramatically higher than their counterparts employing a typical carbonate-based electrolyte (3:7 EC:EMC by volume, 1 M LiPF$_6$, 2% VC by mass). In addition, the LHCE cells with LNO cathodes deliver a capacity only a few mAh g^{-1} lower than the same cathode in the baseline electrolyte, and can still attain > 220 mAh g^{-1} at C/3 rate.

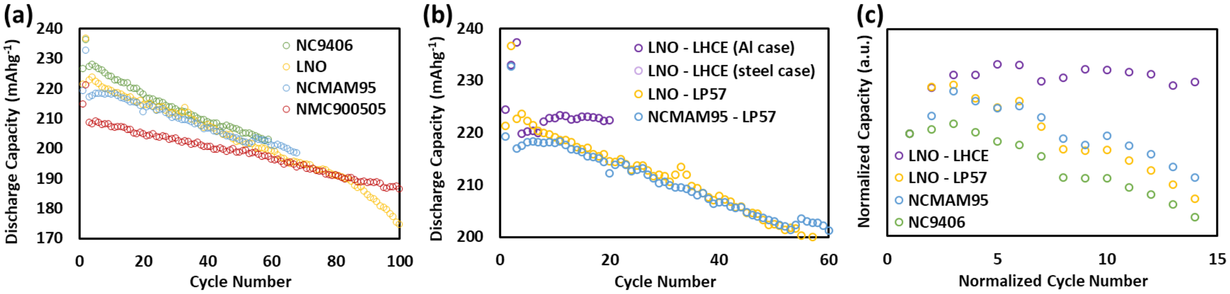

Figure 120. Cycling performance of high-nickel cathodes. (a) Performance of cathodes with various compositions with the baseline electrolyte. (b) Comparison of cells with an LNO cathode and baseline electrolyte to those with a localized high-concentration electrolyte. (c) Capacity of cells immediately before and after an ambient temperature spike. Capacities and cycle numbers are normalized to the cycle immediately before the spike.

The UW team synthesized mesoporous N-doped hard carbon (mN-HC) as a potential alternative for high-energy-density lithium battery anodes. mN-HC prepared via the Stöber method exhibits high specific capacity and high surface area. The as-obtained mN-HC exhibits a uniform spherical morphology with a diameter of ~ 500 nm (Figure 121a). The XRD pattern reveals the amorphous, hard carbon nature of the as-obtained product. The d-spacing value of (002) is 0.408 nm, much larger than that of graphite (0.334 nm), which will facilitate lithium insertion/extraction between the carbon planes. N 1s XPS spectrum of the sample confirmed the doping of nitrogen in the hard carbon. The introduction of nitrogen could enhance the electronic conductivity of carbon and lower the polarization during lithium insertion. The pore size distribution indicates a high portion of mesopores with a pore width of ~ 15 nm. The electrochemical performance of the mN-HC was tested in the LHCE [1.54M LiFSI in DME/TTE (1.2:3 by mol)]. Figure 121b displays the cycling performance of the mN-HC$_{Li}$/LiNi$_{0.8}$Mn$_{0.1}$Co$_{0.1}$O$_2$ (NMC-811) and Li/NMC-811 batteries in LHCE with an N/P ratio of 0.4 (1.6/4). The full cell with lithium anode (1.6 mAh cm^{-2}) exhibits obvious capacity deterioration after 30 cycles, implying continuous lithium loss during repeated lithium plating/stripping. In comparison, the full cell with mN-HC$_{Li}$ anode (1.6 mAh cm^{-2}) shows a capacity retention of 87.3% after 100 cycles with an average CE of 99.8%, indicating high lithiation/delithiation reversibility of the mN-HC$_{Li}$. In addition, the mN-HC$_{Li}$/NMC-811 battery exhibits lower polarization than that of the Li/NMC-811 at the same cycles. This pre-stored lithium could compensate for the inevitable lithium consumption, and hence improve the cycle performance.

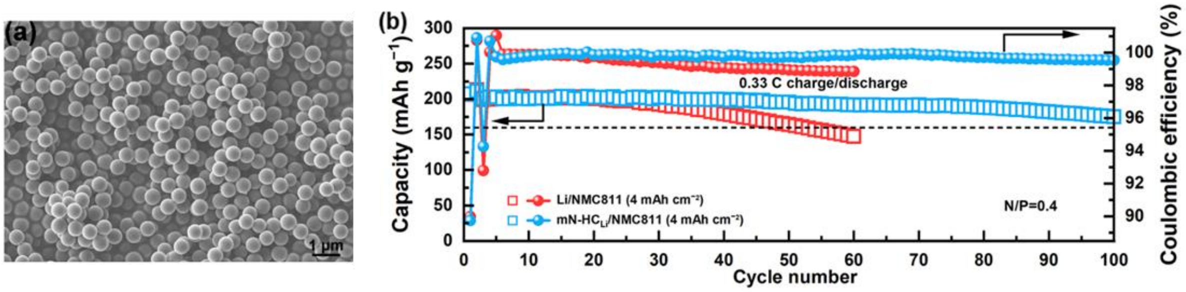

Figure 121. (a) Scanning electron microscopy image of the mesoporous N-doped hard carbon (mN-HC) materials. (b) Cycling performance of Li/NMC-811 and mN-HCLi/NMC-811 batteries in localized high-concentration electrolytes.

The Stanford group investigated Li-metal morphology and SEI structure of new electrolytes developed by their team. Figure 122 shows the design concepts of the synthesized solvents. The Li-metal deposition morphology and SEI nanostructure are carefully studied, as shown in Figure 123. When the 1 M LiFSI/DME or 1 M LiFSI/DMB is applied in Cu|NMC-532 anode-free cells after 10 cycles, the lithium structure on copper is dendritic and porous (Figure 123a-b). By contrast, with the 1 M LiFSI/FDMB electrolyte, the 2.7 mAh cm^{-2} lithium deposited on copper (~ 14-µm thick theoretically, while ~ 20 µm observed) shows densely packed, flat and large grains even after 70 cycles (Figure 123c-d). The morphology is highly beneficial to reducing the surface area for SEI growth as well as suppressing "dead lithium" formation, leading to an ideal cycling performance. Furthermore, cryo-TEM is utilized to characterize the SEI structure. In 1 M LiFSI/DME, the SEI layer is relatively thick (~ 10 nm) and non-uniform; however, an ultra-thin (~ 6 nm) and amorphous SEI is observed on lithium when 1 M LiFSI/FDMB is applied (Figure 123e-f). Instead of containing wrinkles or non-uniform domains as the SEI observed in 1 M LiFSI/DME or other conventional electrolytes, the SEI in 1 M LiFSI/FDMB exhibits extraordinary uniformity according to the fast Fourier transform (FFT, Figure 123e-f insets). This is also one of the thinnest SEIs observed to date. This feature can effectively reduce the lithium consumption from SEI formation during each cycle, thus improving the CE. The F 1s spectra of XPS further support this argument (Figure 123g). The peaks assigned to LiFSI (~ 688 eV) in 1 M LiFSI/FDMB have similar intensities throughout the depth profiling, indicating uniform SEI, while those in 1 M LiFSI/DME show large variation with sputtering.

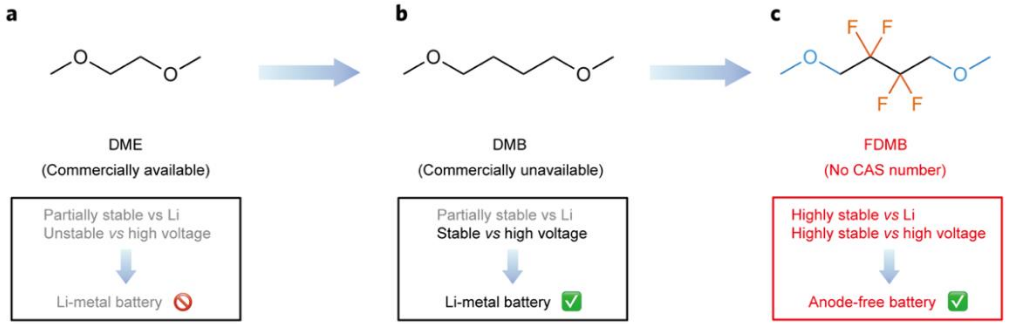

Figure 122. Design concepts of solvent molecules studied in this work. (a-c) Design scheme and molecular structures of three liquids studied in this work: DME (a), DMB (b), and FDMB (c).

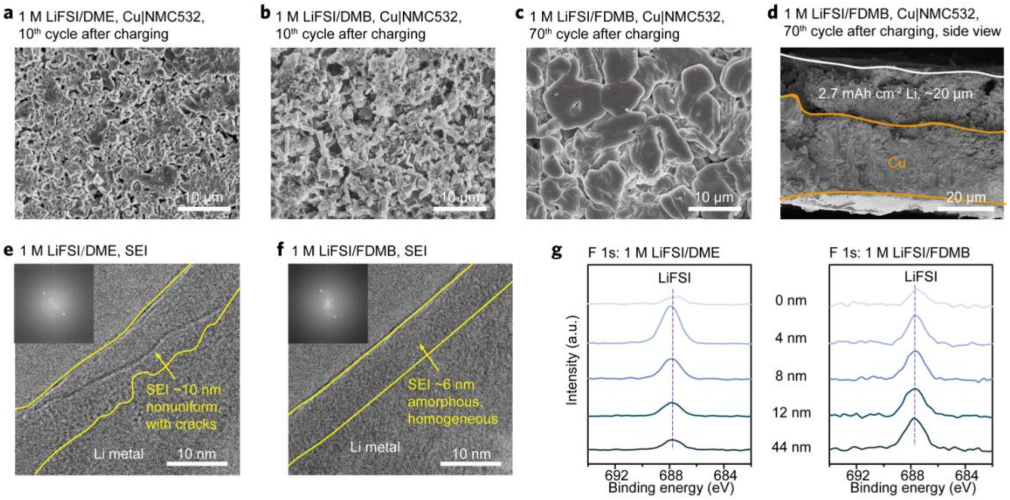

Figure 123. Li-metal morphology and SEI. (a-d) Lithium morphology in anode-free Cu|NMC-532 (2.7 mAh cm^{-2}) coin cells using 1 M LiFSI/DME after 10 cycles (a), 1 M LiFSI/DMB after 10 cycles (b), and 1 M LiFSI/FDMB after 70 cycles (c-d). Cryo-electron microscopy showing the SEI of 1 M LiFSI/DME (e) and 1 M LiFSI/FDMB (f). Insets in (e) and (f): the fast Fourier transform of SEIs. (g) F 1s X-ray photoelectron spectroscopy depth profiles of Li-metal surface in 1 M LiFSI/DME (left) and 1 M LiFSI/FDMB (right).

The PNNL team systematically studied different types of fluorinated solvents, including fluorinated ethers (BTFE, TTE), fluorinated carbonate (BTFEC), fluorinated borate (TFEB), and fluorinated orthoformate (TFEO) as diluents for LHCEs. Significant differences were observed in the LHCEs (based on LiFSI-1.2DME HCE) with these diluents. Among them, BTFEC coordinates with Li^+ in a second solvation shell beyond the first solvation with DME and FSI^-, which partially damages the high-concentration coordinated clusters in the HCE by forming a pseudo-LHCE; thus, the favorable features of HCE are lost in BTFEC-LHCE. BTFE, TTE, TFEB, and TFEO maintain the high-concentration salt clusters, while the overall LiFSI concentration decreases in the electrolytes. In addition to the crucial role of the FSI^- anion in the SEI and CEI properties in LHCEs, the diluent molecules also make great contributions to the interfacial chemistries on both the cathode and the anode. TFEB significantly accelerates oxygen release in the Ni-rich NMC-811 material and causes fast cathode decay because of its electron-deficient nature. BTFE-, TTE-, and TFEO-based LHCEs demonstrated high lithium CEs of 99.4%, 99.5%, and 99.5%, respectively (Figure 124a). For these three LHCEs, the high-voltage Li||NMC-811 cell performance was determined by the CEI chemistries under the testing conditions. The capacity retention of Li||NMC-811 with the tested LHCEs follows the order TFEO-LHCE > TTE-LHCE > BTFE-LHCE > BTFEC-LHCE > SOA electrolyte > TFEB-LHCE. These results reveal the selection rules for diluents to achieve stable cycling of high-voltage Li-metal batteries. The cycled cathodes were also characterized by annular bright-field scanning transmission electron microscopy (ABF-STEM) and HAADF-STEM. The significant amount of LiF found on these cathode primary particles supports previous findings on the critical role of LiF in CEI for effective interfacial protection. With the enhanced protection of a LiF-rich layer, no apparent TM (represented by nickel) dissolution and transport to the cycled LMA is observed in these electrolytes. In TFEO-LHCE, a thicker SEI of 5 nm is obtained on the NMC cathode, which successfully suppresses the cation-mixing phase transition. For the LHCEs studied in this work, the CEI thickness and LiF crystallinity follow the order of BTFE < TTE < TFEO, and the suppression of cation-mixing transformation follows the same order (Figure 124b-f), which is also in good agreement with the cell capacity retention trend shown in Figure 124a.

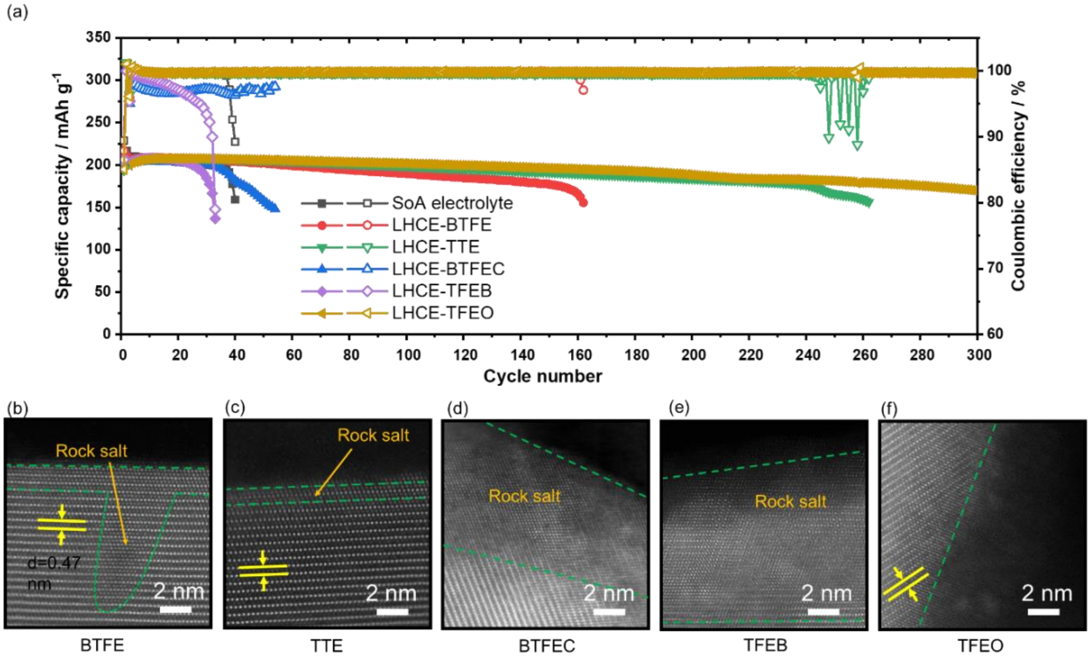

Figure 124. (a) Cycling performance of the Li||NMC-811 cells. (b-e) The annular bright field – transmission electron microscopy images of NMC-811 cathodes after 100 cycles in localized high-concentration electrolytes with different diluents (b) BTFE, (c) TTE, (d) BTFEC, (e) TFEB, and (f) TFEO. The Li||NMC-811 cells were cycled at C/3 after two formation cycles at C/10 with 1.5 mAh cm^{-2} NMC-811, 50-µm lithium, and 75 µL electrolyte.

Highlights of Keystone Project 1

The highlights for this quarter are as follows:

- The Stanford group synthesized a novel electrolyte, 1 M LiFSI/FDMB. Cryo-TEM results show that one of the thinnest SEIs with extraordinary uniformity observed to date was formed in this electrolyte leading to long-term cycling stability of Li/NMC batteries.
- It was discovered that capacity does not directly correlate to nickel content: By adjusting calcination parameters, such as temperature and oxygen pressure, pure-nickel LNO can give superior capacity retention than NC9406 at the cost of reduced capacity.

Keystone Project 2: Electrode Architecture

The goal of Keystone 2 is to design, model, fabricate, and characterize the effect of electrode architecture on electrode and cell performance in support of reaching 500 Wh/kg cell specific energy. Included in this Keystone are Li-metal electrode architectures (UCSD), electrode characterization, and electrolyte optimization for polymeric sulfur (UCSD and BNL). Highlighted this quarter are recent advancements in understanding 3D Li-metal architecture and interfacial characterization for polymeric sulfur that leads to fundamental understanding with guidance for electrolyte optimization.

Porous Copper for Li-Metal Deposition

Last quarter, laboratory XRT was used to quantify the physical properties of the synthesized porous coppers. After obtaining the tortuosity of each porous copper sample with different pore sizes, tortuosity of the 3D current collector was systematically studied by S. Meng's group at UCSD to understand its influence on the Li-metal deposition distribution.

Cross-Section SEM Imaging. The effect of tortuosity was studied by imaging the deposited lithium within the porous copper. Figure 125 shows distribution of the deposited lithium in the porous coppers after being plated for 20 hours at 1 mA/cm^2. The Back-Scattered Electron (BSE) images (Figure 125e-h) give a clear view of how lithium is distributed across the whole porous copper: the brighter region is copper and darker region is lithium. The boundary between vacuum and lithium is marked by white lines for reference. Schematic illustrations were also made to better illustrate the lithium deposition's spatial distribution and morphology in different samples.

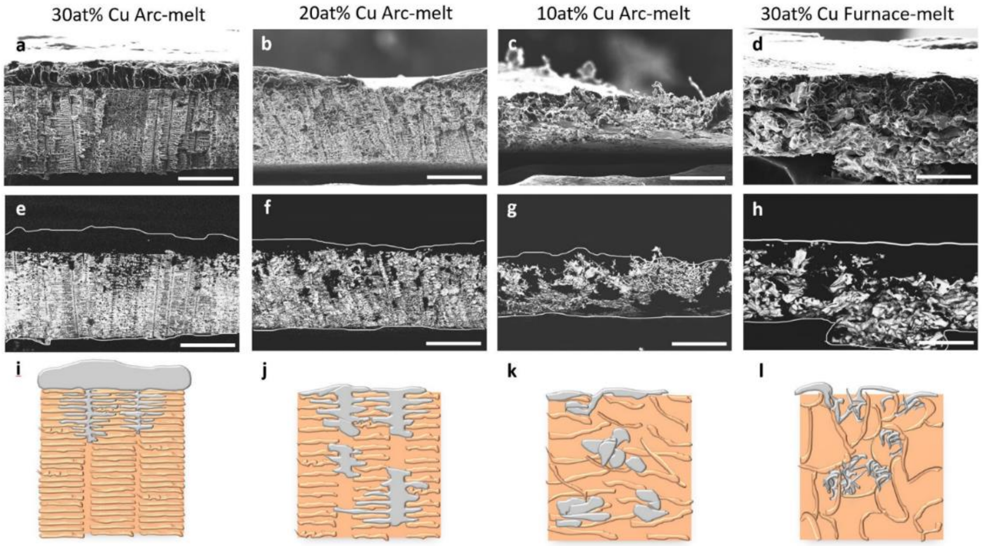

Figure 125. (a-d) Scanning electron microscopy cross section images. (e-h) Back-scattered electron images and (i-l) schematic illustration of lithium distribution in the cross-section of the porous copper with lithium deposited within different parts of the structure. All samples were plated to 20 mAh/cm^2. The scale bars indicate 50 µm in all images.

With the smallest pore diameter (~ 4 µm) and the highest z-directional tortuosity (1.95), the 30Arc samples showed the greatest inhomogeneity of deposited lithium (Figure 125a/e/i). Most of the deposited lithium accumulated near the top surface of the porous copper. The space under the surface, where the lithium was desired to be deposited, was devoid of lithium deposition. This inhomogeneous distribution of deposited lithium can be attributed to the fact that the complex structure of porous copper with small pores and high tortuosity will block the incoming lithium from entering the empty space inside the structure. As a result, most of the lithium deposited near the top surface and the extra surface/pores that was provided in the 3D structure was not utilized.

As the pore size was increased to 10 µm, a decrease in the z-directional tortuosity to 1.60 was observed (from 1.95). The distribution of the deposited lithium in the porous copper changed dramatically (Figure 125b/f/j). More lithium was found to be deposited inside the pores of the porous copper instead of on the top surface. The high utilization of the empty pores can help to increase the contact area between lithium and the copper, which would lower the local effective current density and result in a more uniform morphology.

On further increase in the pore size (~ 20 µm) and decrease in the tortuosity (1.08), more lithium was found to grow further inside the pores (Figure 125c/g/k). The deposited lithium grew in a bulky and cluster-like morphology inside the porous copper, which is less homogenous compared to the 10-µm pore-sized porous sample.

Using porous copper with the largest pore size (~ 25 µm), the distribution of the deposited lithium is similar to the previous 10Arc sample. However, the increase of the pore size also led to the decrease in specific surface area. Therefore, the morphology of the deposited lithium changed from bulky chunk type to whisker-like (Figure 125d/h/l). This change of morphology would eventually lead to the formation of inactive metallic lithium and cause decrease in CE.

Based on these observations, the effect of the tortuosity can be summarized as follows: (1) the narrow and tortuous structures, such as the case in the 30Arc sample (with a tortuosity of 1.95), would largely hinder the diffusion of lithium ions, leading to an inhomogeneous distribution of the deposited lithium; (2) the inhomogeneous distribution would also under utilize the empty space and surface area provided by the 3D structure and possibly lead to the formation of lithium whiskers after the top surface is fully covered by deposited lithium.

STEM-EELS Analysis of Sulfurized Polyacrylonitrile

Sulfurized polyacrylonitrile (SPAN) has emerged as a popular candidate as a cathode material for Li-S batteries due to its ability to mitigate the polysulfide dissolution issue. However, the electrochemical reaction mechanisms between lithium and SPAN are still not clear. Here, STEM EELS was used by S. Meng's group at UCSD to probe the bonding environment evolution of nitrogen, sulfur, and carbon in SPAN cathode fabricated by Liu's group at UCSD at the pristine, discharged, and charged states, which provided insight into the interaction between lithium and SPAN during cycling.

N K-Edge. Figure 126a shows the nitrogen K-edge at three different states. In the pristine state, two peaks that are associated with 1s to π^* and 1s to σ^* transitions are seen, which suggests that nitrogen exists in mostly the sp^2-hybridization state. After discharge, the nitrogen K-edge shows a decrease in the σ^* peak intensity compared to the π^* peak. This change potentially indicates that nitrogen is actively participating in the electrochemical reaction between lithium and SPAN. After charging, the σ^* peak was recovered to a similar intensity as the pristine state. The reversibility of the σ^* peak intensity in nitrogen K-edge suggests that nitrogen plays an active reversible role in the electrochemical reaction.

C K-Edge. Figure 126b shows the carbon K-edge during cycling. In the pristine state, the carbon K-edge shows two peaks that are associated with 1s to π^* and 1s to σ^* transitions, which suggests that the carbon is also in a sp^2-hybridization state. The carbon K-edge and nitrogen K-edge show similar near-edge structures at the pristine state, which indicates that carbon and nitrogen are in similar electronic environment and form an aromatic ring structure, consistent with existing literature. After discharge and charge, the most noticeable change happens in the relative peak intensity of the π* bonding peak. To better illustrate the change in the peak intensity, an intensity ratio π*:σ* is listed in Figure 126d, which shows that the ratio changed from 0.9135 at pristine state to 0.7180 after discharge and then back to 0.7770 after charge. This peak intensity change shows that there is less degree of reversibility in the carbon bonding environment during cycling after the first discharge.

S L-Edge. As shown in Figure 126c, for the sulfur L-edge, the peaks at 165.7 and 228.7 eV corresponding to the sulfur $L_{2,3}$ edge and sulfur L_1 edge confirm the presence of sulfur in the pristine SPAN. While there is no clear feature in the sulfur L-edge after discharge, the sulfur $L_{2,3}$ edge reappeared after charge, which shows a possible reversibility of sulfur in SPAN. The sulfur $L_{2,3}$ edge for Li_2S is also simulated by FEFF9. The simulated spectrum shows two characteristic peaks at 173.2 eV and 180.9 eV, which are not obvious in the measure sulfur $L_{2,3}$ edge from both discharged and charged states. The lack of Li_2S signals in the cycled SPAN might explain why SPAN material shows an excellent stability during cycling, due to material losses into the electrolyte bulk caused by Li_2S oxidation to form polysulfides.

More characterization and analysis are in progress to further decipher the reaction mechanism between lithium and SPAN. Additionally, subsequent cycles will be also analyzed to investigate the large differences in electrochemical voltage profiles of the 1st and subsequent cycles.

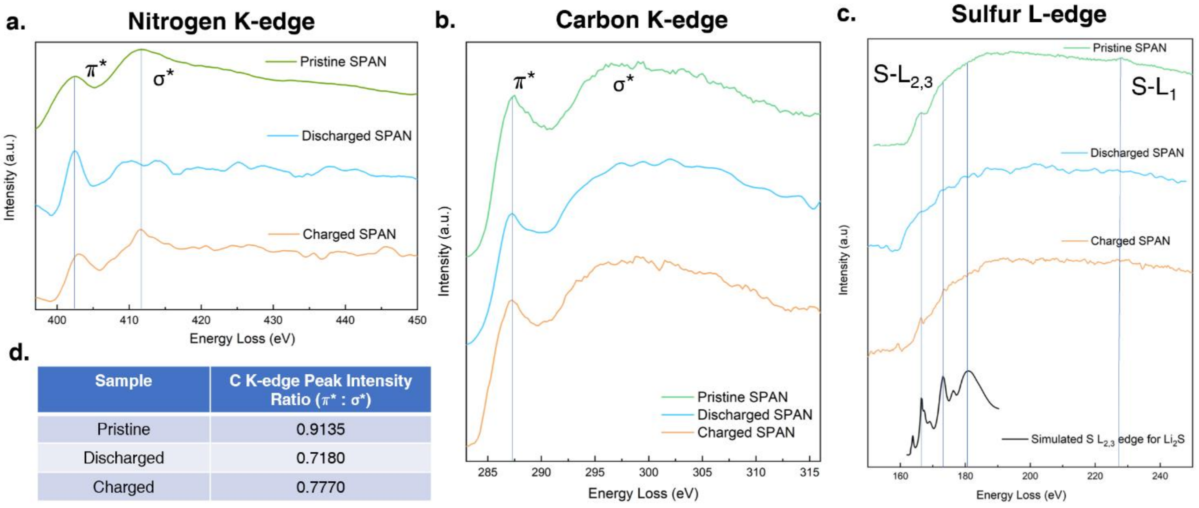

Sample	C K-edge Peak Intensity Ratio (π* : σ*)
Pristine	0.9135
Discharged	0.7180
Charged	0.7770

Figure 126. Scanning transmission electron microscopy electron – energy loss spectroscopy spectrum of (a) nitrogen K-edge, (b) carbon K-edge, and (c) sulfur L-edge in pristine, discharged, and charged sulfurized polyacrylonitrile. (d) Table of carbon K-edge peak intensity ratio (π*: σ*).

In collaboration with Liu's group, Yang's group at BNL applied synchrotron-based diagnostic tools to understand why addition of $LiNO_3$ can enable stable cycling of SPAN in ether-based electrolyte (DME/DOL). This is important because only ether-based electrolyte can be compatible with Li-metal anode. By using spatially-resolved XRF microscopy combined with XAS, it was found that in pure DME/DOL electrolyte, the Li_2S_x that forms on the cathode side after one discharge-charge cycle shuttles to the lithium side, resulting in the fast capacity degradation (Figure 127). After adding $LiNO_3$, the Li_2S_x in the SPAN cathode is retained via the formation of a robust CEI layer, leading to dramatic improvement in the cyclability of SPAN in ether electrolyte. Based on knowledge learned from detailed XRF/XAS and electrochemical study, Liu's group has successfully demonstrated stable cycling of SPAN cathode with high areal loading (> 6.5 mAh cm^{-2}) with lean electrolyte, showing promising Li-SPAN cell performance under practical conditions (Figure 128).

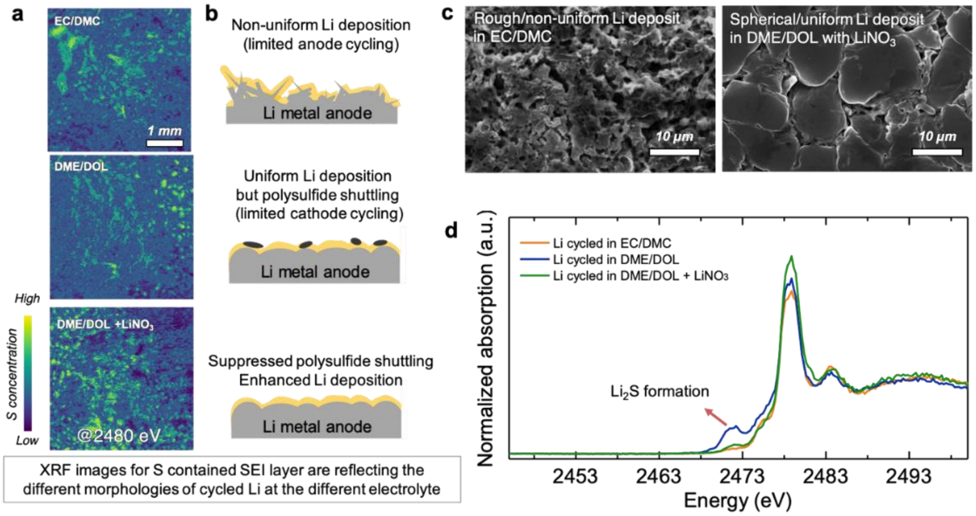

Figure 127. (a) X-ray fluorescence image of Li-metal anodes cycled in EC/DMC, DME/DOL, and DME/DOL with $LiNO_3$, measured at an incident beam energy of 2480 eV. (b) Corresponding schematic sketch of a cross-section view of Li-metal anode for each case. (c) Scanning electron microscopy images for Li-metal anode after 100 cycles in EC/DMC and DME/DOL with $LiNO_3$. (d) Normalized sulfur K – X-ray absorption near-edge spectroscopy measured from the selected area from (a).

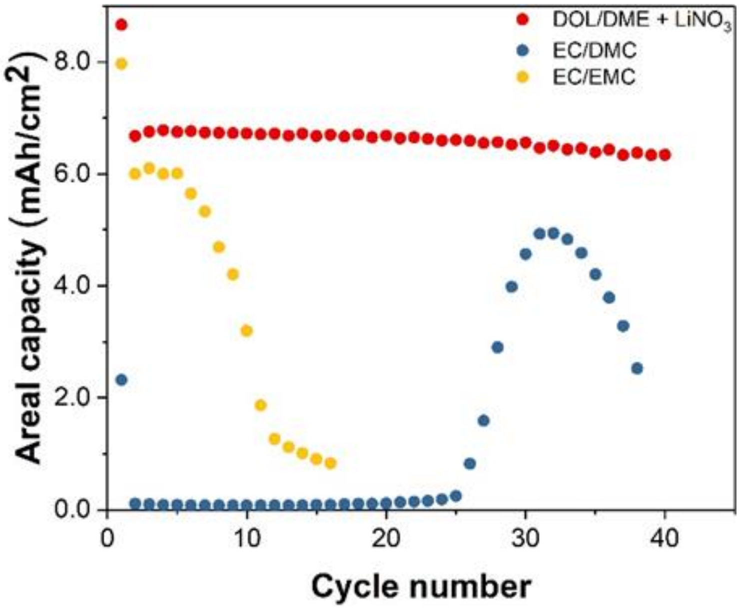

Figure 128. Lean electrolyte (3g/Ah) cycling performance of thick sulfurized polyacrylonitrile electrode in carbonates and DME/DOL with $LiNO_3$ (azure blue dots).

In another effort, W. Xu's group at PNNL evaluated the long-term cycling performance of Li||SPAN coin cells with DME-based LHCE and $LiPF_6$/EC-EMC+VC control electrolyte, in which the high areal loading (> 6.5 mAh cm^{-2}) SPAN cathode (from Liu's group at UCSD), medium-thick (250 μm) lithium, and flooded electrolyte (75 μL) were used. As shown in Figure 129, the discharge areal capacity in LHCE reaches 6.1 mAh cm^{-2} after initial activation and maintains at 5.3 mAh cm^{-2} after 400 cycles at C/5 under 25°C (1C = 6.0 mAh cm^{-2}), corresponding to a capacity retention of 86.9%. Moreover, with LHCE, the Li||SPAN cell exhibits an average CE of ~ 100% during the 400 cycles, indicating inhibited side reactions on the

SPAN cathode and the lithium anode and limited resistance growth during cycling. By comparison, although the Li||SPAN cell with Control exhibits higher capacities during both the formation and the following first 10 cycles than the cell with LHCE, it suffers from a rapid capacity drop after only about 15 cycles at C/5, and the remaining capacity after 50 cycles is negligible. The evaluation of Li||SPAN cells with DME-LHCE under practical conditions will be performed.

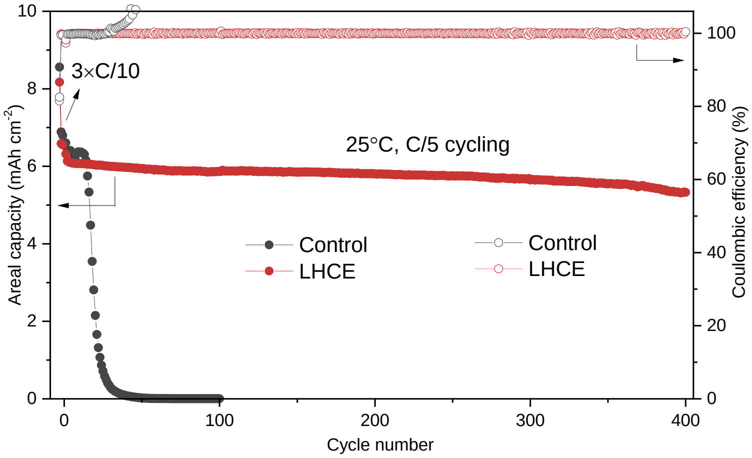

Figure 129. Cycling performance of Li||SPAN coin cells with two different electrolytes of control and localized high-concentration electrolyte at C/5 (1.2 mA cm^{-2}) between 1.0-3.0 V.

Highlights of Keystone Project 2

The highlights for this quarter are as follows:

- STEM-EELS and synchrotron studies revealed the chemistries both within the SPAN bulk electrode and at the electrode-electrolyte interphase. These studies provided insight for designing electrolytes that enable high areal loading (> 6.5 mAh cm^{-2}) SPAN with promising electrochemical performance.
- SEM images revealed the effect of 3D current collector tortuosity on lithium deposition behavior: high tortuosity can hinder the diffusion of lithium ions and lead to inhomogeneous lithium deposition, while small tortuosity can reduce the specific surface area and cause whisker-like lithium that are prone to deactivation.

Keystone Project 3: Cell Fabrication, Testing, and Diagnosis

This quarter, researchers at PNNL developed approaches for large-scale preparation of sulfur electrodes with integrated nano-structured sulfur/carbon (S/C) materials and identified the key challenges for the long-term cycling of high-energy Li–S pouch cells at realistic conditions. High mass-loading sulfur electrodes at 4-6 mg cm^{-2} have been prepared in large scale at PNNL's Advanced Battery Facility (ABF) and used for multiple-layer Li–S pouch cell fabrication (Figure 130a). The S/C composites and high loading electrodes were supplied to other Battery500 teams on request for benchmark or validation research.

Key parameters affecting the practical energy of the Li–S battery were investigated using the Li–S pouch cell as a platform. It is found that reducing the electrolyte content while increasing the active sulfur amount are the two important approaches for substantial cell-level specific energy improvement. A steady increase in cell-level specific energy with increased cathode areal capacity is only feasible when electrolyte and inert weight are tightly controlled. For a sulfur cathode with loading of at least 4 mg cm^{-2}, the amounts of electrolyte and lithium need to be strictly controlled to reach a high specific energy of 350 Wh kg^{-1} in a practical pouch cell. Following cell design, practical pouch cells with different E/S ratios were fabricated and tested (Figure 130d). The lifespan of Li–S pouch cells is highly dependent on the amount of electrolyte used, that is, electrolyte volume / sulfur mass ratio (E/S in unit mLg^{-1}). To clearly understand the effects of E/S ratio on cell cycling life, the cumulative specific discharge capacities (the total discharge capacities delivered in the lifespan) are plotted versus applied E/S ratio (Figure 130e). The cumulative specific discharge capacity decreases almost linearly with the E/S ratio, indicating that Li–S pouch cell cycling is primarily dominated by the electrolyte amount.

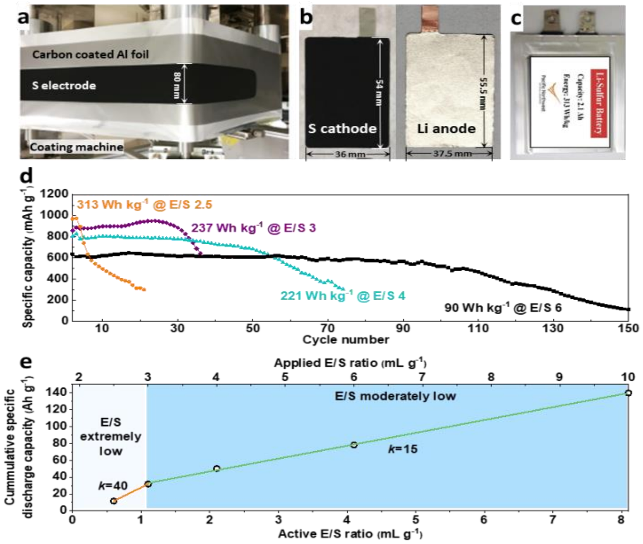

Figure 130. High-energy Li–S pouch cell. (a) Digital photograph of the large-area sulfur electrode on a coating machine. (b) Digital photographs of punched sulfur cathode and lithium anode (thickness = 50 μm) for pouch cell. (c) Digital photograph of the high-energy pouch cell. (d) Cycling performances of Li–S pouch cells with different energy densities and E/S ratios (mL g^{-1}). (e) Relationship of the cumulative specific discharge capacity and applied E/S ratio and active E/S ratio of pouch cells in (d).

To extend cell cycle life at high cell-level specific energy, sulfur electrodes with improved sulfur utilization and electrode density are under development to reduce requirements for excessive thick electrodes and high sulfur loading to increase the amount of available electrolyte.

Researchers at INL studied the formation and aging of Li-S batteries at different cycling rates and temperatures with the aim to better understand guidance on cycling use and implications for future cell designs. Assorted temperatures for formation ranging from 10-45°C and cycling rates C/2-C/20 were investigated. A distinct change in performance was observed when using intermediate temperatures. The capacity retention and aging cycling performance at C/10, C/5, and C/2 C-rates (25°C C/20 formation) suggests a competition between polysulfide shuttle and electrode utilization. Advanced analysis is under way following similar procedures the team used for Li-NMC cells using Battery500 electrolytes and formation process.

In work on Li-NMC, INL has expanded the electrochemical methods that can uniquely show the interplay between cell-level thermodynamic and kinetic aspects, including Kinetic Polarization Hinderance (KPH) for Li-NMC cells.[1, 2] The origin of this KPH effect could include mass transport in the porous media of the electrode, the charge transfer rate at the electrode-electrolyte interface, or the lithium diffusion in the lattice of NMC, etc. By comparing the capacity ratio measured at a *C/n* rate of polarization ($QR_{C/n}$) with the theoretical capacity ratio (QR_T), it is possible to obtain the NMC utilization efficiency ($\varepsilon_{C/n}$) at the *C/n* rate at a specific SOC and cycle number. Further derivation can provide the degree of the KPH effect (η_{KPH}) based on $\eta_{KPH} = QR_{KPH} / QR_{C/n}$. The values of QR_{KPH} are calculated by the incremental amount of $QR_{KPH} = \Delta Q_{KPH} / \Delta SOC$. The quantifications as shown in Figure 131 are very useful to identify and quantify the effects on the materials utilization and capacity loss (reversible or irreversible) with clear separation of the origin of the attributes. Such information will become more critical and quantitative to effectively establish a quantitative measure to improve specific energy and cycle life.

UW and UT Austin researchers have developed a coupled electrochemical-thermal model for Li-S batteries, while also highlighting many of the key challenges that remain in multi-scale battery models including moving boundaries and mechanical aspects that prevail in Li-NMC and Li-S batteries.[3] The Li-S electrochemical model developed this quarter, is based on the model developed by Kumaresan et al.[4] In this model, the overall potential is set by the thermodynamics of individual electrochemical reactions and their overpotentials. The anode is modeled as a constant source of lithium ions. The model explores how the battery dynamics change over the one-dimensional regions of the cathode and the separator. The thermal model was developed based on the work by Pals and Newman. The temperature is a function of ohmic heating and heat due to the electrochemical reactions. For this work, the researchers have developed a single sandwich model, and for future work, the team will be considering more layers to more accurately depict thermal behavior.

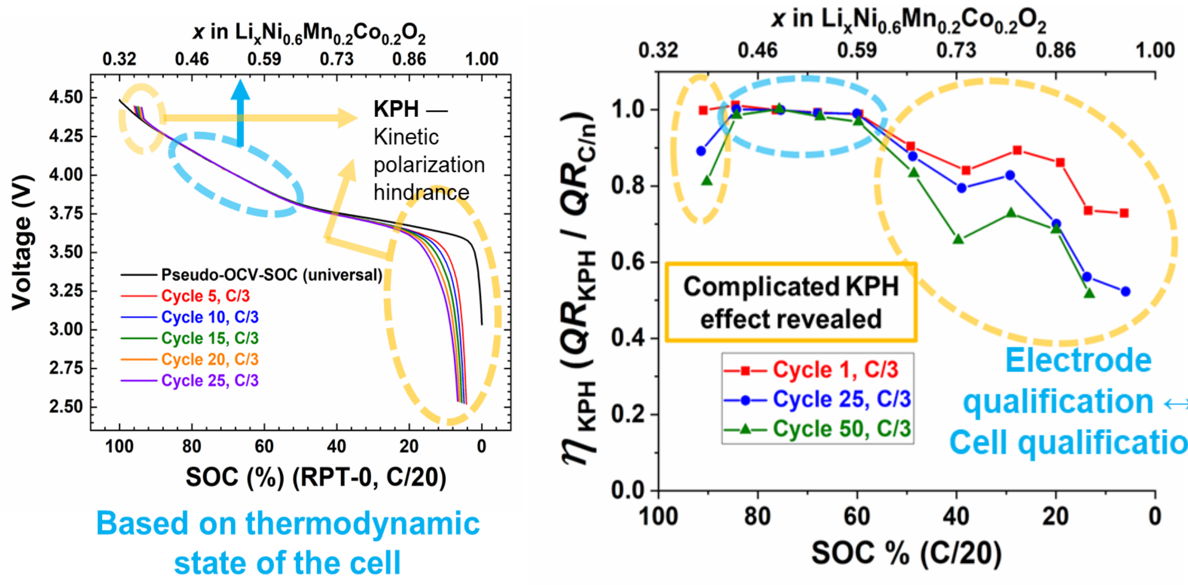

Figure 131. Idaho National Laboratory's electrochemical analytic diagnosis (eCAD) technique can transform a typical charging-discharging curve into a cell infrared (IR)-free voltage versus state-of-charge (SOC) (which corresponds to the lithium content in NMC cathode composition) curve to separate the thermodynamic and kinetic effect attributes. (Left) The transformed curves show regions where NMC potential versus lithium content in the NMC composition (pseudo-OCV versus x in Li$_x$NMC) correlation and the IR-free voltage versus SOC ($V_{IR\text{-}fee}$ versus SOC) correlation are compared. (Right) The effect from an electrode's kinetic polarization hindrance (KPH) can then be derived from the charging-discharging curves as "the degree of KPH effect" (η_{KPH} = QR_{KPH} / $QR_{C/n}$) as a function of SOC and cycle number.

To understand the rate dependence of the thermal behavior, three different rates were compared with low natural convection (h=1 W/m^{2}K). Everything is compared on a capacity basis. As the rate increases, there is increased polarization, and these losses result in depressing the voltage curve and capacity loss at the end of discharge. As expected, the temperature rise increases with increase in rate. The temperature rise is greatest initially, with another increase at the point of inflection between the two plateaus. To understand the heat sources, the heats have been included. As shown in Figure 132, Ohmic heating increases dramatically at the transition between the two plateaus and decreases until another steep increase at the end of discharge, indicating the conductivity is lowest during those rises. The heat generation from the reactions is around an order of magnitude larger than ohmic heating. The reversible heating is larger than the irreversible heat during the first plateau, and then the irreversible heat increases steadily until the end of discharge, indicating the overpotentials are larger in the second half of discharge. For ohmic heating and reaction heats, the increase in rate accompanies a similar increase in Q.

The work for this quarter was development of the preliminary coupled electrochemical-thermal model for Li-S batteries. The thermal part of the model is affected by the electrochemical behavior; however, the other parameters are currently not functions of temperature. For future work, the team would like to collaborate with experimental groups with full-cell data to study the effect of temperature on the kinetic, transport, and thermodynamic parameters.

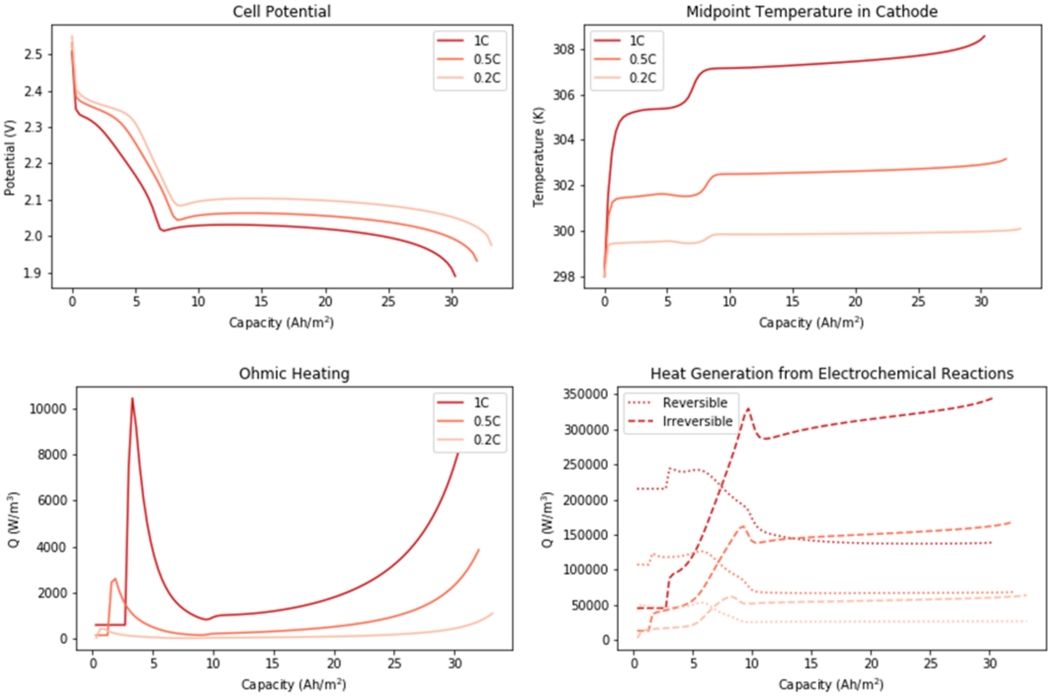

Figure 132. Thermal profiles for assorted rates associated with low convection.

References

[1] Zhang, Y., et al. *Journal of the Electrochemical Society* 167 (2020): 090502.

[2] Zhang, Y., et al. *Journal of Physics: Energy* 2 (2020): 034003.

[3] Shah, K., et al. *Journal of the Electrochemical Society* 167 (2020): 133501.

[4] Kumaresan, K., Y. Mikhaylik, and R. E. White. *Journal of the Electrochemical Society* 155 (2008): A576

Highlight of Keystone Project 3

Electrochemical characterization methods were enhanced to understand utilization of electrode materials. These methods will allow the Battery500 team to directly compare different cycling experiments and advance new cell and electrode design concepts.

Patents/Publications/Presentations

Publications

- Cao, X., L. Zou, B. E. Matthews, L. Zhang, X. He, X. Ren, M. H. Engelhard, S. D. Burton, P. Z. El-Khoury, H-S. Lim, C. Niu, H. Lee, C. Wang, B. W. Arey, C. Wang, J. Xiao, J. Liu, W. Xu, and J-G. Zhang. "Optimization of Fluorinated Orthoformate Based Electrolytes for Practical High-Voltage Lithium Metal Batteries." *Energy Storage Materials* 34 (2021): 76–84, ISSN 2405-8297. https://doi.org/10.1016/j.ensm.2020.08.035. Publication Date (Web): September 4, 2020.
- Xiao, J., Q. Li, Y. Bi, M. Cai, B. Dunn, T. Glossmann, J. Liu, T. Osaka, R. Sugiura, B. Wu, J. Yang, J-G. Zhang, and M S. Whittingham. "Understanding and Applying Coulombic Efficiency in Lithium Metal Batteries." *Nature Energy* (2020): 561–568. Publication Date (Web): June 5, 2020.
- Shi, L., S-M. Bak, Z. Shadike, C. Wang, C. Niu, P. Northrup, H. Lee, A. Y. Baranovskiy, C. S. Anderson, J. Qin, S. Feng, X. Ren, D. Liu, X-Q. Yang, F. Gao, D. Lu, J. Xiao, M. S. Whittingham, and J. Liu. "Reaction Heterogeneity in Practical High-Energy Lithium-Sulfur Pouch Cells." *Energy & Environmental Science* 10 (2020): doi:10.1039/D0EE02088E. Publication Date (Web): September 4, 2020.
- Wang, X., G. Pawar, Y. Li, X. Ren, M. Zhang, B. Lu, A. Banerjee, P. Liu, E. J. Dufek, J. G. Zhang, J. Xiao, J. Liu, Y. S. Meng, and B. Y. Liaw. "Glassy Li Metal Anode for High-Performance Rechargeable Li Batteries." *Nature Materials* (2020). doi:10.1038/s41563-020-0729-1. Publication Date (Web): July 27, 2020.
- Zhang, Y., Q. Wang, B. Y. Liaw, S. C. Nagpure, E. J. Dufek, and C. C. Dickerson. "Cell Degradation Quantification – A Performance Metric-Based Approach." *Journal of Physics: Energy* 2 (2020): 034003. doi:10.1088/2515-7655/ab979b. Publication Date (Web): July 3, 2020.
- Xin, F., and M. S. Whittingham. "Challenges and Development of Tin Based Anode with High Volumetric Capacity for Li-ion Batteries." *Electrochemical Energy Reviews* (2020). doi: 10.1007/s41918-020-00082-3. Publication Date (Web): October 1, 2020.
- Nanda, S., and A. Manthiram. "Lithium Degradation in Lithium-Sulfur Batteries: Insights into Inventory Depletion and Interphasial Evolution with Cycling." *Energy & Environmental Science* 13 (2020): 2501–2514. Publication Date (Web): July 3, 2020.
- Xie, Q., and A. Manthiram. "Long-Life, Ultrahigh-Nickel Cathodes with Excellent Air-Storage Stability for High-Energy-Density Lithium-Based Batteries." *Chemistry of Materials* 32 (2020): 7413–7424. Publication Date (Web): August 4, 2020.
- Li, W., X. Liu, Q. Xie, Y. You, M. Chi, and A. Manthiram. "Long-Term Cyclability of NCM-811 at High Voltages in Lithium-Ion Batteries: An In-depth Diagnostic Study." *Chemistry of Materials* 32 (2020): 7796–7804. Publication Date (Web): August 27, 2020.
- Subramaniam, A., S. Kolluri, S. Santhanagopalan, and V. R. Subramanian. "An Efficient Electrochemical-Thermal Tanks-in-Series Model for Lithium-Ion Batteries." *Journal of the Electrochemical Society*, 167 (2020): 113506. Publication Date (Web): July 29, 2020.
- Shah, K., A. Subramaniam, L. Mishra, T. Jang, M. Z. Bazant, R. D. Braatz, and V. R. Subramanian. "Editors' Choice—Perspective—Challenges in Moving to Multiscale Battery Models: Where Electrochemistry Meets and Demands More from Math." *Journal of the Electrochemical Society*, 167 (2020): 133501. Publication Date (Web): September 24, 2020.
- Kasse, R. M., N. R. Geise, J. S. Ko, J. N. Weker, H-G. Steinrück, and M. F. Toney. "Understanding Additive Controlled Lithium Morphology in Lithium Metal Batteries." *Journal of Materials Chemistry A* 8 (2020): 16960–16972. doi: 10.1039/d0ta06020h. Publication Date (Web): July 30, 2020.

Presentations (Invited)

- StorageX International Symposium, Stanford, California, Virtual (July 17, 2020): "Energy Storage Solutions from -80°C to +100°C: From Liquified Gas Electrolytes to Solid State Electrolytes"; Y. S. Meng.
- Israel National Research Center for Electrochemical Propulsion (September 15, 2020): "Advanced Diagnostic Tools for Characterizing Lithium Metal Batteries and Solid-State Batteries"; Y. S. Meng. Keynote.
- Florida Battery Symposium, Virtual (July 28, 2020): "The Li Battery: From Its Origin to Enabling an Electric Economy"; M. S. Whittingham.
- International Society of Electrochemistry (ISE) Meeting, Belgrade, Virtual (August 31, 2020): "Lithium Batteries: From an Idea to Domination. What's Next?"; M. Stanley Whittingham.
- Materials, Science, and Engineering Seminar, Iowa State University (September 14, 2020): "The Origins of the Lithium Battery and Future Challenges/Opportunities"; M. S. Whittingham.
- Israel National Research Center for Electrochemical Propulsion (September 16, 2020): "The Origins of the Lithium Battery and Future Challenges/Opportunities"; M. S. Whittingham. Nobel Lecture.
- Diamond Jubilee, Indian Institute of Technology, New Delhi, India (September 17, 2020): "The Origins of the Lithium Battery and Future Challenges/Opportunities"; M. S. Whittingham. Inaugural Lecture.
- World Energy Storage Day Conference and Expo (September 22, 2020): "The 2020s – The Decade of Energy Storage: Cleaning the Environment and Mitigating Global Warming"; M. S. Whittingham.
- General Motors (September 22, 2020): "The Origins of the Lithium Battery and Future Challenges/Opportunities"; M. Stanley Whittingham.
- TESTA - International Electric Vehicle Technology Conference and Exhibition, Taiwan (September 24, 2020): "Lithium Batteries: From an Idea to Domination. What's Next?"; M. Stanley Whittingham.
- 2020 Advanced Lithium-Ion Battery and Fuel Cell Conference, Taiwan (September 29, 2020): "Lithium Batteries: From an Idea to Domination. What's Next?"; M. Stanley Whittingham.
- Institute for Materials Discovery and Design (IMDD) Materials Research Science and Engineering Center (MRSEC) Launch Celebration, University of California, San Diego, California (September 29, 2020): "Why Materials?"; M. S. Whittingham.
- India Smart Grid Forum, Online Training Program on Electric Mobility & Charging Infrastructure, New Delhi, India (July 4, 2020): "Battery Technologies and Charging Characteristics"; A. Manthiram.
- StorageX International Symposium, Stanford, California (July 24, 2020): "Oxide Cathode Chemistry for Batteries: Richness and Complexities"; A. Manthiram.
- Indian Institute of Technology, Madras Webinar, Chennai, India (August 14, 2020): "Electrical Energy Storage: A Materials Chemistry Perspective"; A. Manthiram.
- International Advanced Research Centre for Powder Metallurgy and New Materials (ARCI), Chennai, India (August 28, 2020): "Next Generation Battery Chemistries"; A. Manthiram.